UiT The Arctic University of Norway

Faculty of Science and Technology

Department of Physics and Technology

Ice in Norwegian subarctic fjords and coastal regions

An examination of ice formation, properties, and trends based on remote sensing and in situ data

Megan O'Sadnick

A dissertation for the degree of Philosophiae Doctor – June 2022

***Front Page Image**: Breakup of ice cover on Nordkjosbotn, Troms, Norway*
11 March 2020

Abstract

Norwegian fjords act as a natural laboratory to observe the interaction of fresh water, fed by snow melt, rain, and ground water with the ocean, from periods of relative warmth through winters with sub-freezing temperatures. No two are exactly alike with circulation and stratification within the fjord's waters controlled by tides, river runoff, coastal exchange, and wind combined with the bathymetry and shape of the fjord. Often surrounded by high mountains, weather including air temperature, precipitation, and wind patterns can also differ significantly between fjords located within close proximity to each other. The ice that can develop on the surface is likewise variable, a reflection of the environmental conditions at the time of its formation.

Larger fjords along the Norwegian coast are ice free all year due to the influence of warm Atlantic water, however, sea ice can form in the inner parts of fjords and in smaller fjord branches. While a wide breadth of work exists examining mainland Norwegian fjords often focused on water mass dynamics and their link to biological processes, little research has been conducted on specifically sea ice in these locations. The overarching goal of the work presented here is to address this gap in research and knowledge. To do so, first an assessment of ice extent in fjords and other coastal areas along the coast of mainland Norway from 2001 to 2019 between February through May is completed. Through the development of an automated method to estimate quantitatively ice extent in optical satellite imagery, variability in ice extent between years as well as within single seasons is highlighted for regions and specific fjords. An investigation into the factors potentially driving ice formation is conducted with focused placed on air temperature, snowfall, and rainfall plus snowmelt. Next, seven fjords located in northern Norway are studied in-depth through the collection of ice and ocean measurements over the course of three winter seasons spanning 2017 into 2020. Ice stratigraphy, bulk ice salinity and oxygen isotopic composition, ocean temperature, salinity and oxygen isotopic composition, and river isotopic composition are analyzed. Possible connections to temperature and snowfall are revisited in addition to river runoff illuminating further variations not only in ice extent between seasons but also ice properties and the factors driving ice formation. Lastly, bulk ice salinity and oxygen isotopic composition are given a closer look through the inversion of previously derived, separate, relationships of each to growth rate and interface water composition. Results provide a promising method to deduce ocean and weather conditions during ice growth in fjords and coastal areas where continuous measurement through winter is not possible.

Ice alters the physical behavior of a fjord including stratification, the transmission of light in the upper water column, and heat flux from the air to ocean and vice versa, and in turn alter biological conditions. In addition, ice creates an obstacle to those transiting fjords and coastal regions by boat – slowing speed, increasing risk in search and rescue scenarios, and complicating the clean-up of any spilled pollutants such as oil. With industry increasing in the North, a larger number of boats and people are being drawn to these areas. Understanding ice conditions including not only where ice may be present but also the properties of that ice and the factors contributing to its formation will better prepare northern communities for future development.

Acknowledgements

Glancing upward at the steep rocky sides of a fjord with the deep, cold ice and ocean beneath, the surrounding landscape offers whispers of its dramatic past. Glaciers, kilometers deep, fed by icefields extending far up into the mountains once flooded this spot with dense powerful ice, slowly digging, scraping, and carving. These giants of erosive power have left a record of their evolution, written in bedrock and sediment on land and along the ocean's bottom. They also have left a lasting imprint on my own mind, being what brought me into this field of science, of ice. In summer of 2007, I left googly-eyed and in love with ice after exploring the Juneau Icefield, hiking along moraines, peering down at wave ogives in the Gilkey trench, following the meanders of supraglacial streams. My path through academia has twist and turned since then (much like those streams), evolving from glaciers to the microstructure of sea ice in Arctic Alaska, to coastal ice where fresh and seawater collide. So, I first want to thank glaciers for bringing me into this world of ice that continually fascinates and leaves me in awe of its beauty. There are many people (and one animal) I would like to thank as well.

Thank you to my advisors and mentors at Wheaton College (Massachusetts), The Norwegian Polar Institute, University of Colorado Boulder, and University of Alaska Fairbanks, for guiding me through the ups and downs of research and academia including John Collins, Geoffrey Collins, Jack Kohler, Tad Pfeffer, Malcolm Ingham, Erin Pettit, and Hajo Eicken.

Thank you to Camilla Brekke and Jofrid Skarðhamar for your guidance and collaboration throughout the writing of this dissertation, and for the time taken to introduce me to new scientific disciplines. The experience has broadened my world, inspiring me to expand on this research in the future.

Thank you to Chris Petrich for all you have taught me through this time, the long meetings filled with discussion, the occasional day in the field, and development of instrumentation and webpages to further the scope and reach of this work. Your enthusiasm is contagious and always appreciated.

Thank you to my colleagues Nga Dang, Øystein Kleven, Ingeborg Sandvik and the others at SINTEF Narvik in addition to the many other students and researchers I've met along the way who have offered friendship, interesting conversations, and laughs.

Thank you to Caitlin Glover, Courtney Shephard, Tara Clancy, and Meghan Behnke, your friendship means the world to me and has powered me through the most difficult of times.

Thank you to my sisters, Pam Brown and Amy Hills, brothers-in-law Jasen Brown and Rollin Hills, niece Mackenzie Brown, and nephews Leo and Ian Hills, and JJ Brown, although you're far away, I can feel your love from here. You are always close to my heart.

Thank you to Jan André, Mille, and the entire Jansen family for your love, support, the occasional adventure, and many the delicious dinner.

Thank you to my dog Sully who has traveled across the world with me, making sure every day contained fresh air. You truly are the best.

And lastly, thank you to my parents Kathy and Dave O'Sadnick for simply being my North stars.

Table of Contents

List of Figures

List of Tables

List of Abbreviations

CIRFA	Center for Integrate Remote Sensing and Forecasting for Arctic Operations
CTD	Conductivity, Temperature, Depth
GISP	Greenland Ice Sheet Precipitation
HBV	Hydrologiska Byråns Vattenbalansavdelning
HSVA	Hamburgische Schiffbau- Versuchsanstalt GmbH
IRMS	Isotope Ratio Mass Spectrometry
MODIS	Moderate Resolution Imaging Spectroradiometer
NVE	Norwegian Water Resources and Energy Directorate
SAR	Synthetic Aperture Radar
SLAP2	Standard Light Antarctic Precipitation 2
VSMOW	Vienna Standard Mean Ocean Water

Nomenclature

a_f	Sea level amplitude (tidal height)
A_f	Horizontal surface area of a fjord
B_m	Width of the fjord mouth
c_h	Heat exchange coefficient
c_i	Speed of an internal wave
c_i *(Section 3)*	Specific heat capacity of ice
f	Coriolis coefficient
F_c	Conductive heat flux
Fr_{plume}	Froude number for a river plume
Fr_{sill}	Froude number for sill
F_w	Oceanic heat flux
g	Acceleration of gravity
h	Thickness of a water layer
H	Total depth of fjord
H *(Section 3)*	Ice thickness
h *(Section 3.3)*	Vertical height variation
h_{plume}	Thickness of a river plume
k_0	Extinction coefficient of free space
k_a	Extinction coefficient due to absorption
L	Monin-Obukhov length
L *(Section 3.3)*	Latent heat of fusion for freshwater ice
N	Buoyancy frequency
$q_{B,fjord}$	Surface buoyancy flux
Q_f	River discharge
R	Baroclinic radius of deformation
Ri_E	Richardson number for an estuary
S_{si}	Sea ice bulk salinity
t	Time
T	Temperature
T_a	Air temperature
T_f	Freezing temperature
T_{ml}	Temperature of the mixed layer
T_s	Surface temperature
T_{si}	Sea ice temperature
u_{fric}	Frictional velocity
u_{plume}	Velocity of a river plume
u_{tidal}	Tidal velocity
u_w	Vertical flux of momentum from wind
W	Width of an estuary
z	Depth

$\delta^{18}O$	Stable isotope composition
δ_p	Penetration depth
ε	Electric permittivity
ε *(Section 3.4)*	Fractionation coefficient
θ	Freezing degree days
θ *(Section 3.*	Incidence angle
λ *(Section 3.3)*	Wavelength
λ_b	Thermal conductivity of brine
λ_{fw}	Thermal conductivity of freshwater
λ_i	Thermal conductivity of ice
λ_s	Thermal conductivity of snow
λ_{si}	Thermal conductivity of sea ice
λ_{sw}	Thermal conductivity of seawater
ρ	Density
φ	Latitude
ω	Wave frequency

1 Introduction

1.1 Motivation

This research was completed through the Center for Integrated Remote Sensing and Forecasting for Arctic Operations (CIRFA) with support from SINTEF Narvik (previously Norut Narvik). Through enhancing knowledge and advancing methodology of remote sensing data and techniques, CIRFA is developing new technologies to assist in safer maritime operations in the Arctic. Utilizing a variety of platforms, sensors, and surface-based measurements, the research and resultant innovation will benefit industrial operators, the scientific community, and the whole of arctic society through improving forecasts of ocean and sea ice conditions on both regional and local scales.

The work presented here was completed as part of Work Package 3: Oil Spill Remote Sensing. The inspiration came during a data campaign completed at the Hamburgische Schiffbau- Versuchsanstalt GmbH (HSVA) Arctic Environmental Test Basin in Spring 2017. Both electromagnetic (radar and tomographic SAR) and optical (thermal, hyperspectral, and fluorescent) instruments were tested to assess their effectiveness at detecting oil as it rose to the surface of two types of sea ice- one being composed of only columnar ice and the other columnar ice with a granular surface layer (Oggier et al., 2019; Petrich et al., 2018) (Fig. 1.1). The influence of ice type and microstructure has previously been examined in both laboratory and natural sea ice in studies (Brandvik et al., 2010; Dickens, 2011; NORCOR, 1975; Petrich et al., 2013). This connection to microstructure and the factors that will most dominate the rise of oil through ice was a topic of consideration during a small field campaign to a fjord in Winter 2018. The ice sample gathered was nearly fresh in its salinity, having very few pores and clearly differing from the saline ice grown during the HSVA study. This led to the question to be asked, where historically do you find ice along the coast of Norway and what are the properties of this ice? How would our results from the HSVA experiment as well as other ongoing studies on the remote sensing of ice translate to fjords and other similar subarctic coastal regions? It was then the topic of this thesis came into focus as we considered the vulnerable coastal zone and fjords of Norway whose ice, we knew very little about.

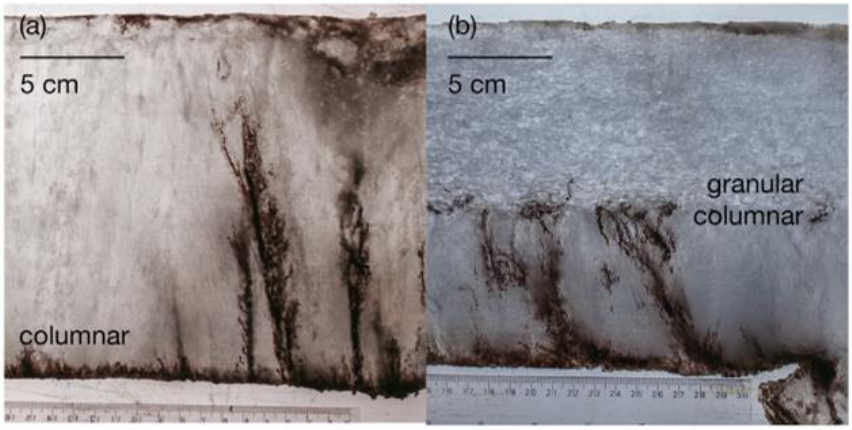

Figure 1.1: Comparison of oil migration upwards in laboratory-grown (a) columnar ice vs (b) granular/columnar ice (from Petrich et al. (2018)).

The bathymetry and geometry of a fjord or coastline combined with variable input from freshwater sources and changing oceanic and atmospheric patterns will influence when and where ice forms and the properties of that ice. Ice, in turn, will have an impact on the surrounding environment, calming surface waves, preventing sunlight from propagating into the water column, potentially disrupting transit but also providing a platform for activity. Through this work it has become increasingly clear that Norwegian fjords and possibly other similar subarctic regions, hold ice that disrupts assumptions on its interaction with oil. In addition, for similar reasons, how this ice is characterized in application to remote sensing, ice mechanics, and its interaction with local fauna must also be considered to account for these potential variations. To ensure safe maritime operations, one must have a thorough understanding of the ice conditions that may be present, from the high Arctic down to the climatic subarctic regions where more populated coastlines exist and much activity is based.

The fjords and the coastal regions of Norway have played a role throughout human history, with many early settlements dating as far back as 9,500- 8,000 BC strategically placed here for access to marine resources (Fig. 1.2). At these locations, fresh water fed by retreating glaciers met the ocean resulting in the mixing of water of varying salinity, temperature, and nutrient levels ideal for a diversity of marine fauna to flourish (Breivik, 2014). In present day, towns and cities line the coast of Norway, not only for their access to traditional industries like fishing but also natural resource developments and shipping activities. Ice can form periodically over the winter yet little systematic documentation exists to provide explanation of when, where, and the implications from both industrial and scientific standpoints. The Norwegian pilot guide offers brief descriptions of ice conditions in selected areas to assist boat and ship captains (Hughes, 2006), but direct observations of sea ice thickness, extent and properties in fjords found throughout mainland Norway are very limited in published literature.

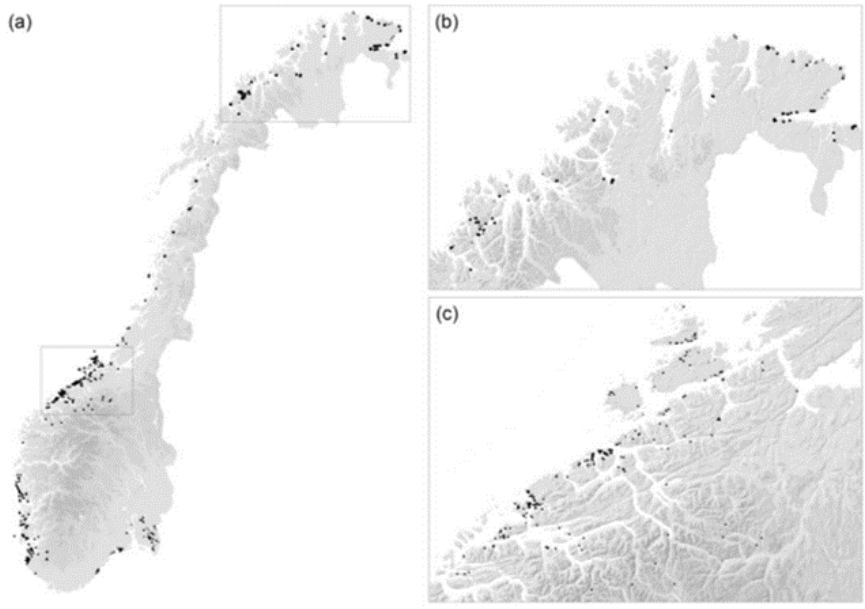

Figure 1.2: Location of early Mesolithic sites throughout Norway (a). (b) Closeup of northern-most Norway. (c) Closeup of western Norway (from Breivik (2014)).

The fjord ice studied here forms on top of a stratified water column characterized by a thin surface layer of very low salinity, an intermediary layer of similar composition to coastal water (approximately 32 psu), and a dense basin layer below sill depth (Stigebrandt, 2012). Studies of sea ice in the Baltic offer similarities particularly in how fresh water interacts with ice and the microstructure of low salinity ice. Baltic seawater is brackish in character throughout, however, differing in the stratified structure of a Norwegian fjord that has a strong influence on ice formation (Granskog et al., 2005; Granskog et al., 2005b; Granskog et al., 2006). Research focused on Arctic estuaries, also provides a basis of work to increase understanding of the interaction between river and sea (Eicken et al., 2005; Macdonald et al., 1999; Macdonald et al., 1995). Application to fjord ice is limited though, as estuaries differ from fjords in their depth, extent, and dynamics.

While there is a wide breadth of work focused on mainland Norwegian fjords (e.g. Asplin, Salvanes, & Kristoffersen, 1999; Cottier et al., 2010; Eilertsen & Skarðhamar, 2006; Jones et al., 2020; Mankettikkara, 2013; Skarðhamar et al., 2018), ice is only mentioned in passing if at all. The role of sea ice in fjords on Svalbard is well studied (for example Cottier et al., 2010; Gerland & Renner, 2007; Hop & Wiencke, 2019; Nilsen et al., 2008; Skogseth et al., 2020) but often cannot be applied to the fjords of mainland Norway where marine-terminating glaciers are absent and both air and ocean temperatures are higher. Thus, this thesis aims to provide the first comprehensive look at Norwegian subarctic fjord and coastal ice to address an intriguing gap in scientific knowledge.

The main contributions of the work presented are:

- Identification of the fjords and coastal areas of Norway where ice has formed in recent history (Paper I)
- Measurement of natural fjord ice from different locations over a three-year timespan to investigate variations in ice thickness, ice type, and ice bulk properties in relationship to fjord geometry, weather patterns, and oceanic conditions (Paper II)
- Determination of water composition at the ice-ocean interface during ice growth and the rate of ice growth using measurements of ice bulk salinity and oxygen isotope composition (Paper III)

1.2 Thesis Outline

There are three separate systems, all independently complexed, colliding when examining the topic of ice formation, properties, and trends in subarctic fjords and coastal environments: ocean, atmosphere, and ice.

In Chapter 2, we begin with an introduction to fjord oceanography, with primary focus placed on the surface layer from which ice forms. An overview of the exchange processes occurring in a fjord's deeper layers is next examined to understand their connection to larger coastal processes. Lastly, a comparison to ice formation in Arctic fjords is provided to reveal one extreme of the potential impact of ice on a fjord system and why subarctic fjord ice is distinctly different from sea ice formed elsewhere.

In Chapter 3, an introduction to ice physics, is provided. The microscale processes that lead to formation, the different types of ice types found in fjords and the ice properties of greatest relevance to the published work are each highlighted. An explanation of the thermal, electrical, and optical properties of ice as well as the evolution of ice bulk salinity and oxygen isotope composition is additionally presented.

In Chapter 4, an overview of the field work completed is offered including a summary of where, when, and what measurements were obtained.

In Chapters 5 – 8, after now having a picture of the fjord environment painted, the three journal papers composed as part of this dissertation are first summarized then presented in full:

Paper I: M. O'Sadnick, C. Petrich, C. Brekke, & J. Skarðhamar **"Ice extent in sub-arctic fjords and coastal areas from 2001 to 2019 analyzed from MODIS imagery"**, Annals of Glaciology, vol. 62, no. 82, pp. 210- 226, 2020.

Paper II: M. O'Sadnick, C. Petrich, C. Brekke, J. Skarðhamar, & Ø. Kleven **"Ice Conditions in northern Norwegian fjords: Observations and measurements from three winter seasons: 2017-2020",** Cold Regions Science and Technology, 2022, accepted with minor revisions, in review.

Paper III: M. O'Sadnick, C. Petrich, & J. Skarðhamar **"The use of ice bulk salinity and $\delta^{18}O$ to investigate changes in the fjord environment over a winter season"**, The Cryosphere, 2022, submitted.

In Chapter 9, this work concludes with a summary of the most significant research findings and potential topics for future research.

2 The Oceanography of Fjords

The water column of a fjord can typically be divided into two, at times three layers, based on gradients in temperature, salinity, and density (Fig. 2.1). The bottom-most layer, from here referred to as basin water, is formed below sill level where exchange with coastal water is limited. Above sill depth, two dominant layers can form- a surface layer being influenced by the inflow of freshwater and thus often fresh or brackish, and the middle, intermediary layer below the influence of surface processes and above sill depth (Farmer & Freeland, 1983; Inall & Gillibrand, 2010). This stratification is a key component of the fjord system and influences circulation and the overall mixing processes throughout the fjord. In turn, the fjord ecosystem, geology, and other physical processes including ice formation are impacted. Here, a summary of processes most pertinent to ice formation is provided including those that may pre-condition a fjord for ice or hinder its formation.

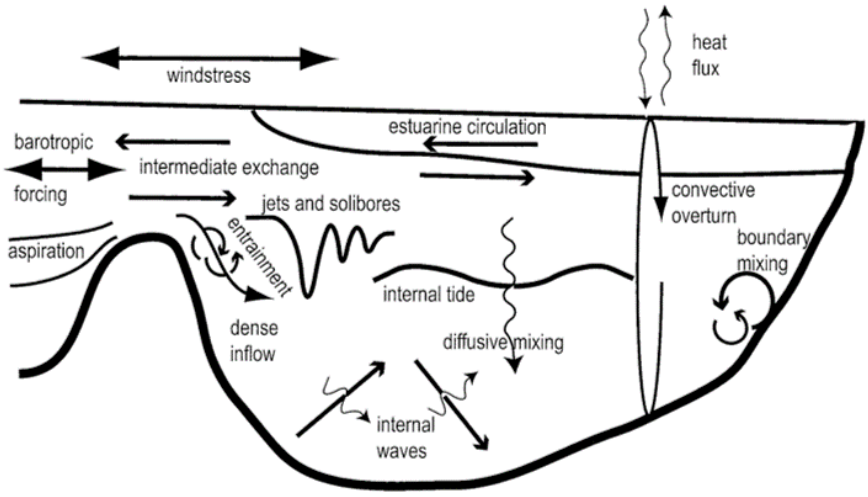

Figure 2.1: Schematic of layering and physical process found in a sill fjord (from Inall & Gillibrand (2010)).

2.1 The Surface Layer: Freshwater flux into a fjord and density gradient

The Norwegian Coastal Current carrying Norwegian Coastal Water that originates in the Baltic Ocean flows northward along the Norwegian coast. Along the way, it can interact with Atlantic Water in the Norwegian Atlantic Current. These currents and their interactions with water masses in the south and west will influence ocean temperature along the Norwegian coastline and subsequently, the temperature of seawater in fjords (Eilertsen & Skardhamar, 2006). It is due to this current that coastal Norway remains largely ice free in comparison to coastlines at similar latitudes, for example, Greenland. Within the inner parts of fjords, however, freshwater runoff will act to lower both the temperature and salinity of a fjord's surface layer enabling the possible formation of ice. The details of this process are discussed in greater depth throughout the following chapters.

The properties of the surface layer including thickness, temperature, and salinity, are determined primarily by the flux of freshwater into the fjord, size of the fjord, and amount of mixing. The first,

freshwater flux, is dependent on the size of the catchment area and amount of rain and snowmelt it receives, with rainfall directly on the fjord surface often negligible in comparison (Inall & Gillibrand, 2010). Along the Norwegian coast, warm and wet summers are contrasted by cold and relatively dry winters. Freshwater flux will therefore increase in the spring as the snowpack begins to melt and precipitation comes more frequently in the form of rain rather than snow. The peak in freshwater flux that results can last into August however periods of rain, such as those that can come in the Fall between September through November, may lead to subsequent but less pronounced peaks (Wassmann et al., 1996). Once winter arrives and temperatures below 0 °C dominate, the flux of freshwater will slow substantially as rivers and lakes freeze and snow replaces rain. In sub-arctic regions such as Norway, freshwater can continue to flow into fjords throughout winter due to periods of above freezing temperatures and rainfall. Such trends are becoming more common in recent years with average annual temperature, precipitation, and runoff in winter increasing over mainland Norway since 1900. For example, in a comparison of winter seasonal runoff from 1971 – 2000 versus 1985 – 2014 Norway, as a whole, experienced approximately 6 % increase in runoff during specifically winter with the northern-most region of Troms and Finnmark recording over an 18 % increase (Hanssen - Bauer et al., 2017).

Additionally, hydroelectric facilities are often located along the rivers that lead into fjords. Freshwater runoff into the fjord can resultantly be impacted by, first, changing the outflow from surrounding watersheds to lead to the reservoir and eventually the fjord. Second, with higher electricity demands in wintertime, reservoirs will often be opened increasing flow during a period of year when this does not occur naturally. The ecology and biogeochemical cycles in the fjord will resultantly be impacted as well as the properties of the surface layer including the greater potential for ice cover in fjords (Green et al., 2004). Winter-time freshwater flux can have a large influence on ice conditions in a fjord, leading at times to rapid formation and subsequent thickening depending on factors including wind and tidal mixing.

2.1.1 Freshwater plume dynamics

The surface layer is largely controlled by the river plumes that feed into a fjord. The fjords of focus here hold rivers substantially smaller than those elsewhere in the Arctic from which many studies of plume dynamics originate (e.g. the Mackenzie River in Canada and Lena River in Russia). The theory behind the spread and evolution of a river plume remains relevant, however, as similar processes may still occur albeit on a different scale. It is useful to consider these processes and how they relate to when and where ice may form and, additionally, to increase understanding of the variations observed across fjords and years. Further research into the spread of river plumes in narrow fjords fed by smaller rivers, their evolution through changing seasons, and interaction with an ice cover is recommended, however.

2.1.1.1 The spread of a river plume

The origin of the surface layer in a fjord is connected to the evolution of river plumes with fjord geometry and bathymetry near the river outlet, freshwater flux, influence of wind, geostrophic controls, tides and current all having an influence on depth and areal extent. The Froude number (Fr_{pl}) of a plume is generally defined as the ratio between inertial and gravitational forces:

$$Fr_{pl} = \frac{u_{pl}}{g' h_{pl}} \tag{2.1}$$

Where, in application to a river plume, u_{pl} is the velocity of upper layer, g' is the $g(\Delta\rho/\rho)$, and h_{pl} is the the thickness of the upper layer. Mixing of the river plume depends on whether conditions are subcritical ($Fr_{pl} < 1$) in comparison to supercritical ($Fr_{pl} > 1$). The presence of ice will additionally play an important role in the fate of the plume. Horner-Devine et al. (2015) define four dynamical regions of a freshwater plume, as depicted in Fig. 2.2:

1) The source region- located within or at the river mouth where the buoyancy and momentum of the freshwater flux from the river originates ($Fr_{pl} < 1$)
2) The near-field region- also referred to as the tidal plume in areas with large tides, it begins where the river plume lifts off and loses contact with the seabed. After this point, the buoyancy of the plume is exceeded by the river's momentum, leading to substantial mixing through sheer instabilities and turbulence ($Fr_{pl} > 1$)
3) The mid-field region- the river jet that characterizes the near-field region begins to lose its dominance with either geostrophic or wind-driven estuarine circulation forces increasing in their influence over the flow of the plume (see Sections 2.1.2.3 & 2.1.2.4).
4) The far-field region- all momentum provided by the initial river plume has dissipated with geostrophic and/or estuarine circulation, stress at the ocean/air interface at the ocean's bed, and buoyancy determining the fate of the plume. Despite mixing, a significant gradient may still exist between the plume and underlying seawater

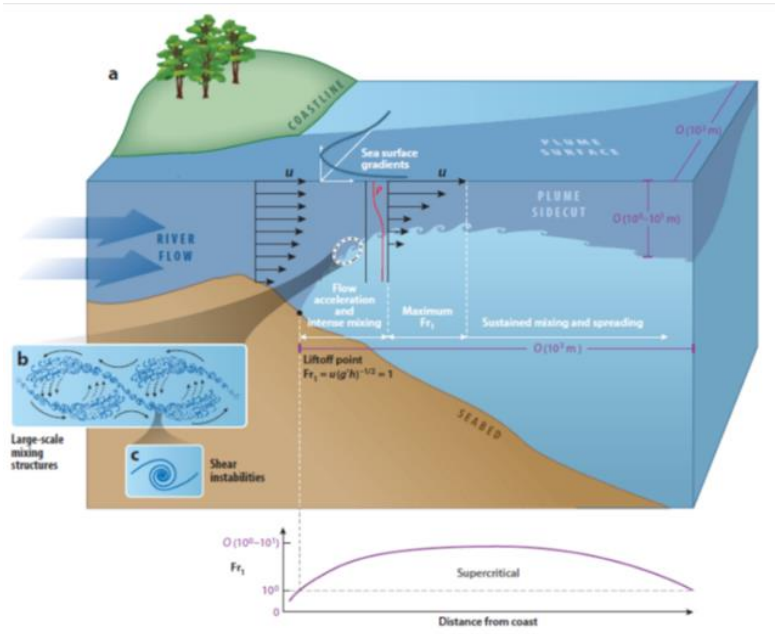

Figure 2.2: (a) Schematic of plume spreading in the source and near-field regions. (b) large scale mixing structures in the near-field region comprised of (c) shear instabilities (from (Horner-Devine et al., 2015))

In a fjord, the movement of a plume is bounded on all but one side with tide playing a key role in the extent of the plume. During periods of flood, the water column will have a higher salinity, with the plume not extending far from the source region. When the tide ebbs, the water column will become

more stratified with greater turbulence and sheer at the interface of the plume and the seawater (Nash et al., 2009). A Richardson number, which provides a description of turbulence, specific to rivers can be defined to provide an approximation of the ratio between turbulent and advective flux given certain river and tidal conditions (Fisher, 1972; Nash et al.,2009; Horner-Divine et al., 2015):

$$Ri_E = g' \left(\frac{Q_f}{W u_{tidal}^3} \right) \quad (2.2)$$

Where Q_f is the river discharge, w is the width of the estuary, and u_{tidal} is the tidal velocity. When $Ri_E <$ ¼, sheer velocity from tidal forces can overcome the stratification that is the result of Q_f, thus creating more turbulence and resultantly mixing.

2.1.1.2 The influence of ice on a river plume

Once an ice cover is present, the movement and evolution of the river plume will change due to the now negligible influence of wind. This will allow the plume to extend further, undisrupted by the mixing that normally occurs at the surface but still hindered slightly by friction at the ice-ocean interface. As a result, stratification of the water column will differ with studies showing freshwater plumes that extend further and are of greater thickness in comparison to when no ice is present. Tidal forces will persist however, limiting plume extent despite potentially a comparatively high freshwater flux. For example, the Great Whale River in Hudson Bay has a discharge upwards 20 times greater than that of the River Siikajoki in Bothnia Bay, yet the extent of the two plumes is approximately the same during the winter. This is due to the tidal forces being considerably greater at the Great Whale River and counteracting the movement of the river plume outward in comparison to River Siikajoki. Once sea ice melts and wind-mixing can take place at the surface, plume extent is drastically altered in Bothnia Bay and River Siikajoki being over 10 times less in summer time versus 4 times less at the Great Whale River (Granskog et al., 2005; Ingram & Larouche, 1987).

The ebb and flow of the tide will also influence the shape and extent of a freshwater plume (Fig. 2.3). During periods of flow, plume extent will be limited as river velocity is counter-acted by tidal forces. Once the tide ebbs, the plume will deepen and extend further outward. The depth can vary depending on the height of the tide and friction experienced at the ice-ocean interface, not always decreasing as distance from the river outlets increase. This is the case during periods of particularly low tide when ice surface can become depressed leading to more turbulence and unstable flow at the ice-ocean interface (supercritical, Fr > 1). As a result, the river plume can deepen after leaving the river mouth where ice plume thickness normally derives (Li & Ingram, 2007).

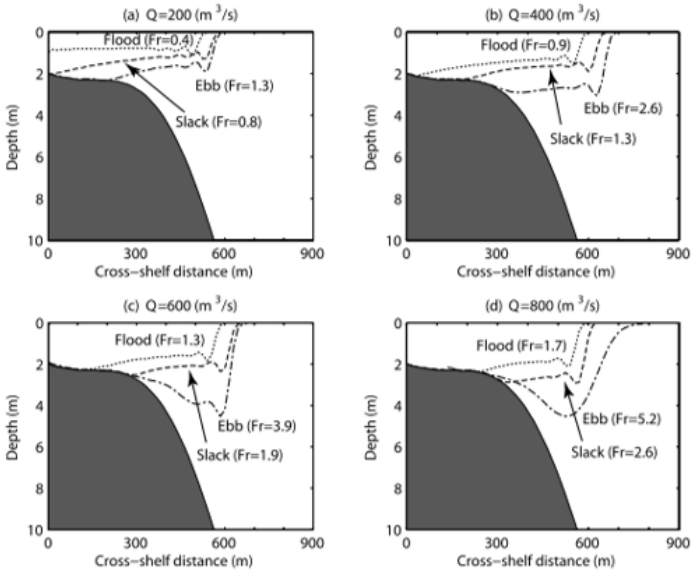

Figure 2.3: Comparison of modeled river plume extent and depth under-ice for ebb and flood cycles (including Fr number) for different river fluxes with friction included, (a) 200 m^3/s, (b) 400 m^3/s, (c) 600 m^3/s, (d) 800 m^3/s (Li & Ingram, 2007)

The extent and depth of a freshwater plume is relevant to consider through the winter as it will determine the water properties at the ice-ocean interface and therefore ice bulk salinity, isotopic signature, and brine volume fraction. In the Baltic, layers of freshwater ice can form under brackish ice having microstructure similar to that of higher salinity ice with interconnected brine pores and channels. Microbiota and algae will inhabit this space meaning that layers of freshwater ice, having lower porosity, will impact their extent. Additionally, this variation in microstructure will influence ice permeability, with lower porosity fresh water ice potentially limiting the exchange between the ocean and high salinity ice (Granskog et al., 2005). In relationship to subsequent growth of sea ice, a plume of fresh water can act to stabilize the water column and limit the turbulent exchange of oceanic heat flux. As a result, such plumes may lead to an increase in growth rate and/or limit bottom melt (Granskog et al., 2005; Omstedt, 1998; Shirasawa & Ingram, 1991). The latter is particularly important to consider in a sub-arctic fjord environment where ocean temperature and heat flux can play a considerable role in the formation and break up/melt of ice.

2.1.2 Evolution of the surface layer

The formation of ice from the surface layer enables quicker subsequent ice formation by: 1) calming surface turbulence that would otherwise prevent ice formation enabling the growth of congelation ice downwards and 2) provides a platform for snow to accumulate leading to the formation of granular, snow ice. Both processes, separate and combined, will lead to the thickening of this ice, making it more resilient to wind, waves, and other currents within the fjord that otherwise would obstruct ice formation or lead to breakup of thinner ice layers. Thus, the formation of the surface layer through the spreading of a plume and the resilience of that plume to resist mixing is of great importance when studying ice formation in sub-arctic fjords. How a surface layer of fresh or brackish water originating from a river plume evolves as it moves outward into the fjord will depend on several factors including the density gradient separating this top layer from the ambient ocean water beneath and the strength of

wind, tidal, and Coriolis forces. Each can influence the extent of mixing of the surface and at times, deeper layers, which can subsequently impact if and where ice formation occurs.

2.1.2.1 Degree of stratification

The fate of a surface layer including the rate it may be mixed downward is related to the degree of stratification in the upper water column characterized by a buoyancy frequency (*N* in 1/s):

$$N^2 = \left(-\frac{g}{\rho_0}\frac{d\rho}{dz}\right) \tag{2.3}$$

Where g is acceleration of gravity, ρ_o is a reference density taken below the surface layer, and $d\rho/dz$ is the change in density over depth (z). A higher frequency represents a more stratified water column, the result of a sharper gradient in density between layers. When a parcel of water is displaced to a layer differing in buoyancy, it will rebound to return to its starting position resulting in turbulence at this boundary. The greater the buoyancy of the surface layer, or in other terms the greater the stratification, the more resilient the surface layer will be to mixing.

2.1.2.2 Convective mixing

Mixing of the surface layer downward can occur without currents or wind. As the surface decreases in temperature, the density of water will increase, sinking downward until it reaches a depth of equal density, thereby setting up convection in this layer and altering the temperature and salinity of the surface layer. The evolution of these properties is dependent on the surface buoyancy flux ($q_{B,fjord}$ in J/(ms)] . For a fjord where a homogeneous layer of fresh water is present, this property can be described (Farmer & Freeland, 1983):

$$q_{B,fjord} = g(\rho - \rho_0)Q_f \tag{2.4}$$

This differs from definitions of surface buoyancy flux in application to the larger ocean where freshwater runoff from land plays little, if any, role. Buoyancy flux is instead defined as function of surface heat exchange and freshwater flux dependent on evaporation and precipitation (Cronin & Sprintall, 2001). For fjords, freshwater flux is dependent on runoff from land with precipitation and evaporation at the fjord surface contributing very little (Inall & Gillibrand, 2010).

The rate of deepening due to convection in the surface layer is defined:

$$\frac{dh}{dt} = \frac{1}{2}\frac{\sqrt{rq_{B,fjord}}}{N\sqrt{t}} \tag{2.5}$$

Where r is a constant describing dissipation of energy ranging between 2 to 6 and t is time in seconds. An increase in freshwater flux or a decrease in stratification will both act to change the depth of this layer at a faster rate over time while a lesser flux or greater stratification leading to comparatively less mixing downward. The latter is what may occur on a calm, winter day a Norwegian fjord when freshwater flux is substantially less than in the summer. If the surface layer is stratified, being fresh or very low salinity, even with cooling it will not sink downwards into the saline water below. Thus, cooling to freezing temperatures will occur quickly in this potentially thin upper layer.

As discussed in Section 2.1.1.2, with the formation of ice, mixing by wind of the surface will end thus placing more focus on the influence of tidal currents. Before ice is present however, it is useful to understand the amount of wind needed to mix a surface layer which may resultantly influence if ice forms as well as the type of ice (See Section 3.1.3). Wind across the surface of the fjord will lead to mixing downward to a depth proportional to the Monin-Obukhov length (L) (Farmer & Freeland, 1983):

$$L = -\frac{u_w^3}{kq_{B,fjord}} \tag{2.6}$$

Here u_w is the vertical flux of momentum from wind and hence, negative in the downward direction and k is a constant. As Eq. 2.6 clarifies, an increase in wind will lead to a deepening of the mixed layer. A thinner layer with less of a buoyancy flux will also be less able to balance the momentum from the wind also leading to deepening. Alternatively, a more stratified water column having a higher buoyancy flux will act to counteract the wind, limiting the thickening of the wind-effected layer.

2.1.2.3 Estuarine circulation

The depth of the wind-effected layer is an important characteristic to consider in relation to circulation throughout the entirety of the fjord (Fig. 2.1). Estuarine circulation is characterized by a surface layer being forced by both wind and current from the river out of fjord. To replace this water, deeper, more saline, water is brought into the fjord beneath the surface layer leading to a conveyor belt-like pattern, called estuarine circulation, along the fjord's length. As this occurs, saltier water will be mixed upwards weaking the density gradient between the surface and intermediary layers.

Estuarine circulation is strongest nearest to river outlets where runoff for a unit area and current from the river is at its the greatest. Moving down fjord, current in the upper surface layer will weaken and mixing between fresh and saline water will increase leading to the water column to become less stratified (Myksvoll et al., 2014). The thicker the upper layer, the lower its velocity as it moves out of the fjord (Stigebrandt, 2012). The ratio between the freshwater flux leading into a fjord and the saltier water brought in is often used to categorize estuaries. The greater the amount of freshwater in comparison to the seawater from outside the fjord, the less mixing is occurring between layers which indicates less estuarine circulation (Inall & Gillibrand, 2010).

Estuarine circulation will lessen considerably, if not stopping entirely, in wintertime due to the decrease in runoff from land. If ice formation does occur, estuarine circulation will be disabled entirely in areas of the fjord that are ice covered. Resultantly, stratification in the fjord under the ice cover will persist even during periods of increased runoff and wind. Thus, by overlooking ice formation in fjords, one risks overestimation of processes like estuarine circulation and its impact on the fjord environment in winter but particularly into spring when widespread melting of snow begins.

2.1.2.4 Geostrophic circulation

The width of a fjord and thickness of the surface layer will determine how strongly circulation within a fjord is influenced by the Coriolis force. The baroclinic radius of deformation (R) is defined as:

$$R = \frac{\sqrt{\frac{g' H_1 H_2}{H}}}{f} \tag{2.7}$$

$$g' = \frac{g(\rho_2 - \rho_1)}{\rho_2} \tag{2.9}$$

$$f = 2\Omega sin\varphi \tag{2.10}$$

Where H is the total depth of the fjord with subscripts 1 and 2, denoting the thickness (H) and density (ρ) of the surface layer and layer beneath respectively, f is the Coriolis coefficient, Ω = 7.2921 x 10^{-5} rad/s, and ϕ is latitude. When the diameter of the fjord is greater than R, it will experience rotation due to the Coriolis force. The thinner the surface layer, the greater the difference in density between the two layers, and the higher the latitude, the smaller R. Given the dependence on stratification and thickness of the surface layer, the radius of deformation will change throughout the year.

Fjords that experience geostrophic circulation consistently over a period can develop circulation patterns not only in the surface layer but through their depths (Fig. 2.4). For example, as wind blows up or down fjord consistently, the surface will be deflected to the right as the result of the Coriolis force and Ekman transport. This will cause the thickness of the surface layer to vary across fjord as well as downwelling to occur along one shoreline while upwelling occurs along the other. Such circulation is often evident in temperature and salinity gradients across the fjord, both of which can influence ice formation (Cottier et al., 2010; Cushman-Roisin et al., 1994; Skardhamar & Svendsen, 2010).

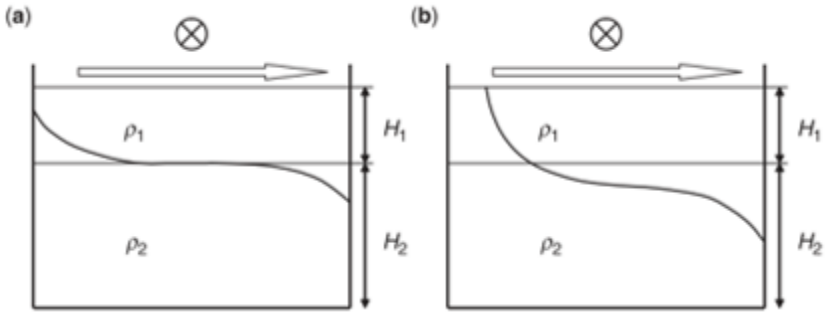

Figure 2.4: Schematic of the two-layer density structure of a fjord before and after continuous down-fjord wind (marked as an X). Due to geostrophic forces and Ekman transport (width of fjord > baroclinic radius of deformation), upwelling and downwelling will occur on the left and right sides of the fjord respectively (from (Cottier et al., 2010)).

An influence by geostrophic circulation was suspected at several of the fjords examined but not investigated in-depth. In Beisfjord for example, ice formation often originates along the northern coastline, to the right when looking down fjord. Deflection of fresh water from the river towards this coastline as well as upwelling/downwelling offers a potential explanation. Measurement of surface salinity during periods of high wind and river runoff would further help to investigate this possibility.

2.2 The Intermediary and Deep Layers

The formation of ice in a fjord is tightly connected to the surface layer. Throughout the depth of the fjord however, currents controlled by differences in sea surface height (barotropic) and density gradients (baroclinic) between coastal and fjord waters will drive mixing and exchange with coastal waters. While processes in deeper layers may have a less defined impact on ice formation and properties, a summary is provided to aid understanding of the fjord environment as a whole and the complex intermingling of factors that may contribute to variability in ice conditions.

2.2.1 Baroclinic Flow

Beneath the water mixed by estuarine circulation and above the sill depth is where an intermediary layer can form. Coastal waters will often differ in density in comparison to seawater at a similar depth within the fjord. As a result, a baroclinic current will form to bring the two to equilibrium. This process, intermediate exchange, will evolve throughout the year as both coastal currents and water within the fjord vary in their density and stratification (Inall & Gillibrand, 2010). Annual stratification cycles in coastal waters lead to exchange to occur over longer, more predictable time periods. Daily and weekly changes to conditions however, such as wind events that lead to coastal upwelling and downwelling or larger inputs of freshwater along the coast, can drive baroclinic movement over shorter time scales. Intermediary circulation depends on three main factors: the depth and width at the fjord mouth, the surface area within the fjord, and the variance in the density gradient directly outside the fjord mouth (Aure et al., 1996). Circulation in the intermediate layer can be significantly greater than that attributed to surface layer (through e.g. estuarine circulation). For this reason, it is important to consider in studies of water quality including nutrients in the water column and pollution that may come from aquaculture, sewage, and other industries present along the fjord (Arneborg, 2004; Aure et al., 1996).

Baroclinic exchange is not limited to the intermediate layer and can impact basin water as well. Coastal water moving into a fjord may be denser than the intermediary layer resulting in its sinking into basin water once it crosses the fjord entrance. An increase in tidal velocity as coastal water passes over a sill, a barotropic flow, can additionally bring water outside the fjord deeper than sill depth into the fjord. If little mixing occurs as this water moves over the sill, it may sink into the basin water potentially to the fjord bottom in what is considered a deepwater renewal event. Such occurrences are important for the health of the fjord environment, displacing stagnant, potentially de-oxygenated, water with nutrient rich coastal water (Darelius, 2020). Full renewal events will occur as fjord waters slowly freshen through convective and turbulent mixing at the surface combined with stronger than normal tides (eg. Equinoxal spring tide) that can pull deeper water from the coast into the fjord (Inall & Gillibrand, 2010). The former factor is relevant to consider in reference to the impact of ice formation on a fjord environment. With ice present, mixing of fresh water downward due to wind and surface currents will not occur. As a result, a full renewal of basin water may be delayed. Renewal events in ice covered fjords environments are researched in Arctic environments (discussed further below). There is an apparent absence of research, however, around the influence of ice on deep water renewal in sub-arctic fjord environments with focus placed instead on only ice-free conditions.

2.2.2 Barotropic Flow

Barotropic flow derives from differences in sea surface height that create a pressure gradient force on the water column. This force is constant with depth however the barotropic flow that results will not be given friction at the bed and its interaction with other coastal features. Tide is the primary driver of barotropic flow with storm surges caused by low pressure, wind, and/or heavy rainfall leading to particularly strong, energetic events (Inall & Gillibrand, 2010).

The barotropic tidal speed entering a fjord is tightly connected to the geometry of a fjord and can be defined as:

$$u = \alpha \cos(\omega t) \tag{2.11}$$

$$\alpha = \omega a_f \frac{A_f}{B_m(H_t - H_B)} \tag{2.12}$$

Where ω is the wave frequency, a_f is the sea level amplitude (tidal height), A_f is the horizontal surface area of the fjord, B_m is the width of the mouth, H_t is the depth of the sill, and H_B is the depth below the sill. Internal waves in a stratified water column are the result of a barotropic tide interacting with bottom topography, specifically a sill. As they enter into a fjord they will travel along the boundary of the intermediary and deep water, at times breaking in places where a slope in the bed is present (Stigebrandt, 1976). This results in vertical mixing and diffusion which will in the decrease in density of deep water discussed in Section 2.2.1. The speed of an internal wave (c_i) in a stratified fjord is calculated as:

$$c_i = \sqrt{g \frac{\Delta\rho}{\rho_0} \frac{H_t H_B}{H_t + H_B}} \tag{2.13}$$

To determine if an internal wave is generated at a fjord entrance, the densimetric Froude number (Fr_{sill}) must follow $Fr_{sill} < 1$ (subcritical) where:

$$Fr_{sill} = \frac{\alpha}{c_i} \tag{2.14}$$

When $Fr_{sill} > 1$, a tidal jet will instead be created (Stigebrandt, 2012). An acceleration in tidal velocity will occur as a water passes over a sill due to the decrease in cross-sectional area thus creating a jet on the lee-side of the sill (Fig.2.1). The narrower the constriction in comparison to the size of the fjord, the greater this acceleration as well as value for α, resulting in a larger value for Fr. A decrease in stratification will also lead to smaller values for c_i, further increasing Fr. Therefore, in cases where Fr is considerably larger than 1, the lesser the likelihood of internal waves whereas if Fr is close to 1, both internal waves and a jet may be created depending on timing within the tidal cycle (Stigebrandt, 1980).

In a jet – type fjord ($Fr_{sill} > 1$), velocity will increase over a sill then decrease quickly as the jet separates from the sill and ocean bed, moving into the deeper and wider fjord. As this occurs, the width of the jet will stay fairly constant, being comparable to the width of the sill. This is an indication of the high dissipation of turbulent kinetic energy, and resultantly mixing, within the jet. Larger

amplitude waves can be created between the jet and underlying water on the lee-side of the sill as well but these have been observed to quickly dissipate (Inall et al., 2004). Such jets may have potential to influence the formation and extent of ice in a fjord environment. The increase in tidal velocity and resultantly turbulent kinetic energy, for example, may disturb surface layers near to the sill which would resultantly increase temperature and salinity of the surface due to mixing with the intermediary layer. In addition, if ice is present, the increase in tidal velocity at the ice – ocean interface will increase oceanic heat flux at this boundary leading to bottom melt (See Section 3.2.1). Neither of these hypotheses were tested as part of this work, however, a relationship between ice extent and bathymetric and coastal features was suspected after observing consistency in the placement of ice edge during certain periods of the year. The impact of some features (e.g. sharp bends in the coastline at Ramfjord and Kattfjord) is easy to surmise given the protection it may offer but others were not. The connection between tidal processes, fjord geometry, and ice formation in a fjord environment is therefore, one more of many, potential pathways for future research.

2.2.3 Atmosphere-ice-ocean interaction in the Arctic

In Arctic fjords, a substantial cover of sea ice can be present from early winter well into spring. The ice that forms is typically of higher bulk salinity than any ice gathered as part of this study- ranging on average between 5 – 8 psu. This is the result of ice in Arctic regions forming from seawater of higher salinity than in sub-arctic fjords where a fresh or brackish surface layer plays an important role in ice formation. Whether ice forms from saline or fresh water plays an important role in the stratification of a fjord's water column and coast- fjord exchange. As ice forms from ocean water, salt is rejected from the ice matrix and expelled at the ice-ocean interface (Fig. 2.5). The brine will be denser than the surrounding seawater due to its high salinity and low temperature (see Section 3.1.3.3) and resultantly sink down the fjord bottom, mixing and displacing deep water present below the sill. In the spring, sea ice melts and more fresh water enters into the fjord from the surrounding land leading to a layer of lower density water to form on the surface. Diffusion and mixing occurs over time leading to a stratified water column to form similar to what has previously been explained with a surface, intermediary, and deep water layer. In the Fall, heat loss from the surface will lead to convection throughout the surface and intermediary layers which will eventually lead to ice formation. Once ice is present, the replacement of deep water will begin again (Cottier et al., 2010).

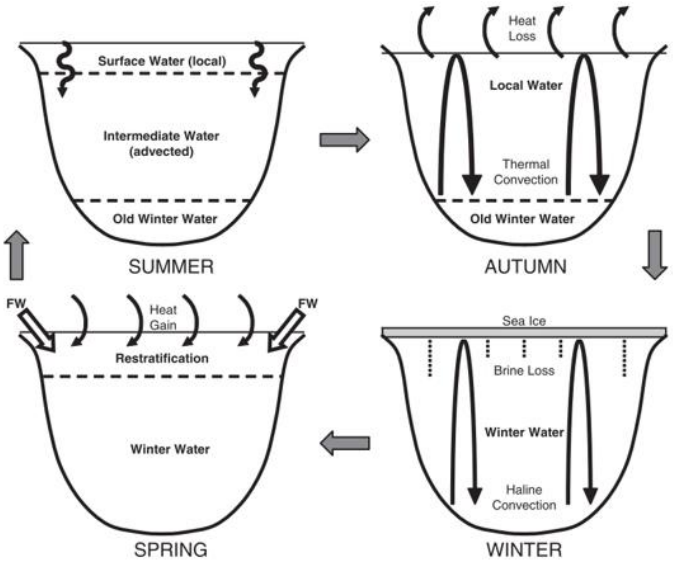

Figure 2.5: The annual evolution of the water column in an Arctic fjord with sea ice present during winter (from (Cottier et al., 2010))

The amount of ice formation in an Arctic fjord will play an important role in exchange with coastal waters. For example, in Svalbard, warm and saline Atlantic water was able to flow into Isfjorden during August and September of 2002. Subsequently, a new population of blue mussels was reported in 2004 at the mouth of Isfjorden that was found to have settled in 2002. Species of both Atlantic cod and salmon, anomalous to the region, were also reported during this time. Nilsen et al. (2008) found the amount of dense, deep water was controlled by the amount of ice production during a given winter. During seasons with high ice production, more deep water was created leading to higher density gradients between shelf and fjord waters. This influenced where and when shelf water was able to penetrate into the fjord and thus impact other parts of fjord system, namely biological activity.

In a sub-arctic fjord environment, the expulsion of brine will be less given the lower salinity of the surface layer. A broad variation in bulk salinity and isotopic signature (linked to the freshwater influence) was found between fjords and years however, meaning that there is potential for such processes to occur, albeit most likely on a smaller scale, in these regions. The influence of ice on circulation and exchange in an Arctic fjord nonetheless offers an important example of the impact of ice formation on a fjord system and its broader implications that should be considered when examining ice in a sub-arctic region.

3 The Physics of Ice

3.1 Ice Formation

3.1.1 Initial cooling

In fresh water, heat loss at the surface leads to convection in the water column down to a temperature of approximately 4 °C, the temperature of maximum density for water of zero salinity. Once this temperature is reached, convection will cease with further cooling only acting to stabilize the upper water column. Ice formation will begin once the surface reaches freezing temperature, 0 °C (Granskog et al., 2006; Weeks & Ackley, 1986). Up until a salinity of approximately 24.7 psu, the temperature of maximum density will be greater than the freezing point of the water with freezing point decreasing as a function of salinity (Fig. 3.1). In water of greater than 24.7 psu, convection will continuously occur until the freezing point of the water is reached, approximately -1.8 °C for seawater with a salinity of 32 psu. Once this point is reached, crystals begin to form in the water column, eventually coalescing until their buoyancy lifts them to the surface leading to a layer of ice to form.

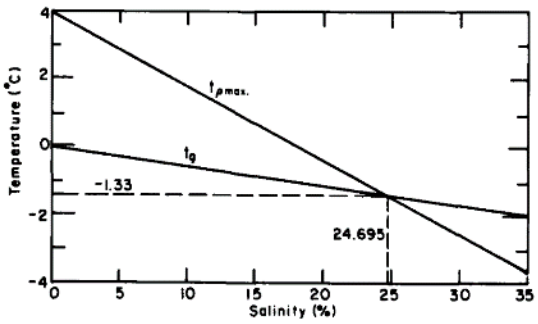

Figure 3.1: Temperature of the maximum density ($t_{p,max}$) and freezing point of seawater (t_g) for different salinities (from Weeks & Ackley (1986)).

3.1.2 The ice crystal lattice

Whether formed from freshwater or seawater, the pure crystal lattice structure of ice, specifically ice Ih, will not differ. This type of ice is the most common found on earth with 'I' representing pressure and 'h', its hexagonal symmetry. The latter characteristic comes from water molecules connected in a tetrahedral pattern where each oxygen atom is connected to four other oxygen atoms through hydrogen bonds (Fig. 3.2). Oxygen atoms lay largely on planes parallel to each other, termed basal planes. Perpendicular to the basal plane, is the axis of maximum rotational symmetry, referred to as the c - axis. The anisotropic crystal structure of ice will largely influence its mechanical, electrical, and thermal characteristics making understanding of its origin relevant. For example, ice will generally fracture along the basal plane due to only two bonds in comparison to four along the c-axis, being present. In addition, growth rate along the basal plane is faster than that along the c-axis (Hillig, 1958; Hobbs, 1974; Weeks & Ackley, 1986) leading to geometric selection and a consistent crystal arrangement. Further references to ice crystal structure, anisotropy, and its implications will be detailed further in subsequent sections

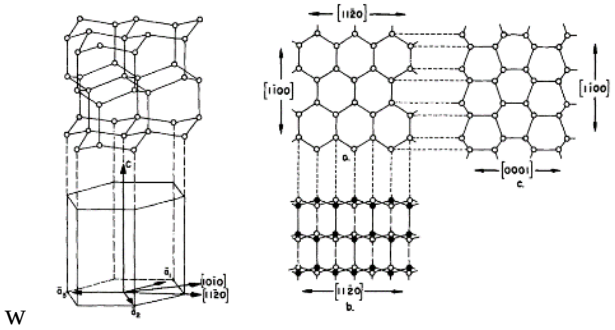

Figure 3.2: Crystal structure of ice (from Weeks & Ackley (1986))

3.1.3 Modes of ice formation and resultant texture

3.1.3.1 Ice nucleation and frazil granular ice formation

With cooling of the upper water column to freezing temperature, ice nucleation will begin as water molecules cluster around impurities like NaCl or biological material. This initial growth of ice may also occur through ice seeding where an external ice crystal (e.g. snowflakes) acts as a nucleation site. In this phase of ice growth, crystals will begin as tiny spheres that quickly grow along the basal plane to form discs (Weeks & Ackley, 1986). As discs continue to grow, to a diameter of approximately 2 – 3 mm, they will diffuse both heat and salt. With an increasing diameter and thus smaller surface area to volume ratio, this process will eventually become unstable leading to the formation of dendrites. Once this occurs, growth rate of crystals will quickly increase as heat and salt are quickly diffused at the crystal- water interface forming platelets, needles, and spicules (Jones & Wells, 2018).

When the water surface is calm, ice crystals can grow outward and converge to form a continuous layer known as an ice skim. In this scenario, the c – axis across the skim has potential to be consistently vertical (Jeffries et al., 2012). Müller-Stoffels et al. (2009) found that unseeded ice grown in freshwater having a positive temperature gradient maintained a vertical c – axis given the growth advantage parallel to the water surface. When ice was seeded, however, cooling of the surface water from the melt of crystal seeds combined with supercooled water pooled between ice crystals, created a growth advantage in the vertical direction. As a result, ice had a horizontal c-axis with the basal plane perpendicular to the ice-ocean boundary. This mode of ice formation was not explored in application to fjord ice but it should be noted as a possibility given the stratified water column with a distinct surface layer that can form in a fjord. Thin, dendritic hand-sized pans of ice, suspected to be growing outward were observed on the surface on several occurrences.

In turbulent conditions, frazil ice crystals will form in a super-cooled water column, eventually rising to the surface to create a slushy layer termed grease ice. With continuous cooling, grease ice will consolidate and harden taking the form of pancakes which will then converge to create a cohesive ice cover from which growth will continue downward (Petrich & Eicken, 2010). This initial layer of ice composed of fine-grained (mm- sized) randomly oriented frazil ice crystals with pores located at grain boundaries is texturally classified as granular ice. Ice texture being the arrangement and geometry of ice crystals, and brine- and air- filled pore space (Lange & Eicken, 1991).

The origin of frazil ice is important to understand in a fjord environment given how it may differ from regions of the Arctic where air temperatures are consistently below freezing and the influence from land-based water is generally less. The formation of frazil ice occurs in four distinct ways as defined by Weeks and Ackley (1982) and emphasized by Jeffries et al. (1994):

- The rise of water flowing out from the base of ice shelves, the resulting adiabatic decompression and supercooling which leads to the formation of platelet ice in the water column. In fjords of mainland Norway, no marine terminating glaciers are present making this mechanism irrelevant. It is primarily considered a characteristic found in Antarctic sea ice.
- Thermohaline convection resulting from the rejection of brine as seawater freezes. As the high density brine sinks downward in the water column, it can undergo supercooling due to double diffusion (heat and salt concentrations diffusing at different rates) leading to formation of frazil ice. Here, we will not consider this as a main mechanism for frazil ice generation given ice forming from often low salinity water where brine rejection may be minimal in comparison to other Arctic and Antarctic regions.
- Wind and wave induced turbulence that cools the upper water column to freezing, enabling the formation of frazil ice crystals. While this mechanism may contribute to ice formation, we note here that without influence by freshwater masses of lower temperature, the water column in northern Norwegian fjords rarely reaches the freezing temperature for seawater. If frazil ice forms in the water column, it will likely be constrained to a fresh or brackish surface layer which has a maximum density at a temperature higher than its freezing point. Due to the lack of convection, without turbulence from for example wind, the frazil layer has potential to be very thin.
- The confluence of two water masses of different salinities but near to their respective freezing points. In other studies of the Arctic, it is assumed that water of lower salinity collides with seawater of both higher salinity and lower temperature. In a fjord environment in northern Norway, this is not the case with the fresh water from rivers being colder given their origin at high altitudes where ice cover is present. As the water flows down the river, at times under substantial ice cover, frazil ice can begin to form. Velocity will slow considerably once reaching the fjord thus allowing for any frazil crystals to accumulate. If frazil crystals are not already present, restricted cooling on a cool day given the stratification may enable formation of frazil crystals in this layer and possibly help cool the underlying more saline layer.

The thickness of a frazil ice – derived granular layer was often limited to only a few centimeters in the cores gathered as part of this study but have potential to be much thicker due to the mode of formation, prolonged mixing and turbulence in a water column (Carnat et al., 2013; Granskog et al., 2003; Lange & Eicken, 1991).

3.1.3.2 Geometric selection and the transition layer

Initially, crystals can be inclined with c – axes placed at various angles. Through a transition layer, however, crystals having a horizontal c – axis will dominate due to their growth advantage in the vertical along the basal plane. In a process termed geometric selection, crystals will begin to align, growing to be cm – sized and progressively more elongated in the vertical. The transition layer appears as a mixed of granular and columnar ice and will vary in its thickness and placement

depending on conditions specific that location (Granskog et al., 2003; Weeks & Ackley, 1986). Factors enabling quicker and more pronounced geometric selection are discussed further in Section 3.2.

3.1.3.3 Congelation columnar ice formation

Congelation growth will occur at the ice-ocean interface after a layer of frazil ice has formed that dampens turbulence at the surface, leading to a transition and eventual quiescent growth downward. Characterized by elongated crystals having a horizontal c-axis that lengthen with depth, this ice is texturally classified as columnar and grows from both freshwater and seawater. Distinct differences do exist between ice grown from these two sources, differing in their microstructure- the size, shape, and connectivity of pores- despite being of the same textural ice type. The rejection of brine from the ice matrix and the process of desalination drives these variations in microstructure between fresh and sea ice as detailed further in Section 3.2. The composition of water at the ice – ocean interface is, therefore, relevant to consider when investigating ice properties of fjord ice. In Paper 2, this topic is explored in greater depth as bulk ice salinity and oxygen isotope measurements are utilized to estimate the proportion of freshwater in relation to seawater at the ice – ocean interface during ice formation.

3.1.3.4 Granular Snow Ice

Granular ice can form when seawater floods a snow-covered surface along an ice edge or when enough snow accumulates that the ice surface is depressed under the ocean's surface resulting in negative freeboard and a slushy layer to form at the ice-snow interface. The water will freeze forming a layer of fine- grained granular ice having both air and brine filled pores. In crystallographic analysis, granular ice formed from snow versus formed from frazil ice can be indistinguishable making the measurements of oxygen isotope composition particularly useful to determine the ratio of snow ice to other ice types.

For granular snow ice to form, only a thin platform of ice is needed thus, it can act as a significant mechanism for the thickening of ice. In opposition, snow can also lead to ice to be thinner due to its insulative properties. Therefore, having an estimate of snowfall throughout a season can assist in understanding the mechanisms behind ice formation and growth rate (Granskog et al., 2017; Merkouriadi et al., 2017; Wang et al., 2015; Webster et al., 2018). In the samples collected as part of this work, granular snow ice often composed large portions of cores with two being entirely composed of granular snow ice. Snow ice is a characteristic more closely associated with Antarctica due to the thinner ice historically found due to higher oceanic heat fluxes although recently it is becoming more common in the Arctic (Provost et al., 2017). Ice thickness in sub-arctic fjords is also limited due to both air temperatures (fewer freezing degree days) and oceanic heat flux, providing a thinner ice cover that can more easily be depressed below the surface. The influence of snow on ice growth however, was not consistent over the period of observation with some cores being nearly devoid of this type of ice. Given the difference between granular and columnar ice in terms of microstructure and related physical properties, an understanding of the influence of snow on ice formation specific to sub-arctic fjords is important to investigate further.

3.2 Desalination

3.2.1 Sea ice

As ice grows from seawater, salt is rejected from the ice matrix and collects in pores and channels generally located at crystal boundaries. In granular ice, pores and channels will be randomly dispersed, a reflection of the crystal size and orientation itself being variable. Being denser than the ambient seawater, brine will flow downwards (gravity drainage), following the path of least resistance. In granular ice, connected pathways can display less consistency and greater tortuosity although vertically oriented channels may form (Oggier et al., 2019). As ice transitions to columnar, rejected brine will accumulate between the basal planes of crystals, often described as plates or lamellae. Brine flows downwards through thinner channels before meeting broader vertical brine channels and brine tubes where flow is well established (Fig. 3.3c).

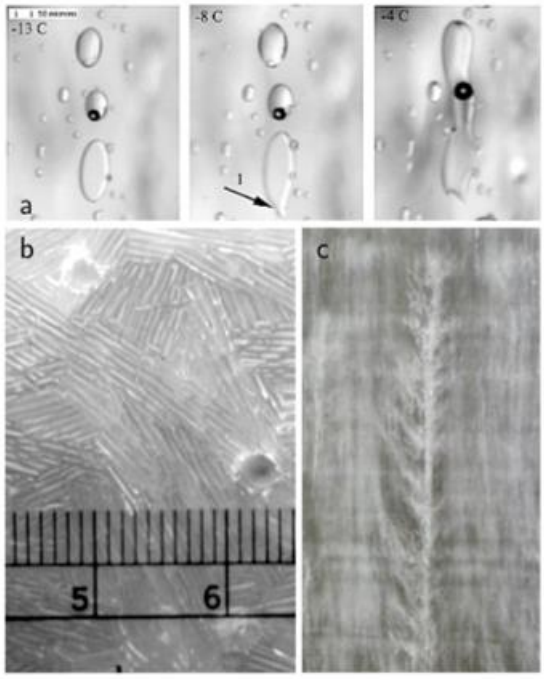

Figure 3.3: (a) Example of the evolution of pore size and connectivity with temperature increase, (b) lamellae present at the ice-ocean interface with outlets of brine tubes present, (c) a brine tube with feeder channels (Hunke et al., 2011)

At the ice – ocean interface, rejected salt can accumulate, increasing the salinity of a thin layer at this boundary, eventually diffusing towards the less saline ocean or being advected in the form of a brine plume once ice reaches a critical thickness (Wettlaufer et al., 1997). The former, diffusion, is not likely to play a considerable role in the fjord ice examined here given currents and, relatedly, turbulence at the interface that will disrupt this process and transport salt away. Independent of this point, however, convection through the ice volume will result as high salinity brine is replaced by seawater leading to lower bulk ice salinity, or in other terms, desalination. The interface temperature holds constant at freezing point during this time, thus due to thermodynamic equilibrium, the increase in salinity will be accompanied by a decrease in temperature. Ice lamellae protruding into this layer

will have a pronounced growth advantage forming what is often referred to as the skeletal layer, characterized by high porosity (approximately 30 %) and permeability (Fig. 3.3b) (Petrich & Eicken, 2010; Weeks & Ackley, 1986). In areas where a current persists, lamellae will align perpendicular to the current (c-axis parallel to current). This is likely due to greater salt transport away from the interface and resultantly faster growth for perpendicularly orientated lamellae. It is the presence of these lamellae, particularly when aligned with current, that causes sea ice to be highly anisotropic, a characteristic reflected in both its thermal and electrical properties (Langhorne, 1983). In addition, the skeletal layer provides habitat for diatoms and other microorganisms, which in turn attracts grazers. It therefore plays an essential part in the sea ice and arctic ecosystem.

As ice growth continues, porosity will decrease due to decreases in temperature and salinity resulting in a less-connected network of pores which prevents further desalination (Fig. 3.3a). Large brine tubes may persist through portions of ice however, with diameters greater than the spacing between lamellae (Fig.3.2(c)) (Petrich & Eicken, 2010; Weeks & Ackley, 1986). The resultant bulk ice salinity will be related to the growth rate of ice with a slower growth rate associated with ice of lower bulk salinity. There are other factors to consider, however, namely the density gradient in the bottom layer in the ice that drives convection. This along with thermal diffusivity of the ice, the thickness of the permeable layer, and viscosity of the brine will all influence the vertical volume flux and resultant salinity in the ice (Notz & Worster, 2008; Notz & Worster, 2009; Petrich et al., 2011). In Paper 3, equations incorporating the interchange of these relationships are examined to determine if accurate growth rates utilizing measurements of bulk ice salinity and oxygen isotope can be obtained.

The microstructure of columnar sea ice will evolve throughout the season being highly dependent on temperature (Fig.3.3(a)). In the winter when heat flux is directed upwards, the coldest ice will be located at the ice surface with a linearly increasing temperature downward to the freezing temperature of ice. The salinity profile of the ice during this time will be c – shaped with the highest salinities at the bottom of the ice, in the highly porous skeletal layer, and the top of the ice (Fig. 3.4). The latter, although hydrostatically unstable, is due to the stopping of brine movement downward once ice porosity decreases to the point that a connected network of pores is no longer present. Nearer to the ice – ocean interface and into the interior of the ice, desalination can continue to occur as higher density brine moves downward and is replaced by lower salinity seawater. In the spring, as air temperatures warm, porosity will begin to increase in the upper layers of the ice and melt pools will form on the surface. Once a critical porosity is reach, high salinity brine trapped in the top layers will flow downwards along with meltwater leading to the interior of the ice to drop in salinity (Eicken et al., 2004; Petrich et al., 2006). Ice temperature during this time will become increasingly homogeneous as the ice approaches its melting point.

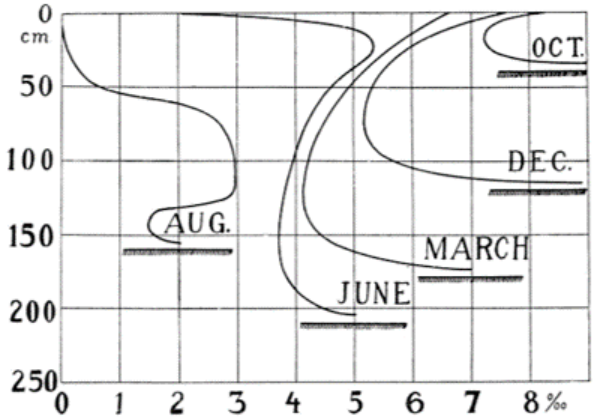

Figure 3.4: Evolution of ice bulk salinity from ice formation (here in October) for Arctic ice (originally from Malmgren (1927), taken from Hunke et al. (2011))

In the fjords examined here, ice was often of low salinity as well as temperature near to 0 °C. The c-shaped salinity profiles characteristic of sea ice were not observed as a result. However, in fjords located in regions where temperatures further below freezing persist, such patterns may be present (e.g. Porsangerfjorden, Finmark). Variability between fjords and years is, again, highlighted as an important factor to consider.

To this point, temperature and salinity have both been mentioned in relation to porosity, often referred to as brine volume fraction in studies of sea ice. The three are well intertwined with established relationships to allow estimate of brine density and salinity, ice density, and ice brine volume fraction through measurement of temperature and salinity. Methods to calculated brine volume fraction are described in Cox & Weeks (1983) for ice below -2 °C and Leppäranta & Manninen (1988) for ice between -2 to 0 °C.

3.2.2 Brackish water and Freshwater

When ice is frozen from fresh water, the distinct growth advantage that leads to the pronounced pattern of lamellae is absent. Crystals may be oriented so the faster-growing basal plane lays either horizontal or perpendicular to the ice-ocean interface depending on conditions at the time (See Section 3.1.3.1) with the interface characterized as planar and having low porosity (Weeks & Ackley, 1986). This has repercussions on the thermal, electrical, and optical properties of the ice, discussed further in Sections 3.3 – 3.5. Considering optical properties, for example, freshwater ice can have an albedo up to 10 times less than that of sea ice. A fact important to consider when estimating the amount of light that may be transmitted to the ocean below and surface energy balance (Petrich & Eicken, 2010).

In between these two extremes, ice formed from brackish water is known to have microstructure similar to that of sea ice having brine pores and channels (Granskog et al., 2005; Granskog et al., 2003; Ikävalko, 1998). Weeks & Lofgren (1967) observed through laboratory measurements, a transition from a planar to lamellar surface at the ice – ocean interface at seawater salinities of 1 psu. This finding was supported by Gow et al. (1992) who made observations of natural brackish ice in the Bay of Bothnia formed from seawater of approximately 4 psu finding a similar pattern of lamellae.

Considering the process of desalination described above, even when ice is formed from water having lower salinity, salt will be rejected and subsequently flow downward through any pathways that exist.

In the fjords studied here and presumably throughout Norway, brackish water and freshwater are contained to the upper-most water layer with ambient seawater being higher than 30 psu. The ice that forms can come from very thin layers on the surface that varies between fresh, brackish, and saline throughout the winter. Thus, it is useful to consider the proportion of fresh versus seawater in an ice sample to deduce its pore structure and other related characteristics like permeability and the habitable space it may offer to microbiota.

3.3 Thermal properties of ice

Throughout the study of fjord ice presented here, the transfer of heat from ocean to air through the ice and vice versa is a fundamental concept of indirect but repeated focus through analysis of ice thickness in relationship to air temperature and ice growth rate deduced from ice properties. At 0 °C, the thermal conductivity of ice (λ_i) is approximately 2.0 W m^{-1} K^{-1} while the thermal conductivity of brine (λ_b) is significantly lower being approximately 0.5 W m^{-1} K^{-1}. The relationship of both to temperature (T in °C) differs with λ_i increasing while λ_b decreases, as temperature decreases. This behavior is described by the following functions presented by Yen et al. (1991):

$$\lambda_i = 1.16\ \mathrm{W}\, m^{-1}K^{-1}(1.91 - 8.66 \cdot 10^{-3}T + 2.97 \cdot 10^{-5}T^2) \quad \text{, for T < 0 °C} \tag{3.1}$$

$$\lambda_b = 0.4184\ \mathrm{W}\, m^{-1}K^{-1}(1.25 + 0.030T + 0.00014T^2) \tag{3.2}$$

The thermal conductivity of sea ice (λ_{si}) will be dependent on brine volume fraction with recent models also taking into consideration microstructure, for example the vertical connectivity of the pore space (Ono, 1968; Schwerdtfeger, 1963). While the thermal conductivity of brine is impacted by changes in salinity, this influence is found to be considerably less than that of temperature. In a study conducted by Sharqawy (2013), the ratio between the thermal conductivity of freshwater (λ_{fw}) and seawater (λ_{sw}) was found to be:

$$\frac{\lambda_{fw}}{\lambda_{sw}} = A \cdot S + 1 \tag{3.3}$$

Where *S* is the salinity of the water in g/kg and *A* is constant determined empirically through the study equal to 0.00022. Therefore, with an increase in salinity, thermal conductivity will decrease.

The thermal conductivity of air (λ_a) is approximately 0.025 W m^{-1} K^{-1}. Thus, air-filled pores can also have a dramatic impact on the thermal conductivity of ice. For cores containing granular snow ice, this is particularly important to consider. Snow ice can be considered as another stage in the metamorphosis of snow on a sea ice surface. In Sturm et al. (2002), measured values of conductivity including snow ice were predicted accurately following an empirical relationship originally meant for snow presented in Sturm et al. (1997):

$$\lambda_s = 0.138 - 1.01\rho_s + 3.233{\rho_s}^2 \qquad \text{for } 0.156 < \rho_s < 0.6 \tag{3.4}$$

Where ρ_s is the density of snow in g cm^{-3}.

In the ice samples gathered here, ice varied considerably in its characteristics with some samples containing brine channels and elongated pores, others being nearly transparent, and also ice with a high density of more rounded, less connected pores indicative of either snow or superimposed ice. Given differences between ice, brine, and air each ice sample had potential to vary in its thermal conductivity, not only between fjords and years but within singular cores given clear layers containing different microstructure.

Knowing the thermal properties of ice is necessary to determine the evolution of ice growth and melt through a season. Using thermal conductivity, the conductive heat flux (F_c) through the ice of thickness, z, is calculated:

$$F_c = -\lambda_{si}\left(\frac{dT}{dz}\right) \tag{3.5}$$

Where T is temperature. Specific heat capacity and latent heat of fusion will both also depend on the thermal conductivity. Sea ice differs from pure ice because a temperature change will also be accompanied by a phase transition as brine pores grow or contract to stay in thermodynamic equilibrium. This phase transition will be accompanied by a release of latent heat. The specific heat capacity of sea ice (c_{si}) can be represented as the following:

$$c_{si} = c_i - m_m L\frac{S_{si}}{T^2} \tag{3.6}$$

Where c_i = 2.11 kJ kg^{-1} K^{-1} is the specific heat capacity of ice, m_m = -0.05411 K is the slope of the liquidus, L= 333.4 KJ kg^{-1} is the latent heat of fusion for freshwater ice, S_{si} is the bulk salinity of sea ice, and T is the temperature of sea ice in °C. These relationships apply for ice having a constant bulk salinity and therefore not experiencing, for example, brine drainage. In measurements of c_{si}, values increase significantly above approximately -5 °C meaning that more energy is needed to raise ice temperature 1 K from -5 to 0 °C than in comparison to lower temperatures. This behavior is a reflection of the latent heat of fusion, increasing or decreasing ice temperature as temperature approaches freezing thus making the second term important to include (Petrich & Eicken, 2010; Weeks & Ackley, 1986). Without it, c_{si} would be underestimated leading to models to show a greater thinning of ice.

Through integration of specific heat capacity (c_{si}) from a given temperature to the melting temperature, latent heat is defined for melting ice as:

$$L_{si} = L_i - c_i T + c_i m_m S_{si} - m_m L\frac{S_{si}}{T} \tag{3.7}$$

In comparison to the latent heat of pure ice (L_i), L_{si} will be less due to the presence of pores and the exchange of sensible heat between ice and brine. A unique characteristic of sea ice in comparison to pure ice is also a slight difference in the latent heat of fusion while ice is melting in comparison to freezing with the latter being approximately 2% smaller in sea ice. This is due to the freezing point of

sea ice melt, being of a lower salinity and being nearer to 0 °C than the freezing point of ocean water (Ono, 1968; Petrich & Eicken, 2010; Weeks & Ackley, 1986).

3.3.1 Estimation of sea ice growth rate

Throughout this work, sea ice growth rate is a focus. With measurements of ice thickness, ice properties, and atmospheric data, the general approach is to first compare measured ice thickness to calculated ice thickness. The latter, summarized further below, is determined through use freezing degree days between ice formation and the day of measurement (Eq. 3.12) substituted into Eq. 3.13. This approach is summarized in Paper 2. The use of bulk ice salinity and oxygen isotope measurements to determine water conditions at the ice-ocean interface and ice growth rate is the focus of paper 3. For further description of theory behind this work, please see the respective papers for thorough background. Presented here is a more complete description of how one may go about estimating ice growth rate if complete data sets of atmospheric, oceanic, ice and snow conditions are available, a perfect world per se. To better understand the formation of ice in sub-arctic fjords and relatedly ice properties useful in other work, such approaches are recommended to take and are offered here to provide a complete picture of this topic.

3.3.1.1 Using Atmospheric and Oceanic Data

The growth rate of ice is dependent on the exchange of heat at the ice-ocean interface combined with the thermal properties of the ice (Fig. 3.5):

$$-F_c + F_w + \rho_i L_{si} \frac{dH}{dt} = 0 \tag{3.8}$$

Where F_c is the conductive heat flux through the ice, F_w is the oceanic heat flux at the ice-ocean interface, and dH/dt, is the change in ice thickness overtime (Petrich & Eicken, 2010). Oceanic heat combined with latent heat released during freezing will limit the amount of ice growth due to conductive heat flux.

Conditions at the ice-atmosphere interface will largely control ice growth with several sources of energy at this interface contributing (Parkinson & Washington, 1979; Persson et al., 2002):

- Shortwave flux: Radiation in the wavelengths 0.3 – 4 μm. Both the albedo of the surface and the amount of radiation that penetrates through the ice to ocean below will decrease this value.
- Longwave flux: Radiation in the wavelengths 4 – 100 μm, the net balance between infrared radiation absorbed and emitted by the surface.
- Turbulent sensible and latent heat flux – the energy absorbed or released to the atmosphere as a function of wind speed. Latent heat being specific to changes in phase while sensible heat specific to changes in temperature with no phase change (Parkinson & Washington, 1979; Rutgersson et al., 2007).
- Heat flux due to surface melt
- Conductive heat flux

In much of Norway, little to no shortwave radiation reaches the ice during ice growth given the complete absence of sun during periods of the winter. Further south, sun may appear but be limited in

the length of time it is present given the steep sides of the fjords providing shade. Shortwave radiation as well as heat flux due to surface melt are therefore often not incorporated into models of ice growth. Surface and air temperature offer a first order estimate of several other sources of energy - the net longwave radiation, sensible heat flux, and latent heat flux. Through determination of a heat transfer coefficient between the air surface (k), these sources can be combined to be described as a net atmospheric flux (F_a):

$$F_a = -k(T_a - T_s) \tag{3.9}$$

Where T_a is air temperature and T_s is temperature at the surface. For a constant surface temperature, $F_a = F_c$.

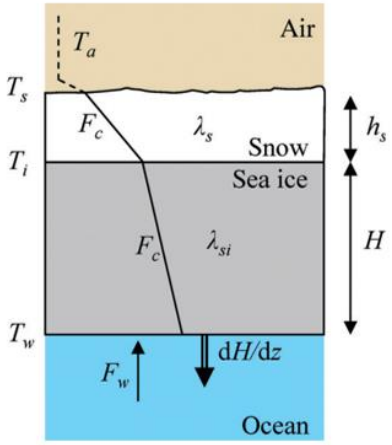

Figure 3.5: Schematic of heat flux through an ice volume (Petrich & Eicken, 2010)

Often a layer of snow separates the surface from the ice interface (Fig. 3.5). In such cases, the insulative properties of the snow must also be incorporated with the thermal conductivity of snow (λ_{sn}) approximately equal to $0.1\lambda_{si}$ and thus potentially having a large impact on the net conductive heat flux from the ocean to air. Atmospheric and conductive flux can be included into Eq. 3.8 to arrive at a new relationship linking growth rate to heat transfer between air and the snow surface, the thermal properties of ice and snow, and the net heat flux from the ocean (Petrich & Eicken, 2010):

$$\frac{dH}{dt}\rho_i L_{si} = -\frac{T_a - T_w}{\frac{1}{k} + \frac{H}{\lambda_{si}} + \frac{h_{sn}}{\lambda_{sn}}} - F_w \tag{3.10}$$

Determination of the oceanic heat flux (F_w) is a non-trivial process as one must consider the turbulent heat exchange at the ice-ocean interface as a current moves underneath. McPhee (1992) defines turbulent oceanic heat flux as deviation from the mean vertical velocity (the turbulent component, w') multiplied by the deviation from the mean temperature (T') equal to:

$$F_w = w'T' = c_h u_{fric}(T_{ml} - T_f) \tag{3.11}$$

Where c_h is the heat exchange coefficient, u_{fric} is the frictional velocity, T_{ml} is the temperature of mixed layer under the ice, and T_f is the freezing temperature. Current and relatedly frictional velocity will be largely dependent on the geometry and size of the fjord combined with the tidal height. In addition, frictional velocity will evolve as water flows under the ice. All these components are difficult to account for making numerical modelling that incorporates variations in currents through a fjord an ideal approach to obtain the best approximation. One more challenge specific to sub-arctic fjords is the potential influence of a freshwater plume moving under the ice on oceanic heat flux. First, the interaction between the tidal current and freshwater plume, particularly near the river mouth, may alter u_*. Freshwater will also decrease salinity leading to an increase in T_f. Lastly, freshwater can act to stabilize the water column at the ice-ocean interface, limiting the efficiency of turbulent heat exchange and therefore the influence of oceanic heat flux (Granskog et al., 2005; McPhee, 1992; Shirasawa & Ingram, 1991).

While continuous measurement of ice thickness and temperature are ideal, simpler models exist to determine ice thickness through only air temperature and specifically the number of freezing degree days (θ in °C days) derived by summing all average daily air temperatures (T_a) below freezing point (T_f) from a start date (i=1) to end date (i=N):

$$\theta = \sum_{i=1}^{N} \Delta t \begin{cases} T_f - T_{a,i}, & T_{a,i} < T_f \\ 0, & T_{a,i} \geq T_f \end{cases} \tag{3.12}$$

Where Δt= 1 day in the studies presented here. Anderson (1961) derived a relationship linking ice thickness (H_i in cm) to θ:

$$H_i^2 + 5.1H_i = 6.7\theta \tag{3.13}$$

Ice growth rate (dH/dt) can therefore be estimated and potentially compared to measured growth rates to better understand the influence of ocean heat flux and/or insulation by snow. Perhaps the best approach (which is an aim of future field campaigns) is through measurement of conductive heat flux (F_c). Although this may be determined roughly using air temperature and the freezing temperature of ice, ideally, temperature measurements are gathered throughout the ice volume to accurately determine dT/dz. This, in turn, can be a used to estimate oceanic heat flux (F_w). Nevertheless, given the difficulty associated with obtaining accurate measurements of F_w at the many unique fjords in regions like Norway, such residual approaches may at times be the simplest to obtain an order of magnitude approximation.

3.3.1.2 Modeling snow ice formation

Through the observation and measurements of fjord ice made throughout this study, it became evident that snow ice formation played an important role in thickening the ice. In particularly the Antarctic, snow ice can often compose large portions of ice cores gathered. As mentioned previously, seawater may flood the surface at ice edges where waves have potential to splash onto the surface. Alternatively, when ice is depressed below sea level, seawater may percolate upward through either cracks in the ice surface or through the pore space. The latter is dependent on the permeability of the ice and the existence of pathways from the ocean to the ice surface (Eicken et al., 1995; Maksym &

Jeffries, 2000). For this reason, despite ice having a negative freeboard, the ice surface may remain dry and therefore snow ice unable to form until cracks form in the surface.

Maksym & Jeffries (2000) present two models to estimate growth of the congelation ice in combination with snow ice and resultant ice bulk salinity. While the first model incorporates the physics of brine percolation upward including displacement of brine and heat exchange, the second model takes a more simplified approach assuming seawater reaches the surfaces in select areas where brine tubes and cracks are present. The two models differed in their results, with the first showing a greater dependence on climatic conditions early on in ice formation. For example, if too much snow fell too early permeability of the ice decreased, a result of brine channels contracting due to brine being displaced into colder ice, this led to limited snow ice growth (see Fig. 3.6). In the second, simpler model, snow ice formation was found to be strongly dependent on the total snow load and was overall more accurate.

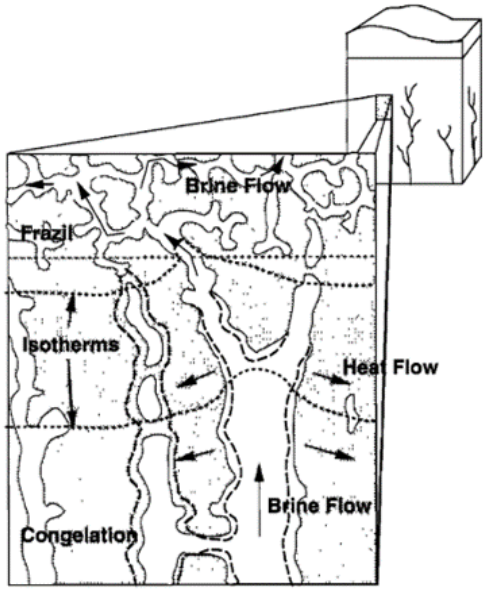

Figure 3.6: Schematic of sea ice microstructure as snow deflects the surface downwards leading to brine flow upwards, displacing isotherms (dotted lines) in the same direction. Heat flow will occur from brine channels to the surrounding ice, leading to brine channels to freeze and narrow while unconnected grow in size (Maksym & Jeffries, 2000).

Through this work on sub-arctic fjords, it became evident that the timing of weather events including above and below freezing temperatures, snowfall, wind, and freshwater flux will influence the amount of ice and its properties. This is supported by the variation in ice thickness and properties observed between the fjords and within single fjords over the three years of observation. How and when seawater and freshwater reach the ice surface is one more piece of the puzzle. In addition, such findings are relevant to studies of snow ice in a sub-arctic fjord environment, as the proportion of freshwater in the upper water column during congelation growth may influence brine volume fraction and relatedly permeability (Freitag & Eicken, 2003; Golden et al., 2007; Petrich & Eicken, 2010). While much of the ice measured was of low salinity and brine volume fraction, all fjords also experienced tides most frequently between 2 – 3 m. This cyclic movement of the ice surface up and

down can produce cracks. This is particularly evident along the shoreline but may occur throughout the ice cover (Kovalev et al., 2020).

In addition to seawater flooding the surface, both rain and melt can also contribute to snow ice as well as superimposed ice formation (Wang et al., 2015). This must be considered as a strong possibility in subarctic regions where both rainfall and above freezing temperatures are common throughout the winter. The measurement of salinity and oxygen isotope composition will assist in determination of the mechanism for formation of snow ice. Snow flooded by seawater will be higher in salinity and hold a different oxygen isotope composition signature than snow flooded by rain. The latter, while possibly of the same salinity will differ in oxygen isotope composition from snow mixed with snowmelt (see Section 3.4). The proportion of snow to water will impact these measurements as well.

3.4 Remote sensing of ice

In the work presented here, the optical and electric properties of ice are of interest due to their relationship to remote sensing. Remote sensing, in the most basic sense, is the ability to observe something, in this case ice, from a distance as opposed to direct contact. Cameras, satellites, and other instruments positioned on land, the sky, or space may be used to gather information about an ice volume. In this work, remote sensing technology including camera and satellite imagery was used to determine dates of ice formation and breakup and ice extent during that time.

There are two categories of remote sensing- passive and active - both of which were used here. The former is based on the measurement of energy at different frequencies emitted or reflected (from sunlight) from the Earth's surface and atmosphere. In comparison, active remote sensing uses instruments that transmit pulses of radiation at specific frequencies and measure the reflected signal received back (Woodhouse, 2006). Both passive and active remote sensing depend on physical characteristics of the ice being measured and surface roughness in relationship to the frequency of the signal (Fig. 3.7).

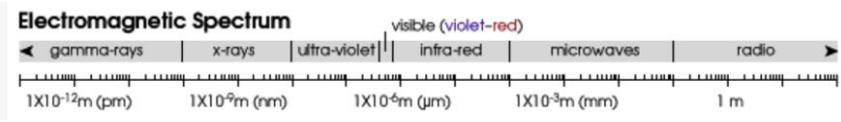

Figure 3.7: The electromagnetic spectrum and related wavelengths. MODIS and Sentinel instruments work in the visible through microwave frequency.

3.4.1 Optical properties of ice

In Paper 1, a dataset gathered by the satellite-based Moderate Resolution Imaging Spectroradiometer (MODIS) was analyzed. This passive sensor collects data ranging from the visible through infrared wavelengths (0.620 – 14.385 μm). Three bands were used as part of the study: Band 3, in the visible part of the spectrum (459 – 479 nm), reflects well off snow and ice while Band 6 (1628 – 1652 nm) and Band 7 (2105 – 2155 nm) are both absorbed. Reflectance in the latter two are indicative of cloud cover, of concern given the possibility of cloud cover along the coast of Norway. Thus, by using the three bands in combination, the impact of cloud cover on results was minimized.

In northern Norway, snowfall is common throughout winter. Thus, MODIS imagery allowed a simple way to identify ice without much further interpretation due to the high reflectivity of the snow-covered surface. Being of low density with many air pockets, snow will scatter all visible wavelengths resulting in its stark white appearance. Reflectivity in the visible as measured by MODIS instrumentation is akin to albedo, the difference being the former measures scatter directed towards the sensor specifically (Woodhouse, 2006). The latter, albedo, accounts for all outgoing and incoming radiation and can be defined as the amount of incident irradiance that is returned from the surface at a given wavelength. The visible color of ice is dependent on both specular and scattered reflection at the surface as well as by scattering and absorption in the volume (Fig.3.8) (Perovich, 1998). Fig. 3.8 depicts the relationship between the scattering coefficient (a function of porosity), the depth of the layer, and resultant color. Without snow on the surface, ice can appear dark in optical imagery, at times showing little contrast to the ocean given transmittance and absorption in the visible wavelengths. Sea ice, however, will have higher albedo than freshwater ice given the number of brine inclusions (greater scattering coefficient) as noted previously in Section 3.2.2. The thicker the sea ice, the greater number of scatterers and the higher the albedo (Perovich, 1998; Petrich & Eicken, 2010). In the fjords of focus here, the density of scatterers varied widely. While some samples were nearly devoid of air and brine inclusions, others were not, particularly when either snow ice or superimposed ice were present on the surface.

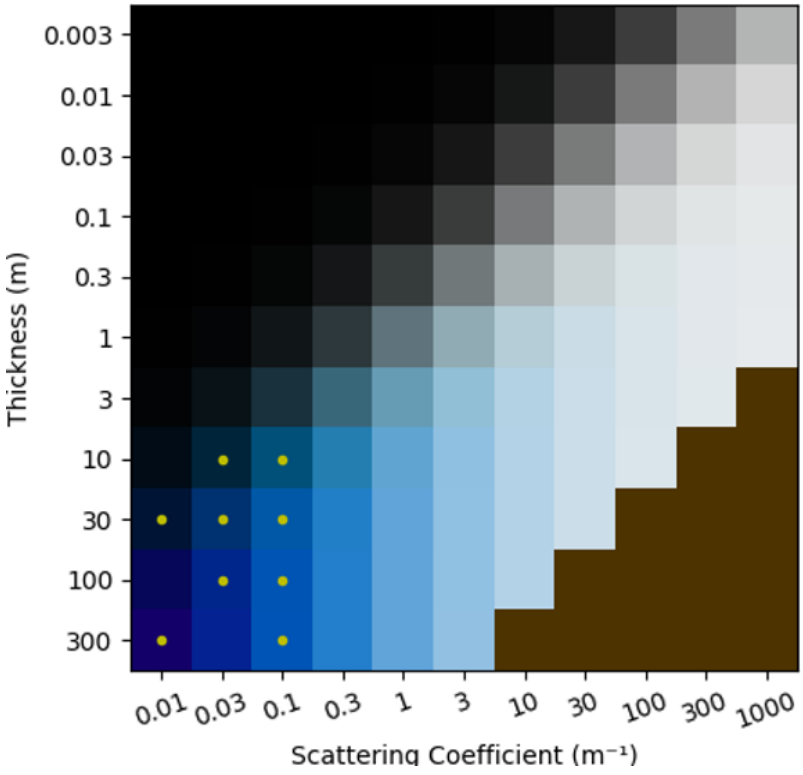

Figure 3.8: The relationship between the depth of a snow or ice layer, the scattering coefficient (dependent on porosity), and resultant color of the ice (from Petrich (2019)). Yellow dots are colors outside the sRGB gamut. Brown squares (lower right corner, are uncalculated values. Calculation done assuming no Colored Dissolved Organic Matter (CDOM)

While the use of passive optical imagery proved to be a useful tool, it does have downfalls including the requirement of daylight. In regions located at the high latitudes, where winter brings the polar night, imagery is not available throughout much of the winter. Active systems like synthetic aperture radar (SAR), are therefore needed to obtain continuous imagery of the earth's surface throughout the year. In addition, sensitivity to clouds as well as specular reflection off waves on a windy day both may lead to misidentification of an ice surface in MODIS imagery. Therefore, it is imperative to take adequate processing steps to address these issues and possibly other sources of misidentification to ensure accurate interpretation of images.

3.4.2 Dielectric permittivity of ice and scattering

In Paper 2, SENTINEL- 1 C-band SAR images were used in combination with MODIS imagery to determine freeze-up and break-up dates for the seven specific fjord of interest. Operating at a frequency of 5.404 GHz (λ = 5.55 cm), the strength of the backscatter received will depend on the dielectric properties of the ice, discrete scatterers within the ice volume, and surface roughness and large-scale geometry.

Dielectric properties determine how electromagnetic waves propagate and attenuate when interacting with a volume (Hallikainen & Winebrenner, 1992). The frequency will largely control the depth of penetration (δ_p) of an electromagnetic wave:

$$\delta_p = \frac{1}{k_a} = \frac{\sqrt{\varepsilon'}}{k_0 \varepsilon''} \tag{3.14}$$

Where k_a is the contribution to the extinction coefficient by absorption, k_0 is the extinction coefficient of free space, and ε' and ε'' are the real and imaginary parts of the electric permittivity:

$$\varepsilon = \varepsilon' - i\varepsilon'' \tag{3.15}$$

ε' describes the contrast in comparison to free space (ε'_{air}=1) and ε'' represents the dielectric loss being dependent on conductivity (σ) and angular frequency (ω):

$$\varepsilon'' = \frac{\sigma}{\varepsilon_0 \omega} \tag{3.16}$$

Due to this dependence on conductivity, a clear difference exists between water and ice, with ε'' being several magnitudes smaller in ice. For a porous medium, dielectric properties will be determined by the properties of the constituent phases and temperature. In application to sea ice, this means the distribution, size, and shape of brine and air inclusions in the pure ice matrix. Therefore, freshwater ice devoid of brine inclusions will interact differently with an electromagnetic wave in comparison to saline, sea ice depending on the frequency used (Hallikainen & Winebrenner, 1992; Petrich & Eicken, 2010). In other terms, the volume scattering differs between these two types of ice (Fig. 3.9). When considering the use of remote sensing technology to monitor fjord ice, one must consider variations in salinity and ice type with saline congelation ice, freshwater congelation ice, and granular snow ice all differing. In addition, while dry snow is easily penetrable at C-band frequencies, as the liquid water content increases due to melt or rain (common in winter in northern Norway), the penetration depth

will decrease significantly. As a result, the ice and its properties will be much more challenging to resolve. Interpretation of fjord ice SAR images is non-trivial. The main method to determine ice extent was through manual inspection of images for an ice edge, a hard target scatterer, which is illuminated by the double bounce from the ocean to the ice edge, and back to the sensor (Fig. 3.9). The ice surface, in comparison, was challenging to interpret given variation in surface characteristics.

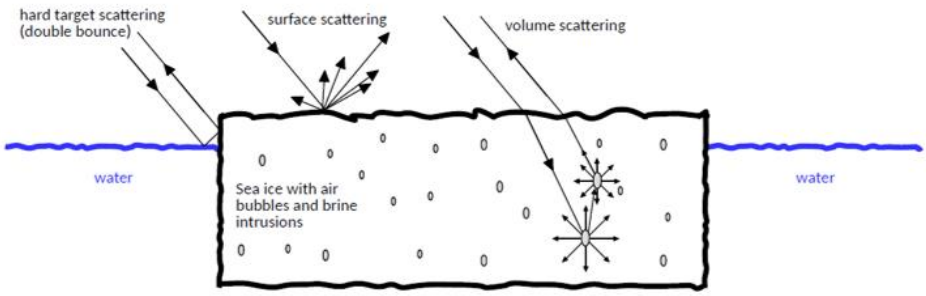

Figure 3.9: Schematic of scattering mechanisms by an ice cover (from Lohse (2020)).

Surface scattering is dependent on roughness, better defined as the vertical height variation (h), in comparison to wavelength (λ) and incidence angle (θ) (the Rayleigh criterion):

$$h < \frac{\lambda}{8cos\theta} \tag{3.17}$$

When this criterion is met, specular scattering will occur with the transmitted signal being reflected off the surface in the forward direction, away from the sensor. As a result, the surface appears dark in a SAR image. When surface roughness is greater than h, diffuse scattering results leading to a portion of the transmitted signal to be reflected back to the sensor (Lohse, 2020). During initial ice formation, specular scattering may occur. If the ocean surface is rough, this may allow for clear identification of ice however given that ice in fjords generally occurs on calm days, this is often not the case. Additionally, through time the fjord ice surface may become rough due to melt/freeze cycles combined with snow and superimposed ice. This will further complicate interpretation of images.

SAR data is a useful tool to obtain information on fjord ice having both better spatial and temporal resolution in comparison to optical MODIS imagery. In addition to challenges with interpretation however, the oblique angle of the transmitted signal combined with the narrow width and high mountains surrounding many fjords in Norway may result in shadowing, preventing the acquisition of data in these regions. While this was not encountered in the imagery examined as part of this work, it is a relevant factor to consider if automatic detection and identification of ice type is pursued in fjord environments.

3.5 Stable isotopic signature of ice

The oxygen and hydrogen atoms that compose a water molecule can differ in their isotopic signature. Isotopes are chemically identical atoms that have the same number of protons but differ in number of

neutrons and therefore mass. In the work presented here, ^{16}O and ^{18}O are the two isotopes of greatest interest given their connection to the water composition from which ice is grown and sensitivity to ice growth rate. The two are linked through definition of oxygen isotope signature, $\delta^{18}O$:

$$\delta^{18}O = \left[\frac{\left(\frac{^{18}O}{^{16}O}\right)_s}{\left(\frac{^{18}O}{^{16}O}\right)_{VSMOW}} - 1 \right] * 1000\ ‰ \tag{3.18}$$

Where *s* refers to the ratio of ^{18}O to ^{16}O of the sample while *VSMOW* is the ratio for Vienna Standard Mean Ocean Water. Therefore, seawater will have a $\delta^{18}O$ near to 0 ‰ with measured values for $\delta^{18}O$ ranging as high as approximately 2 ‰ at lower latitudes down to approximately -3 ‰ in regions of the arctic (LeGrande & Schmidt, 2006). The dependence on latitude is linked to cycles of evaporation and precipitation in addition to significant contribution from freshwater sources. The greatest amount of precipitation originates from ocean evaporation. At lower latitudes, a greater amount of evaporation occurs and freshwater influence is less. As ^{18}O is heavier, it takes more energy for its evaporation in comparison to ^{16}O leading to higher values of $\delta^{18}O$. $\delta^{18}O$ is often used as a climate proxy for this reason, with periods of warm weather characterized by a greater amount of water molecules holding ^{18}O evaporated and thus lower values of $\delta^{18}O$ in comparison to colder periods indicated by higher values of $\delta^{18}O$. Similarly, as precipitation falls more commonly as snow rather than rain during periods of cold, snow itself will generally be depleted in heavier isotopes in comparison to rain (Beria et al., 2018). A schematic summarizing these factors is presented in Fig. 3.10.

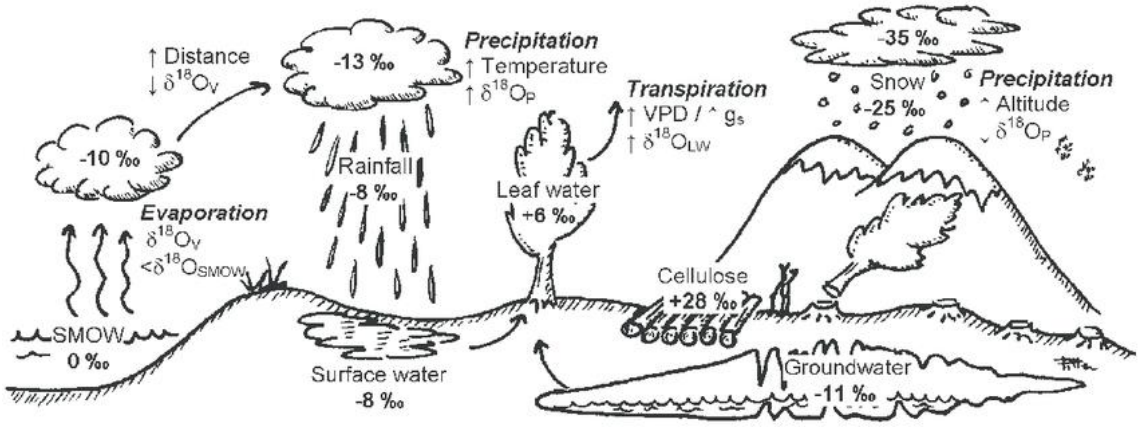

Figure 3.10: Processes determining the isotopic signature of water sources including distance from the initial source (ocean) connected to the type of precipitation. Each can influence the isotopic signature of river water leading into a fjord (Serrano et al, 2005).

Due to their greater mass, water molecules holding ^{18}O will also be preferentially precipitated. This leads to differences in ^{18}O of freshwater sources on land. The farther away from the ocean, the more depleted precipitation will be of the heavier ^{18}O isotope and thus lower values of $\delta^{18}O$ (see Eq. 3.18). The isotopic signature of fresh river water across the globe ranges from -41.42 ‰ to 14.75 ‰ with an average $\delta^{18}O$ of -10.59 ‰. In Norway specifically, this range narrows to approximately -4 ‰ in southern Norway, down to approximately -12 ‰ in northern Norway (Nan et al., 2019). The rivers discharging into fjords are often fed by many tributaries located higher into the surrounding mountains

each potentially varying in their characteristic isotopic composition. When determining the isotopic signature of freshwater leading into a fjord, it is therefore ideal to gather samples near to the river mouth where all freshwater sources are thoroughly mixed.

When ice formation occurs, ^{18}O is more quickly incorporated into the ice due to a lower vibrational energy in comparison to ^{16}O (Eicken, 1998). The difference between $\delta^{18}O$ in water and ice is termed the fractionation coefficient (ε):

$$\varepsilon = \delta^{18}O_{ice} - \delta^{18}O_{water} \tag{3.19}$$

Under isotopic equilibrium, whereby ice is grown in laboratory at a rate slow enough to allow for mixing of the boundary layer, ε is estimated to be 2.91 ‰ for pure freshwater ice (Lehmann & Siegenthaler, 1991). For sea ice, under laboratory conditions at the slowest of growth rates, fractionation was measured to be 2.7‰ (Craig & Hom, 1968). Many examples of measurements of natural ice of differing thickness and salinity exist in the literature, varying, for example between 2.09 ‰ (Melling & Moore, 1995) , 2.57 ‰ (Macdonald et al., 1995), 2.23 ‰ (Macdonald et al., 1999), and 1.88 ‰ (Toyota et al., 2013). Fractionation, ε, is therefore not constant, with growth rate influencing its value. For the latter, the slower the ice grows, the more time available for fractionation to occur leading to a higher value for $(^{18}O/^{16}O)_s$ and, hence, $\delta^{18}O$ in the ice (Eicken, 1998; Toyota et al., 2013).

As noted in Section 3.1.3.3, bulk ice salinity is also dependent on seawater properties (salinity) at the ice-ocean interface and ice growth rate. For the former, salinity and $\delta^{18}O$ are positively correlated, seawater with higher salinity and $\delta^{18}O$ will lead to ice of higher bulk salinity and $\delta^{18}O$. Growth rate will have an opposite effect on salinity however, with a slower growth rate leading to lower bulk salinity given a greater amount of time for desalination to occur. The connection between ice properties, seawater properties, and growth rate is the topic considered in Paper 3 where measurements of ice bulk properties, seawater properties, and freshwater properties are applied to estimate ice growth rate and the composition of water at the ice-ocean interface. A complete overview of the theory, relevant literature, and derived method is presented therein.

4 Fieldwork

Seven fjords located in northern Norway were chosen for ice characterization based on knowledge that they held ice in recent years, determined through satellite imagery and in-situ observation, as well as their accessibility (Fig. 4.1). Measurements were performed over the winter of 2017/2018, 2018/2019, and 2019/2020 with samples collected toward the end of the ice-growth period (Table 1). In one fjord, Beisfjord, measurements were made more frequently due to its proximity to Narvik.

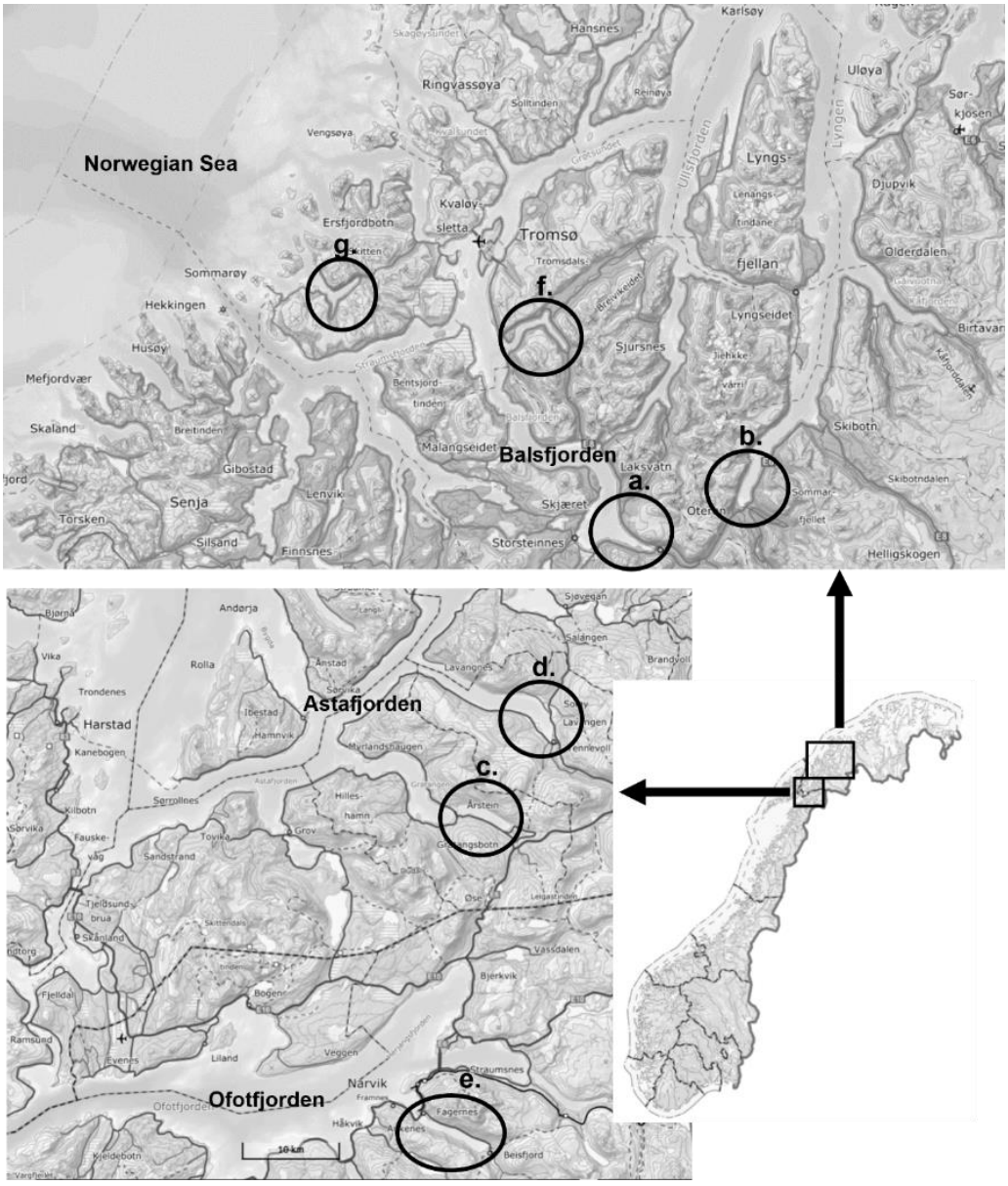

Figure 4.1: Location of Norwegian fjords where measurements were gathered, ordered according to freezing degree days (FDD) from highest to lowest. a) Nordkjosbotn, b) Storfjord, c) Gratangsbotn, d) Lavangen, e) Beisfjord, f) Ramfjord, g) Kattfjord. ©norgeskart.no

4.1 Field Measurements

A summary of when and where measurements were obtained of both ice and ocean is presented in Table 4.1. Here a description of the different measurements and method is provided. Before ice samples were removed, any snow on the surface was shoveled away to provide a clean area from which to drill ice cores. Up to three cores were gathered at each location. A stratigraphy core for transport back to our home office for subsequent thin sectioning and analysis of ice crystal structure, a core to measure ice temperature, and a core to measure of ice salinity. To measure temperature, small holes were drilled 0.05 m apart upon the removal of the core. Next, a Fluke 54IIB thermometer having an accuracy of ± 0.05% + 0.3 °C and resolution of 0.1 °C was placed into the hole and held for approximately 15 seconds before a stable temperature reading was obtained.

For salinity measurements, the core was removed and laid horizontal immediately to minimize brine drainage. Using a saw, the core was sliced into 0.05 m sections and double bagged. Samples were melted at room temperature before salinity was measured using a YSI Pro30 temperature/conductivity probe with resolution of 0.1 on the practical salinity scale (psu) (Fofonoff & Millard, 1983) and accuracy of ±0.1 (psu) or ±1% of the reading, whichever is greater. It is noted that the sampling procedure is meant to minimize brine drainage, but it still can occur being largely dependent on the brine volume fraction (porosity) of the ice. The remaining seawater from the melted ice samples was placed in glass bottles with cone liners and stored at 4 ℃ for stable oxygen isotope analysis. Samples were analyzed at the Stable Isotope Laboratory at the Centre for Arctic Gas Hydrate, Environment and Climate (CAGE) located at UiT The Arctic University of Norway, Tromsø, Norway. A 0.5 mL sample from each melted core slice was pipetted into a 12 mL Labco glass vial which was next flushed with a 0.3% CO2 in He gas mixture, equilibrated at 25°C for >24h. Calibration was done through measuring three inhouse standards of $\delta^{18}O$ between -1 and -36 ‰ that had previously been calibrated against international standards VSMOW2, GISP, and SLAP2. When a line was fit to true vs. measured vales of $\delta^{18}O$, the R2 value of the line was 1.0, with error between separate readings most often being less than 0.01‰ but with a standard deviation <0.05‰. A Thermo-Fisher MAT253 IRMS with a Gasbench II was used to measure of the quantity of $\delta^{18}O$.

For all fjords, seawater temperature and salinity were measured with a CTD (CastAway-CTD, Sontek) at the ice-sampling location just after the ice cores were collected. Slush was removed from one of the holes before measuring the vertical distribution of temperature and salinity in the water column below the ice by lowering the CTD manually from the drill hole to the seabed. The CTD had a resolution and accuracy of 0.01°C and 0.05 °C respectively for temperature, 0.01 (psu) and ±0.1 (psu) for salinity, and 0.01 m and ±0.25% of the measured value for depth. Two casts were made at each location to ensure that consistent measurements were obtained. The data presented here were taken during the upcast, with measurements of pressure, temperature, and conductivity converted to depth and salinity automatically by the instrument using the UNESCO equations (Fofonoff & Millard, 1983). The CTD sampled at a frequency of 5 Hz and was raised at approximately 0.5 m/s. Only upcasts were used due to the presence of ice that sometimes formed around the sensor while in between measurements. This resulted in a clear error in measurements of the upper water column in the downcast as the ice was melted and/or dislodged. Seawater samples from 0.20 down to 2.0 m below the bottom of the ice were collected for isotopic measurements using a manual water pump attached to a rubber hose. The hose

was rinsed with water from the desired depth and two cone-lined bottles were filled and stored at the lab facility at SINTEF Narvik at 4 °C until analysis at the UiT stable isotope laboratory.

Table 4.1: Summary of the field measurements obtained over three seasons and seven fjords.

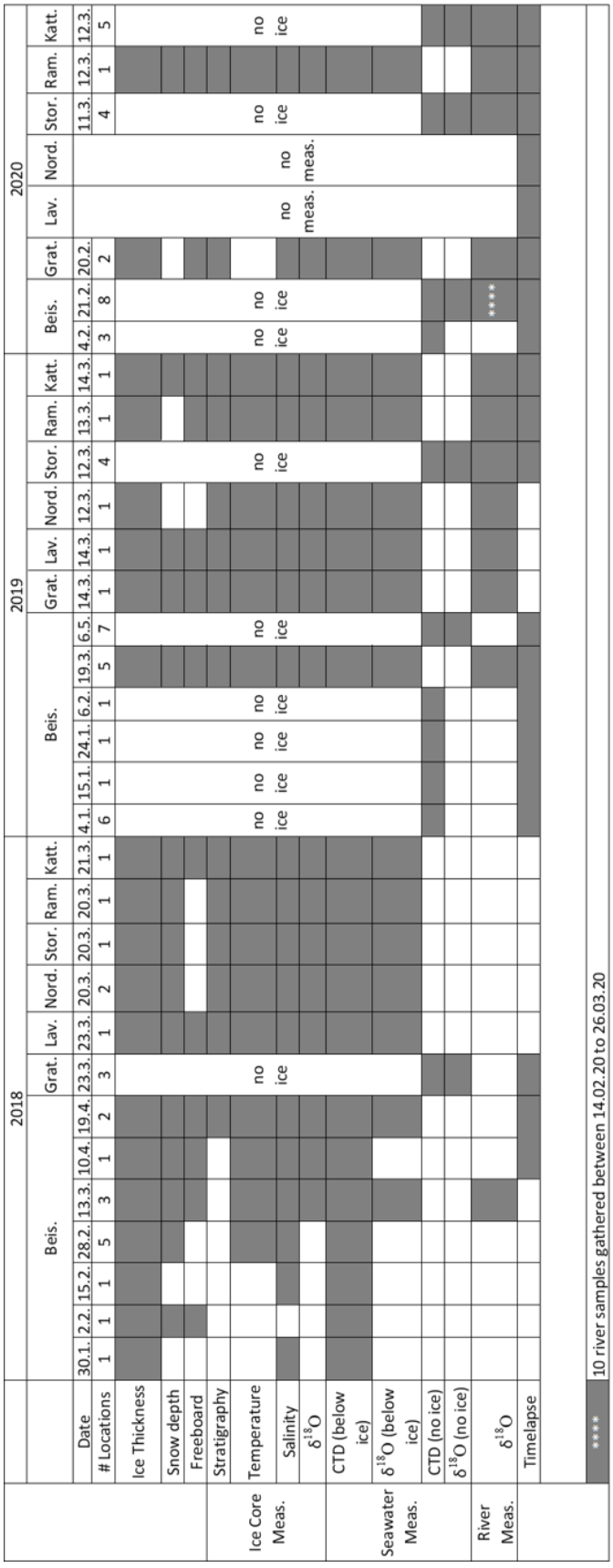

4.2 Ancillary data

4.2.1 Determining ice freeze up and break up

UOVision UM 565 and UM785 trail cameras were used to collect timelapse images at all fjords. This allowed for tracking of weather events as well as determination of ice freeze up and break up. As images were not consistently gathered at all fjords throughout the three seasons of data collection, satellite imagery was also used to track ice conditions, primarily the formation and breakup of ice (see Section 3.3). Two products were used for this purpose - SENTINEL-1 C-band Synthetic aperture radar (SAR) and imagery from Terra satellite MODIS sensor, specifically the MOD09A1.006 Terra Surface Reflectance 8-Day Global 500m product. For the former, Ground Range Detected (GRD) scenes were evaluated with Google Earth Engine (Gorelick et al., 2017). Processing steps for MODIS imagery are described in Paper 1. Ice formation and break up can occur several times throughout the season. In this work, freeze up is defined as the first day of consistent ice coverage, with no further break ups occurring before the day of measurement. The ice edge often deteriorated over time, with rarely a single event leading to all ice dispersing. The date of break up represents the first day where the fjord was entirely ice free.

4.2.2 Weather data

Values for average daily air temperature, accumulated snow cover, and runoff were obtained from the openly available web portal seNorge.no (Lussana et al., 2018), providing spatially interpolated observational data by the Norwegian Meteorological Institute and the Norwegian Water Resources and Energy Directorate (NVE). Values for both runoff and accumulated snow cover are derived using the Hydrologiska Byråns Vattenbalansavdelning (HBV) hydrology model. Runoff (Q) in m/day is a function of several parameters including precipitation and evapotranspiration as well as changes over time in the amount of water stored in the soil, snow, and bodies of water (Bergström, 1992).

5 Overview of Publications

5.1 Paper Summaries

5.1.1 Paper 1

Paper I: M. O'Sadnick, C. Petrich, C. Brekke, & J. Skarðhamar **"Ice extent in sub-arctic fjords and coastal areas from 2001 to 2019 analyzed from MODIS imagery"**, Annals of Glaciology, vol. 62, no. 82, pp. 210- 226, 2020.

Ice extent in 386 fjords and coastal regions from February through May, 2001 to 2019, was assessed using imagery collected by the Moderate Resolution Imaging Spectroradiometer (MODIS) with processing completed in Google Earth Engine. Frequent cloud cover is common along the coast of Norway, thus, the MOD09A1.006 Surface Reflectance 8-Day Global 500 m dataset was selected for use given its automatic selection of one value over an 8-day period for each pixel based on cloud cover and solar zenith. To locate ice in these images, Band 3, in the visible part of the spectrum (459–479 nm) which reflects well off ice was used in combination with Band 6 (1628–1652 nm) and Band 7 (2105– 2155 nm). The latter two are both absorbed by ice but reflected by clouds. By subtracting the sum of Bands 6 and 7 from Band 3, ice is illuminated while further minimizing the impact of cloud cover on results. To ensure only ice on the ocean surface was considered and no pixels of snow-covered land or in-land ice were included, the MOD44W.005 Land Water Mask was also applied.

Results showed 47 fjords with over 5 km^2 of ice at least once during the time period examined with many others having a measurable amount of ice throughout that time as well. Fjords were subsequently grouped into ten geographical regions to examine the possible drivers behind ice formation, comparing findings of ice extent to air temperature, snowfall, and rainfall plus snowmelt. Six out of the ten regions were found to be significantly correlated to air temperature as defined by freezing degree days (see Eq. 3.12), while two were correlated to snowfall, and one was correlated to rainfall plus snowmelt. Seasonal trends in ice extent also appeared when comparing regions in southern Norway and moving up the coastline to northern Norway. In the former, ice showed a tendency to breakup and reform throughout a winter season while further north, ice coverage was more consistent.

Through examining differences in ice extent from year to year between regions but also individual fjords located near to each other, our understanding of how certain factors combine to allow for ice formation can be improved. Of particular consideration are fjords displaying similar patterns in ice extent that may differ in the factors contributing to ice formation. For example, both a cold, calm year with little precipitation to form a brackish layer may display the same ice extent as a year with more precipitation but with strong winds in the days directly following. Such unpredictability in both ice extent as well as ice properties has potential to impact boat traffic, local communities, marine life, and oil spill cleanup efforts. Future work is recommended to expand on findings presented in this paper including the collection of in situ measurements of ice and further investigation into the influence of weather conditions.

5.1.2 Paper 2

Paper II: M. O'Sadnick, C. Petrich, C. Brekke, J. Skarðhamar, & Ø. Kleven **"Ice Conditions in northern Norwegian fjords: Observations and measurements from three winter seasons: 2017-2020",** Cold Regions Science and Technology, 2022, accepted with minor revisions, in review.

Over the period of three winters between 2017 and 2020, ocean and ice conditions and properties were monitored in seven northern Norwegian fjords chosen based on knowledge of previous ice coverage. Ice thickness, stratigraphy, bulk salinity, and the oxygen isotope composition ($\delta^{18}O$) were all measured as well as ocean salinity, temperature, and oxygen isotopic measurements of seawater, snow, and river water. Findings revealed ice thicknesses ranging from non-existent up to 0.8 m with ice bulk salinity varying from 0 psu to 5.6 psu and $\delta^{18}O$ from -13.3 ‰ and 0.2 ‰. In addition, the proportion of congelation and granular ice changed between both seasons and fjords with the first season being primarily columnar ice, the second season being a mix of granular and columnar, and the third season being primarily granular. Despite often low values for ice bulk salinity and $\delta^{18}O$ characteristic of ice frozen from freshwater, seawater salinity near to the ice – ocean interface was primarily above 31 psu with $\delta^{18}O$ between -1 to 0 ‰. This finding indicates de-coupling between the surface and intermediary layers of the fjord likely playing an important role in ice formation in Norwegian fjords.

An investigation into the relationship between ice thickness, properties, and pore structure and several weather-related variables including freezing degree days, snowfall, and runoff was performed to understand the influence of each on the ice and ocean conditions observed. The use of freezing degree days as a predictor of ice thickness was found to be undependable due likely to the timing and amount of snowfall and oceanic heat flux. The importance of understanding how weather and oceanic conditions overlap between seasons and fjords was subsequently highlighted, including not only the weather variables analyzed but also wind, tide, and fjord-coast water exchange. Such timing will determine when, how much and what type of ice will form. From these findings, the inadequacy of single year measurements in Norwegian fjords is noted especially for use in prediction of ice conditions over long time spans.

5.1.3 Paper 3

Paper III: M. O'Sadnick, C. Petrich, & J. Skarðhamar **"The use of ice bulk salinity and $\delta^{18}O$ to investigate changes in the fjord environment over a winter season"**, The Cryosphere, 2022, submitted.

Measurements of bulk salinity and oxygen isotope composition ($\delta^{18}O$) first presented in Paper 2 are further examined in Paper 3. Focus is placed on the 2017- 2018 season, chosen due to the sustained period of subfreezing temperatures and minimal snowfall allowing for the greatest amount of columnar ice growth between the three seasons. Both properties of the ice can be related to growth rate and properties of water at the ice – ocean interface through previously defined equations found in Petrich et al. (2011) and Toyota et al. (2013). A method was thus developed to invert bulk ice salinity and $\delta^{18}O$ simultaneously to determine the history of growth rate and interface water composition of ice samples the ice samples gathered. Needed are only measurements of ice properties as well as seawater salinity and $\delta^{18}O$ and river water $\delta^{18}O$.

In regions where growth rate and interface composition can vary constantly, bulk ice salinity was found to correlate well to composition of the water at the ice – ocean interface while $\delta^{18}O$ correlated best to growth rate. Periods where air temperatures were near to freezing or above freezing had large potential to bias results. For example, if temperatures are warm enough to cause either sea ice melt, snow melt, or both, all can alter $\delta^{18}O$ at the interface-ocean due to changes to endmember values. When not accounted for in the inversion, higher values of $\delta^{18}O$ in ice due to the refreezing of sea ice meltwater will result in predictions of growth rate slower than it should be. Snowmelt, however, will have an opposite effect, leading to $\delta^{18}O$ of ice to decrease and an overestimation of ice growth rate. These findings were supported by determination of the approximate time of formation for sections of ice cores which could then be aligned with known values of air temperature, snowfall, and runoff. With these biases noted, it was found that five of the six investigated sites had ice grown from a brackish layer with between 0 and 40% seawater content, while one site had ice grown from water with between 50 and 90% seawater content.

When the limitations of the inversion are understood, the method presented provides a valuable estimate of conditions in ocean and air at the time of ice formation in environments where continuous measurement is challenging. Results are most sensitive to the properties of the dominating water mass, i.e. inversion of ice with predominantly seawater origin will be most sensitive to knowledge of seawater properties. In the current study, sensitivity was highest to uncertainties in the isotopic composition of the river water. As supported by findings presented in Paper 2, the dominating water mass at the ice-ocean interface in Norwegian fjords may differ between seasons making accurate measurement of freshwater endmembers of upmost importance if applying the method presented here.

5.2 Other Publications

As First Author

O'Sadnick, M., Petrich, C., Kleven, Ø., Brekke, C., Skarðhamar, J., & Dang, N. P. (2018). Observations of ice conditions and properties in Norwegian fjords during the winter of 2018 and implications for oil spill response. In *Proceedings of the Forty-first AMOP Technical Seminar, Environment and Climate Change*, Ottawa, Canada (pp. 123 – 137).

O'Sadnick, M., Petrich, C., Kleven, Ø., Skardhamar, J., & Brekke, C. (2020). Ice Formation in Norwegian Fjords–Findings from the 2018-2019 Field Season. In *Proceedings of the 25th International Symposium on Ice*, Trondheim, Norway.

As Co-author

Petrich, C., O'Sadnick, M., Brekke, C., Myrnes, M., Maus, S., Salomon, M. L., ... & Reimer, N. (2018). An overview of the MOSIDEO/CIRFA experiments on behavior and detection of oil in ice. In *Proceedings of the forty-first AMOP Technical Seminar, Environment and Climate Change*, Ottawa, Canada (pp. 112-122).

6 Paper 1

Ice extent in sub-arctic fjords and coastal areas from 2001 to 2019 analyzed from MODIS imagery

M. O'Sadnick, C. Petrich, C. Brekke, & J. Skarðhamar

Published in:
Annals of Glaciology, vol. 62, no. 82, pp. 210- 226, 2020.

Annals of Glaciology

Paper

Cite this article: O'Sadnick M, Petrich C, Brekke C, Skarðhamar J (2020). Ice extent in sub-arctic fjords and coastal areas from 2001 to 2019 analyzed from MODIS imagery. *Annals of Glaciology* 1–17. https://doi.org/10.1017/aog.2020.34

Received: 1 December 2019
Revised: 4 May 2020
Accepted: 4 May 2020

Key words:
Ice/atmosphere interactions; remote sensing; sea ice; sea-ice growth and decay; ice/ocean interactions

Author for correspondence:
Megan O'Sadnick,
E-mail: megan.osadnick@norut.no

Ice extent in sub-arctic fjords and coastal areas from 2001 to 2019 analyzed from MODIS imagery

Megan O'Sadnick[1,2], Chris Petrich[1], Camilla Brekke[2] and Jofrid Skarðhamar[3]

[1]SINTEF Narvik, Narvik, Norway; [2]UiT – The Arctic University of Norway, Tromsø, Norway and [3]Institute of Marine Research, Tromsø, Norway

Abstract

Results examining variations in the ice extent along the Norwegian coastline based on the analysis of Moderate Resolution Imaging Spectroradiometer (MODIS) images from 2001 to 2019, February through May, are presented. A total of 386 fjords and coastal areas were outlined and grouped into ten regions to assess seasonal and long-term trends in ice extent. In addition, three fjords were examined to investigate how ice extent may vary over short distances (<100 km). Of the 386 outlined, 47 fjords/coastal areas held >5 km^2 of ice at least once between 2001 and 2019. Over this span of time, no statistically significant trend in ice extent is found for all ten regions; however, variations between regions and years are evident. Ice extent is assessed through comparison to three weather variables – freezing degree days (FDD), daily new snowfall and daily freshwater supply from rainfall plus snowmelt. Six out of ten regions are significantly positively correlated ($p < 0.05$) to FDD. In addition, ice in two regions is significantly positively correlated to daily new snowfall, and in one region negatively correlated to rainfall plus snowmelt. The importance of fjord geometry and bathymetry as well as other weather variables including wind is discussed.

1. Introduction

The coast of mainland Norway is dominated by the presence of fjords. Often subjected to air temperatures below freezing, sea ice has the possibility to form in these regions. The larger fjords are mostly ice free in winter due to the inflow of warm oceanic water, but ice often forms in the inner parts of fjords and fjord arms, with variable duration and extent of the ice cover (Eilertsen and Skardhamar, 2006). It is understood that one condition important, often necessary, for ice to form in fjords is a layer of brackish water on the surface (Gade, 1986). This water can be less dense than the warmer ocean water below, leading to little vertical mixing and a stable water column that promotes cooling and ice formation at the surface (Manak and Mysak, 1989; Ogi and Tachibana, 2001). Calm oceanic and atmospheric conditions must be present to allow for the stratified water column to form. These requirements of fresh water and calm conditions make ice formation a local effect, likely to vary between fjords and years.

Very little systematic work has been done on ice in mainland Norwegian fjords. The Norwegian pilot guide offers brief descriptions of ice extent in selected fjords to assist boat and ship captains (Hughes, 2006). However, the guide is based primarily on limited data with little focus on interannual variability. There is a wide breadth of work examining Norwegian fjords from physical and biological perspectives (e.g. Hopkins and others, 1984; Stigebrandt and Aure, 1989; Svendsen, 1995; Asplin and others, 1999; Eilertsen and Skardhamar, 2006; Skardhamar and others, 2018). In these works, focus is primarily placed on the warmer, summer months with ice conditions in the winter mentioned only occasionally. One can turn to research focused on fjords found in Arctic regions such as Svalbard which have been closely investigated regarding sea ice (Cottier and others, 2010; Nilsen and others, 2008; Smedsrud and Skogseth, 2006). These regions differ from coastal Norway, given longer periods of cooler temperatures.

Ice can alter the physical behavior of a fjord, i.e. the transmission of light through the water column and heat flux from the air to ocean and vice versa, and in turn alter biological conditions (Gradinger, 2009; Arndt and Nicolaus, 2014; Arrigo and others, 2014). In addition, ice can create an obstacle to those transiting certain areas by boat – slowing speed, increasing risk in search and rescue scenarios and complicating the clean-up of any spilled pollutants such as oil (Arctic Marine Shipping Assessment, 2009). With industry increasing in the North, a larger number of boats and people are being drawn to these areas. Understanding ice conditions including not only where ice may be present but the properties of that ice, i.e. thickness, porosity and permeability, will better prepare northern communities for future development (Petrich and others, 2019). Previous work has examined the relationship of oceanic, atmospheric and hydrologic variables to ice extent in estuaries and other areas where rivers interact with marine environments; however, little focus has been placed on the Norwegian coastline (Manak and Mysak, 1989; Ogi and Tachibana, 2001; Granskog and others, 2005; Kuzyk and others, 2008). Here we first present findings of ice extent determined

from the analysis of Moderate Resolution Imaging Spectroradiometer (MODIS) satellite images from 2001 through 2019, February through May for each year, with focus placed on fjords but including coastal areas where similar oceanic and weather conditions may exist enabling ice formation. We next examine correlations between ice extent and several variables related to weather: air temperature, new snowfall and rainfall plus snowmelt.

2. Data and Methods

2.1 Analysis of imagery and measurement of ice extent

Many of the fjords along the Norwegian coastline are narrow (<2 km wide), with steep slopes, and often experience cloudy weather; 24 h darkness also occurs in the northern-most regions. For these reasons, remote sensing of fjords along the Norwegian coast can be challenging. In a previous study examining ice cover in the northern Norwegian fjord of Porsangerfjorden, false color images were manually examined to determine changes in ice extent through time (Petrich and others, 2017). Here, a similar approach is taken but automated using Google Earth Engine.

The MOD09A1.006 Surface Reflectance 8-Day Global 500 m dataset was chosen to be analyzed (Vermote, 2015). This dataset provides surface spectral reflectance values of Terra, a NASA satellite that began collecting environmental data in 2000, MODIS bands 1 through 7 with corrections for atmospheric conditions including gasses and aerosols. For each pixel, one value is chosen over an 8-day period based on cloud cover and solar zenith. Given the frequency of cloud cover along coastal Norway, an instrument performing daily passes is ideal. Additionally, through using the 8-day composite, corrections are made to decrease, but do not remove all, the possible influence of clouds on results. If several pixels over the 8-day period are found to be of equal quality, the one having the lowest reflectance in channel 3 is used. To illuminate ice, the following formula was applied:

Ice Index = Band 3 – (Band 6 + Band 7).

These three bands are commonly used in false color images. Band 3, in the visible part of the spectrum (459–479 nm), reflects well off ice while Band 6 (1628–1652 nm) and Band 7 (2105–2155 nm) are both absorbed. Reflectance in the latter two is indicative of cloud cover, of concern given the possibility of cloud cover in these regions over periods of time longer than the 8-day time span composite is created. Thus, by using the three bands in combination, ice is illuminated while further minimizing the impact of cloud cover on results. To ensure only ice on the ocean surface was considered and no pixels of snow-covered land or in-land ice were included, the MOD44W.005 Land Water Mask was applied. Having a resolution of 250 m, this mask is derived from the MODIS and Shuttle Radar Topography Mission (SRTM) data (Carroll and others, 2017).

Prior to the calculation of ice extent, all images were filtered based on quality and cloud cover using Quality Assessment (QA) and State Quality Assessment (StateQA) data, respectively. For QA data, the first 30 bits were examined with only pixels defined as being of 'ideal quality' for all bands included in analysis, thus filtering out any pixels marked as 'less than ideal quality' or not corrected for atmospheric effects due to clouds. For StateQA data, the first three bits were processed which provide a description of cloud state and cloud shadow. Pixels were filtered to include only those having a 'clear' cloud state (as opposed to 'cloudy', 'mixed', 'not set') and no cloud shadow. The majority of the following analysis was completed using results from images filtered using both QA and StateQA data. A comparison to results produced when only QA data were used is still provided however due to the observed frequency of cloud cover by the authors in northern Norway in wintertime (Fig. 3). Filtering using QA and StateQA may result in an underestimation despite the 8-day composite being used to select images with the lowest cloud cover. On average, ice extent was 38% lower in results filtered using both QA and StateQA data. The four most southern regions, Oslo–Kristiansand, Kristiansand–Stavanger, Stavanger–Bergen and Bergen–Ålesund, showed the greatest similarity between the two types of filtering, falling below this average. The remaining six regions were above.

For analysis, focus was placed primarily on fjords but also included several narrow channels and areas with a high density of small islands and inlets. Smaller fjords/inlets were also often grouped together (Figs 1 and 2) given the length of the coastline. A region of interest (ROI) was created around each, a total of 386, with boundaries determined subjectively by the coastline and natural breaks (i.e. abrupt changes in fjord width, direction, etc.). Each ROI was drawn manually in Google Earth Engine using the polygon tool to output a geometry object and are specific for use in this work, not being used previously. Pixels that are partially (>0.50%) within the ROI are weighted based on the fraction of the pixel included in the region. Visually inspecting the land mask shows generally good agreement, but areas where there is not perfect alignment are evident. This can introduce an overestimation due to land being mistaken as water with snow cover being identified as ice. Through creating ROIs that follow the coastline closely, the possibility of misidentification is further prevented. In addition, through normalization of ice extent by maximum ice extent, any remaining error is lessened assuming more constant conditions (snow or no snow) on land than in the water. Any fjords having an ice extent >5 km^2 were also manually examined to further ensure accurate results.

To determine ice extent, the number of pixels within each ROI having an ice band value above 0.3 were counted. Given an array of ice (e.g. homogeneous snow covered, meltwater, bare ice) and atmospheric conditions, setting a threshold proved non-trivial. Depending on the region and fjord, ice band values for pixels holding ice could vary from where the threshold was set, 0.3, upwards to ~0.7. Pixels with high reflectances (indicative of ice) in band 3 also could have high values in bands 6 and 7. The result often led to ice band values between 0.2 and 0.3; however, while such a pixel could have held ice, clouds were also possibly present influencing results. Such pixels were often filtered out using StateQA data; however, by applying the 0.3 threshold, further reassurance is provided that only ice is counted.

The sum of pixels holding ice was multiplied by the area of the pixel, often varying slightly from 0.25 km^2 (expected for a 500 m pixel) given MODIS is produced in a geographic coordinate system and referenced to a spheroid. The calculation was done at a scale of 500 m, the average value of a pixel within the spheroid and the resolution of the MOD09 dataset. The land mask was therefore downscaled to a lower resolution. For fjords above the Arctic Circle, no images are gathered between 1 November and 2 February. Values of maximum ice extent therefore apply to ice observed between 2 February and 24 May. It is important to note however that ice may have been present and extended further during the period no images were gathered.

For every fjord/coastal area, a maximum ice extent for each year of analysis, 2001–2019, was obtained. These data acted as a starting point to determine if any significant trends existed as well as revealed the spread of values for ice extent in individual fjords, highlighting which showed particularly high extent, >5 km^2. Given the large number of fjords outlined, the majority of analysis here is presented with ROIs grouped into regions, created based primarily on features in the coastline (Figs 1 and 2), namely Oslo–Kristiansand (a), Kristiansand–Stavanger (b), Stavanger–Bergen (c), Bergen–Ålesund (d), Ålesund–Vik (e), Vik–Bodø (f), Bodø–Narvik (g), Narvik–Lofoten–Harstad (h),

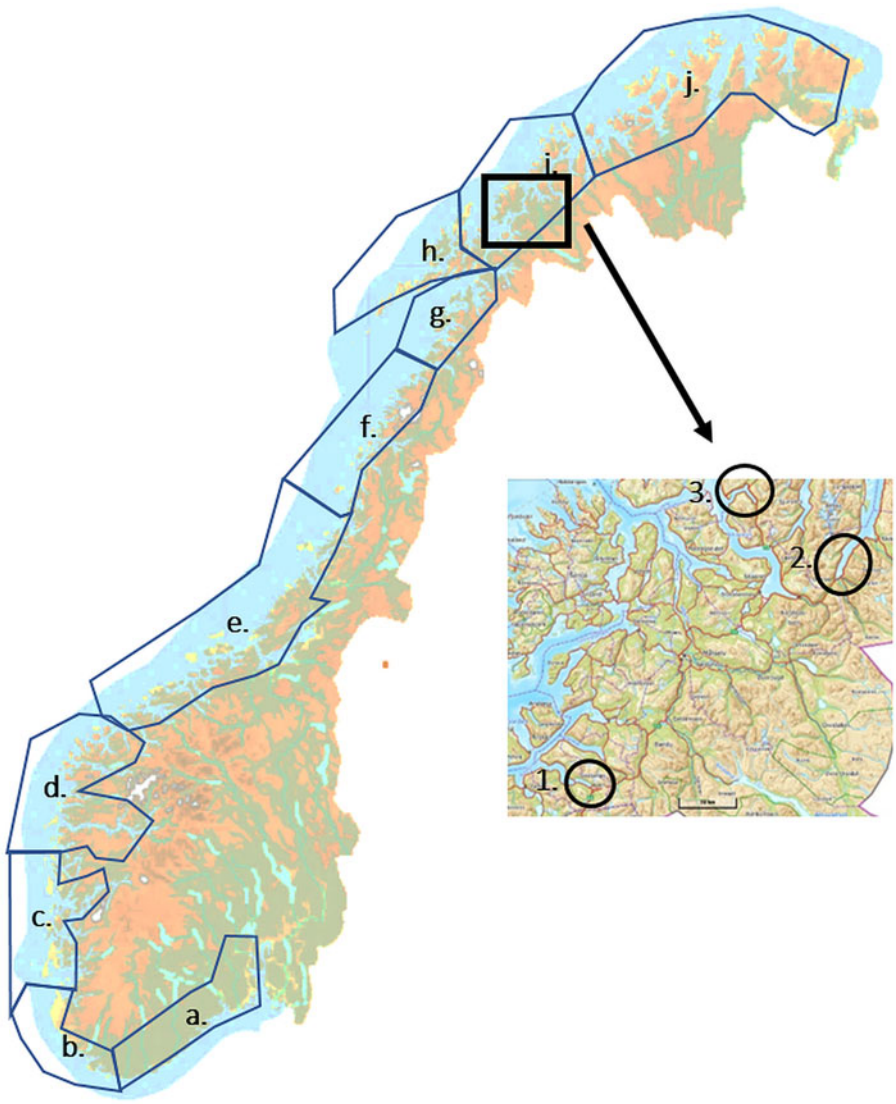

Fig. 1. Norwegian coastline with regions used for analysis outlined. (a) Oslo–Kristiansand; (b) Kristiansand–Stavanger; (c) Stavanger–Bergen; (d) Bergen–Ålesund; (e) Ålesund–Vik; (f) Vik–Bodø; (g) Bodø–Narvik; (h) Narvik–Lofoten–Harstad; (i) Harstad–Skjervøy; (j) Skjervøy–Kirkenes. The boxed area shows the three fjords examined closer, (1) Gratangsbotn, (2) Storfjord and (3) Sørbotn/Ramfjord.

Fig. 2. Example of region-of-interest (ROI) placement and point selection for weather data for the Skjervøy–Kirkenes (j) region.

Harstad–Skjervøy (i) and Skjervøy–Kirkenes (j). Through grouping the numerous ROIs, analysis can begin examining the variations between years and possible causes, potentially directing future studies where individual fjords are examined. To provide an example of how regional findings may differ from that of individual fjords, three fjords from the Harstad–Skjervøy region were selected Gratangsbotn (a), Storfjord (b) and Sørbotn/Ramfjord (c) (Fig. 1).

Ice extent was summed between all fjords in a region for each date included in the time span investigated, with a maximum ice extent found for each year (Fig. 3). For each region, the yearly maximum was normalized by the highest maximum of ice extent observed from 2001 through 2019. This was done for results obtained when images were filtered using only QA data, to remove pixels of poor quality, and QA and StateQA data, to remove pixels of poor quality and those with clouds present. The normalized ice extent for each region was used in the subsequent analysis comparing ice extent to ancillary data.

2.2 Analysis of ancillary data

The relationship was examined between ice extent and two variables enabling fjord ice formation, cold weather and a source of fresh water. Estimates of daily new snowfall, daily snow melt

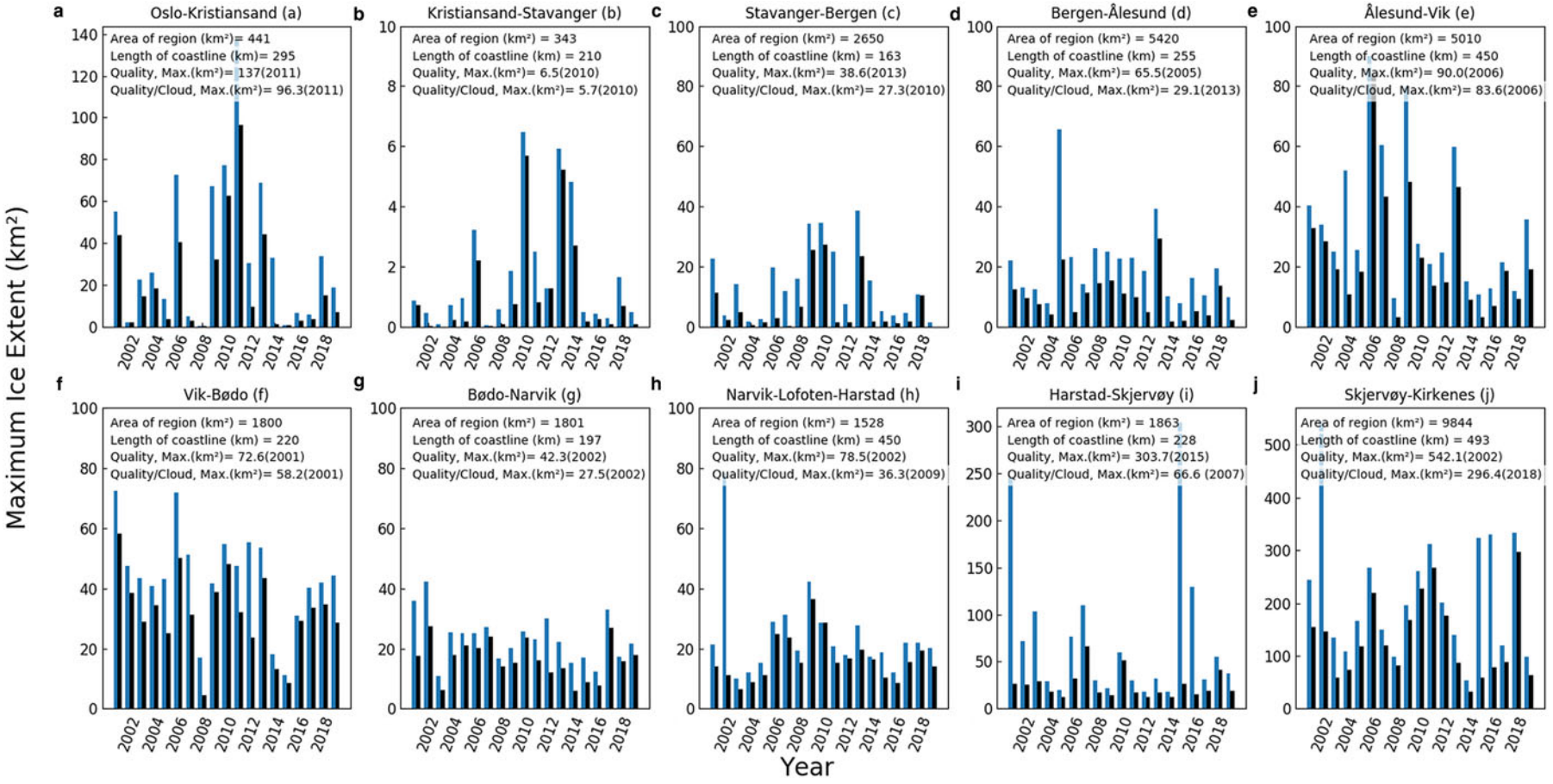

Fig. 3. Maximum ice area for each region and year with comparison between filtering methods using only quality, QA, data (blue) and quality and cloud, QA and StateQA, data (black). The area, length of outer coastline and maximums for both filtering approaches are also provided for each region. (a) Oslo–Kristiansand; (b) Kristiansand–Stavanger; (c) Stavanger–Bergen; (d) Bergen–Ålesund; (e) Ålesund–Vik; (f) Vik–Bodø; (g) Bodø–Narvik; (h) Narvik–Lofoten–Harstad; (i) Harstad–Skjervøy; (j) Skjervøy–Kirkenes. Note, while the *y*-axis scale is generally consistent, it differs on plots for regions (b), (i) and (j).

and rainfall, and daily average temperature were obtained through seNorge (Lussana and others, 2016). This open online database provides several datasets including rain, snow and temperature used most often for the monitoring and prediction of hazards including avalanches, floods and landslides. Data are only available for land-based locations. Temperature data are interpolated at 1 km resolution from point observations from ~230 measurement stations across Norway. Values for daily rainfall plus snowmelt in millimeters provide an estimate of total water supply and are based on point measurements from ~400 stations that are interpolated onto a 1 km grid (Engeset, 2016). Daily new snowfall in millimeters is provided by the Norwegian Water Resources and Energy Directorate (NVE) and is calculated from models using the temperature and precipitation data described above. Both snow and weather data have a resolution of 1 km and a time resolution of 24 h.

Given unknowns as to where runoff may end up and subsequently mix with fjord water, total runoff from the catchment area around a fjord was not considered. Representative temperature, new snowfall, and rainfall plus snowmelt data for each region were obtained by selecting one point at the head of each fjord near to sea level for all contained in each region (Fig. 2). Through using only one location from each fjord/coastal area, an understanding of the general weather patterns and their potential impact on fresh water in the fjord for a given year is provided. This allows for examination of how such weather patterns may influence ice formation without introducing unknown artifacts, for example, some fjords may have strong gradients in temperature throughout the fjord while others not as much, some fjords may have many river inlets while others only have one main source of water. Using the approach outlined here, an understanding of the general weather patterns and their influence on ice extent over the time span examined can begin to form with findings useful in future studies focused on specific regions or weather variables.

For correlation analysis, cumulative daily new snowfall and daily rainfall plus snowmelt were calculated from 1 November to 30 April of each year. This range of dates differs from the period ice extent is examined to account for the possible influence of snowfall and rainfall/snowmelt prior to freeze-up. Freezing degree days (FDD), the sum of average daily temperatures below 0°C, was determined during this time period as well. As fresh water may enable formation, the freezing temperature of fresh water (0°C) was set as the threshold to calculate FDD, although this may vary depending on the fjord and timing of freeze-up in relation to weather events (e.g. Weeks and Ackley 1982).

3. Results

3.1 Maximum ice extent in fjords

While the majority of the analysis presented here focuses on the ten selected regions, results from individual fjords and areas along the coast were also examined to understand if and how many contributed most to higher values of ice extent. Often this led to manually sorting through images to ensure accuracy. Of the 386 fjords/coastal areas examined, 47 had over 5 km^2 of ice during at least one season between 2001 and 2019. The majority of areas with high ice extent were found in the Skjervøy–Kirkenes region, 22 out of 47, while Ålesund–Vik came in second with seven out of 47. Additionally, Vik–Bodø had five out of 47; Bergen–Ålesund had four out of 47; Oslo–Kristiansand, Stavanger–Bergen, Narvik–Lofoten–Harstad and Harstad–Skjervøy all had two each out of 47; and Bodø–Narvik had one. While these values are driven by the overall area of the ROI (the reason why the following results are presented normalized), they provide context for where ice may be expected and to what degree. Additionally, such findings motivate the continuing analysis of why some fjords/coastal areas display years with high extent and relatedly, how ice varies through a season and between years and the main contributing factors.

Table 1. Results from linear least-squared regression trend analysis for ice extent by region from 2001–2019

	Correlation coefficient (r)	p-value
Oslo–Kristiansand	−0.14	0.58
Kristiansand–Stavanger	0.12	0.63
Stavanger–Bergen	−0.03	0.91
Bergen–Ålesund	−0.22	0.36
Ålesund–Vik	−0.33	0.16
Vik–Bodø	−0.33	0.17
Bodø–Narvik	−0.24	0.32
Narvik–Lofoten–Harstad	0.08	0.74
Harstad–Skjervøy	−0.13	0.59
Skjervøy–Kirkenes	−0.03	0.9

3.2 Trends in regional ice extent

3.2.1 Trends from 2001 to 2019

No statistically significant trend ($p < 0.05$) was found between ice extent and variations between 2001 and 2019 when a linear least-squared trend regression analysis was performed (Table 1). Between years and through individual seasons however, variations were observed sometimes consistently and sometimes unique to each region. In the following, the factors driving these findings are of focus.

3.2.2 Patterns in seasonal and interannual ice extent

Depending on the year, the area of ice in a region was non-existent, increased and decreased gradually, or showed abrupt changes between images (Fig. 7). In the southern three regions, Oslo–Kristiansand (a), Kristiansand–Stavanger (b) and Stavanger–Bergen (c), several years revealed a total ice extent <0.20 the maximum or no ice at all (Fig. 4). For example, 2007 was a year of very low ice extent in these three regions. Additionally, between 2014 and 2017, regions (a), (b) and (c) have had ice extents consistently lower than 0.50 the maximum. In 2018, ice extent increased but returned to similarly low values in 2019. The next two regions, Bergen–Ålesund (d) and Ålesund–Vik (e), also show a similar pattern but with longer periods having a small area of ice each year.

For the regions of Vik–Bodø (f), Bodø–Narvik (g), Narvik–Lofoten–Harstad (h), Harstad–Skjervøy (i) and Skjervøy–Kirkenes (j), ice is consistently observed each year over varying lengths of time. Gradual increases and decreases in ice extent were also more commonly observed in these regions, for example, in 2006 where all five regions generally increased to a maximum between 21 March and 6 April before a decrease. Additionally, further north, measured ice extent was more consistent between years with yearly maximum ice extent often above 0.50–0.60 of the overall maximum. Harstad–Skjervøy (i) region differs slightly with 2010 and 2018 showing noticeable extremes with all other years being more similar in total ice extent being 40–60% of the maximum.

In regions (a), (b) and (c), outside of 2013, ice was not measured after March except at very low quantities. In regions (d) and (e), the period of time where ice was observed extended into the first 2 weeks of April with the possibility of ice at very low values until May (Fig. 4). Further north, in the regions (f) and (g), ice was often found at higher quantities at the beginning of April but showed low values by 30 April with very little observed in May. The remaining two regions, (f) and (j), revealed

ice seasons extending more frequently into May but with very little ice measured after 16 May.

3.3 Correlation of maximum ice extent with weather variables

For each fjord/coastal area in a region, FDD, cumulative daily new snowfall and daily rainfall plus snowmelt were calculated. The values in Figs 5–7 represent an average over all areas within a region with std dev. also determined.

A Pearson's correlation coefficient (r) and p-value were calculated between each variable – daily snowfall, daily rainfall plus snowmelt and FDD – in comparison to maximum ice extent from 2 February and 24 May (Fig. 8, Table 2). Four out of the ten regions examined – Oslo–Kristiansand (a), Kristiansand–Stavanger (b), Stavanger–Bergen (c) and Vik–Bodø (d) – had a significant correlation between ice extent and FDD (p-value <0.05) when both filtering methods were used (Fig. 8a, Table 2). Two additional regions – Bergen–Ålesund (d) and Skjervøy–Kirkenes (j) – showed a significant correlation only when images were filtered using QA and StateQA data. Lastly, Harstad–Skjervøy (i) showed a correlation to FDD but of slightly lower significance, $p = 0.078$. The three regions that showed no

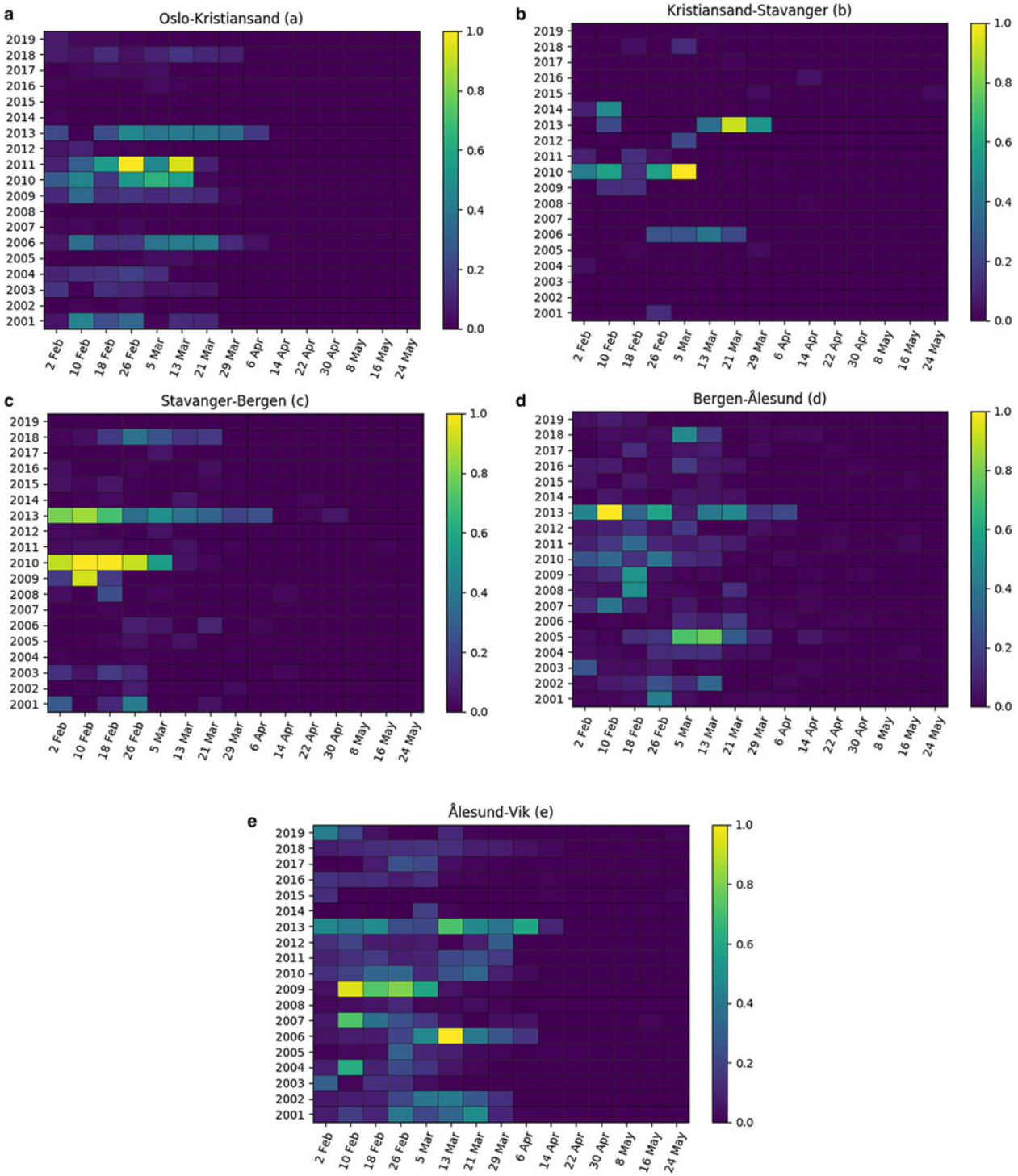

Fig. 4. Total ice extent, determined using QA and StateQA filtering, in each region for dates 2 February through 24 May, 2001 through 2019 normalized by the maximum ice extent measured during this time period. (a) Oslo-Kristiansand, (b) Kristiansand-Stavanger, (c) Stavanger–Bergen, (d) Bergen–Ålesund, (e) Ålesund–Vik, (f) Vik–Bodø, (g) Bodø–Narvik, (h) Narvik–Lofoten–Harstad, (i) Harstad–Skjervøy, (j) Skjervøy–Kirkenes.

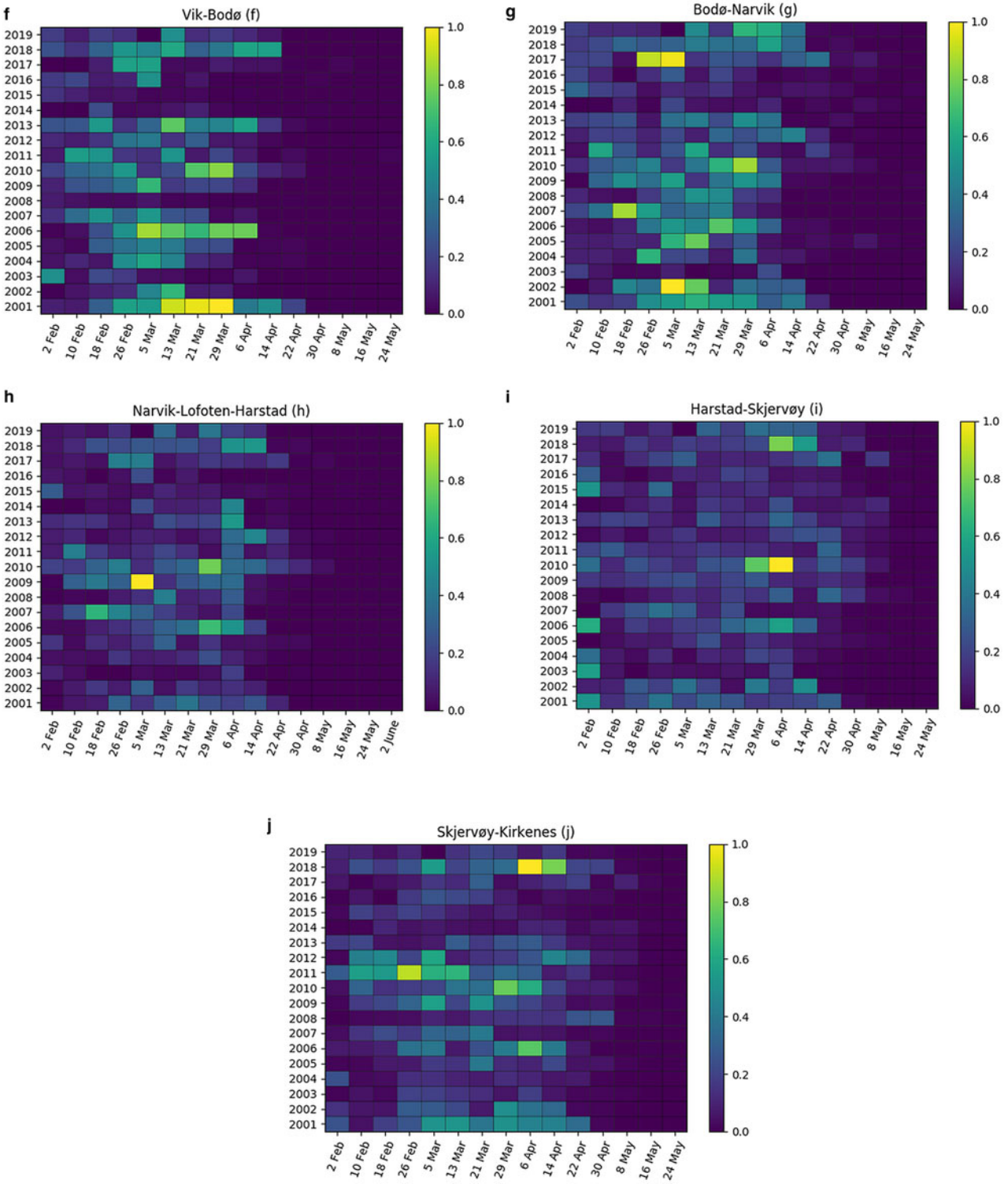

Fig. 4. Continued.

significant correlation to FDD were Ålesund–Vik (e), Bodø–Narvik (f) and Narvik–Lofoten–Harstad (i). Significant correlations to the two other variables presented were less frequent. Stavanger–Bergen (c) showed a significant negative correlation to rain plus snowmelt using both filtering methods (Fig. 8b, Table 2). Both Oslo–Kristiansand (a) and Bodø–Narvik (g) showed a significant correlation to snowfall, the latter only when using QA/StateQA filtering (Fig. 8c, Table 2). Seven out of ten regions showed good agreement between the two filtering methods used. The three regions where filtering by QA/StateQA versus only QA showed disagreement resulting in no significant correlation were Bergen–Ålesund (d), Narvik–Lofoten–Harstad (h) and Harstad–Skjervøy (i).

3.4 Selected fjords in the Harstad–Skjervøy region

3.4.1 Ice extent

To begin addressing smaller scale, local variations in ice extent, we chose three fjords located within 100 km of each other – Gratangsbotn, Storfjord and Sørbotn/Ramfjord, each located in the Harstad–Skjervøy region (i) (Fig. 1). The shape of each fjord offers an example of the variety one can expect

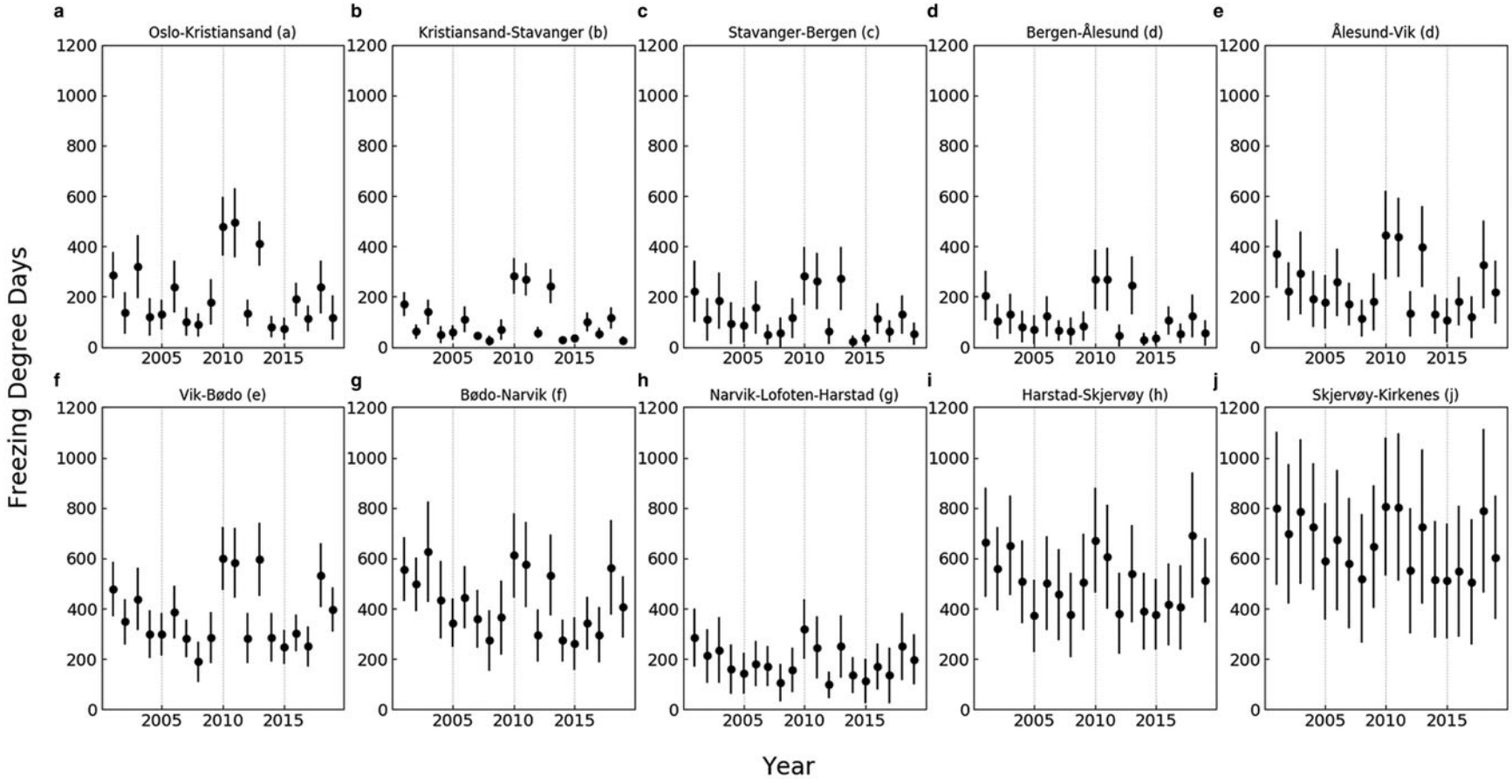

Fig. 5. Average freezing degree days for each region and year, calculated between 1 November and 30 April, with bars representing std dev.. (a) Oslo–Kristiansand; (b) Kristiansand–Stavanger; (c) Stavanger–Bergen; (d) Bergen–Ålesund; (e) Ålesund–Vik; (f) Vik–Bodø; (g) Bodø–Narvik; (h) Narvik–Lofoten–Harstad; (i) Harstad–Skjervøy; (j) Skjervøy–Kirkenes.

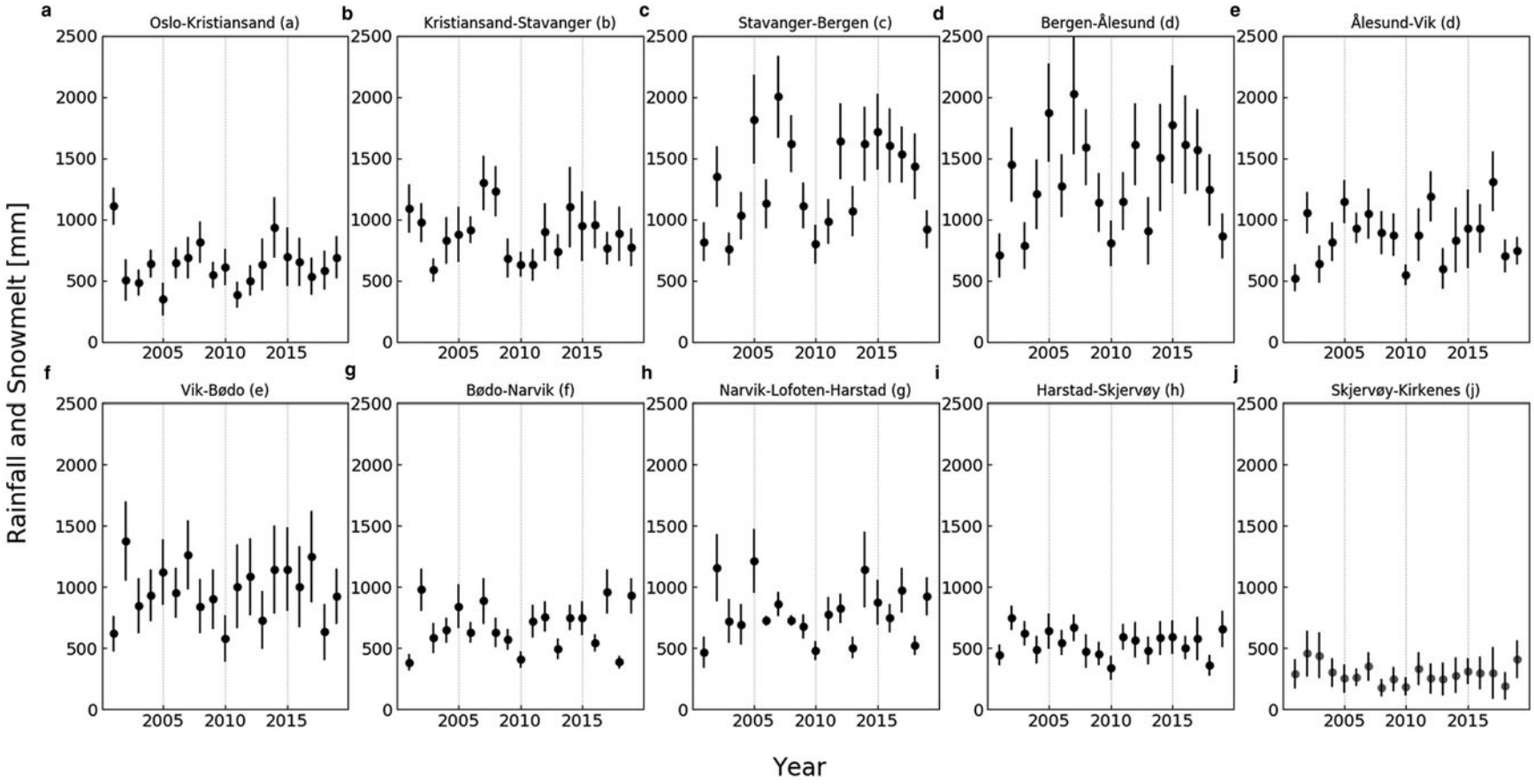

Fig. 6. Average sum of rainfall plus snowmelt for each region and year, calculated between 1 November and 30 April, with bars representing std dev. (a) Oslo–Kristiansand; (b) Kristiansand–Stavanger; (c) Stavanger–Bergen; (d) Bergen–Ålesund; (e) Ålesund–Vik; (f) Vik–Bodø; (g) Bodø–Narvik; (h) Narvik–Lofoten–Harstad; (i) Harstad–Skjervøy; (j) Skjervøy–Kirkenes.

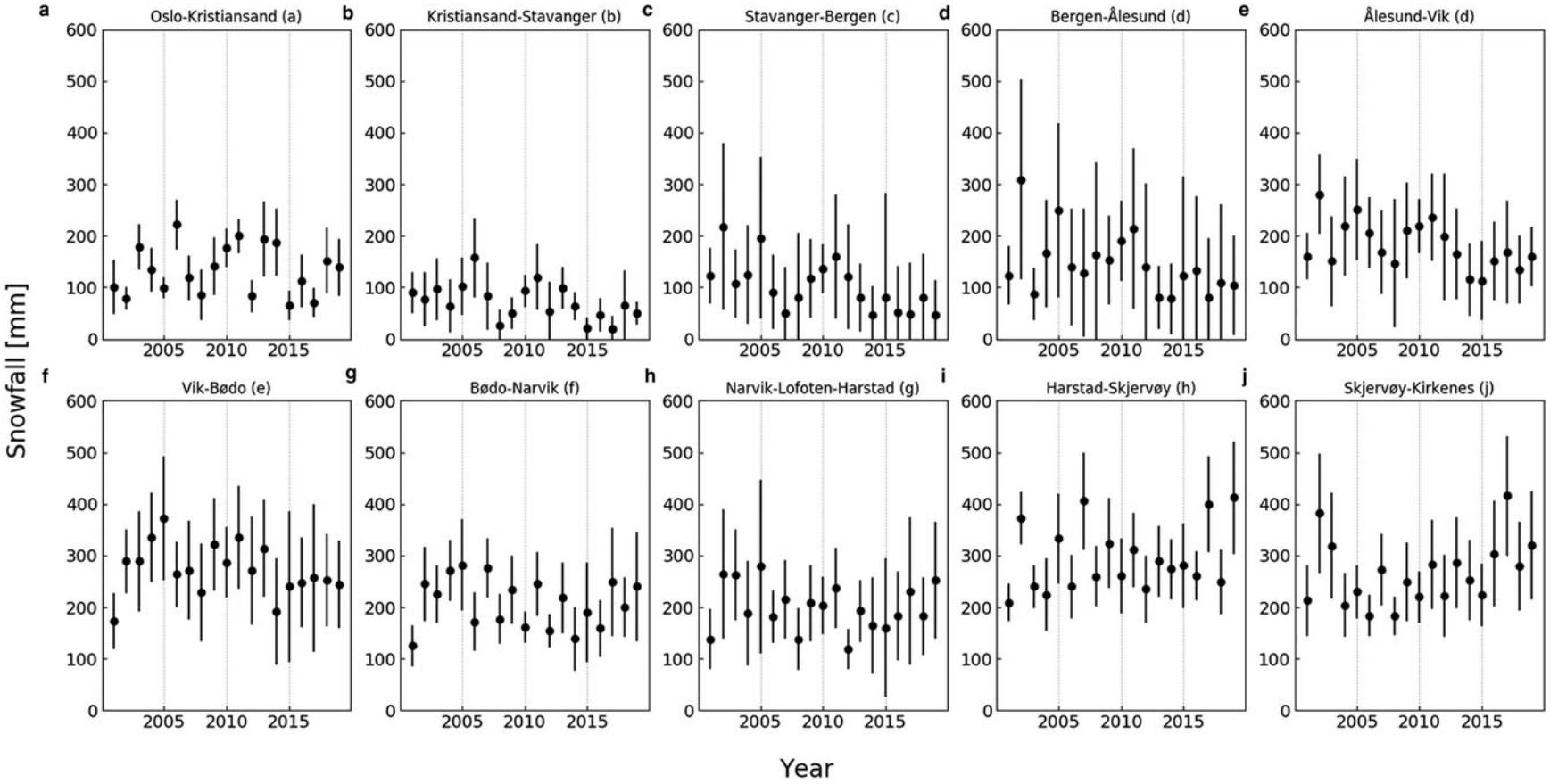

Fig. 7. Average sum of snowfall for each region and year, calculated between 1 November and 30 April, with bars representing std dev. (a) Oslo–Kristiansand; (b) Kristiansand–Stavanger; (c) Stavanger–Bergen; (d) Bergen–Ålesund; (e) Ålesund–Vik; (f) Vik–Bodø; (g) Bodø–Narvik; (h) Narvik–Lofoten–Harstad; (i) Harstad–Skjervøy; (j) Skjervøy–Kirkenes.

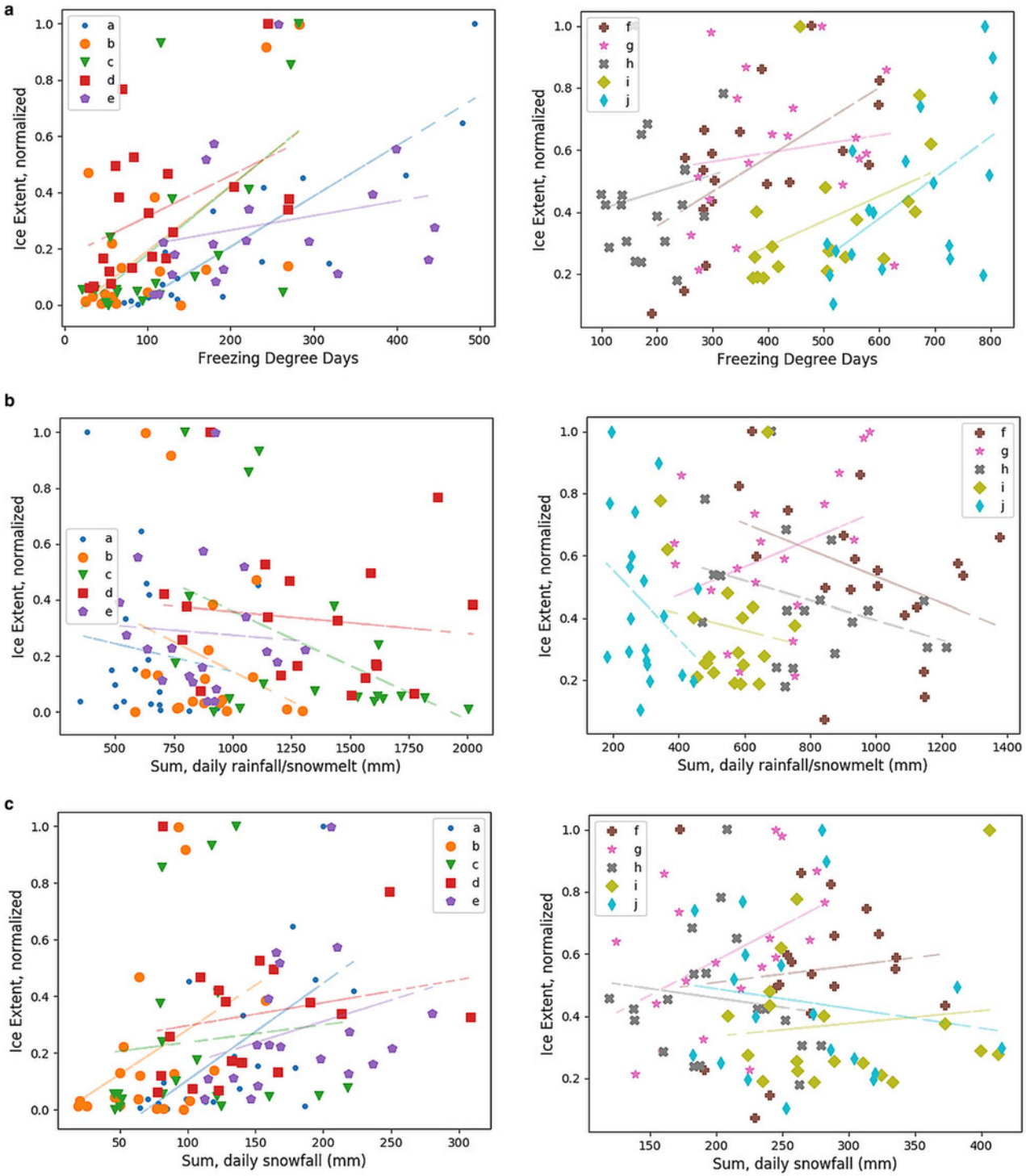

Fig. 8. Normalized ice extent filtered using QA and StateQA data compared to (a) freezing degree days, (b) sum of daily rainfall plus snowmelt and (c) sum of daily new snowfall for regions. A linear trend line for each region is included to highlight the relationship between and spread of data points. (a) Oslo–Kristiansand; (b) Kristiansand–Stavanger; (c) Stavanger–Bergen; (d) Bergen–Ålesund; (e) Ålesund–Vik; (f) Vik–Bodø; (g) Bodø–Narvik; (h) Narvik–Lofoten–Harstad; (i) Harstad–Skjervøy; (j) Skjervøy–Kirkenes.

when examining these regions closer (Fig. 9). Gratangsbotn (Fig. 9a) has a fairly consistent width of ~1 km except at its mouth where the fjord narrows to 300 m and the depth decreases to <10 m. Sørbotn/Ramfjord (Fig. 9c), while also having a consistent width between 800 m and 1 km, has a distinct nearly 90° turn with variations in depth throughout. Storfjord (Fig. 9b) is wider being 1.5–2 km in width where ice is known to form. The fjord is substantially longer, extending nearly 75 km, widening and breaking off into other smaller fjords along the way.

Ice extent for the three fjords since 2001 is presented in Figure 10. Each fjord differs in seasonal and annual variations in ice extent. In Gratangsbotn, years of low ice extent are separated by peaks where ice is present often over a period of time upwards of 2 months in length (Fig. 10a). During the years with ice, the maximum ice extent reached is relatively consistent with >0.50 of the maximum (2010) reached in five separate years. Storfjord showed fewer years of similar ice extent (Fig. 10b), with years of very little or no ice separated by years with none or short-lived ice. In 2018 however, ice was observed

Table 2. Pearson's correlation coefficient and *p*-value between ice extent and three variables for each region

	Ice area and freezing degree days		Ice area and rain + snowmelt		Ice area and snowfall		Filtering method QA/StateQA and only QA
	QA/State QA	QA	QA/State QA	QA	QA/State QA	QA	
Oslo–Kristiansand (a)	0.886 (0.000)	0.815 (0.000)	0.132 (0.589)	0.137 (0.575)	0.617 (0.005)	0.713 (0.001)	0.961 (0.000)
Kristiansand–Stavanger (b)	0.647 (0.003)	0.62 (0.005)	−0.282 (0.243)	−0.285 (0.237)	0.372 (0.117)	0.412 (0.079)	0.963 (0.000)
Stavanger–Bergen (c)	0.608 (0.006)	0.721 (0.000)	−0.451 (0.053)	−0.476 (0.039)	0.094 (0.703)	0.048 (0.845)	0.844 (0.000)
Bergen–Ålesund (d)	0.454 (0.051)	−0.285 (0.237)	−0.122 (0.619)	−0.053 (0.829)	0.197 (0.419)	0.055 (0.823)	−0.284 (0.239)
Ålesund–Vik (e)	0.242 (0.319)	0.14 (0.567)	−0.063 (0.796)	−0.083 (0.734)	0.29 (0.228)	0.334 (0.162)	0.909 (0.000)
Vik–Bødo (f)	0.617 (0.005)	0.528 (0.020)	−0.411 (0.08)	−0.298 (0.215)	0.114 (0.643)	0.143 (0.559)	0.880 (0.000)
Bødo–Narvik (g)	0.15 (0.541)	0.107 (0.663)	0.357 (0.134)	0.34 (0.154)	0.459 (0.048)	0.162 (0.508)	0.785 (0.000)
Narvik–Lofoten–Harstad (h)	0.166 (0.498)	0.168 (0.491)	−0.343 (0.151)	0.204 (0.403)	−0.135 (0.582)	0.281 (0.244)	0.318 (0.185)
Harstad–Skjervøy (i)	0.414 (0.078)	0.088 (0.721)	−0.13 (0.595)	−0.001 (0.997)	0.121 (0.623)	−0.221 (0.364)	0.271 (0.262)
Skjervøy–Kirkenes (j)	0.576 (0.01)	0.303 (0.208)	−0.336 (0.159)	0.203 (0.405)	−0.155 (0.525)	0.203 (0.404)	0.506 (0.027)

Significant correlations ($p < 0.05$) marked in gray. Those with $0.05 > p < 0.1$ marked in light gray. (a) Oslo–Kristiansand; (b) Kristiansand–Stavanger; (c) Stavanger–Bergen; (d) Bergen–Ålesund; (e) Ålesund–Vik; (f) Vik–Bodø; (g) Bodø–Narvik; (h) Narvik–Lofoten–Harstad; (i) Harstad–Skjervøy; (j) Skjervøy–Kirkenes.

throughout the season. Sørbotn/Ramfjord (Fig. 10c) has the most constant ice extent between all years reaching ice extents often above 0.70 of the maximum. Ice was observed every year in Sørbotn/Ramfjord although in 2016 ice extent did not reach above 0.2 of the maximum.

Comparing between fjords during specific years, differing behavior is apparent despite each being located near to each other. For instance, in 2018, Storfjord held ice from approximately 26 February to 14 April, with an abrupt break around 21 March likely due to cloud coverage. Conversely at Gratangsbotn, 2018 was a year with no to little ice, while in Sørbotn/Ramfjord, ice extent stayed below 0.4 the maximum until later in the season. In 2019 however, Storfjord had less consistent ice coverage while Gratangsbotn and Ramfjord/Sørbotn experienced the opposite.

3.4.2 Correlation to weather variables

Out of the three fjords examined individually, only Gratangsbotn showed a significant, albeit moderate, positive correlation – ice extent filtered using only QA data and snowfall (Fig. 11, Table 3). Sørbotn/Ramfjord showed a moderate positive correlation but of less significance between ice extent when filtered using QA/StateQA data and FDD. These findings are therefore partially in alignment with the Harstad–Skjervøy (Table 2) region where all three are located, which had a moderate positive correlation of lower significance to temperature for QA/StateQA filtered ice extent. Snowfall does not appear to have played a dominant role when examining the region as a whole.

4. Discussion

4.1 Connecting ice conditions to weather events

Through comparison of FDD to measurements of ice thickness, Anderson (1961) derived a relationship between these two variables to provide an accurate estimation of ice thickness knowing only FDD. Although ice extent, not ice thickness, is considered here, FDD provides a method to examine ice formation based purely on the transfer of heat between air and water. Past studies have used this measurement to look at trends in ice conditions and their possible connection to other variables such as the presence of marine and terrestrial organisms (Petrich and others, 2014). In fjords where FDD is not found to be correlated to ice extent, other factors may be playing a more dominant role in ice formation. The influence of temperature appears to be most prominent in the southern regions of Oslo–Kristiansand (a), Kristiansand–Stavanger (b) and Stavanger–Bergen (c). Moving north, this relationship is less consistent being significant (using both filtering methods) in one region located midway up the coast, Vik–Bodø (f) as well as the most northern region, Skjervøy–Kirkenes (j) using QA/StateQA filtering.

Snowfall and rainfall plus snowmelt have similarities in their potential impact on ice formation through supplying fresh water to a fjord's surface. Rainfall plus snowmelt may not contribute substantially to creating a freshwater layer when applied directly to the surface of a fjord. What likely has a larger impact is the accumulation of rain and snowmelt in rivers and streams leading into a fjord, which can create a freshwater plume and a stratified water column closer to river outlets (Ingram and others, 1996; Granskog and others, 2005). Snowfall while not leading to a thick layer of fresh water may assist in ice formation through further cooling the surface and enabling ice formation through seeding the ice. The initial enabling formation of a thin ice layer is capable of dampening small waves allowing for further ice formation (Martin and Kauffman, 1981). In addition, once a thin ice layer is created, it allows for accumulation of more snow on top, thickening and strengthening the ice to better withstand fluctuations in weather conditions. If snowfall occurs after a cohesive ice cover has formed however, this snow may alternatively slow ice formation, insulating the ice from the top and allowing more melt from below. Deeper investigation is required to assess which of the two processes, snowfall on the fjord surface versus rainfall plus snowmelt flowing into the fjord, triggers ice formation more efficiently. The mechanism for ice formation, potentially different in southern versus northern fjords, may also lead to differences in ice properties, a topic discussed more below.

The timing of both snowfall and rainfall plus snowmelt events to colder weather likely explains much of the variance in ice extent observed between years and fjords. While a thin ice layer may be able to form a number of times throughout the season, it is vulnerable to break-up given waves, tides or variations in air and water temperature. For ice to stay in place depends on the thickness, or primarily its ability to withstand changing conditions.

It is through examining specific fjords that the unique conditions needed in different regions and even fjords become more apparent. The lack of significant correlations to the three weather variables examined except Gratangsbotn's relation to snowfall illustrates the absence of a general formula combining an input of fresh water, cold weather and their respective timing. Instead, other factors impact ice formation significantly, potentially unique to individual fjords.

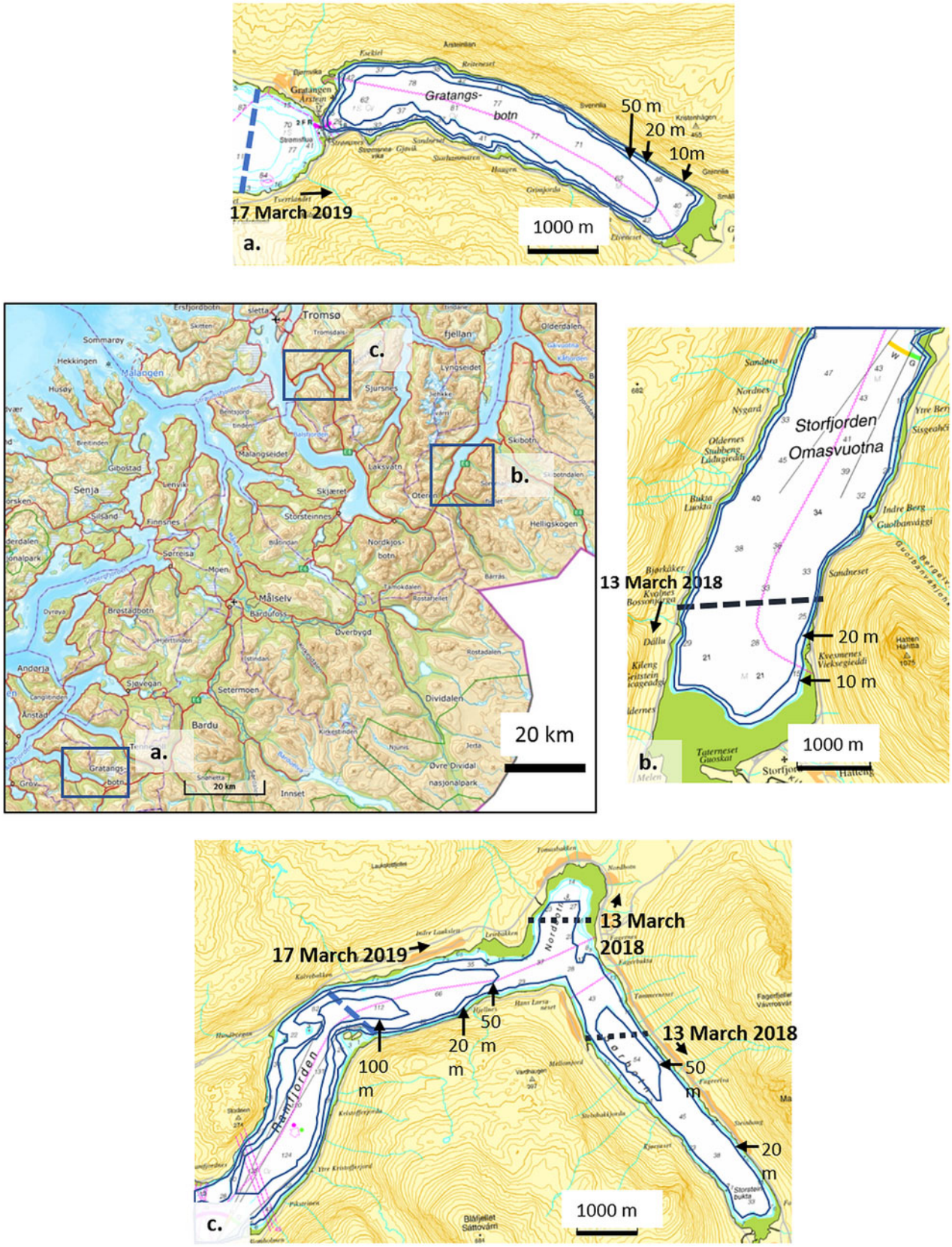

Fig. 9. Region where the three fjords discussed further are found with each separate fjord boxed and presented on a smaller scale. (a) Gratangsbotn (only ice in 2019), (b) Storfjord (only ice in 2018), (c) Sørbotn/Ramfjord. Ice extent in 2018 and 2019 for each fjord marked with a long-dash black line and short-dash blue line, respectively, and arrows pointing in direction of ice. Fjord bathymetry and depth also marked.

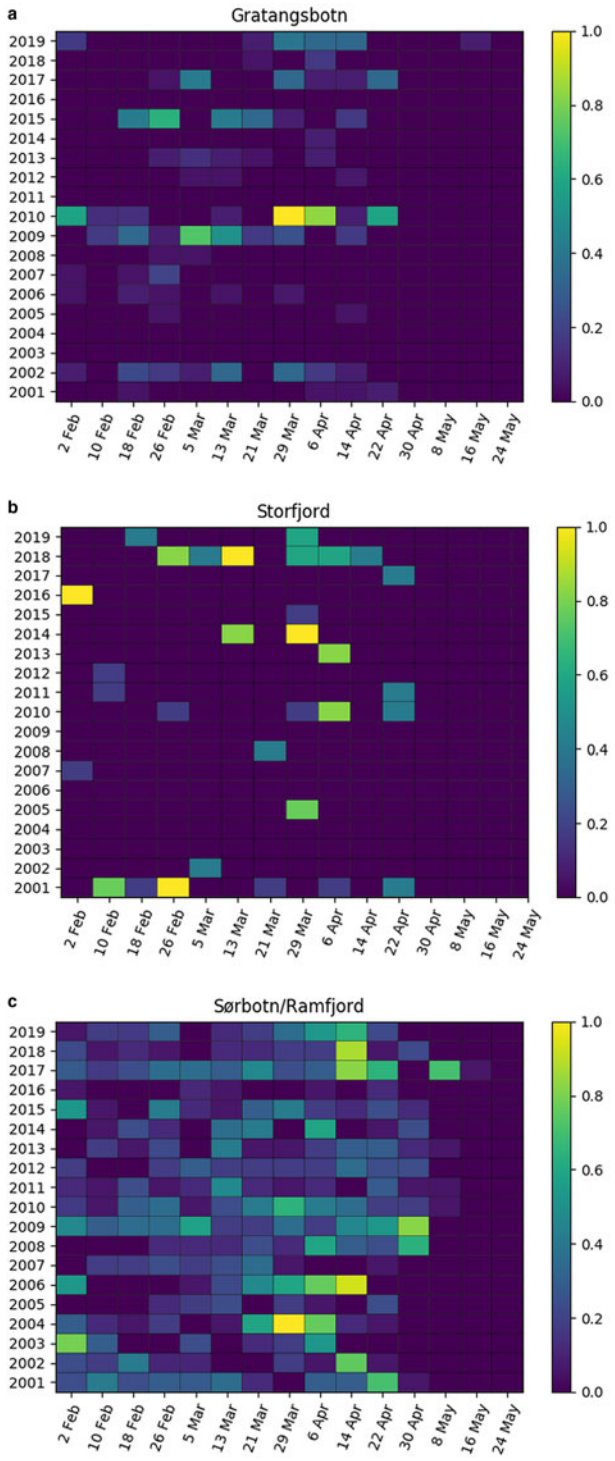

Fig. 10. Total ice extent in three fjords for dates 2 February through 24 May, 2001 through 2019 normalized by the maximum ice area measured during this time period. (a) Gratangsbotn, (b) Storfjord, (c) Sørbotn/Ramfjord.

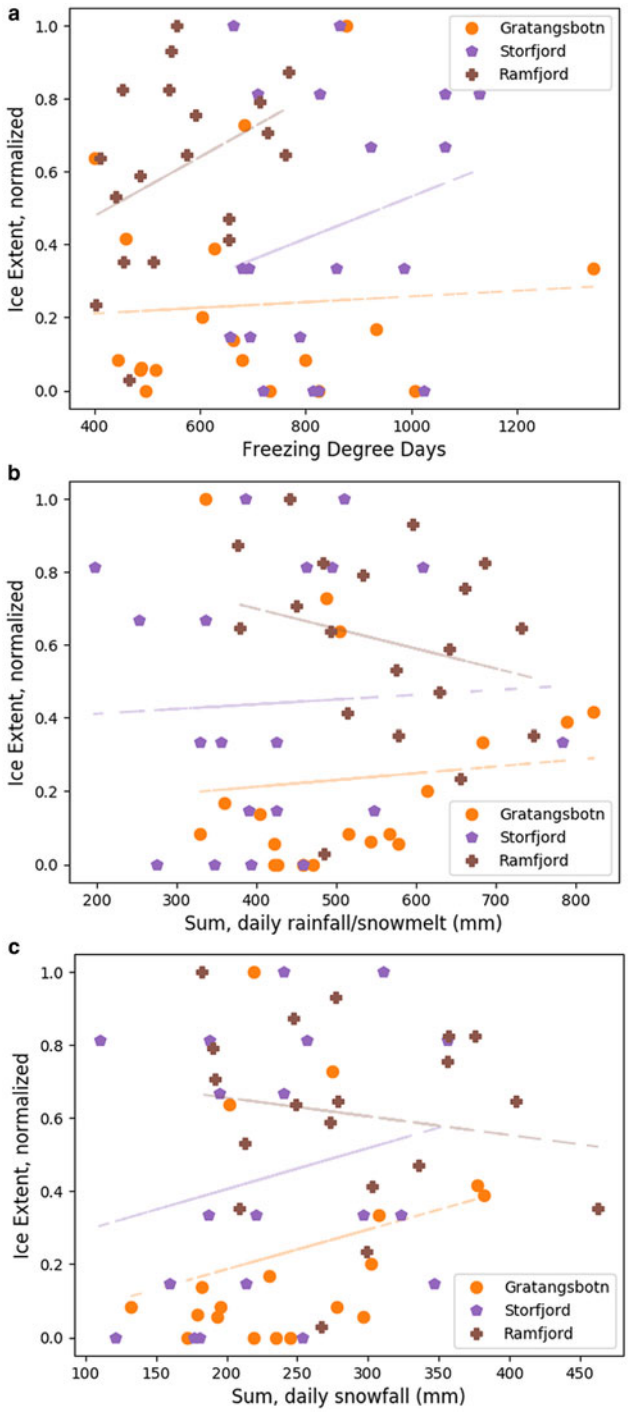

Fig. 11. Normalized ice extent filtered using QA and StateQA data compared to (a) freezing degree days, (b) sum of daily rainfall plus snowmelt and (c) sum of daily new snowfall for Gratangsbotn, Storfjord and Sørbotn/Ramfjord (marked as Ramfjord). A linear trend line for each region is included to highlight the relationship between and spread of data points.

4.2 Additional factors to consider

4.2.1 Other weather and oceanic conditions

While several weather variables are considered here, one important factor remaining is wind. Wind provides mixing energy that may act to prevent a cooler, fresher layer of water from forming ice (Manak and Mysak, 1989). Additionally, any thin ice that may be formed during a calmer period is at risk if and when wind may increase, creating waves to break-up or push ice to another area. Wind strength and direction is difficult to obtain in each individual fjord given the impact of topography which can act to shelter a fjord or conversely to funnel wind to alter predicted wind patterns. Weather models used to predict wind are often produced at resolutions too large for many of the fjords examined. In situ measurements are also limited. The impact of wind on ice conditions in fjords is an important topic that should not be overlooked when analyzing variations in ice conditions in fjords through time. The lack of a significant correlation between ice extent and the variables examined in the regions of Ålesund–Vik (e), Narvik–Lofoten–Harstad (h) and Harstad–Skjervøy (i) and additionally Bodø–Narvik (g) and Skjervøy–Kirkenes (j)

Table 3. Correlation and associated *p*-value between ice extent for each fjord of focus versus the three weather variables discussed

	Ice area and freezing degree days		Ice area and rain + snowmelt		Ice area and snowfall		Filtering method QA/StateQA and only QA
	QA/State QA	QA	QA/State QA	QA	QA/State QA	QA	
Gratangsbotn	0.065 (0.791)	0.125 (0.609)	0.091 (0.711)	0.329 (0.169)	0.260 (0.283)	0.477 (0.039)	0.942 (0.000)
Storfjord	0.019 (0.939)	−0.141 (0.564)	−0.071 (0.773)	−0.174 (0.475)	0.154 (0.528)	−0.056 (0.820)	0.703 (0.001)
Sørbotn/Ramfjord	0.380 (0.109)	0.296 (0.219)	−0.241 (0.321)	−0.019 (0.940)	−0.157 (0.521)	−0.056 (0.819)	0.857 (0.000)

Significant correlations ($p < 0.05$) marked in gray.

when both filtering methods are considered alludes to the influence of other factors, wind likely being one. In future studies, this is recommended to be examined more closely.

Another factor that may lead to mixing and disruption of the stratification that can enable ice formation is tides. Measurements of water temperature in the upper 6 m of the water column in a northern Norwegian fjord known to have ice cover show fluctuations in water temperature aligned with tidal cycles (O'Sadnick and others, 2018). Tides bring in ocean water that may also be of a different salinity, potential mixing and sweeping away layers of fresh or brackish water formed due to water runoff. They also can influence the presence of currents in a fjord (Stigebrandt, 1980; Stigebrandt and Aure, 1989) which may also impact mixing at varying depths in the water column. Modeling currents within a specific fjord is not simple due to the interaction of current with bed topography and features in the coastline. Understanding the movement of water within a fjord however is useful in determining ocean temperature and related oceanic heat flux, how it may change throughout a day, month or year and if it has potential to control ice extent.

4.2.2 Fjord geometry and bathymetry

Gratangsbotn, Sørbotn/Ramfjord and Storfjord offer an example of the diversity in fjord shape one can encounter within a region. Gratangsbotn has a distinct narrowing where a shallow sill is present. In addition, its shape and bed resemble a bathtub with depth increasing quickly a short distance from the coastline, consistent around its rim (Fig. 6). It is the only fjord out of the three that was significantly correlated to any variable examined, that being snowfall. Additionally, Gratangsbotn displayed large differences in ice extent from year to year, with ice either being non-existent or extending throughout the entirety of the fjord.

The lack of distinct features in the bed or coastline likely contributes to the consistent ice cover when it is present. This is in comparison to Sørbotn/Ramfjord where ice extent appears related to the sharp turn in its coastline as well as areas of varying water depth throughout its length. Ice extent may also be tied to the location of input and amount of fresh water entering a fjord by way of streams and rivers. In Sørbotn/Ramfjord, ice appears to form at the head of the fjord where two rivers enter. Gratangsbotn only has one main river, which itself is smaller than in many other rivers leading into fjords in the area. Given that Gratangsbotn often has a similar ice extent and also a significant correlation to snowfall, one can surmise that the river may not influence ice coverage to the same degree as in other locations like Sørbotn/Ramfjord.

Storfjord displays often the opposite behavior of Gratangsbotn (Figs 10a and b), having greater ice extent in years where Gratangsbotn has lesser or none. The fjord geometry and bathymetry of Storfjord lack abrupt changes in the coastline and ocean bed where ice is present but is considerably wider than the other two examined here, 2 km versus nearer to 1 km. When ice is present, it only extends at most a maximum of 4 km outwards despite a much longer fjord (Fig. 9b). This may be a result of currents and wind on a fjord that due to its width and length, offers less protection against the elements. The last year with substantial ice formation occurred in the winter of 2018, a notably cold and dry season. If conditions were comparatively calm with little wind and resultantly mixing, congelation ice formation due purely to cooling of the ocean from the surface downward may have been possible. Given the lack of a correlation to FDD however, it may be the relationship to another factor such as wind that played the more important role. In comparison, in a fjord such as Gratangsbotn, temperature and FDD may also not be the most important factor but rather a trigger for ice formation, i.e. snowfall just before calm conditions that allow for a strong, cohesive ice cover to form.

Through examining differences in ice extent from year to year between fjords located near to each other, our understanding of how certain factors combine to allow for ice formation can be improved. Fjords displaying similar patterns in ice extent can also be of interest however as the factors contributing may not be the same. For example, both a cold, calm year with little precipitation to form a brackish layer may display the same ice extent as a year with more precipitation but with strong winds in the days directly following. Each fjord may have a different combination of factors leading to variations in ice conditions. For each fjord or region, the questions become:

(1) What factors initiate ice formation?
(2) What factors support an increase in ice extent?
(3) What factors lead to break-up of the initial ice cover, both thin or of substantial thickness?

Understanding historically where ice is present and how it has changed between years in relation to weather and oceanic conditions, as well as its own geometry and bathymetry, helps to identify these factors.

4.3 Implications

Grouping together fjords into regions as done here allows for a first-order analysis of the factors that may be most important when examining trends in sea-ice cover. In future work, focus may be placed more on specific fjords to determine what variables contribute most to sea-ice formation and why, determining if patterns exist between fjords that show stronger correlations to such factors as FDD, snowfall or rainfall/snowmelt. Knowing what factors, and combinations of factors, are most likely to lead to ice formation in each region or fjord allows also for understanding of the properties of the ice such as thickness and porosity that are likely to result.

Ice formed primarily from snow accumulating on a layer of slush or thin ice which turns into a cohesive cover as sea water floods the surface and refreezes is termed granular ice. Such ice typically has a high porosity with pores being connected in all directions through meandering networks of channels. High porosity enables fractures to propagate more easily; this is ideal for boats looking to break through an ice cover but may cause a safety risk if traveling across (Timco and Frederking, 1982). Once it is

emplaced on top of the ocean's surface however, granular ice cover can enable and quicken the growth of congelation ice downward due to its dampening effect on waves. This process requires temperatures cold enough to counteract oceanic heat flux, the latter possibly varying between years. Congelation ice forms directly from the source water, that being either seawater or fresh water. It occurs under quiescent conditions, allowing for slow growth favoring large ice crystals. If fresh water is the source, this ice will be the lowest in porosity, appearing nearly transparent with only air bubbles throughout. In ice formed from saltwater, porosity is higher, the result of salt being rejected from the ice crystal matrix. The pores are connected particularly in the vertical dimension and have a predictable structure based on the temperature of the ice (Petrich and Eicken, 2010). The failure mechanisms differ for sea ice versus freshwater ice, the former deforming before breaking thus allowing for some animals or even humans to walk across if they have the correct technique. For all ice types, temperature will largely influence its strength (Assur, 1960).

Ice permeability, an indicator of pore connectivity, is also an important characteristic to consider when investigating how ice may interact with the surrounding environment. Given fewer pores in freshwater congelation ice, there is a lack of habitat for marine microbiota. Freshwater ice also does not offer favorable conditions for under-ice algae to grow, a potential source of nutrients for marine life during the winter and initiator of phytoplankton blooms in the summer when ice melts (Granskog and others, 2003; Kaartokallio and others, 2007). In sea ice, a connected pore space provides microbiota a pathway to move upward into the ice where they are protected from predators and can subsist on nutrients in the high salinity brine. Relatedly, algae can be found at the ice–ocean interface in the highly porous skeletal layer (Arrigo and others, 2010).

Permeability also determines how a pollutant, such as oil, may pass through the ice. Given a cover of congelation sea ice, oil has the potential to migrate up through the volume, pooling eventually on the surface allowing for cleanup. In freshwater ice, oil does not have a pathway to the surface and therefore can remain under or entrapped in the ice until warmer conditions allow for break-up (Oggier and others, 2019). These two types of ice, although similar in many aspects in the way they may impact transit through and across, may therefore have a big impact on how one would respond in the case of an oil spill cleanup.

Due to variations in weather and oceanic conditions throughout one season, ice has the possibility to fall between the categories described above – in terms of microstructure and related physical properties. Through considering the factors that ice formation in specific regions or fjords is correlated to, hypotheses can begin to be made in terms of resultant ice conditions. To determine the relation between the factors examined here (i.e. weather, fjord geometry, bed topography), further work must be done. This includes in situ ice sampling of ice properties and the analysis of remote-sensing datasets sensitive to microstructural differences at least in the upper layers of the ice (Hallikainen, 1994; Tucker and others, 1994). Unpredictable and inconsistent ice conditions present a very real risk in an Arctic where traffic is increasing. Therefore, ice conditions both in Norwegian fjords and regions with similar characteristics such as the coast of Greenland or northern Canada where fjords are numerous are an important topic of study.

5. Conclusions

The coast of Norway offers a natural laboratory to explore how differing weather, oceanic conditions, bathymetry and coastal geometry may influence ice extent, conditions and properties important for the safety of the community, those working in these regions, and the environment as a whole. From the work presented here, the following conclusions can be drawn.

- No statistically significant trend in ice extent was found when individual fjords/coastal areas were grouped into regions and total maximum ice extent analyzed between 2001 and 2019.
- Of the 386 fjords and coastal areas chosen, 47 held >5 km^2 at least once between 2001 and 2019.
- FDD, a simple measurement of how cold a winter may be in relation to potential ice growth, was significantly correlated to six out of ten regions studied. Additionally, cumulative new snowfall was significantly correlated to ice extent in two regions, and rainfall plus snowfall in one region.
- Seasonal patterns in ice cover are apparent in each region with those lying in the south appearing to break-up and reform while a more consistent ice cover is present in northern regions. The mechanisms of ice formation may influence ice properties, namely ice porosity which will determine ice strength, backscatter signal and permeability.
- The potential impact of unpredictable ice extent and ice properties on boat traffic, local communities, marine life and oil spill cleanup efforts should be considered in future studies. It is recommended to expand the analysis to incorporate more in situ measurements of ice and weather conditions, the latter including wind. Additionally, other regions of the Arctic where fjords are prevalent including northern Canada and Greenland should be examined under a similar lens to determine if similarities exist.

Acknowledgements. This work is funded by the Centre for Integrated Remote Sensing and Forecasting for Arctic Operations (CIRFA), a Centre for Research-based Innovation (Research Council of Norway project number 237906). In addition, we thank the two anonymous reviewers whose constructive feedback greatly added to the presentation and text of the final paper.

References

Anderson DL (1961) Growth rate of sea ice. *Journal of Glaciology* **3**(30), 1170–1172. doi: 10.3189/S0022143000017676

Arctic Marine Shipping Assessment (2009) Arctic Council April 2009, second printing. Tromsø: Arctic Council.

Arndt S and Nicolaus M (2014) Seasonal cycle and long-term trend of solar energy fluxes through Arctic sea ice. *Cryosphere* **8**, 2219–2233. doi: 10.5194/tc-8-2219-2014

Arrigo KR and 6 others (2014) Phytoplankton blooms beneath the sea ice in the Chukchi sea. *Deep-Sea Research Part II: Topical Studies in Oceanography* **105**, 1–16. doi: 10.1016/j.dsr2.2014.03.018

Arrigo K, Mock T and Lizotte M (2010) Primary producers and sea ice. In Thomas D and Dieckmann G (eds), *Sea Ice*, 1st Edn. Oxford: Wiley-Blackwell, pp. 283–326.

Asplin L, Salvanes AGV and Kristoffersen JB (1999) Nonlocal wind-driven fjord-coast advection and its potential effect on plankton and fish recruitment. *Fisheries Oceanography* **8**(4), 255–263. doi: 10.1046/j.1365-2419.1999.00109.x

Assur A (1960) Composition of sea ice and its tensile strength. *SIPRE Research Report* **44**.

Carroll ML and 5 others (2017) MOD44W MODIS/Terra land water mask derived from MODIS and SRTM L3 global 250 m SIN grid V006 [data set]. NASA EOSDIS land processes DAAC. Available at doi: 10.5067/MODIS/MOD44W.006

Cottier FR, Nilsen F, Skogseth R, Tverberg V, Skarðhamar J and Svendsen H (2010) Arctic fjords: a review of the oceanographic environment and dominant physical processes. *Geological Society, London, Special Publications* **344**(1), 35–50.

Eilertsen HC and Skardhamar J (2006) Temperatures of north Norwegian fjords and coastal waters: variability, significance of local processes and air-sea heat exchange. *Estuarine, Coastal and Shelf Science* **67**(3), 530–538. doi: 10.1016/j.ecss.2005.12.006

Engeset R (2016) How are weather and snow data produced for seNorge.no and XGEO.no ? Available at https://www.nve.no/Media/4816/weatherandsnowdata_v2_en.pdf

Gade HG (1986) Features of fjord and ocean interaction. In Hurdle BG ed. *The Nordic Seas*. New York, NY: Springer, 183–190. doi: 10.1007/978-1-4615-8035-5_7.

Gradinger R (2009) Sea-ice algae: major contributors to primary production and algal biomass in the Chukchi and Beaufort Seas during May/June 2002. *Deep-Sea Research Part II: Topical Studies in Oceanography* **56**(17), 1201–1212. doi: 10.1016/j.dsr2.2008.10.016

Granskog MA, Ehn J and Niemelä M (2005) Characteristics and potential impacts of under-ice river plumes in the seasonally ice-covered Bothnian Bay (Baltic Sea). *Journal of Marine Systems* **53**(1–4), 187–196. doi: 10.1016/j.jmarsys.2004.06.005

Granskog MA, Kaartokallio H and Shirasawa K (2003) Nutrient status of Baltic Sea ice : evidence for control by snow-ice formation, ice permeability, and ice algae. *Journal of Geophysical Research* **108**, 3253. doi: 10.1029/2002JC001386.

Hallikainen M (1994). Microwave remote sensing of low-salinity sea ice. In Carsey FD (ed.), *Microwave Remote Sensing of Sea ice*, 68th Edn. American Geophysical Union, 361–373. doi: 10.1029/GM068

Hopkins CCE, Tande KS and Grønvik S (1984) Ecological investigations of the zooplankton community of Balsfjorden, Northern Norway. *Journal of Experimental Marine Biology and Ecology* **82**, 77–99.

Hughes N (2006) *NP57A, NP57B, NP58A, NP58B Norway Pilot. Sea Ice Conditions: West Coast of Norway from: Lindesnes to Statlandet, Statllandet to Risværfjorden. Offshore and Coastal Waters of Norway from: Risværfjorden to the North Part of Vesterrålen, Andfjorden to Varang*. Argyll, UK: Scottish Association for Marine Science.

Ingram RG, Wang J, Lin C, Legendre L and Fortier L (1996) Impact of freshwater on a subarctic coastal ecosystem under seasonal sea ice (southeastern Hudson Bay, Canada). I. Interannual variability and predicted global warming influence on river plume dynamics and sea ice *. *Journal of Marine Systems* **7**, 221–231.

Kaartokallio H, Kuosa H, Thomas DN, Granskog MA and Kivi K (2007) Biomass, composition and activity of organism assemblages along a salinity gradient in sea ice subjected to river discharge in the Baltic Sea. *Polar Biology* **30**, 183–197. doi: 10.1007/s00300-006-0172-z

Kuzyk ZA, Macdonald RW, Granskog MA and Scharien RK (2008) Sea ice, hydrological, and biological processes in the Churchill River estuary region, Hudson Bay. *Estuarine, Coastal and Shelf Science* **77**, 369–384. doi: 10.1016/j.ecss.2007.09.030

Lussana C, Tveito O and Uboldi F (2016) Senorge v2.0: an observational gridded dataset of temperature for Norway. Met. No Report 14.

Manak DK and Mysak LA (1989) On the relationship between arctic sea-ice anomalies and fluctuations in Northern Canadian air temperature and river discharge. *Atmosphere-Ocean* **27**(4), 682–691. doi: 10.1080/07055900.1989.9649361

Martin S and Kauffman P (1981) A field and laboratory study of wave damping by grease ice. *Journal of Glaciology* **27**(96), 283–313. doi: 10.3189/s0022143000015392

Nilsen F, Cottier F, Skogseth R and Mattsson S (2008) Fjord–shelf exchanges controlled by ice and brine production: the interannual variation of Atlantic Water in Isfjorden, Svalbard. *Continental Shelf Research* **28**(14), 1838–1853.

Oggier M, Eicken H, Petrich C, Wilkinson J and O'Sadnick M (2020) Crude oil migration in sea-ice: laboratory studies of constraints on oil mobilization and seasonal evolution. *Cold Regions Science and Technology* **174**, 102924.

Ogi M and Tachibana Y (2001) Does the fresh water supply from the Amur River flowing in the sea of Okhotsk affect sea ice formation? *Journal of the Meteorological Society of Japan* **79**(1), 123–129.

O'Sadnick M and 5 others (2018) Observations of ice conditions in Norwegian fjords during the winter of 2018 and implications for oil spill response. In *Proceedings of the 41st AMOP Technical Seminar on Environmental Contamination and Response*. Ottawa, ON, Canada.

Petrich C and 6 others (2019) Mosideo/cirfa tank experiments on behavior and detection of oil in ice. In *Proceedings of the 25th International Conference on Port and Ocean Engineering under Arctic Conditions*. Delft, The Netherlands.

Petrich C and Eicken H (2010) Growth, structure, and properties of sea ice. In Thomas D and Dieckmann G (eds), *Sea Ice*, 2nd Edn. Oxford: Wiley Blackwell, pp. 23–78.

Petrich C, O'Sadnick ME and Dale L (2017) Recent ice conditions in North-Norwegian Porsangerfjorden. *Proceedings of the International Conference on Port and Ocean Engineering under Arctic Conditions, POAC*.

Petrich C, Tivy AC and Ward DH (2014) Reconstruction of historic sea ice conditions in a sub-Arctic lagoon. *Cold Regions Science and Technology* **98**, 55–62. doi: 10.1016/j.coldregions.2013.10.011

Skardhamar J and 6 others (2018) Modelled salmon lice dispersion and infestation patterns in a sub-arctic fjord. *ICES Journal of Marine Science*, **75**(5), 1733–1747. doi: 10.1093/icesjms/fsy035

Smedsrud LH and Skogseth R (2006) Field measurements of Arctic grease ice properties and processes. *Cold regions science and technology* **44**(3), 171–183.

Stigebrandt A (1980) Some aspects of tidal interaction with fjord constrictions. *Estuarine and Coastal Marine Science* **11**, 151–166.

Stigebrandt A and Aure J (1989) Vertical mixing in basin waters of fjords. *Journal of Physical Oceanography* **19**, 917–926.

Svendsen H (1995) Physical oceanography of coupled fjord-coast systems in northern Norway with special focus on frontal dynamics and tides. *Ecology of Fjords and Coastal Waters*. Amsterdam: Elsevier, 149–164.

Timco G and Frederking RM (1982) Flexural strength and fracture toughness of sea ice. *Cold Regions and Technology* **8**, 35–41.

Tucker W, Perovich DK, Gow AJ, Weeks WF and Drinkwater MR (1994) Chapter 2. Physical properties of sea ice relevant to remote sensing. In Carsey FD ed. *Microwave Remote Sensing of Sea ice*, 68th Edn.American Geophysical Union, 9–28. doi: 10.1029/GM068.

Vermote E (2015) MOD09A1 MODIS/terra surface reflectance 8-day L3 global 500 m SIN grid V006. *NASA EOSDIS Land Processes DAAC* **10**.

Weeks WF and Ackley SF (1986) The growth, structure, and properties of sea ice. In *The geophysics of sea ice*Boston, M: Springer, pp. 9–164.

7 Paper 2

Ice Conditions in northern Norwegian fjords: Observations and measurements from three winter seasons: 2017-2020

M. O'Sadnick, C. Petrich, C. Brekke, J. Skarðhamar, & Ø. Kleven

Accepted with minor revisions, in review (as of 30 June 2022):
Cold Regions Science and Technology, 2022

Ice conditions in northern Norwegian fjords: Observations and measurements from three winter seasons, 2017-2020.

Megan O'Sadnick[1,2*], Chris Petrich[2], Camilla Brekke[1], Jofrid Skarðhamar[3], & Øystein Kleven[2]

[1]UiT The Arctic University of Norway, Tromsø, Norway

[2]SINTEF Narvik, Narvik, Norway

[3]Institute of Marine Research, Tromsø, Norway

Abstract

Freshwater provided by rivers beginning deep within the mountains, feeds into fjords along the coast of Norway, often forming a brackish surface layer that will change in its salinity, thickness, and extent throughout the year. As temperature drops below freezing, ice can form from this layer along the entire coastline from 71° N down to 58° N. The influence of freshwater combined with changing weather and oceanographic conditions, can lead to ice that varies not only in its thickness and extent but its properties including crystal fabric, bulk salinity, and pore structure. Resultantly, how ice interacts with the surrounding environment including communities that use the ice for winter activities, boats transiting through fjords, pollutants like oil, and the biota living within the ice and fjord waters, will be impacted.

To enhance understanding of the drivers of ice formation and resultant properties in Norwegian fjords, seven fjords located in northern Norway were monitored over three winter seasons between 2017 and 2020. Measurements of ice thickness, stratigraphy, bulk salinity, and $\delta^{18}O$ were gathered along with measurements of ocean salinity, temperature, and $\delta^{18}O$ of both snow and river water. Ice thickness ranged from non-existent up to 0.8 m with the proportion of congelation to granular ice changing

*Corresponding author- email: megan.osadnick@sintef.no, telephone: +47 468 44599

between seasons and fjords. While ocean salinities directly below the ice on the day of measurement were primarily above 31 psu, ice bulk salinity varied from 0 psu to 5.6 psu with values of $\delta^{18}O$ between -13.3 ‰ and 0.2 ‰, indicating ice frozen from fresh water as well as seawater. Findings support that ice conditions in a single fjord or in a geographic region should not be generalized, with substantial variations measured between years and locations. We examine openly accessible interpolated weather and runoff data obtained through seNorge for possible causes for the variable ice conditions observed. Results reveal freezing degree days are not a dependable predictor of ice thickness when applied to Norwegian fjords, and substantial consideration of the date of onset of ice formation and snow cover are needed. Freshwater runoff and snowfall as well as the timing of weather and oceanic conditions throughout the three winter seasons are also presented to highlight their potential to influence ice formation considerably.

Keywords: sea ice, fjords, ice-ocean interaction, coastal processes

1. Introduction

The coast of mainland Norway is dominated by the presence of fjords cutting into the adjacent mountains, with the glaciers that carved these fjords now receded into higher terrain if not gone entirely (Holtedahl, 1967; Porter, 1989). Fjords differ in width, length, depth, and orientation with these characteristics transferring to the physical and biological characteristics of fjords including weather, oceanography, and the plants and biota present (Eilertsen & Skarðhamar, 2006; Rikardsen et al., 2004). Often subjected to temperatures below freezing, fjords have the possibility to form ice. While the Norwegian pilot guide offers brief descriptions of ice conditions in selected areas to assist boat and ship captains (Hughes, 2006), no studies exist that make direct observations of sea ice thickness, extent and properties in fjords found throughout mainland Norway. Ice conditions in the pilot guide are themselves

based primarily off aging data published in older editions mixed with examination of visible and infrared satellite images gathered in February and March 2005.

The larger fjords along the Norwegian coast are ice free all year due to the influence of warm Atlantic water (Aure et al 1997; Eilertsen & Skarðhamar 2006). However, sea ice often forms in the inner parts of fjords and in smaller fjord branches (O'Sadnick et al. 2020). There is a wide breadth of work in mainland Norwegian fjords focusing on water mass dynamics, often linked to biological processes in open waters (Asplin, Salvanes, & Kristoffersen, 1999; Cottier et al., 2010; Eilertsen & Skarðhamar, 2006; Jones et al., 2020; Mankettikkara, 2013; Skarðhamar et al., 2018). However, little research has so far been conducted on sea ice in Norwegian fjords (O'Sadnick et al 2020), while the role of sea ice in fjords on Svalbard is well studied (for example Cottier et al., 2010; Gerland & Renner, 2007; Hop & Wiencke, 2019; Nilsen et al., 2008; Skogseth et al., 2020).

When ice forms on the surface of a fjord, it creates a barrier between the ocean and air, altering the exchange of mass and energy (Petrich & Eicken, 2010). In addition, ice creates a biologically rich environment of brine-filled pores that offer a sheltered place for algae and other microbiota to grow (Arrigo et al., 2010; Brandon et al., 2010; Gradinger et al., 1999). Studies of sea ice in the Baltic Sea offer descriptions of ice grown from sea water of lower salinity, brackish in character, as well as the impact of fresh water plumes on local ecology (Granskog et al. 2005a; Granskog et al., 2005b; Kaartokallio et al., 2007). However, these studies may be difficult to apply to fjord ice where a stratified water column is often observed characterized by a surface layer that is reduced in salinity due to freshwater, an intermediary layer similar in composition to coastal water, and a basin holding the densest water below the depth of a sill (Stigebrandt, 2012). Fjords are also well contained by coastline and bed topography impacting currents and fjord-coast water exchange.

Though little work is available documenting observations of specifically Norwegian fjords in winter (Walker et al. 2021; Eilertsen & Skarðhamar 2006), research focused on the more general field of Arctic estuaries does exist from e.g. North America and Russia. Macdonald et al. (1995), Macdonald et al. (1999), and Eicken (2005) attempted to quantify the fraction of ice grown from river discharge in coastal sea ice by examining the isotopic signature of both the ice and the water from which it is grown. The isotopic composition $\delta^{18}O$ is defined as:

(1) $$\delta^{18}O = \left(\frac{\left(\frac{^{18}O}{^{16}O}\right)_{sample}}{\left(\frac{^{18}O}{^{16}O}\right)_{standard}} - 1 \right) * 1000$$

where the standard is Vienna Standard Mean Ocean Water (VSMOS).

Similarly to salinity, the stable isotope ratio in ice is sensitive to both source water and growth rate. For the former, fresh water for example may come from a river, snow melt, or ice melt to mention a few possible sources. A study by Nan et al. (2019), found the isotopic signature of fresh river water to vary across the globe with values in Norway, specifically, ranging from approximately -12‰ in the north up to -4‰ further south. For ocean water, the Vienna Standard has a $\delta^{18}O$ of 0‰ while values as high as approximately 2‰ at lower latitudes down to -3‰ in regions of the arctic have been measured (LeGrande & Schmidt, 2006). Therefore, even if all sources carry the same salinity, $\delta^{18}O$ can differ. Additionally, growth rate will impact values of $\delta^{18}O$. A decrease in growth rate will increase isotopic fractionation (increasing values of $\delta^{18}O$, cf. Eq.1) (Eicken, 1998).The opposite impact is seen in measurements of bulk salinity which decreases in magnitude with a decrease in growth rate.

Through using measurements of $\delta^{18}O$, the above authors were able to trace events of larger freshwater flux during the winter and approximate the size and movement of freshwater plumes under the ice. The extent of these plumes is important as they disable convection under the ice, diluting and sweeping away brine rejected from the ice and changing the overall oceanographic conditions within the area.

Granskog et al. (2005) examine the impact of such plumes in the Baltic Sea, noting that plumes of fresh water can also act to stabilize the water column reducing heat exchange with the ocean and causing faster ice growth.

Freshwater under the ice can lead to the formation of ice layers of low porosity that are essentially impermeable to fluid flow. These layers can disrupt the convection of brine through the ice and the exchange of nutrients that enables the growth of ice-algal communities. Ingram et al. (1996) investigated the impact of freshwater on an ecosystem under sea ice through linking the sea water salinity at the ice interface to various environmental and biological response variables including bulk ice salinity, light attenuation, chlorophyll a, and algal diversity. The authors stressed the need for further work examining coastal zones in northern areas; placing focus on the impact of freshwater flow on the hydrodynamics and the ecology of an area.

Whether caused by an influx of freshwater or other factors such as changing weather or oceanic conditions, the microstructure of sea ice and the connectivity of pore space are often a focus in scientific studies. While measurements of temperature, bulk salinity, and stable isotopes are useful, visual examination of sea ice thick sections has proven useful in determining the cause of patterns in sea ice microstructure. For example, banding, simply described as the variation in transmittance of light through the ice, can reveal where pore shape and connectivity may change. Cole et. al (2004) studied banding in first year sea ice present in Utqiaġvik (previously Barrow, Alaska) over the course of three seasons. In the Arctic, first year sea ice can be found along much of the coastline. This ice often has a bulk salinity between 5 and 8 (psu) and is distinguished from freshwater ice in crystal structure and the presence of pores holding brine. As the ice warms in spring, these pores connect in the vertical direction allowing for fluid flow through the ice when temperature is above approximately -5 °C. Cole et al. (2004) analyzed the shape and geometry of the pores present in bands of high and low porosity, i.e., light and dark bands respectively. Results provided a first order description and estimate of pore density, structure, and

variability. In addition, Turner et al. (2017), examined banding in Antarctic ice focusing primarily on the appearance of thin, recurring bands. They determined that such a pattern is related to the changing boundary layer conditions that result from tidal currents.

Layers of freshwater ice have implications for operations in ice-covered waters. As marine traffic increases in Arctic coastal regions, the risk of an oil spill, either from ships or oil production, is also becoming more of a concern. Previous studies examining the interaction of oil and ice, have focused on sea ice of columnar structure that undergoes a predictable evolution through the ice season. In such ice, oil emplaced under and possibly frozen into the ice, would rise to the surface during spring warming as pores connect and a pathway through the ice to the surface are created (Dickens, 2011; Petrich et al., 2013). If layers of lower porosity or possibly impermeable ice are present, this process will be disrupted resulting in a less predictable and likely more challenging approach to oil clean up. This risk applies not only to Norwegian fjords but any area where freshwater interacts with sea ice during the ice growth period. Additionally, freshwater ice and sea ice have different mechanical properties, a characteristic due largely to the former having greater strength because of lower porosity. A simple explanation isthat fewer pores means there is more “solid ice” within the sample (Timco & Weeks, 2010). Relatedly, ice porosity will alter the electrical signature of the ice impacting how ice is seen by remote sensing instruments (Tucker et al., 1992). All these factors are important for operations in the Arctic and sub-Arctic regions. Therefore, the findings presented here have implications for science and industry including biology, shipping and transit in Arctic and sub-Arctic regions, safety for local communities, and oil spill response methods.

The objective of this study is to investigate the ice conditions and properties in northern Norwegian mainland fjords, and how and why the fjord ice varies between years and between neighboring fjords. We present measurements from seven fjords in northern Norway collected over the span of three winter seasons between 2017 to 2020 combined with openly available weather and runoff data. The

measurement data include ice thickness, extent, bulk ice salinity and ice $\delta^{18}O$, as well as seawater salinity, temperature, and $\delta^{18}O$. Additionally, ice crystal and pore structure are examined in relation to these properties.

2. Methods

2.1 Study Area

Seven fjords located in northern Norway were chosen for ice characterization based on knowledge that they held ice in recent years, determined through satellite imagery and in-situ observation, as well as their accessibility (Fig. 1). Measurements were performed over the winter of 2017/2018, 2018/2019, and 2019/2020 with samples collected toward the end of the ice-growth period (Table 1). In one fjord, Beisfjord, during the 2018/2019 season a transect to collect several cores at increasing distance from the river was also completed.

Table 1- Overview of ice conditions in the fjords. Dates of formation of consistent ice cover and when the fjords were ice free are from observations with cameras and/or satellite imagery. Ice thickness, snow depth and freeboard were measured on the dates given. Gray, shaded entries represent visits where only ocean and fresh water measurements were obtained. When ice was present but no measurement made, the season length in days is provided. n/m = not measured, n/a= no ice.

Nordkjosbotn							
Season	**Ice formation**	**Ice free**	**Date of measurement**	**Fraction of season complete**	**Ice thickness [m]**	**Snow depth [m]**	**Freeboard [m]**
2017/18	29-30 Dec	27-30 Apr	20 Mar 2018	81/122	0.76	0.06	n/m
2018/19	29-30 Jan	16-24 Apr	13 Mar 2019	43/76	0.15	n/m	n/m
2019/20	6-8 Mar	16-20 Mar	n/m	-/14	n/m	n/m	n/m
Storfjord							
2017/18	15-20 Feb	20-23 Apr	20 Mar 2018	33/67	0.36	0.10-0.15	n/m
2018/19	n/a	n/a	12 Mar 2019	n/a	n/a	n/a	n/a
2019/20	n/a	n/a	11 Mar 2020	n/a	n/a	n/a	n/a
Gratangsbotn							
2017/18	n/a	n/a	23 Mar 2018	n/a	n/a	n/a	n/a
2018/19	27-29 Jan	16 - 24 Apr	14 Mar 2019	46/87	0.27	0.21	negative
2019/20	4 - 10 Dec	22 Apr	20 Feb 2020	78/140	0.21	0.11	negative
Lavangen							
2017/18	27- 28 Jan	20 - 23 Apr	23 Mar 2018	55/86	0.37	0.16	n/m
2018/19	20 - 23 Jan	16 - 24 Apr	14 Mar 2019	53/94	0.26	0.02	0.03
2019/20	1 - 5 Feb	31 Mar - 4 Apr	n/m	-/63	n/m	n/m	n/m
Beisfjord							
2017/18	1 - 5 Feb	5 - 11 May	19 Apr 2018	77/99	0.42	0.10	n/m
2018/19	3 Mar	21 Apr	19 Mar 2019	16/49	0.24 (a)/0.235 (b)/ 0.18 (c)/ 0.08 (d)	0.0	0.01
2019/20	9 Dec	20 - 26 Jan	22 Feb 2020	-/48	n/m	n/m	n/m
Ramfjord							
2017/18	28-29 Jan	5 - 11 May	20 Mar 2018	51/103	0.49	0.2	n/m
2018/19	20 Dec	7 May	13 Mar 2019	83/138	0.46	n/m	negative
2019/20	15 Oct	24 May	12 Mar 2020	148/222	0.30	0.20	negative
Kattfjord							
2017/18	5 - 10 Jan	5 - 11 May	21 Mar 2018	75/126	0.59	0.23	negative
2018/19	14 Jan	26-27 Apr	14 Mar 2019	59/103	0.35	0.37	negative
2019/20	n/a	n/a	12 Mar 2020	n/a	n/a	n/a	n/a

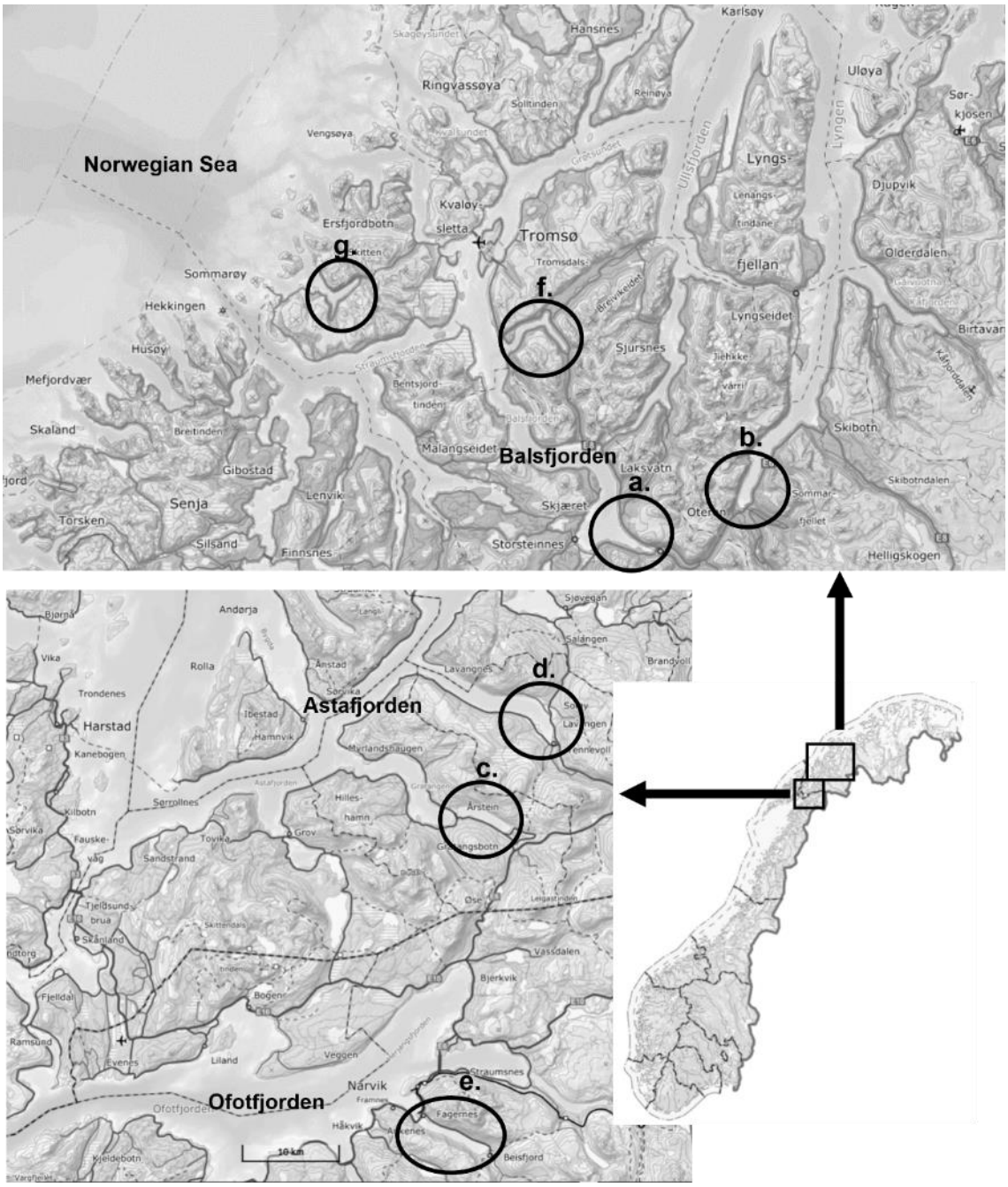

166

167 Fig.1: Location of Norwegian fjords where measurements were gathered, ordered according to freezing degree
168 days (FDD) from highest to lowest. a) Nordkjosbotn, b) Storfjord, c) Gratangsbotn, d) Lavangen, e) Beisfjord, f)
169 Ramfjord, g) Kattfjord. ©norgeskart.no

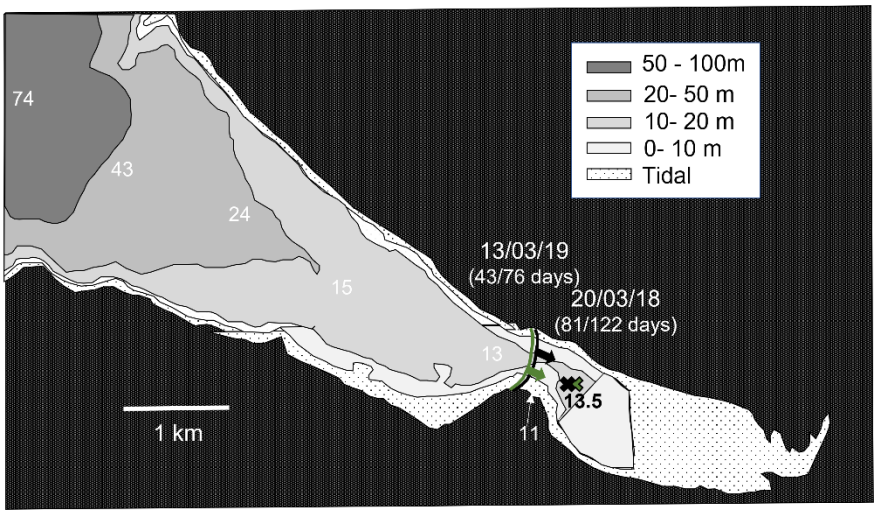

Fig.2- Nordkjosbotn, in the inner part of Balsfjorden. Water depth in meters marked along the length of the fjord, contours are also shown. Ice extent on the day of measurement (indicated, see text for details) and measurement location are marked with a line across the fjord and a cross, respectively, for seasons 2017/18 (black), and 2018/19 (green).

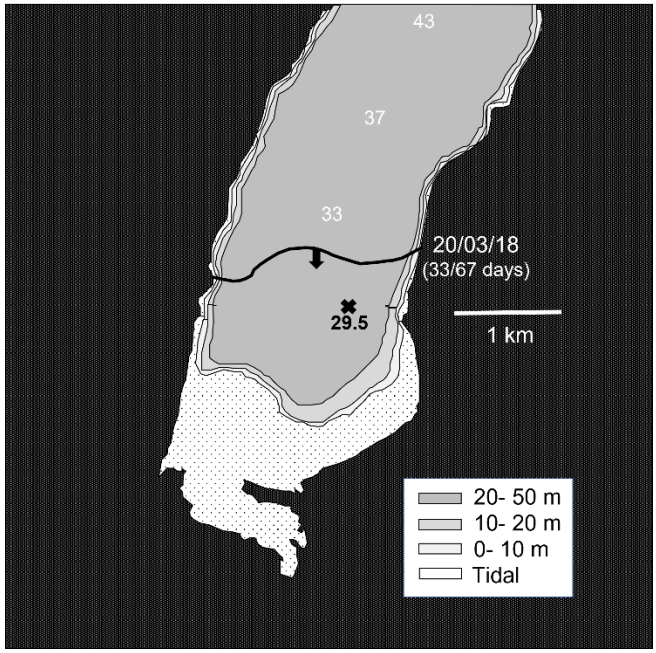

Fig. 3- Storfjord. Water depth in meters marked along the length of the fjord, contours also shown. Ice extent on the day of measurement and measurement location marked with a line across the fjord and a cross, respectively, for the 2017/18 season.

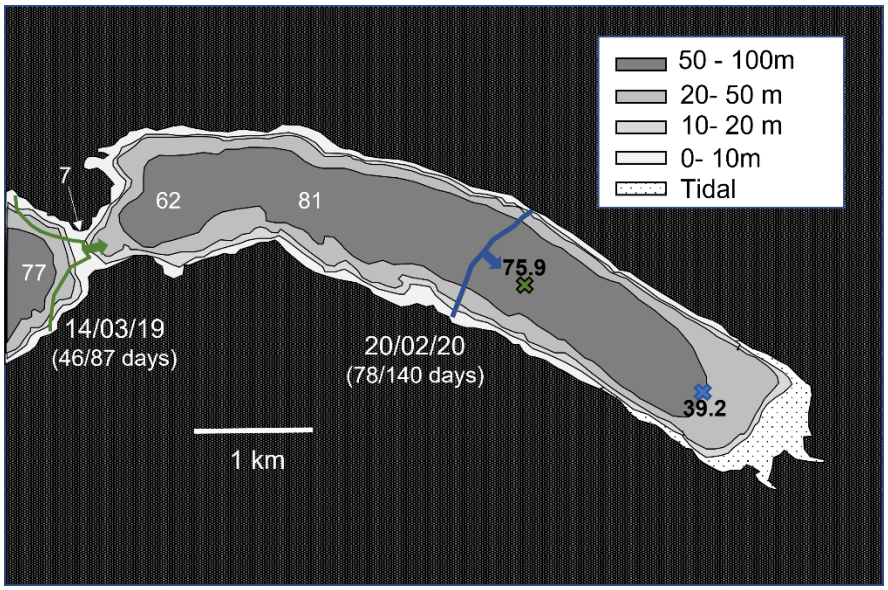

179

180 Fig.4- Gratangsbotn. Water depth in meters marked along the length of the fjord, contours also shown. Ice extent
181 on the day of measurement and measurement location marked with a line across the fjord and a cross,
182 respectively, for seasons, 2018/19 (green), and 2019/20 (blue).

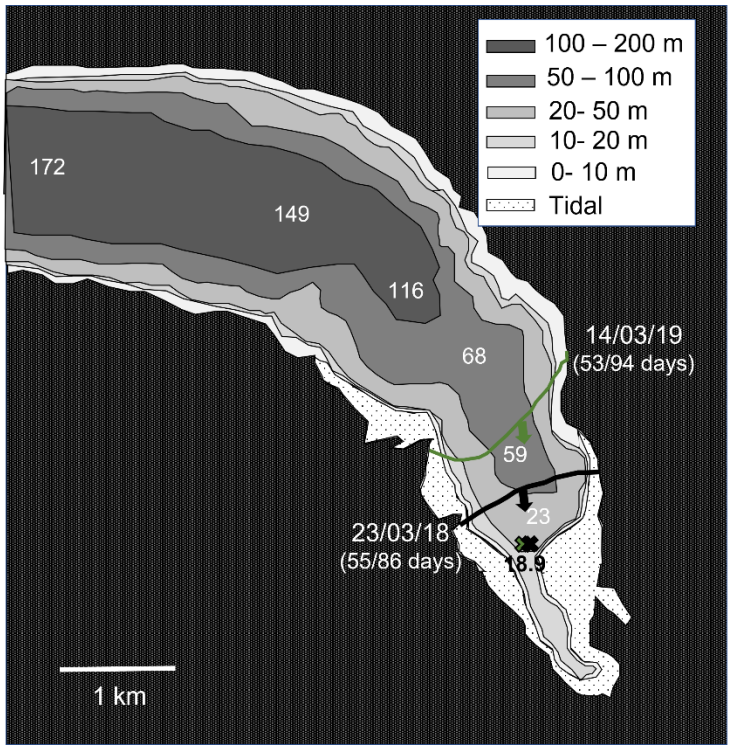

183

184 Fig.5- Lavangen. Water depth in meters marked along the length of the fjord, contours also shown. Ice extent on
185 the day of measurement and measurement location marked with a line across the fjord and a cross, respectively,
186 for seasons 2017/18 (black), 2018/19 (green),.

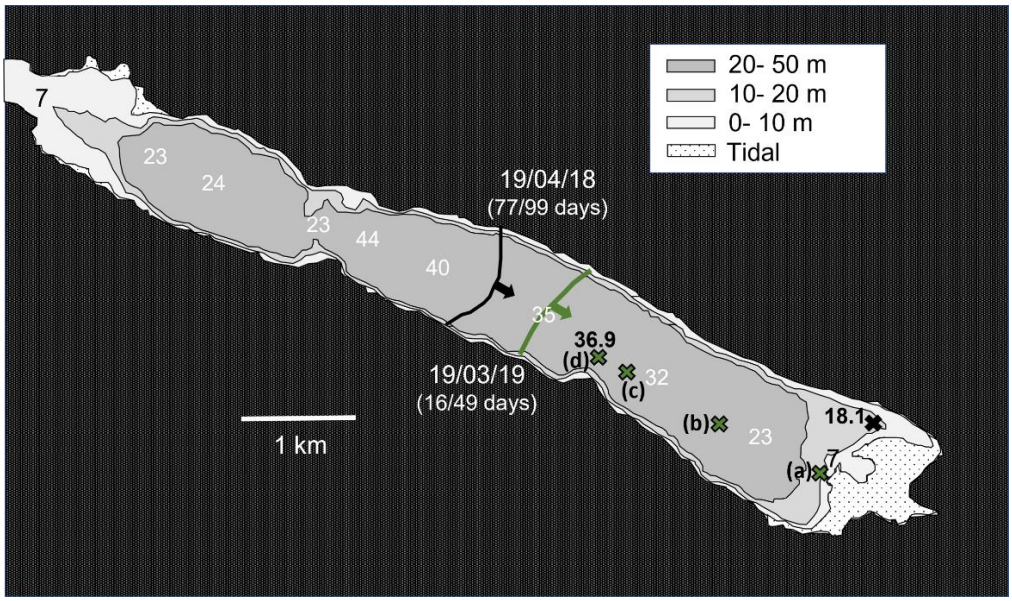

187

188 Fig.6- Beisfjord. Water depth in meters marked along the length of the fjord, contours also shown. Ice extent on the
189 day of measurement and measurement location marked with a line across the fjord and a cross, respectively, for
190 seasons 2017/18 (black), 2018/19 (green).

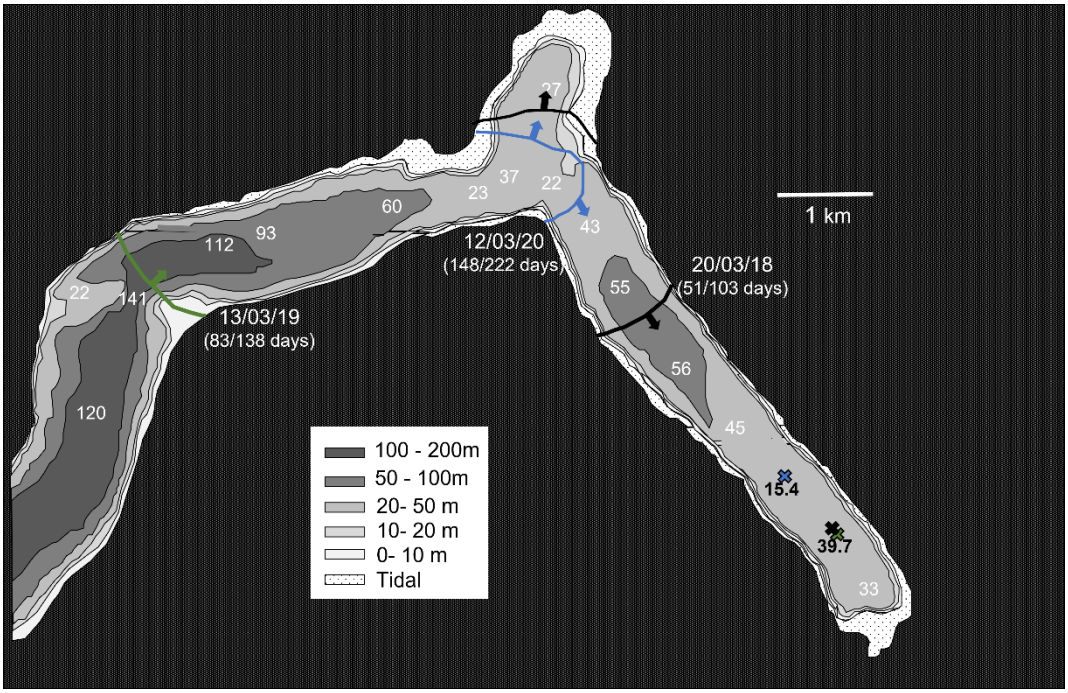

191

192 Fig.7- Ramfjord. Water depth in meters marked along the length of the fjord, contours also shown. Ice extent on
193 the day of measurement and measurement location marked with a line across the fjord and a cross, respectively,
194 for seasons 2017/18 (black), 2018/19 (green), and 2019/20 (blue).

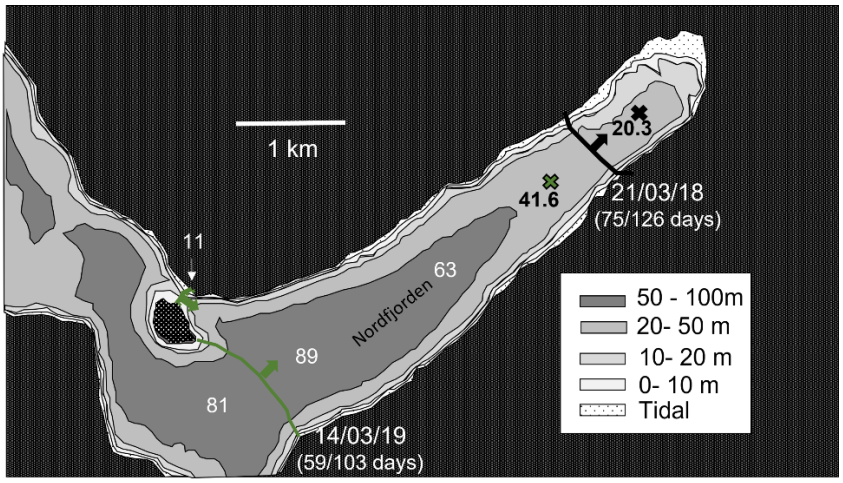

195

196 Fig.8- Kattfjord. Water depth in meters marked along the length of the fjord, contours also shown. Ice extent on the
197 day of measurement and measurement location marked with a line across the fjord and a cross, respectively, for
198 seasons 2017/18 (black) and 2018/19 (green).

199 The fjord Kattfjord (Fig.1g and 8), is located the furthest north out of the fjords selected. The area of the
200 inner part of the fjord, also referred to as Nordfjorden (Fig. 8), is 5 km long and 1.3 km wide, with a
201 maximum depth of 90 m. Kattfjord has a sharp bend to the northwest accompanied by a decrease in
202 depth to a sill with water depth 54 m and 11 m on each side of an island. Past this point (not shown), the
203 fjord continues before branching in two and eventually meeting the Norwegian sea. The only other fjord
204 that is directly connected to the Norwegian sea, i.e., not being a branch of a larger fjord, is Storfjord (Fig.
205 1b and 3) which is the inner part of Lyngenfjorden. Being over 80 km long, its head is located further
206 south than Kattfjord while the mouth is further north and leads into the Norwegian sea. Fjord ice formed
207 from the head of the fjord outward 2 - 3 km, where depth is approximately 33 m and width
208 approximately 1.8 km. Storfjord is primarily straight with no abrupt bends. The nearest sill to the ice
209 edge is roughly 29 m deep and located 8 km from the head of the fjord.

210 There were two study sites in Balsfjorden; Ramfjord (Fig. 1f and 7) and Nordkjosbotn (Fig. 1a and 2).
211 Ramfjorden stands out amongst the other fjords given the abrupt 90 degree turn it takes as one first
212 moves northeast into the fjord from Balsfjorden eventually turning to the southeast. From the head of

the fjord, depth increases quickly to 56 m before decreasing to the first sill of 22 m depth. As the fjord changes direction, depth again increases to 133 m decreasing only to 118 m at the mouth of the fjord. The width of the fjord is fairly consistent along its 13 km length, being generally 0.7 – 1 km. Nordkjosbotn (Fig.2) is a small area located over the innermost 7 km of Balsfjorden. Samples were collected on the eastside of a constriction, less than 500 m in width, where water depth is only 11 m. To the west of the constriction, depth increases gradually towards the main fjord basin of Balsfjorden.

The remaining three fjords are located over 85 km to the southwest. Both Lavangen (Fig. 1d) and Gratangsbotn (Fig. 1c) are branches of Astafjorden. While near to each other, they differ significantly in depth and geometry. Lavangen (Fig.5) varies between 1.5 to 2 km in width as it bends smoothly from the southeast to east back to the southeast. Measurements were only collected at the head of Lavangen where width decreases to less than 1 km and depth to less than 45 m. At its deepest Lavangen measures 202 m with a sill located where it meets Astafjorden about 17 km from the head of the fjord, 106 m deep. In Gratangsbotn (Fig. 4) ice was found to the east of a narrow constriction and sill, 300 m wide and 7 m deep respectively. Depth in the inner part of this part of the fjord, 6 km in length, reaches a maximum of 80 – 85 m while width is consistently between 0.9 and 1 km. To the west of this constriction, the fjord bends several times over 14 km while depth increases to nearly 200 m before meeting another sill only 30 m in depth.

The furthest south fjord, Beisfjord (Fig.1e and 6) is a small side fjord to Ofotfjorden. Being 8 km in length, and 0.8-1.0 km wide, depth reaches a maximum of 44 m before a sill with a depth of 23 m. Moving northwest to the head of the fjord, depth stays fairly constant at approximately 24 m before decreasing again to only 3 – 4 m at the mouth of the fjord. At this point the fjord also narrows from just over 1 km to 350 m.

2.2 Field Measurements

Measurements of ice and water were made once a year at each fjord after a solid layer of ice had formed, if any at all. Before ice samples were gathered, any snow on the surface was removed to provide a clean area from which to drill ice cores. At least two cores were taken at each location for ice bulk salinity, stable isotopes, and ice stratigraphy. For salinity measurements, the core was removed and laid horizontal immediately to minimize brine drainage. Using a saw, the core was sliced into 0.05 m sections and double bagged. Samples were melted at room temperature before salinity was measured using a YSI Pro30 temperature/conductivity probe with accuracy of 0.1 on the practical salinity scale (psu) (Fofonoff & Millard, 1983) and resolution of ±0.1 (psu) or ±1% of the reading, whichever is greater. It is noted that the sampling procedure is meant to minimize brine drainage, but it still can occur being largely dependent on the brine volume fraction (porosity) of the ice. The remaining seawater from the melted ice samples was placed in glass bottles with cone liners and stored at 4 °C for stable oxygen isotope analysis. Samples were analyzed at the Stable Isotope Laboratory at the Centre for Arctic Gas Hydrate, Environment and Climate (CAGE) located at UiT The Arctic University of Norway, Tromsø, Norway. A 0.5 mL sample from each melted core slice was pipetted into a 12 mL Labco glass vial which was next flushed with a 0.3% CO2 in He gas mixture, equilibrated at 25°C for >24h. Calibration was done through measuring three inhouse standards of $\delta^{18}O$ between -1 and -36 ‰ that had previously been calibrated against international standards VSMOW2, GISP, and SLAP2. When a line was fit to true vs. measured vales of $\delta^{18}O$, the R^2 value of the line was 1.0, with error between separate readings most often being less than 0.01‰ but with a standard deviation <0.05‰. A Thermo-Fisher MAT253 IRMS with a Gasbench II was used to measure of the quantity of $\delta^{18}O$.

The stratigraphy core was stored at -18 °C to ensure minimal brine drainage before being sliced in a cold room set to -12 °C. Vertical sections of the stratigraphy core had a thickness of 1 – 1.2 cm. Using both light transmission and cross-polarizers, ice type and transitions with depth were examined.

For all fjords, seawater temperature and salinity were measured with a CTD (CastAway-CTD, Sontek) at the ice-sampling location just after the ice cores were collected. Slush was removed from one of the holes before measuring the vertical distribution of temperature and salinity in the water column below the ice by lowering the CTD manually from the drill hole to the seabed. The CTD had a resolution and accuracy of 0.01°C and 0.05 °C respectively for temperature, 0.01 (psu) and ±0.1 (psu) for salinity, and 0.01 m and ±0.25% of the measured value for depth. Two casts were made at each location to ensure that consistent measurements were obtained. The data presented here were taken during the upcast, with measurements of pressure, temperature, and conductivity converted to depth and salinity automatically by the instrument using the UNESCO equations (Fofonoff & Millard, 1983). The CTD sampled at a frequency of 5 Hz and was raised at approximately 0.5 m/s. Only upcasts were used due to the presence of ice that sometimes formed around the sensor while in between measurements. This resulted in a clear error in measurements of the upper water column in the downcast as the ice was melted and/or dislodged. Seawater samples from 0.20 down to 2.0 m below the bottom of the ice were collected for isotopic measurements using a manual water pump attached to a rubber hose. The hose was rinsed with water from the desired depth and two cone-lined bottles were filled and stored at the lab facility at SINTEF Narvik at 4 °C until analysis at the UiT stable isotope laboratory.

2.3 External Measurements

2.3.1 Determining ice freeze up and break up

UOVision UM 565 and UM785 trail cameras were used to collect time-lapse images at all fjords except Nordkjosbotn. This allowed for tracking of weather events as well as determination of ice freeze up and break up. As images were only gathered in the last season, 2019-2020, satellite imagery was needed to track the formation and breakup of ice during the first two seasons. Two products were used for this purpose - SENTINEL-1 C-band Synthetic aperture radar (SAR) and imagery from Terra satellite MODIS

sensor, specifically the MOD09A1.006 Terra Surface Reflectance 8-Day Global 500m product (Copernicus Sentinel data 2019). For the former, Ground Range Detected (GRD) scenes were evaluated with Google Earth Engine (Gorelick et al., 2017). Processing steps for MODIS imagery were described in detail by O'Sadnick et al. (2020). Ice formation and break up can occur several times throughout the season. Here, freeze up is defined as the first day of consistent ice coverage, with no further break ups occurring before the day of measurement. The ice edge often deteriorated over time, with rarely a single event leading to all ice dispersing. The date of break up provided here represents the first day where the fjord was entirely ice free.

2.3.2 Weather data and calculation of freezing degree days

Values for average daily air temperature, accumulated snow cover, and runoff were obtained from the openly available web portal seNorge.no (Lussana et al., 2018), providing spatially interpolated observational data by the Norwegian Meteorological Institute and the Norwegian Water Resources and Energy Directorate (NVE). Values for both runoff and accumulated snow cover are derived using the Hydrologiska Byråns Vattenbalansavdelning (HBV) hydrology model. Runoff (Q) in m/day is a function of several parameters including precipitation and evapotranspiration as well as changes over time in the amount of water stored in the soil, snow, and bodies of water (Bergström, 1992).The resolution of the HBV model is 1 km. The following approach was used to find the normalized daily runoff ($Q_{fjord,\ norm}$) for each fjord:

(2) $$Q_{fjord,norm} = \frac{Q_{fjord}}{A_{fjord}}$$

(3) $$Q_{fjord} = \sum_{WS\ 1} Q_{pixel} + \sum_{WS\ 2} Q_{pixel} + \cdots$$

(4) $$Q_{pixel} = QA_{pixel}F$$

where A_{pixel} is the area of a pixel equal to approximately 10^6 m^2, F = fraction of the pixel within the watershed (*WS*), Q_{pixel} is the volume of runoff for a pixel in m^3/day, Q_{fjord} is total volume of runoff leading into the fjord in m^3/day based on each individual watershed (*WS*), and $Q_{fjord,\ norm}$ is the amount of runoff into the fjord normalized by A_{fjord}, given in m/day (m^3/day per m^2). Boundaries of water sheds were provided by NVE through their watershed database, REGINE ("Nedbørfelt (REGINE)," 2020). Fjord area is defined here as the area of the fjord connected to these watersheds. In Figs. 2- 8, the area of the fjord shown is approximately the area of the fjord used in these calculations.

Accumulated snow cover and air temperature presented here come from the selection of one pixel at the head of each fjord, located at sea level. While this method does not account for variability throughout the fjord it provides a general view of temperature and snow conditions at sea level.

To better understand the overall potential for ice growth in each fjord, freezing degree days (FDDs) were calculated from 1 October to 1 May. Additionally, FDDs were calculated starting from the day of ice formation in each individual fjord until the day ice thickness was measured. FDDs are derived by summing all average daily air temperatures (T_a) below freezing point (T_f) from a start date (i=1) to end date (i=N):

(3)

$$FDD = \sum_{i=1}^{N} \Delta t \begin{cases} T_f - T_{a,i}, & T_{a,i} < T_f \\ 0, & T_{a,i} \geq T_f \end{cases}$$

Here Δt= 1 day. Given the uncertainty in the salinity of the surface water at the time of ice formation, FDDs were calculated for both T_f= 0 °C, representing freezing temperature of fresh water, and T_f= -2 °C representing sea water. Freezing degree days are useful in the prediction of ice thickness which is approximated in the following using the equation derived by (Anderson, 1961),

(4) $$H^2 + 5.1H = 6.7\theta,$$

where *H* is ice thickness in cm and ϑ is freezing degree days in °C days. In this work, fjords are primarily ordered according to freezing degree days, moving from the fjord with the highest value of FDD (coldest) to the lowest (warmest).

3. Results

3.5 Weather Conditions

Storfjord and Nordkjosbotn where the fjords with lowest air temperatures, as displayed by the number of FDDs each year with temperatures frequently dipping below -10 °C or as in the 2017/18 season, below -15 °C (Fig. 9, Table 2). Kattfjord had the highest air temperatures consistently above -10 °C throughout the winter (Fig. 9b) and the lowest numbers of FDDs.

Table 2- Freezing degree days in °C days for each fjord and winter season using 0 °C and -2 °C, calculated for the period 1 Oct-1 May.

	Nordkjosbotn		**Storfjord**		**Gratangsbotn**		**Lavangen**		**Beisfjord**		**Ramfjord**		**Kattfjord**	
	0 °C	**-2 °C**	**0 °C**	**-2 °C**	**0 °C**	**-2 °C**	**0 °C**	**-2 °C**	**0 °C**	**-2 °C**	**0 °C**	**-2 °C**	**0 °C**	**-2 °C**
2017/18	1159	1136	1134	1115	1008	972	977	943	885	851	777	749	573	537
2018/19	866	846	854	835	702	679	679	651	610	587	592	564	437	401
2019/20	762	732	756	725	560	518	533	495	446	409	516	484	368	313

For all fjords but Beisfjord, the lowest values of accumulated snowfall on land adjacent to the fjord occurred during the 2017/18 season and the highest values during the 2019/20 season. In Beisfjord, 2019/2020 began with higher values of snowfall but did not maintain the consistent increase shown in other fjords. Additionally, Beisfjord had the lowest snowfall values in comparison to other fjords for the last two seasons.

For all fjords, runoff was generally low between December into March and even April except in Kattfjord where events leading to runoff (i.e., warm spells) occurred all three years in January. Another exception

346 can be seen at the end of February during the 2018/19 season, when the runoff increased in all fjords,

347 being largest in Kattfjord and smallest in Beisfjord.

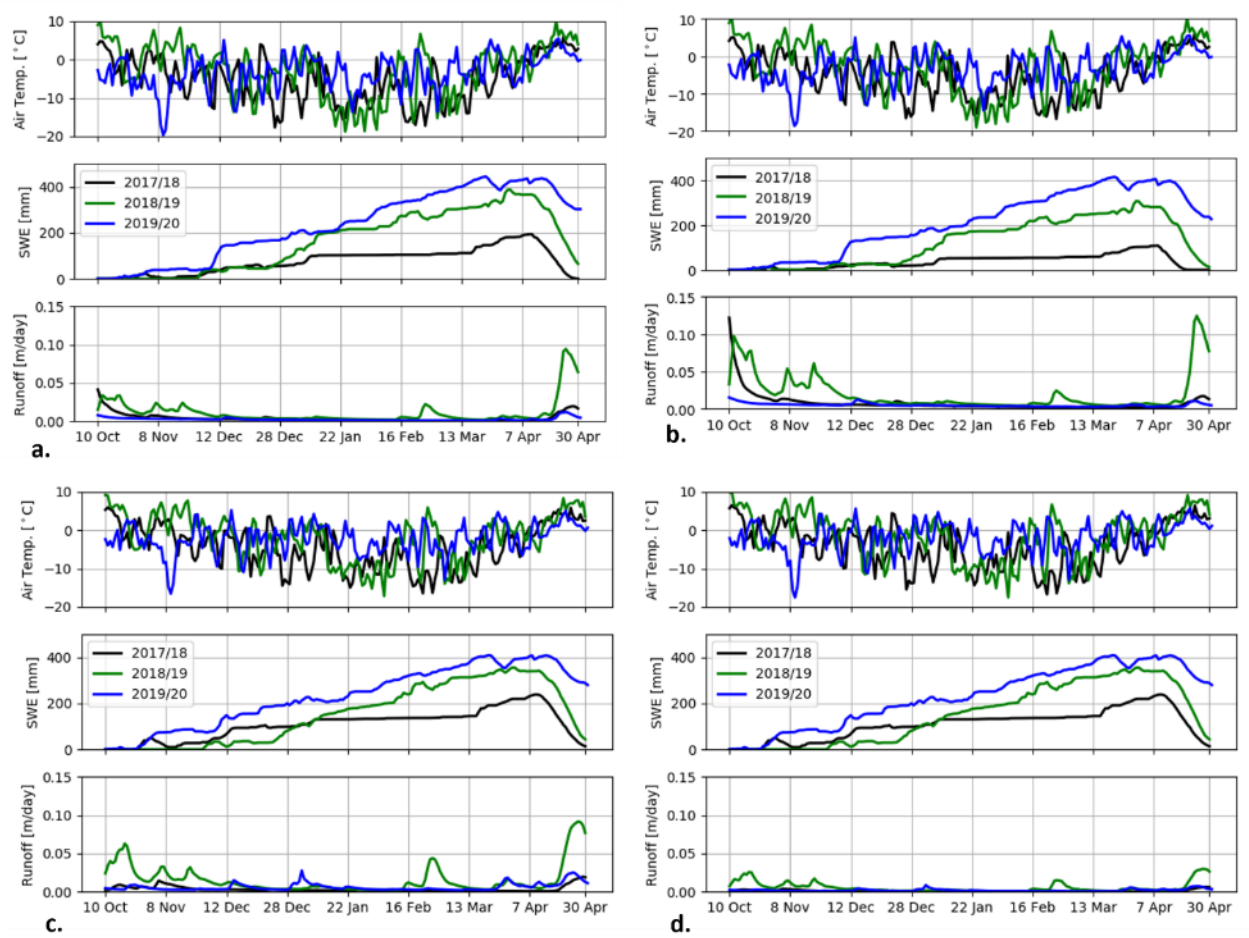

348

349 Fig.9- Spatially interpolated daily average air temperature, accumulated snowfall measured as snow water

350 equivalent (SWE) and runoff ($Q_{fjord,norm}$) for each fjord and year, extracted from seNorge. a) Nordkjosbotn, b)

351 Storfjord, c) Gratangsbotn, and d) Lavangen.

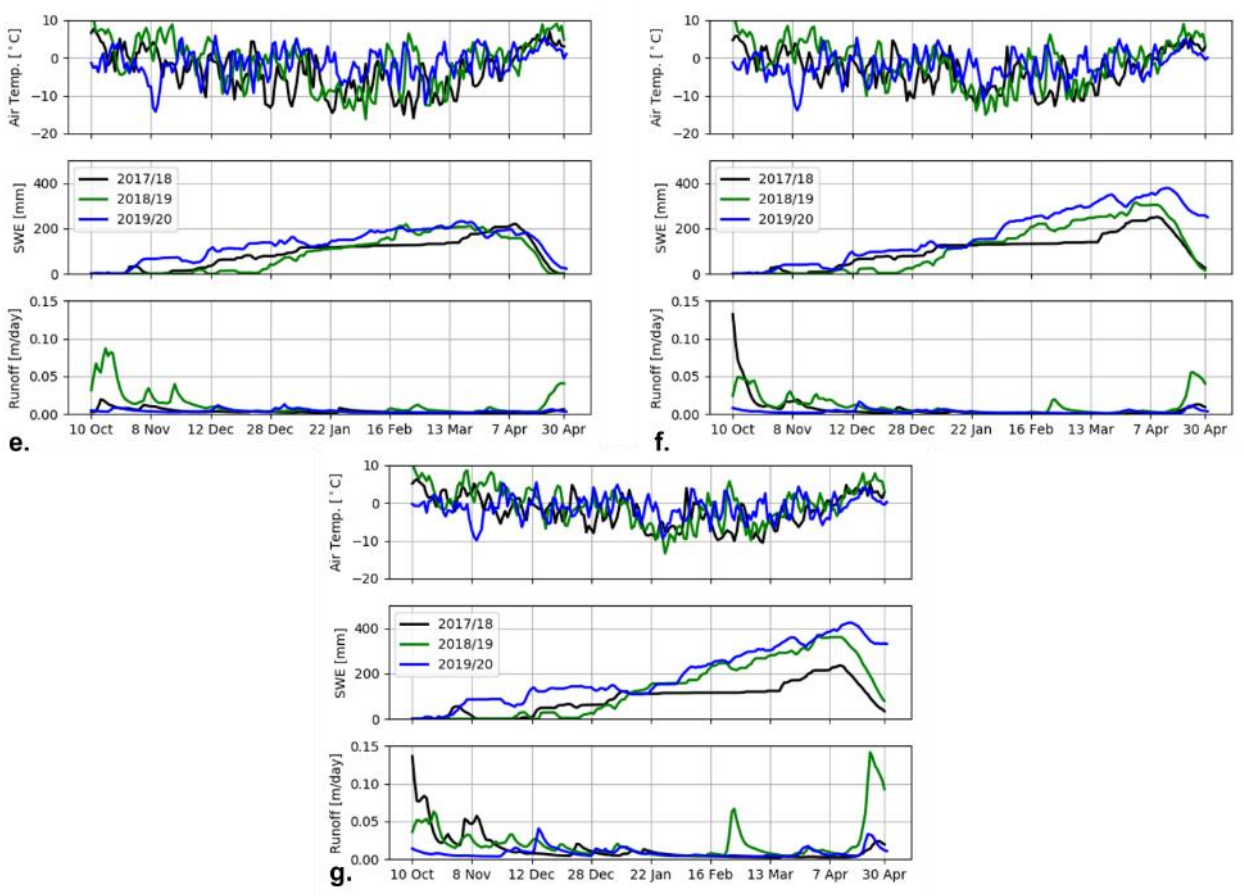

Fig.9 (continued) Spatially interpolated daily average air temperature, accumulated snowfall measured as snow water equivalent (SWE) and runoff ($Q_{fjord,norm}$) for each fjord and year. e) Beisfjord, f) Ramfjord, g) Kattfjord.

3.1 Length of time with ice cover, ice thickness, and ice area

The observed duration of ice cover and thickness of ice varied between fjords and between years (Table 1). The longest period of consistent ice coverage, 222 days, occurred in Ramfjord during the 2019/20 season. For Kattfjord, Storfjord, Gratangsbotn, and Beisfjord, 2017/18 had the longest period of ice coverage while Lavangen had a nearly the same length of time with ice in the first two seasons, with a shorter season during 2019/2020. Ice was thickest for all fjords on the day of measurement in 2018 except for Gratangsbotn where no consistent ice cover was observed. In contrast, ice extent on the day of measurement was greatest in 2019 for all except Storfjord and Beisfjord with both having the greatest extent of ice in 2018 (Figs. 2 – 8).

3.2 Ice Core Measurements

The ice core measurements revealed large variability in ice structure and crystallography between fjords and years (Figs 10 and 11). The greatest fraction of congelation ice was found in 2018 (Fig. 12). The following year, cores had a mixture of columnar and granular ice while in the final year, the two fjords where ice was sampled had cores composed entirely of granular ice (Fig.12). When the ice cores were illuminated only by light (Fig. 10), layers of pores differing in size and shape, changing between years and fjords, are apparent within both granular and congelation ice. In the latter, cores from 2018 season have the most examples of elongated pores, characteristic of saline sea ice, for example in Nordkjosbotn where a brine pore runs from 35 – 55 cm depth. In Ramfjord, a pore approximately 6 cm in length is also visible (marked in Fig.10). However, in all other cores, pores are generally thinner (approximately < 1 mm) and shorter (approximately < 2 cm) or inhomogeneous in shape with layers of spherical or asymmetric pores varying in density.

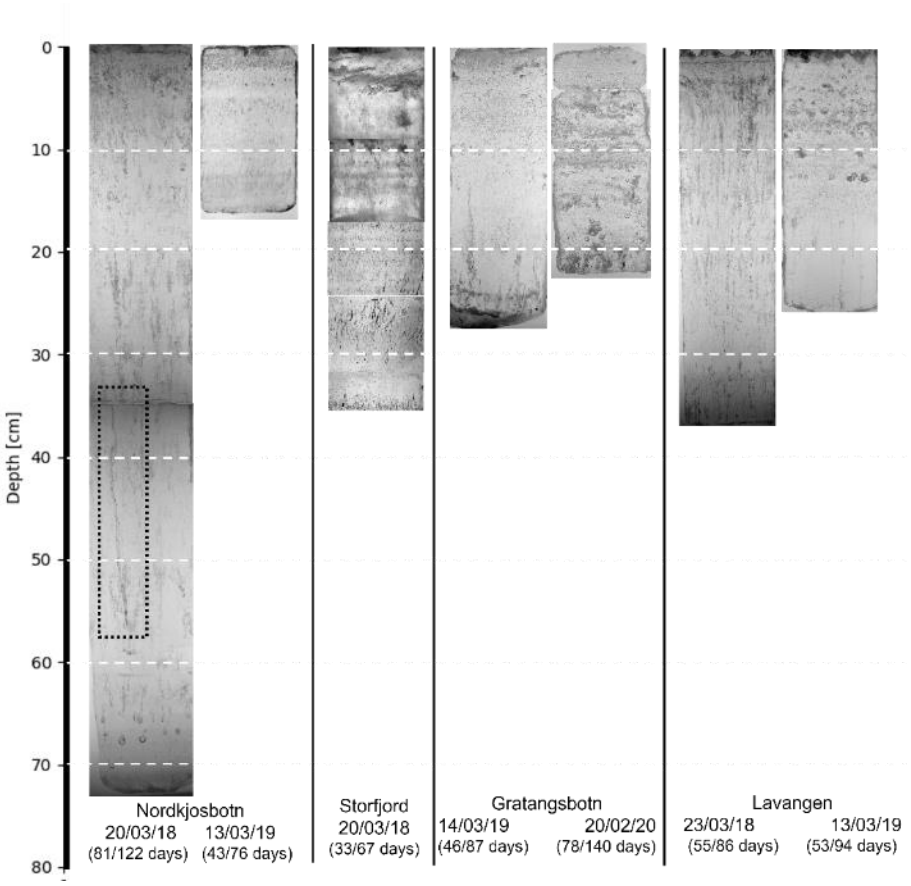
Depth [cm]
0
10
20
30
40
50
60
70
80
Nordkjosbotn
20/03/18 (81/122 days)
13/03/19 (43/76 days)
Storfjord
20/03/18 (33/67 days)
Gratangsbotn
14/03/19 (46/87 days)
20/02/20 (78/140 days)
Lavangen
23/03/18 (55/86 days)
13/03/19 (53/94 days)

377

378

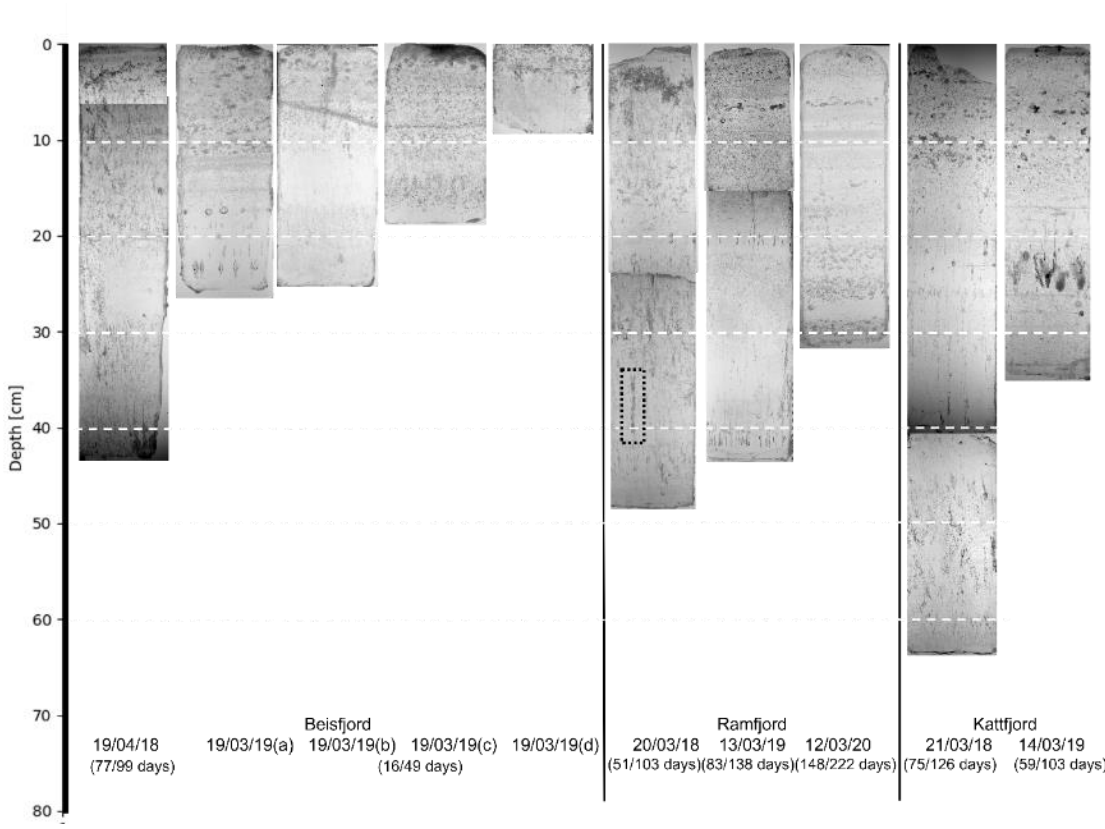

379

380 Fig.10- Backlit vertical thick sections of ice cores to highlight variations in pore structure and density between fjords
381 and years. In general, the less transmittance of light, the greater the scattering of light, signifying a greater number
382 and/or size of pores. To highlight variations in pore shape, two cores are featured independently in Figs. 18 and 19.
383 Dashed boxes used to highlight two elongated pores referenced in text.

384

385

386

387

388

389

390

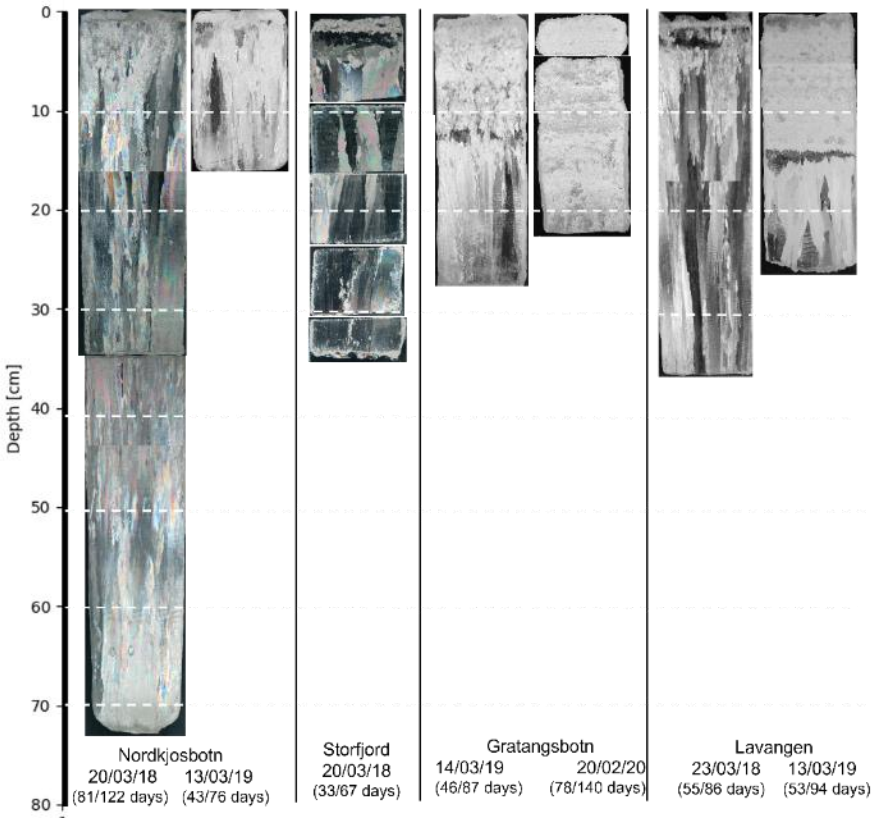
Depth [cm]
0
10
20
30
40
50
60
70
80
Nordkjosbotn
20/03/18 (81/122 days)
13/03/19 (43/76 days)
Storfjord
20/03/18 (33/67 days)
Gratangsbotn
14/03/19 (46/87 days)
20/02/20 (78/140 days)
Lavangen
23/03/18 (55/86 days)
13/03/19 (53/94 days)

391

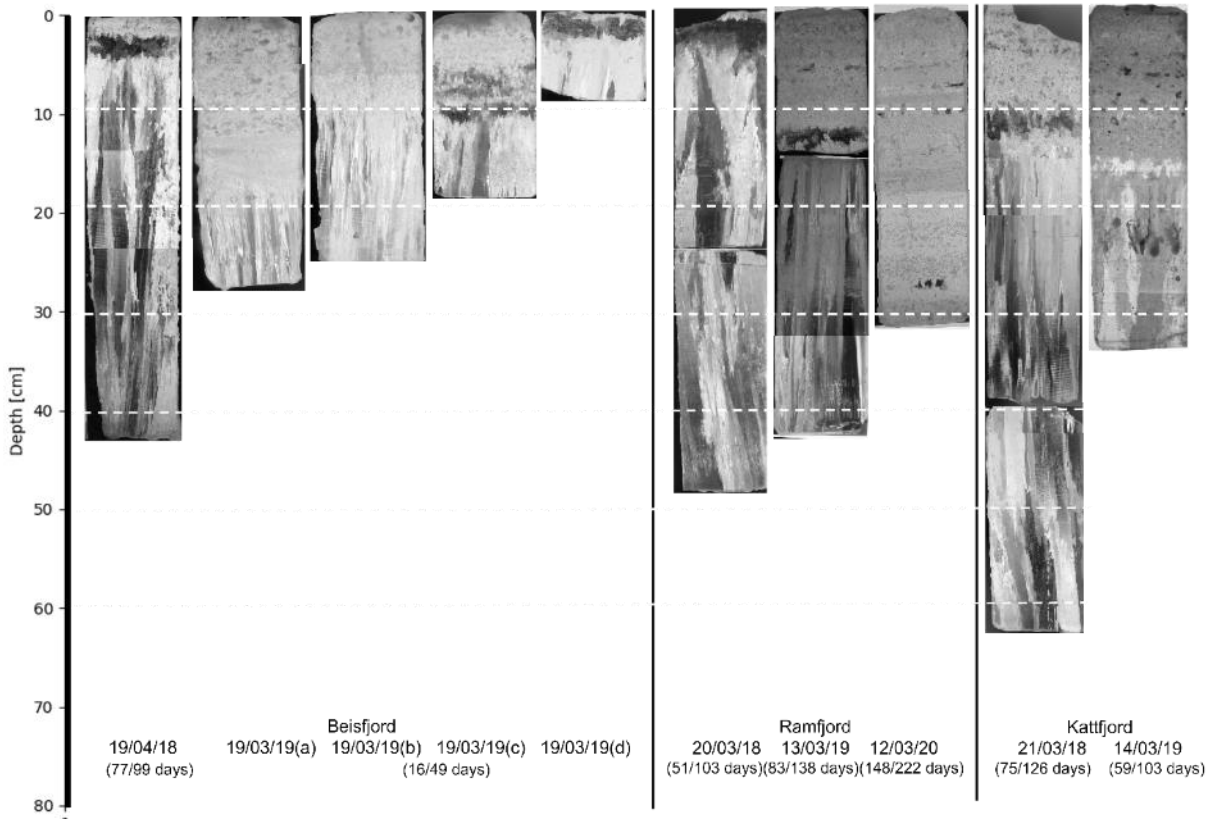

Fig.11- The same vertical thick sections as shown in Fig.9, seen through cross-polarized filters to highlight transitions in ice crystal structure. Smaller crystals, less homogeneous in shape, size and orientation are characteristic of granular ice, typically located in the upper part of the core. Elongated crystals are identified as columnar ice.

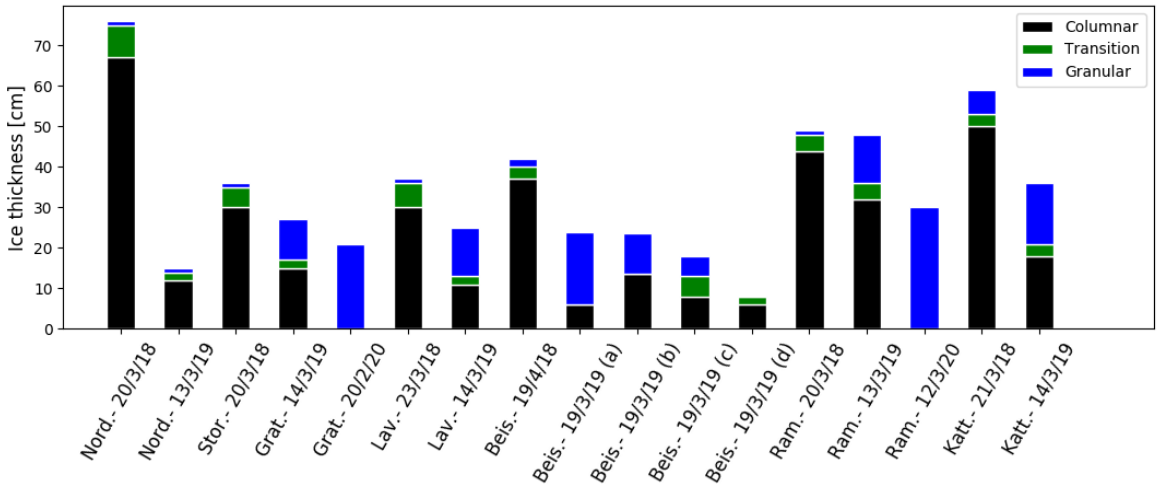

399

400 Fig. 12- Simplified view of cores showing division between columnar, transition, and granular ice. For further
401 information on cores, see Table 1.

402 ## 3.3 Ice Core Measurements – Salinity and $\delta^{18}O$

403 Profiles of ice bulk salinity and $\delta^{18}O$ are shown in Fig. 13. The fjord with the highest bulk salinity and $\delta^{18}O$
404 throughout the entire core came from Storfjord in March 2018. Second to this is a core gathered in
405 Beisfjord in 2019/20 that had high values of salinity in the upper 10 cm granular ice that quickly
406 decreased as depth increased. In all other cores, bulk salinity did not exceed 3 psu with measurements
407 being as low as 0 psu.

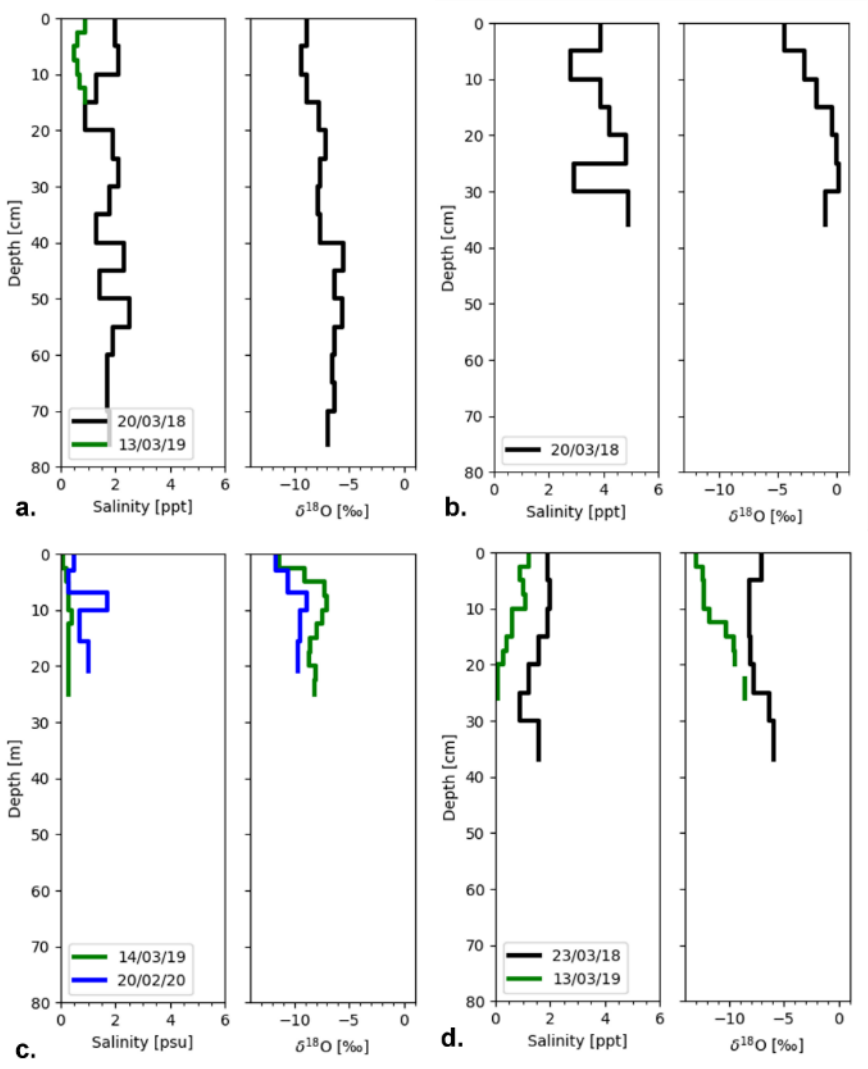

408

409 Fig.13- Profiles of bulk ice salinity and $\delta^{18}O$ for a) Nordkjosbotn, b) Storfjord, c) Gratangsbotn, and d) Lavangen

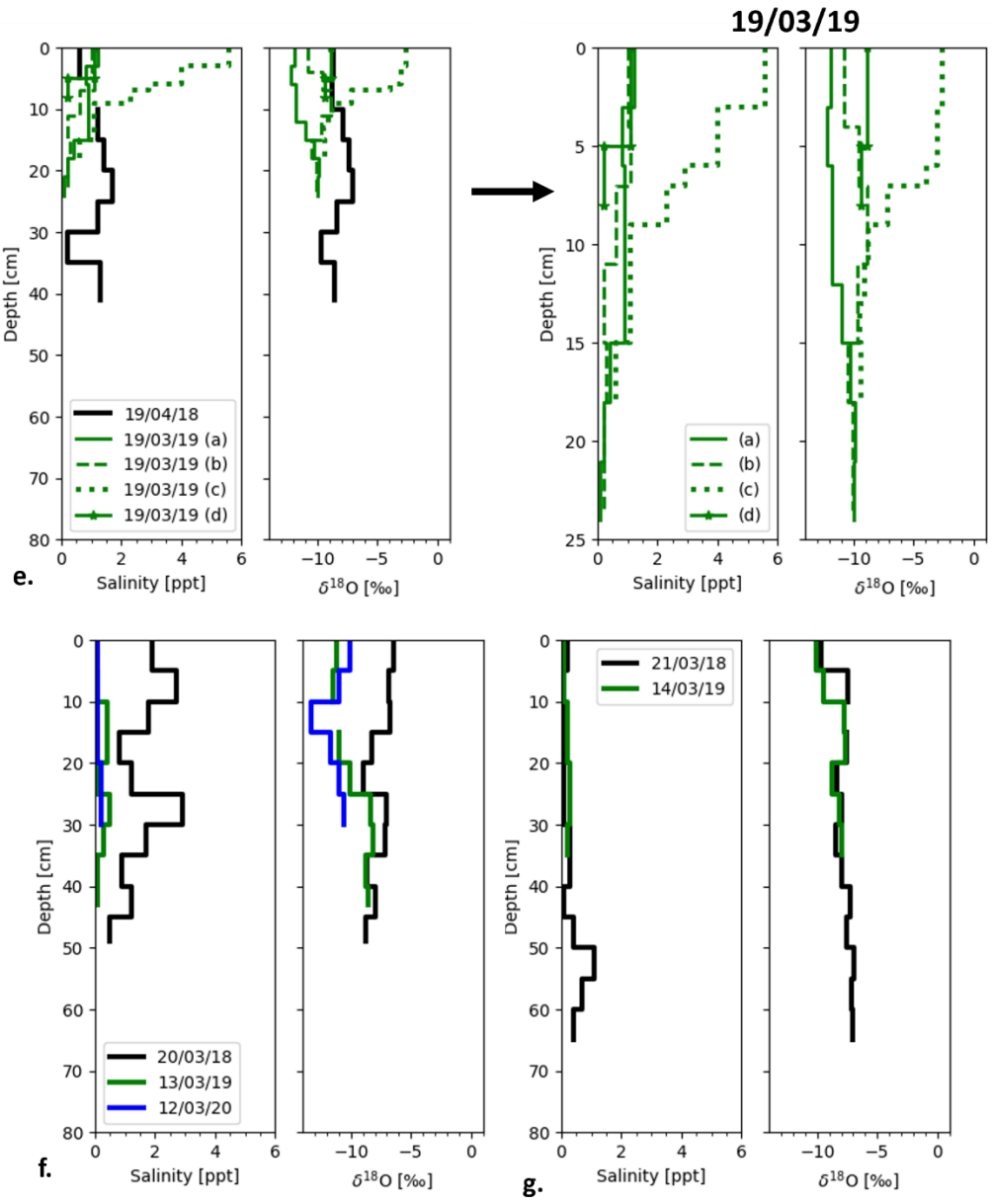

410

411 Fig. 13 (continued)- Profiles of bulk ice salinity and $\delta^{18}O$ for e) Beisfjord, f) Ramfjord, and g) Kattfjord

412

413

414

3.4 Seawater – CTD Measurements

CTD measurements reveal a relatively large variation in water temperature between the three field campaigns (Figs 14). The coldest water for all seven fjords was measured in March 2018. In all three years the four furthest north fjords (Nordkjosbotn (Fig.14a), Storfjord (Fig.14b), Ramfjord (Fig.14f), and Kattfjord (Fig.14g)) were cooler than the southern three (Gratangsbotn (Fig.14c), Lavangen (Fig. 14d), and Beisfjord (Fig.14e)), most noticeably in 2018 with the latter three fjords being upwards of 2 °C warmer. All fjords had water temperature above 0 °C except Storfjord where a temperature of -0.11 °C was measured in March 2018, which was the only year with measurements and ice in this location.

At depths greater than 1 m below the ice-ocean interface, salinity remained consistently above 32 psu for four fjords – Gratangsbotn, Nordkjosbotn, Storfjord, and Ramfjord. In Beisfjord, ocean salinity was slightly lower than the other fjords at depth being between 31 and 32 psu all three seasons. When density is considered, all fjords display an increase with depth with values ranging consistently between 1025 and 1027 kg/m^3 except for the uppermost measurements in Gratangsbotn, Lavangen, Beisfjord, and Ramfjord that dropped to, at a minimum, 1020 kg/m^3. From these CTD measurements, it is apparent that all fjords were stably stratified.

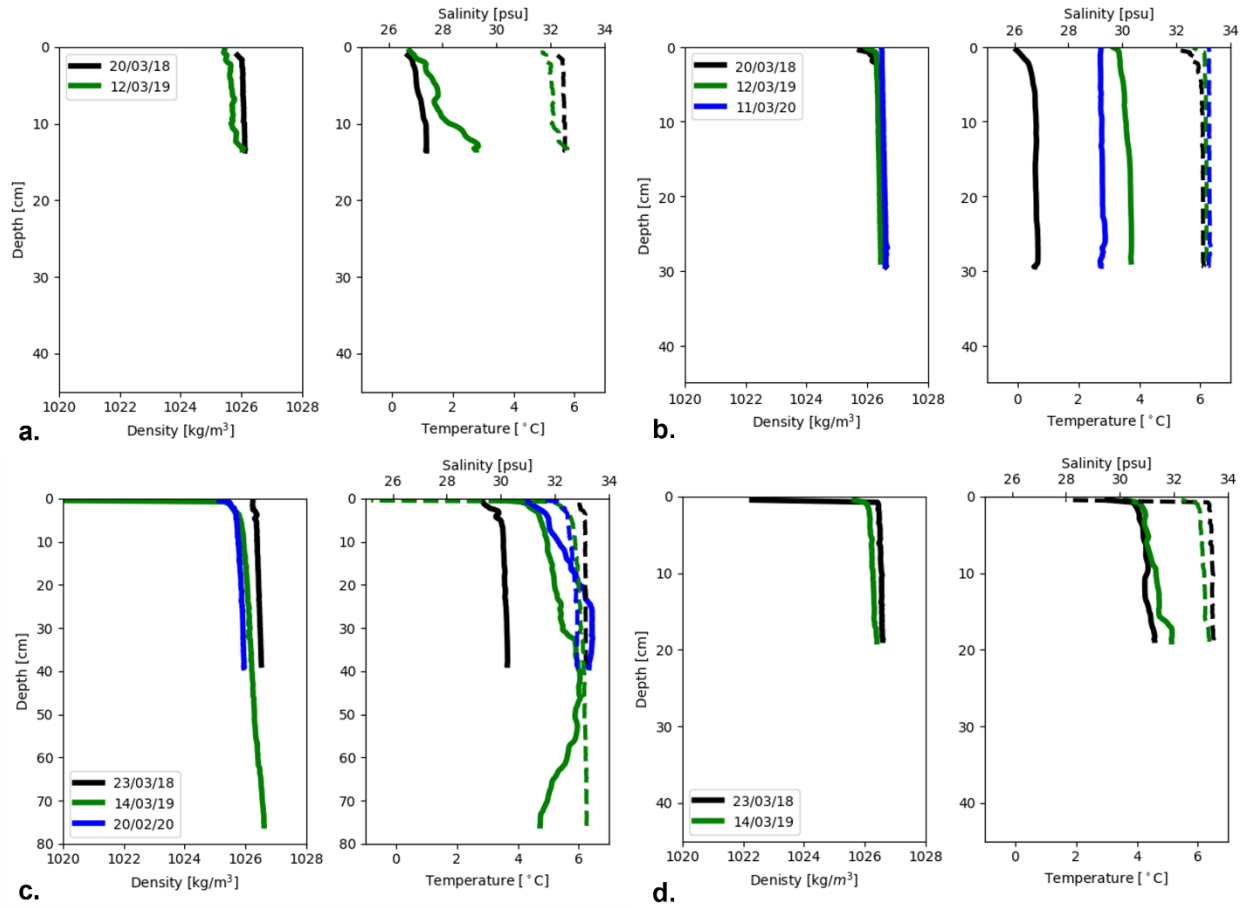

Fig.14- Profiles of seawater salinity (dashed line) and temperature (solid line) for each fjord and year. Zero depth represents the ocean surface with measurements starting at or slightly below the ice-ocean interface. a) Nordkjosbotn, b) Storfjord, c) Gratangsbotn, and d) Lavangen.

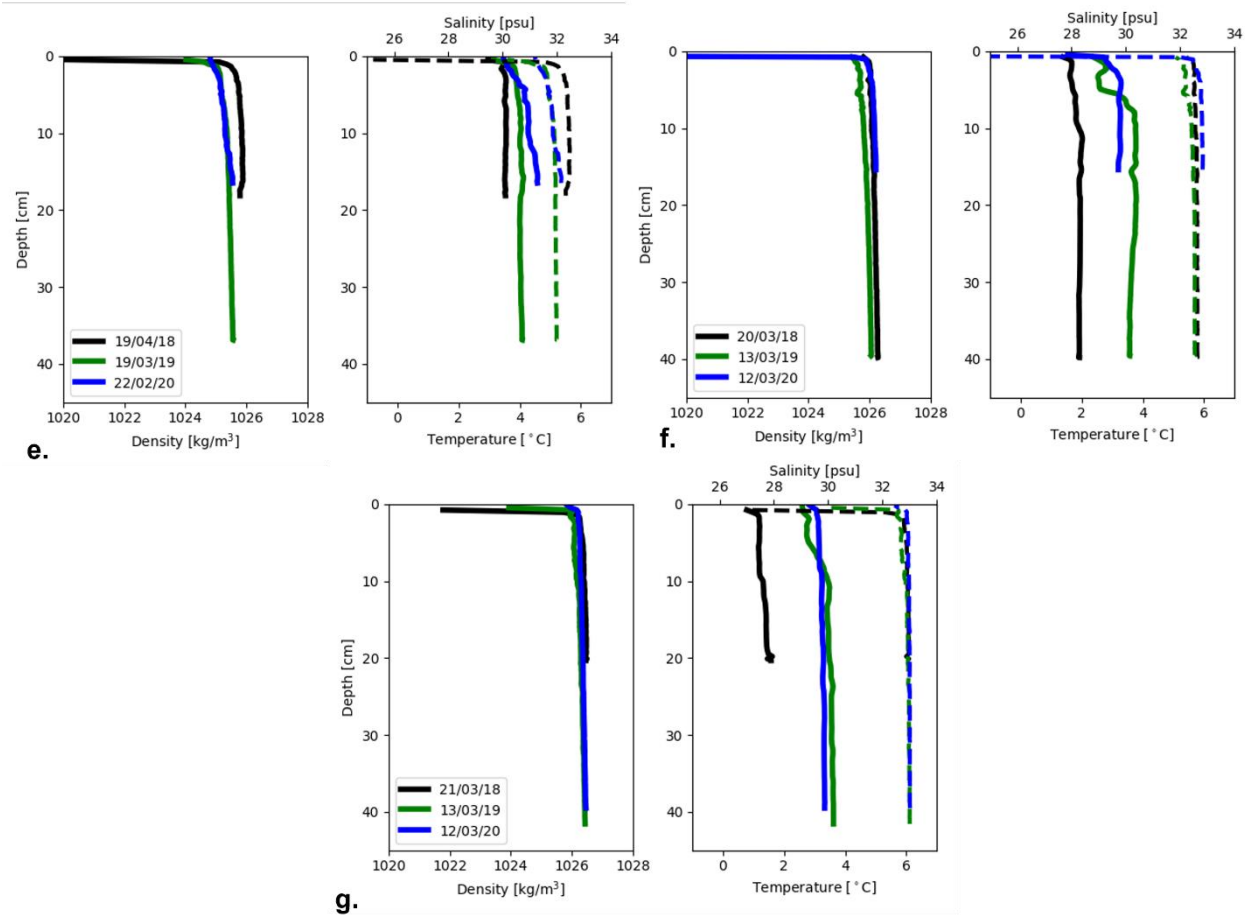

Fig.14 (continued)- Profiles of seawater salinity (dashed line) and temperature (solid line) for each fjord and year. Zero depth represents the ocean surface with measurements starting at or slightly below the ice-ocean interface. e) Beisfjord, f) Ramfjord, and g) Kattfjord

3.6 $\delta^{18}O$ in River, Ocean and Snow

The lowest $\delta^{18}O$ value measured of -13.02 ‰ occurred in the snow of Ramfjord in 2019 (Table 3). River values of $\delta^{18}O$ were near to that of snow but show differences between fjords. In Ramfjord and Nordkjosbotn, river water consistently had values of $\delta^{18}O$ below -12 ‰. For Storfjord, Ramfjord and Lavangen, $\delta^{18}O$ ranged between -11 and -12 ‰ while Kattfjord was consistently between -10 and -11 ‰. Gratangsbotn had a higher value of -10.86 ‰ in 2019 in comparison to 2020 where $\delta^{18}O$ was measured to be -11.25 ‰. Ocean water gathered at depths ranging from 0.8 m to 1.5 m from the bottom of the ice, had $\delta^{18}O$ values ranging between -1 and 0 ‰ with only two instances of lower values in 2019, in Ramfjord and in one location in Beisfjord.

Table 3- Measurements of $\delta^{18}O$ taken from seawater with depth below the ice surface in m marked in parentheses, river leading into the fjord, and snow on top of the ice. n/m = not measured.

Nordkjosbotn				**Storfjord**			
	$\delta^{18}O$ [‰]				**$\delta^{18}O$ [‰]**		
Date of measurement	**Seawater**	**River**	**Snow**	**Date of measurement**	**Seawater**	**River**	**Snow**
20 Mar 2018	n/m	n/m	n/m	20 Mar 2018	-0.17 (1.5)	n/m	n/m
13 Mar 2019	-0.17 (1.5)	-12.15	n/m	12 Mar 2019	-0.08 (1.5)	-11.55	n/m
12 Mar 2020	n/m	-12.30	n/m	11 Mar 2020	0.09 (1.5)	-11.82	n/m
Gratangsbotn				**Lavangen**			
	$\delta^{18}O$ [‰]				**$\delta^{18}O$ [‰]**		
Date of measurement	**Seawater**	**River**	**Snow**	**Date of measurement**	**Seawater**	**River**	**Snow**
23 Mar 2018	-0.28 (0.4)	n/m	n/m	23 Mar 2018	-0.12 (1.0)	n/m	n/m
14 Mar 2019	-0.92 (1.0)	-10.86	-12.55 (at surface)	14 Mar 2019	-0.53 (1.0)	-11.34	n/m
20 Feb 2020	-2.42 (1.0)	-11.25	n/m	2020	n/m	n/m	n/m
Beisfjord				**Ramfjord**			
	$\delta^{18}O$ [‰]				**$\delta^{18}O$ [‰]**		
Date of measurement	**Seawater**	**River**	**Snow**	**Date of measurement**	**Seawater**	**River**	**Snow**
19 Apr 2018	-0.56 (1.0 m)	-12.57	n/m	20 Mar 2018	-0.81 (1.5)	n/m	n/m
19 Mar 2019	-1.57 to - 0.7 (1.4 m)	-12.49	n/m	13 Mar 2019	-1.06 (0.80)	-11.14	-13.02 (surface)
22 Feb 2020	-0.81 (1.5 m)	-12.52	n/m	12 Mar 2020	-0.51 (1.0)	-11.55	nm
Kattfjord							
	$\delta^{18}O$ [‰]						
Date of measurement	**Seawater**	**River**	**Snow**				
21 Mar 2018	-0.12 (1.5)	n/m	n/m				
14 Mar 2019	-0.72 (0.80)	-10.24	-11.94 (surface)				
12 Mar 2020	-0.16 (1.5)	-10.65	n/m				

4. Discussion

Clear variations were observed in ice thickness, crystal structure, and properties between fjords and years. Here the drivers of ice formation and the differences in ice properties between seasons and fjords are examined. Analysis and discussion are included of the relationship of ice thickness and pore structure to several weather-related variables to better understand if and to what extent each may

influence ice formation in a fjord environment. In addition, the relation to fjord geometry and bathymetry with focus placed largely on the influence of freshwater flow into the fjord and the creation and persistence of a brackish surface layer is presented.

4.1 Freezing degree days and the prediction of ice thickness

With lower temperatures and a greater number of freezing degree days comes thicker ice as defined by Eqns. 3 and 4 above. However, in the data presented here, this relationship is at times weak and inconsistent. While there is a significant positive correlation ($p=0.012$) between ice thickness and freezing degree days accumulated from the start of ice formation until the date of thickness measurement during the 2017/18 season (Fig. 15a), ice growth in the 2018/19 season appears to be almost independent of this value. During the latter season, observed ice thickness ranged from 0.15 to 50 cm although FDDs only varied slightly, falling around approximately 350 °C days for all except the Beisfjord core. The number of measurements in season 2019/20 was too low to draw conclusions. When FDDs calculated from 1 Oct to 30 April is examined, only a weak positive trend is revealed (Fig.15b). Eqns. 3 and 4 provide a starting point to examine the connection between air temperature, ice growth and the factors that may disrupt this relationship. Surface melt, for example, is not included in this estimation although it can contribute to ice thickness being less than that predicted (Fig. 15a). The longest period of above freezing average daily air temperatures experienced by all fjords occurred from approximately 23 – 28 February 2019. Outside of this event, such periods of above freezing temperatures generally lasted only 1 – 3 days. The only exception was during the notably long 2019/20 season at Ramfjord, where average air temperature was above 0 °C from 7 – 14 January 2020. With above freezing days scattered amongst days of below freezing temperatures, surface melt has potential to refreeze forming superimposed ice further complicating estimations of ice thickness.

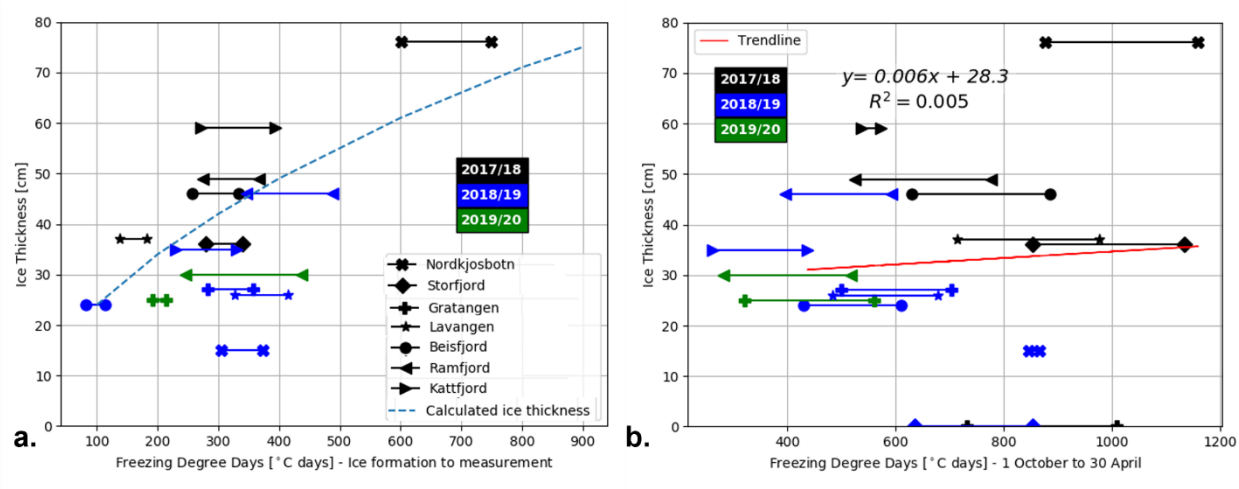

Fig.15- Ice thickness compared to freezing degree days calculated from the day of ice formation to measurement for 2017/18 season (black), 2018/19 season (blue), and 2019/20 season (green). (a) and total freezing degree days (b) from 1 October to 30 April. Two values for each fjord are shown connected- FDDs calculated using -2 °C and 0 °C. Dashed line in (a) represents the calculated ice thickness (Eq. 4). The solid, red line in (b) represents the linear trend fitted to the data with equation and R^2 marked also provided.

Oceanic heat flux is another, likely significant, contributor to the disagreement between calculated and measured ice thickness. Being dependent on coastal and tidal currents, the shape and depth of the fjord, and seasonal evolution of currents and temperature, oceanic heat flux is non-trivial to determine, and requires time series of measurements from a highly variable environment. Future work examining the topic of oceanic heat flux and its relationship to ice in fjords will therefore use detailed measurements of ocean temperature, salinity, and currents in combination with numerical model simulations.

Retardation of ice growth due to the insulating properties of snow and formation of snow-ice are also candidates that could explain the failure of FDDs to explain ice thickness in season 2018/19. To investigate the impact of particularly snow, we compare snow cover, expressed as snow water equivalent (SWE) on the day of measurement, to measurements ice thickness across all three seasons in Fig.16. The significant relationship ($p = 0.014$) supports that higher cumulative snowfall over the entirety of the season, 1 October – 30 April, is associated with thinner ice in the cores gathered. While this

517 relationship is not apparent in the winter of 2017/18 we attribute this to a larger snowfall event only
518 several days before field observations therefore having minimal influence on ice growth.

519 While the retarding effect of snowfall on ice thickness may be intuitive there is another, contradictory,
520 impact of snow at work - its ability to increase ice thickness from the ice surface, upwards. In Ramfjord,
521 as noted above, the composition of the ice between the three years varied substantially, from majority
522 congelation ice, to a mixture between congelation and granular ice, to entirely granular on the day of
523 measurement the last season (Fig. 11 & 12). Therefore, while snow may have slowed ice growth for years
524 where a solid layer of congelation ice was present, snow also likely played an important role in
525 thickening ice at times, for example in 2019/20. The identification of snow ice in comparison to columnar
526 ice using $\delta^{18}O$ is a common method to determine the fraction of each ice type. In the cores studied here,
527 this approach is complicated by the substantial amount of meteoric water, water that originates as
528 precipitation like rain or snow including runoff from rivers, in the upper water column contributing to ice
529 formation. Low values for $\delta^{18}O$ cannot therefore be attributed to only snow ice but also frazil or
530 congelation ice formed from fresh or brackish water or snow flooded by fresh and brackish water instead
531 of seawater. Each will have a distinct signature for $\delta^{18}O$ that reflects both the mixture of fresh and ocean
532 water present at the ice-ocean interface and growth rate. The samples collected show $\delta^{18}O$ values
533 consistently below 0‰, the point often used as the delineator between snow ice and congelation sea ice
534 (Eicken et al., 1994; Jeffries et al., 1994; Smith et al. , 2012). The only core with values above 0‰ was
535 taken in Storfjord. Granular ice having a lower $\delta^{18}O$ value is present in the upper 5 cm however as ice
536 transitions to congelation ice, $\delta^{18}O$ is shown to increase gradually with no abrupt jumps to signal a
537 boundary.

538 The proportion of snow ice is an important factor to consider as it can have an impact on, for example,
539 the biologic productivity of the ice (Granskog et al., 2003), the approach to accidents like an oil spill
540 (Oggier et al., 2019), the interaction between ice and structures (Timco & Weeks, 2010), and how ice

conditions may evolve through the season (Polashenski et al., 2012). The timing of snowfall events, air and ocean temperature, and other variables like wind and tides that cause mixing, can all contribute to the balance between congelation and granular ice growth- this topic specific to a fjord environment would benefit from further examination.

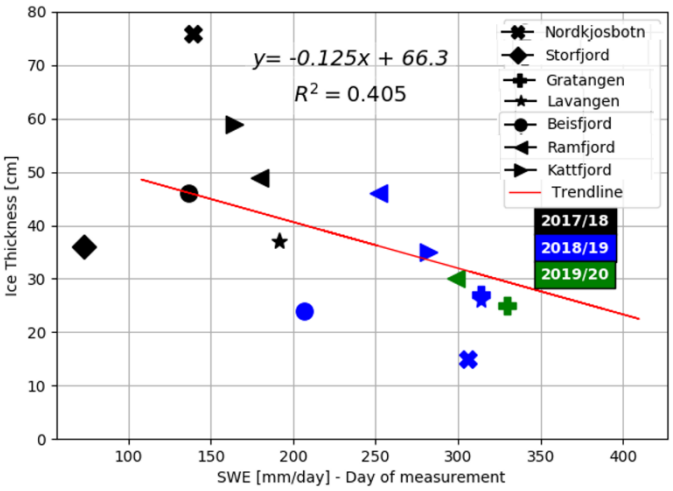

Fig. 16- Ice thickness compared to snow water equivalent (SWE) on the day of measurement for 2017/18 season (black), 2018/19 season (blue), and 2019/20 season (green). The solid line represents the linear trend fitted to the data with equation and R^2 marked also provided.

Another factor that may impact the relationship between freezing degree days and ice thickness and the general formation of ice growth in fjords is freshwater which, when combined with limited mixing with the saline ocean water below, can cause a decoupling between the surface and intermediary layer. Through cooling of this upper-most surface layer, ice can begin to form. For ice grown from seawater of approximately 33 psu, ice bulk salinity values between 4 – 8 psu have been both modelled and observed during the ice growth phase in the Arctic (Petrich & Eicken, 2010; Petrich et al., 2011). Measurements of ice bulk salinity primarily below 3 psu and often below 1 psu, are indicative of brackish or fresh water at the ice-ocean interface at the time of ice growth yet ocean salinity on the day ice cores were gathered

was not often measured below 31 psu. For the fjords considered, there was an insignificant relationship found between ice thickness and total runoff from ice formation to the day of measurement and over the entire season ($p= 0.466$ and $p=0.372$ respectively) (Fig. 17). When a linear relationship is applied, the two show opposing relationships- runoff and ice thickness being negatively correlated when considering only the ice growth period, and positively related when the entire season is considered. In both cases however, the spread of values is large. The brackish or fresh water was, therefore, likely confined to a temporary layer at the ice–ocean interface controlled by the amount of freshwater flow leading into the fjord and mixing by tides and currents.

While the number of variables at play in a fjord environment makes it difficult to determine the influence of freshwater flux on ice growth rate, its most significant role may come during the initial formation of the ice. Fresh water will mix with the upper surface layer of the ocean as it enters the fjord, decreasing its salinity to become brackish and decreasing its temperature. The latter, the result of runoff coming from higher elevations where lakes and rivers are frozen and water temperature is often near to 0 °C in winter. The thicker this brackish surface layer and the greater the difference in density between it and the intermediary layer, the greater the amount of energy needed to mix and disperse this layer (Myksvoll et al., 2014). Heat loss may resultantly be largely confined to the brackish surface layer enabling ice formation during periods of sub-freezing temperatures as well as subsequent ice growth. Local knowledge supported by scientific studies highlight the relationship between fresh water flux in winter and ice formation as noted by Green et al. (2004) when examining the impact of hydropower dams on fjords. While seawater temperatures below 0 °C were measured in 2017/18 in Storfjord, in all other fjords and years (see Fig. 14), seawater temperature was several degrees above even the freezing temperature of fresh water on the day of measurement. The 2018/19 season, in particular, displays the possible relationship between a strong gradient in density in the upper water column, a pycnocline, and onset of ice formation. Although warmer than 2017/2018 based on FDDs (see Table 2), runoff is seen to

fluctuate through the beginning of December in all fjords with another event occurring at the end of February (Fig.9). We hypothesize that these events created a fresh/brackish surface layer that led to the formation of ice over a larger area of the fjord when temperatures dropped below freezing (Li & Ingram, 2007).

Once a layer of ice forms, turbulence at the surface that may have initially prevented ice growth will decrease enabling congelation ice growth downward as exemplified by cores gathered in March 2018 where congelation ice dominated (Fig. 11 & 12). Alternatively, a thin layer of ice can provide a platform for snow to accumulate, depressing the surface and leading to flooding of the snowpack and the formation of granular, snow ice once seawater refreezes. The latter is likely the primary process driving the thickening of ice sampled in 2020. In 2019, both mechanisms of growth are clear in the cores with all exhibiting both congelation and granular ice.

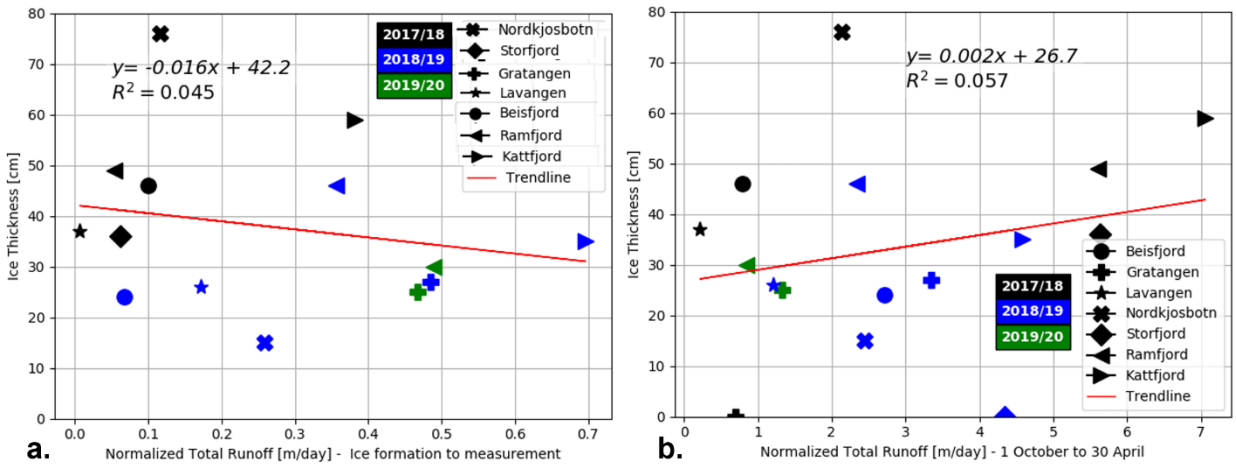

Fig. 17- Ice thickness compared to total runoff up to the day of measurement (a) and over the entire season (b) for 2017/18 season (black), 2018/19 season (blue), 2019/20 season (green). The line represents the linear trend fitted to the data. The trends are not significantly different from 0.

4.2 Conditions at the ice-ocean and ice-air interface and relationship to variations in pore structure

The proportion of granular to congelation ice is the clearest indicator of different ice conditions in the seven fjords observed (Fig. 12). Through examining bands of different pore structure and density and the associated fluctuations in bulk salinity and $\delta^{18}O$ a more detailed description of how the ice formed may be formulated.

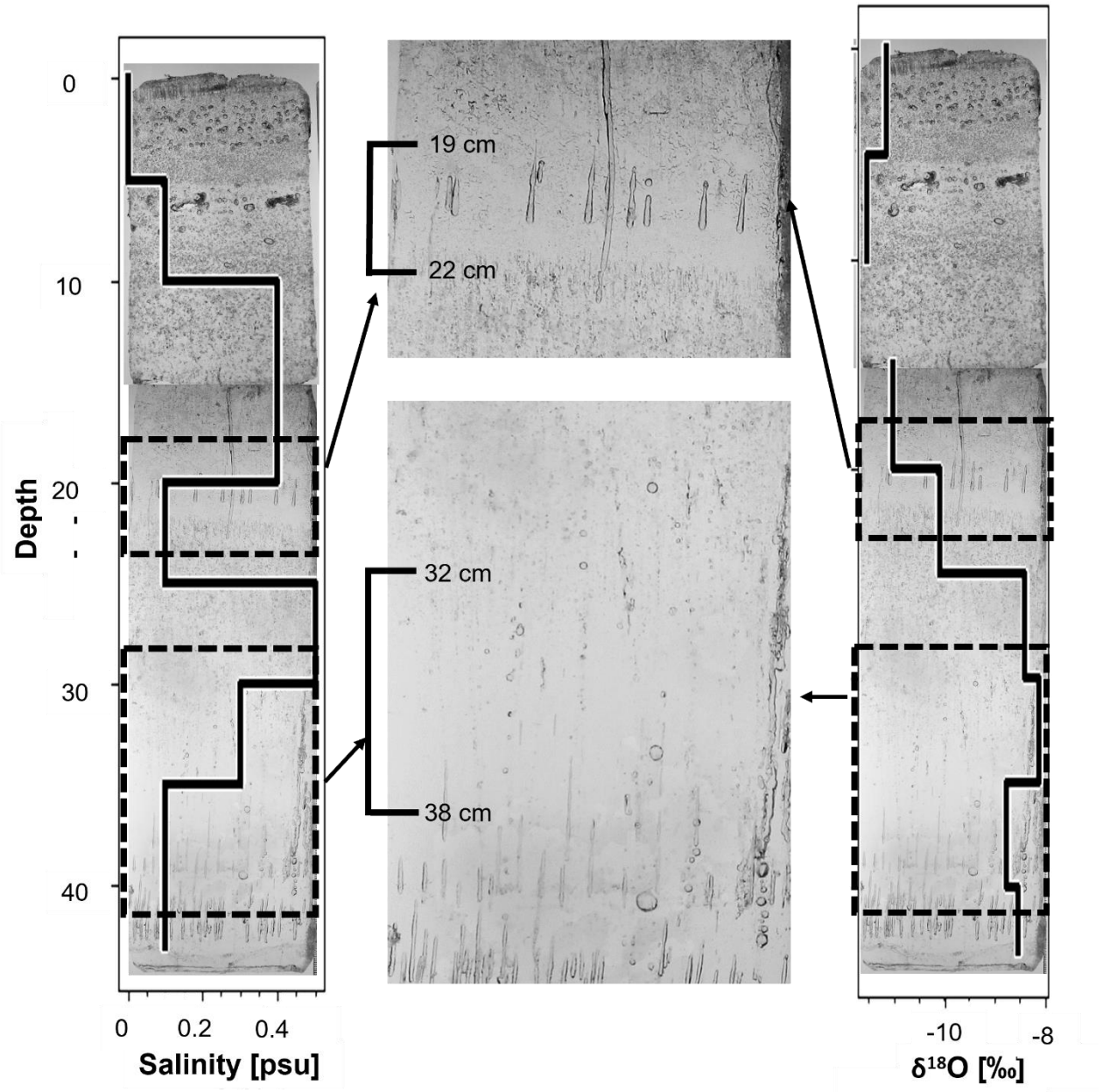

603

604 Fig.18- Backlit thick section of Ramfjord ice core gathered during the 2018/19 season with measurements of bulk
605 salinity and $\delta^{18}O$ overlain with close-up view of two sections.

606 The cores presented in Fig.10 provide many examples of obvious changes in pore shape, size, and density
607 for example in the congelation ice of the Ramfjord core gathered March 2019. Shown again in Fig. 18
608 with salinity and $\delta^{18}O$ overlain, pores at 19 cm depth are nearly 2 cm in length and clearly separated then

become much smaller and densely packed around 22 cm. Transitions are also apparent at approximately 32 cm and 38 cm with bulk salinity and $\delta^{18}O$ showing clear variation with the two properties at times being negative correlated as at 20 cm depth, or positively correlated as at 35 cm depth. These shifts in pore shape and size, may be caused at least in part to the source of the water, namely the amount of freshwater, in combination with other factors such as ice temperature and growth rate, and flow rate of surface water. Additionally, not all pores will hold liquid brine but be air-filled pores also contributing to the variation in pore characteristics (Light et al., 2003). How these factors combine and the resultant impact on bulk salinity and $\delta^{18}O$ values and ice microstructure are currently poorly understood with further investigation recommended in the specific application of fjord environments.

4.3 The impact of freshwater entry point, fjord geometry, and bathymetry

Multiple cores collected in Beisfjord in 2019 provide an example of how ice conditions may vary along a fjord due to location of freshwater input and pathways it follows. Four cores were gathered along a transect reaching 2.5 km out from the head of the fjord (Fig.6). In the first two cores, (a) and (b), salinity is similar being less than 1.0 psu while (a) has lower $\delta^{18}O$ than (b) (see Fig. 13e). This may be due to a difference in growth rate but given the increasing distance from the river, this slight difference might represent a lessening amount of river water at the ice-ocean interface. The third core, (c), has less granular ice (Figs 10 & 11) but some of the highest values of salinity and $\delta^{18}O$ in the upper 10 cm, gradually decreasing with depth. It is hypothesized that the water that infiltrated the snowpack and refroze in (c) was possibly higher in salinity due to timing or distance from the river. The final core, (d) was composed primarily of nearly transparent ice due to very low porosity (Figs. 10 & 11). In the bottom 8 cm of (c) and the entirety of (d), $\delta^{18}O$ measured between -9.0 to -9.5 ‰. It is hypothesized that the water that led ice at (d) to form from the surface down was also present at the ice-ocean interface of (c), forming the bottom section of this core. The similar decrease in $\delta^{18}O$ found in cores (c) and (d) was not observed in cores (a) and (b). Here, ice had values of $\delta^{18}O$ consistently below 9.0 ‰, often below 10 ‰.

633 The water at the ice-ocean interface at (a) and (b) may therefore have differed from that at (c) and (d)
634 during the period ice was present.

635 Fjord geometry and bathymetry are also important factors to consider when examining where, when,
636 and what type of ice was present. A constriction, shallow sill, or both can lead to a higher tidal velocity
637 and resultantly heat flux. Significant bends in a fjord's coastline may also act to alter tidal velocity and
638 shelter parts of a fjord from oceanic currents and waves as well as weather patterns, e.g. wind that
639 blows preferentially from certain directions. In Ramfjord particularly, these bathymetric and coastal
640 features appear to influence the extent of ice. From observation supported by timelapse and satellite
641 imagery, ice formation began at the head of the fjord near the river's entrance and extended out to the
642 sill and abrupt bend soon after initial ice formation in 2019 and 2020. In 2019, ice eventually rounded
643 the corner stopping where a constriction is present. As time progressed, after the day of measurement,
644 the ice pulled back to a similar location as the ice edge observed in 2020 holding more stably before
645 further recession and melt occurred. Further research is recommended to investigate the relationship
646 between ice extent and break-up to coastal geometry and bathymetry.

647 5. Conclusions

648 The conditions along coastal Norway may parallel other locations in the Arctic and sub-Arctic regions
649 with similar variability in freshwater flux during the winter months, and weather and oceanic conditions.
650 Along with potentially altering the safety of the ice for access, there are also implications for structures
651 placed in these areas, boats trying to transit through, response to oil spills, as well as the overall health
652 and ecology of fjords and coastal regions. From the work presented here the following conclusions can
653 be drawn:

654 - De-coupling between the surface and intermediary layer of the fjord plays an important role in
655 ice formation in Norwegian fjords as demonstrated by the distinct difference in ice bulk salinity

656 and $\delta^{18}O$ in the fjord ice versus the fjord water below. This is exemplified by the low values of ice
657 bulk salinity and $\delta^{18}O$ measured, characteristic of ice frozen from fresh water, not seawater.
658 - The use of freezing degree days may not be a dependable predictor of ice thickness when
659 applied to Norwegian fjords. Substantial consideration must be given to the actual date of onset
660 of ice formation and snow cover. Other factors that may contribute include an influx of warmer
661 water into the fjord and runoff.
662 - Single-year measurements of ice in Norwegian fjords provide little insight into ice properties one
663 should expect over longer time spans since interannual variability is high.
664 - Timing is an important factor in ice formation in fjords. How weather and oceanic conditions
665 overlap, including cold weather, runoff, snowfall, wind, tides, and fjord-coast water exchange,
666 will determine when, how much and what type of ice will form.

667 6. Acknowledgements

668 This work was funded by the Centre for Integrated Remote Sensing and Forecasting for Arctic Operations
669 (CIRFA), a Centre for Research- based Innovation (Research Council of Norway project number 237906),
670 and partners. The authors would also like to thank the two anonymous reviewers and editor, Knut
671 Høyland, who offered many helpful comments to increase the quality of this paper.

672 7. Works Cited

673 Anderson, D. L. (1961). Growth rate of sea ice. *Journal of Glaciology*, *3*(30), 1170–1172.

674 Arrigo, K., Mock, T., & Lizotte, M. (2010). Primary Producers and Sea Ice. In D. Thomas & G. Dieckmann
675 (Eds.), *Sea Ice* (2nd ed., pp. 283–326). Oxford: Wiley-Blackwell.

676 Asplin, L., Salvanes, A. G. V., & Kristoffersen, J. B. (1999). Nonlocal wind-driven fjord-coast advection and

its potential effect on plankton and fish recruitment. *Fisheries Oceanography*, *8*(4), 255–263. https://doi.org/10.1046/j.1365-2419.1999.00109.x

Bergström, S. (1992). The HBV model - its structure and applications, SMHI Reports RH 4. *Swedish Meteorological and Hydrological Institute, Norrköping*, *4.*

Brandon, M., Cottier, F., & Nilsen, F. (2010). Sea Ice and Oceanography. In David N Thomas & G. Dieckmann (Eds.), *Sea Ice* (2nd ed., pp. 79–112). Oxford: Wiley-Blackwell.

Cole, D. M., Eicken, H., Frey, K., & Shapiro, L. H. (2004). Observations of banding in first-year Arctic sea ice. *Journal of Geophysical Research: Oceans*, *109 (C8).* https://doi.org/10.1029/2003JC001993

Cottier, F. R., Nilsen, F., Skogseth, R., Tverberg, V., Skarðhamar, J., & Svendsen, H. (2010). Arctic fjords: a review of the oceanographic environment and dominant physical processes. *Geological Society, London, Special Publications*, *344*(1), 35–50. https://doi.org/10.1144/SP344.4

Dickens, D. (2011). Behavior of oil spills in ice and implications for Arctic spill response. *Proceedings of the Arctic Technology Conference*, Houston, Texas, USA, 7-9 February.

Eicken, H, Lange, MA and Wadhams, P (1994) Characteristics and distribution patterns of snow and meteoric ice in the Weddell Sea and their contribution to the mass balance of sea ice. *Annales de Geophysique 12(1)*, 80–93. doi: 10.1007/s00585-994-0080-x.

Eicken, H., Bock, C., Wittig, R., Miller, H., & Poertner, H. O. (2000). Magnetic resonance imaging of sea-ice pore fluids: Methods and thermal evolution of pore microstructure. *Cold Regions Science and Technology*, *31*(3), 207–225. https://doi.org/10.1016/S0165-232X(00)00016-1

Eicken, H., Dmitrenko, I., Tyshko, K., Darovskikh, A., Dierking, W., Blahak, U., … & Kassens, H. (2005).

Zonation of the Laptev Sea landfast ice cover and its importance in a frozen estuary. *Global and Planetary Change*, *48(1-3)*, 55–83. https://doi.org/10.1016/j.gloplacha.2004.12.005

Eicken, H. (1998). Deriving Modes and Rates of Ice Growth in the Weddell Sea from Microstructural, Salinity and Stable-Isotope Data. *Antarctic Sea Ice: Physical Processes, Interactions and Variability, Antarct. Res. Ser*, *74*, 89–122. https://doi.org/10.1029/ar074p0089

Eilertsen, H. C., & Skarðhamar, J. (2006). Temperatures of north Norwegian fjords and coastal waters: Variability, significance of local processes and air-sea heat exchange. *Estuarine, Coastal and Shelf Science*, *67*(3), 530–538. https://doi.org/10.1016/j.ecss.2005.12.006

Fofonoff, N., & Millard, R. (1983). Algorithms for computation of fundamental properties of seawater. *Unesco Technical Papers in Marine Science*, *44*.

Gerland, S., & Renner, A. H. H. (2007). Sea-ice mass-balance monitoring in an Arctic fjord. *Annals of Glaciology*, *46*, 435–442. https://doi.org/10.3189/172756407782871215

Gorelick, N., Hancher, M., Dixon, M., Ilyushchenko, S., Thau, D., & Moore, R. (2017). Google Earth Engine: Planetary-scale geospatial analysis for everyone. *Remote Sensing of Environment, 202,* 18-27. https://doi.org/10.1016/j.rse.2017.06.031.

Gradinger, R., Friedrich, C., & Spindler, M. (1999). Abundance, biomass and composition of the sea ice biota of the Greenland Sea pack ice. *Deep-Sea Research Part II: Topical Studies in Oceanography*, *46*(6–7), 1457–1472. https://doi.org/10.1016/S0967-0645(99)00030-2

Granskog, M. A., Ehn, J., & Niemelä, M. (2005). Characteristics and potential impacts of under-ice river plumes in the seasonally ice-covered Bothnian Bay (Baltic Sea). *Journal of Marine Systems*, *53*(1–4), 187–196. https://doi.org/10.1016/j.jmarsys.2004.06.005

718 Granskog, M.A., Kaartokallio, H., Kuosa, H., Thomas, D. N., & Vainio, J. (2006). Sea ice in the Baltic Sea - A
719 review. *Estuarine, Coastal and Shelf Science*, *70*(1–2), 145–160.
720 https://doi.org/10.1016/j.ecss.2006.06.001

721 Granskog, M. A., Kaartokallio, H., & Shirasawa, K. (2003). Nutrient status of Baltic Sea ice : Evidence for
722 control by snow-ice formation, ice permeability, and ice algae. *Journal of Geophysical Research:*
723 *Oceans*, *108*(C8). https://doi.org/10.1029/2002JC001386

724 Granskog, M.A., Kaartokallio, H., Thomas, D. N., & Kuosa, H. (2005). Influence of freshwater inflow on the
725 inorganic nutrient and dissolved organic matter within coastal sea ice and underlying waters in the
726 Gulf of Finland (Baltic Sea). *Estuarine, Coastal, and Shelf Science 65*(1-2), 109–122.
727 https://doi.org/10.1016/j.ecss.2005.05.011

728 Green, J. A. M., Molvaer, J., & Stigebrandt, A. (2004). Hydrographic response of Holandsfjord to changed
729 freshwater runoff. *Journal of Geophysical Research: Oceans*, *109*(C7).
730 https://doi.org/10.1029/2004JC002295

731 Holtedahl, H. (1967). Notes on the Formation of Fjords and Fjord-Valleys. *Geografiska Annaler. Series A,*
732 *Physical Geography*, *49*(2), 188–203.

733 Hop, H., & Wiencke, C. (2019). The Ecosystem of Kongsfjorden, Svalbard. In H. Hop & C. Wiencke (Eds.),
734 *Advances in Polar Ecology*. Springer: Cham. https://doi.org/https://doi.org/10.1007/978-3-319-
735 46425-1_1

736 Hughes, N. (2006). *NP57A, NP57B, NP58A, NP58B Norway Pilot. Sea Ice Conditions: West coast of*
737 *Norway from: Lindesnes to Statlandet, Statllandet to Risværfjorden. Offshore and coastal waters of*
738 *Norway from: Risværfjorden to the north part of Vesterrålen, Andfjorden to Varang*. Argyll, UK:
739 Scottish Association for Marine Science. *Engineering under Arctic Conditions, POAC*.

Inall, M. E., & Gillibrand, P. A. (2010). The physics of mid-latitude fjords: a review. *Geological Society, London, Special Publications*, *344*(1), 17–33. https://doi.org/10.1144/SP344.3

Ingram, R. G., Wang, J., Lin, C., Legendre, L., & Fortier, L. (1996). Impact of freshwater on a subarctic coastal ecosystem under seasonal sea ice (southeastern Hudson Bay , Canada). I . Interannual variability and predicted global warming influence on river plume dynamics and sea ice. *Journal of Marine Systems*, 7(2-4), 221–231.

Jeffries, M.O., Shaw, R.A., Morris, K., Veazey, A.L. and Krouse, H.R. (1994) Crystal structure, stable isotopes (δ18O), and development of sea ice in the Ross, Amundsen, and Bellingshausen seas, Antarctica. *Journal of Geophysical Research: Oceans 99*, 985–995. doi: 10.1029/93JC02057.

Jones, E. M., Renner, A. H. H., Chierici, M., Wiedmann, I., Lødemel, H. H., Biuw, M., & Miller, L.A. (2020). Seasonal dynamics of carbonate chemistry, nutrients and CO2 uptake in a sub-Arctic fjord. *Elementa: Science of the Anthropocene, 8.* https://doi.org/10.1525/elementa.438

Kaartokallio, H., Kuosa, H., Thomas, D. N., Granskog, M. A., & Kivi, K. (2007). Biomass , composition and activity of organism assemblages along a salinity gradient in sea ice subjected to river discharge in the Baltic Sea. *Polar Biology*, *30(2)*, 183–197. https://doi.org/10.1007/s00300-006-0172-z

LeGrande, A. N., & Schmidt, G. A. (2006). Global gridded data set of the oxygen isotopic composition in seawater. *Geophysical Research Letters*, 33(12).

Li, S. S., & Ingram, R. G. (2007). Isopycnal deepening of an under-ice river plume in coastal waters: Field observations and modeling. *Journal of Geophysical Research: Oceans*, *112*(C7). https://doi.org/10.1029/2006JC003883

Light, B., G. A. Maykut, & Grenfell, T.C. (2003) Effects of temperature on the microstructure of first-year

Arctic sea ice, *Journal of Geophysical Research, 108*(C2), 3051, doi:10.1029/2001JC000887.

Lussana, C., Saloranta, T., Skaugen, T., Magnusson, J., Tveito, O.E., & Andersen, J. (2018). SeNorge2 daily precipitation, an observational gridded dataset over Norway from 1957 to the present day. *Earth System Science Data*, *10*(1), 235–249. https://doi.org/10.5194/essd-10-235-2018

Macdonald, R.W., Carmack, E. C., & Paton, D. W. (1999). Using the δ18O composition in landfast ice as a record of Arctic estuarine processes. *Marine Chemistry*, *65(1-2)*, 3–24.

Macdonald, R.W., Paton, D. W., Carmack, E. C., & Omstedt, A. (1995). The freshwater budget and under-ice spreading of Mackenzie River water in the Canadian Beaufort Sea based on salinity and 18O/16O measurements in water and ice. *Journal of Geophysical Research: Oceans*, *100*(C1), 895–919.

Mankettikkara, R. (2013). *Hydrophysical characteristics of the northern Norwegian coast and fjords*. (Doctoral dissertation, Universitetet i Tromsø).

Myksvoll, M. S., Sandvik, A. D., Asplin, L., & Sundby, S. (2014). Effects of river regulations on fjord dynamics and retention of coastal cod eggs. *ICES Journal of Marine Science*, *71*(4), 943–956. https://doi.org/10.1093/icesjms/fst113

Nan, Y., Tian, F., Hu, H., Wang, L., & Zhao, S. (2019). Stable isotope composition of river waters across the world. *Water*, 11(9), 1760.

Nedbørfelt (REGINE). (2020). Retrieved from https://www.nve.no/karttjenester/kartdata/vassdragsdata/nedborfelt-regine/

Nilsen, F., Cottier, F., Skogseth, R., & Mattsson, S. (2008). Fjord-shelf exchanges controlled by ice and brine production: The interannual variation of Atlantic Water in Isfjorden, Svalbard. *Continental*

Shelf Research, *28*(14), 1838–1853. https://doi.org/10.1016/j.csr.2008.04.015

O'Sadnick, M., Petrich, C., Brekke, C., & Skarðhamar, J. (2020). Ice extent in sub-arctic fjords and coastal areas from 2001 to 2019 analyzed from MODIS imagery. *Annals of Glaciology, 61*(82), 210-226. https://doi.org/10.1017/aog.2020.34

Oggier, M., Eicken, H., Petrich, C., Wilkinson, J., & O'Sadnick, M. (2019). Crude oil migration in sea-ice: Laboratory studies of constraints on oil mobilization and seasonal evolution. *Cold Regions Science and Technology*, *174,* 102924.

Petrich, C., & Eicken, H. (2010). Growth, Structure, and Properties of Sea Ice. In D. Thomas & G. Dieckmann (Eds.), *Sea Ice* (2nd ed., pp. 23–77). Oxford: Wiley Blackwell.

Petrich, C., Karlsson, J., & Eicken, H. (2013). Porosity of growing sea ice and potential for oil entrainment. *Cold Regions Science and Technology*, *87*, 27–32.

Petrich, C., Langhorne, P., & Eicken, H. (2011). Modelled Bulk Salinity of Growing First-Year. In *Proceedings of the 21st International Conference on Port and Ocean Engineering under Arctic Conditions*.

Polashenski, C., Perovich, D., & Courville, Z. (2012). The mechanisms of sea ice melt pond formation and evolution. *Journal of Geophysical Research: Oceans*, *117*(C1). https://doi.org/10.1029/2011JC007231

Porter, S. C. (1989). Some geological implications of average Quaternary glacial conditions. *Quaternary Research*, *32(3)*, 245–261. https://doi.org/10.1016/0033-5894(89)90092-6

Rikardsen, A. H., Haugland, M., Bjørn, P. A., Finstad, B., Knudsen, R., Dempson, J. B., … Holm, M. (2004). Geographical differences in marine feeding of Atlantic salmon post-smolts in Norwegian fjords.

Journal of Fish Biology, *64(6)*, 1655–1679. https://doi.org/10.1111/j.0022-1112.2004.00425.x

Skarðhamar, J., Albretsen, J., Sandvik, A. D., Lien, V. S., Myksvoll, M. S., Johnsen, I. A., … Bjørn, P. A. (2018). Modelled salmon lice dispersion and infestation patterns in a sub-arctic fjord. *ICES Journal of Marine Science*, *75*(5), 1733–1747. https://doi.org/10.1093/icesjms/fsy035

Skogseth, R., Olivier, L. L., Nilsen, F., Falck, E., Fraser, N., Tverberg, V., … Falk-Petersen, S. (2020). Variability and decadal trends in the Isfjorden (Svalbard) ocean climate and circulation – An indicator for climate change in the European Arctic. *Progress in Oceanography*, *187*, 102394. https://doi.org/10.1016/j.pocean.2020.102394

Smith, I. J., Langhorne, P. J., Frew, R. D., Vennell, R., & Haskell, T. G. (2012). Sea ice growth rates near ice shelves. *Cold Regions Science and Technology*, 83, 57-70.

Stigebrandt, A. (2012). Hydrodynamics and Circulation of Fjords. In L. Bengtsson, R. W. Herschy, & R. W. Fairbridge (Eds.), *Encyclopedia of Lakes and Reservoirs. Encyclopedia of Earth Sciences Series.* Dordrecht: Springer. https://doi.org/10.5860/choice.50-3613

Timco, G. W., & Weeks, W. F. (2010). A review of the engineering properties of sea ice. *Cold Regions Science and Technology*, *60*(2), 107–129. https://doi.org/10.1016/j.coldregions.2009.10.003

Tucker, W. B., Perovich, D. K., Gow, A. J., Weeks, W. F., & Drinkwater, M. R. (1992). Physical properties of sea ice relevant to remote sensing. *Microwave Remote Sensing of Sea Ice*, *68*, 9–28.

Turner, K. E., Smith, I. J., Tison, J. L., Verbeke, V., McGuinness, M., Ingham, M., ... & Trodahl, J. (2017). Sea ice growth rates from tide-driven visible banding. *Journal of Geophysical Research: Oceans*, 122(6), 4675-4684.

Walker, E., Wiedmann, I., Renner, A., Nikolopoulos, A., & Skarðhamar, J. (n.d.). Pelagic ecosystem dynamics between late autumn and the post spring bloom in a high latitute fjord. *Submitted, In Review*.

8 Paper 3

The use of ice bulk salinity and $\delta^{18}O$ to investigate changes in the fjord environment over a winter season

M. O'Sadnick, C. Petrich, & J. Skarðhamar

In Review (as of 30 June 2022):
The Cryosphere

The use of ice bulk salinity and $\delta^{18}O$ to investigate changes in the fjord environment over a winter season

Megan O'Sadnick[1,2], Chris Petrich[2], Jofrid Skarðhamar[3]

[1]Department of Physics and Technology, UiT The Arctic University of Norway, Tromsø, 9019, Norway
[2]SINTEF Narvik, Narvik, 8517, Norway
[3]Institute of Marine Research, Tromsø, 9007, Norway

Correspondence to: Megan O'Sadnick (megan.osadnick@sintef.no)

Abstract. Ice that forms in the fjords of northern Norway often undergo temperature fluctuations, rising above and below freezing, throughout winter and experiences variable conditions at the ice-ocean interface due to changes in freshwater runoff from surrounding land. Ice samples gathered from this region, resultantly offer a unique opportunity to examine the connection between bulk ice properties like salinity and $\delta^{18}O$ and environmental conditions including growth rate and the composition of water at the interface. Using relationships from the literature, a method was developed to invert bulk ice salinity and $\delta^{18}O$ simultaneously to determine the history of growth rate and interface water composition of ice samples gathered in March 2018 from six fjords located in northern Norway. Quantitative results depend on knowledge of salinity and $\delta^{18}O$ of both the seawater and freshwater leading into the fjord. When growth rate or interface conditions are not constant, profiles of bulk ice salinity appear indicative of growth rate history while the $\delta^{18}O$ profile represents well the amount of seawater present at the interface. It was found that five of the six investigated sites had ice grown from a brackish layer with between 0 and 40% seawater content, while one site had ice grown from water with between 50 and 90% seawater content. Given the significant amount of freshwater present at the interface, accurate measurement of $\delta^{18}O$ obtained from rivers leading into each respective fjord was found to be of greatest importance. The impact of sea ice melt and changes to the $\delta^{18}O$ value of freshwater were also investigated, revealing that both have the potential to lead to considerable underestimations or overestimations of growth rate respectively. This study supports the use of easily obtained measurements of ice, seawater, and freshwater properties to obtain an understanding of environmental conditions at the time of ice formation.

1 Introduction

Norwegian fjords act as a natural laboratory to observe the interaction of fresh water, fed by snow melt, rain, and ground water with the ocean from periods of relative warmth through winters with sub-freezing temperatures. Fjord circulation is controlled by water exchange with coastal waters, tides, river runoff, local and regional winds combined with the bathymetry and shape of the fjord (Asplin et al 1999, Aure et al 1996, Inall & Gillibrand 2010; Stigebrandt 2012). Fjords are often surrounded by high mountains with no two fjords exactly alike in their weather including air temperature, precipitation, and

wind patterns (Cottier et al., 2010). The ice that can develop on the surface is likewise variable, a reflection of the environmental conditions at the time of its formation. In Norway, 47 fjords and coastal areas of 386 examined were found to have > 5 km^2 of ice between 2001 and 2019 (O'Sadnick et al., 2020). The ice that forms in the sub-arctic fjords of Norway can differ substantially from Arctic fjords by being composed largely or entirely of snow ice, and greatly influenced by the freshwater draining into the fjord during the winter (Green et al.,2004; Skreslet & Loeng, 1977). In comparison, on Svalbard the fjord ice is mainly frozen seawater. This contrast is reflected in the different salinities found in sub-arctic and arctic fjord ice. These characteristics are not consistent however and generalizations about ice properties in Norwegian fjords are problematic. With increasing warming in the arctic, the physical processes observed in fjords including the influence of freshwater at the ice-ocean interface, its incorporation into ice and potential impact on other properties such as microstructure are an important area of focus (Alkire et al., 2015; Kujawa et al., 2021). Coastal regions are diverse in their ecology (Vonnahme, 2020; Wassmann et al., 1996) and also heavily traversed by humans (Olsen et al., 2019; Svavarsson et al., 2021).Understanding how and why ice may form and its properties are imperative to the future environmental management of these regions.

To obtain a description of growth conditions and enhance understanding of why ice differs from fjord to fjord and between years, ice bulk salinity and $\delta^{18}O$ are two characteristics of ice that are helpful to measure. The latter, the ratio of ^{18}O to ^{16}O, is the isotopic signature of the ice and defined as:

$$\delta^{18}O = \left[\frac{\left(\frac{^{18}O}{^{16}O}\right)_s}{\left(\frac{^{18}O}{^{16}O}\right)_{VSMOW}} - 1 \right] * 1000\ ‰\ , \quad (1)$$

where s represents the ratio of the sample and $VSMOW$ refers to Vienna Standard Mean Ocean Water. $\delta^{18}O$ can differ between samples having equal values for salinity due to its link to the origin of fresh water that mixes with seawater at the ice-ocean interface. The isotopic signature of fresh river water varies considerably across the globe from -41.42 ‰ to 14.75 ‰ with an average $\delta^{18}O$ of -10.59 ‰ (Nan et al., 2019). This broad range in values is due to a variety of factors including the composition of precipitation and degree of evaporation. In Norway specifically, this range narrows to approximately -4 ‰ in southern Norway, down to approximately -12 ‰ in northern Norway (Nan et al., 2019). The isotopic signature of ocean water is also not a constant. While Vienna Standard mean ocean water has a $\delta^{18}O$ of 0 ‰, values as high as approximately 2 ‰ at lower latitudes to as low as approximately -3 ‰ in regions of the arctic have been measured (LeGrande & Schmidt, 2006).

As ice forms, ^{18}O is preferentially incorporated into the ice due to its lower vibrational energy in comparison to ^{16}O (Eicken, 1998). The difference between $\delta^{18}O$ in the seawater and ice is termed the fractionation coefficient (ε):

$$\varepsilon = \delta^{18}O_{ice} - \delta^{18}O_{water}\ , \quad (2)$$

Under isotopic equilibrium, whereby ice is grown in a laboratory at a rate slow enough to allow for mixing of the boundary layer, ε is estimated to be 2.91 ‰ for pure freshwater ice (Lehmann and Siegenthaler, 1991). For sea ice, under laboratory conditions at the slowest of growth rates, fractionation was measured to be 2.7 ‰ (Craig and Hom, 1968). Many examples of measurements of natural sea ice of differing growth rate exist in the literature, with ε values of, for example, 2.09 ‰ (Melling and Moore, 1995) , 2.57 ‰ (Macdonald et al., 1995), 2.23 ‰ (Macdonald et al., 1999), and 1.88 ‰ (Toyota et al., 2013).

To link fractionation to growth rate, Eicken (1998) utilized the stagnant layer boundary model originally derived by Burton et al. (1953). The thickness of the boundary layer at the ice-ocean interface is determined by the rate of ice growth and diffusion of, in this application, $H_2{}^{18}O$. The thinner the boundary layer the greater the amount of fractionation that will occur as seawater freezes to sea ice. This, in turn, will lead to higher values of $\delta^{18}O$ in the ice. Based on these processes, Eicken (1998) derived an empirical relationship between ε and growth rate by assuming values for diffusion, the thickness of the boundary layer, and an equilibrium fractionation factor that describes the isotopic ratios in the solid and liquid phases. Smith et al. (2012) showed that this model often underestimates values of growth rate in sea ice based on field data obtained in Antarctica. Laboratory and observational data from another study focused on the Sea of Okhotsk further support this finding (Toyota et al., 2013). In the latter, the authors work to improve the fit of the Eicken (1998) model to data gathered on laboratory- grown and natural sea ice, using a least-squares fitting procedure to determine values for boundary layer thickness and the fractionation coefficient. While it was necessary to apply two procedures, fitting separately to lab and field measurements, a single formula for the effective fractionation coefficient for sea ice ($\varepsilon_{eff,si}$) was derived to cover growth rates of 0.8×10^{-7} m s^{-1} to 9.3×10^{-7} m s^{-1}.

Bulk ice salinity is a more common measurement given the simplicity, needing only a handheld salinometer, and use to estimate ice brine volume fraction. Like $\delta^{18}O$, it depends on conditions at the ice-ocean interface and growth rate. A greater fraction of fresh water will lead to lower interface salinity and resultantly in the ice. For this reason, profiles of $\delta^{18}O$ and bulk salinity often show increases and decreases at the same depths. Growth rate, however, has an opposite impact on bulk ice salinity. A faster growth rate leads to less time for salt to be rejected from the ice as it is forming leading to higher bulk salinity (Eicken, 1998; Petrich et al., 2011).

Exploration of the relationship between bulk ice salinity, source water, and growth rate has often focused on the initial rejection of salt during formation with studies presenting relationships between growth velocity and a segregation coefficient (e.g. Weeks and Lofgren, 1967; Cox and Weeks, 1975; Nakawo and Sinha, 1981). The latter is used to quantify the ratio of salt in the ice to that in the water at the ice-ocean interface after Burton et al. (1953). This work, however, was based off datasets where seawater salinity was often greater than 30 psu. Granskog et al. (2006) focused on Baltic sea ice forming from seawater having a mean salinity of 3.2 psu. It was found that previous models overestimate the segregation coefficient in

application to low-salinity water and ice. In more recent works examining the formation of sea ice and the desalination processes, greater focus is placed on gravity drainage of brine often applying concepts described by mushy layer theory (Hunke et al., 2011; Notz & Worster, 2009; Worster, 1997). In line with these more recent studies, Petrich et al. (2011) sought an explicit expression for bulk salinity segregation of a steadily growing layer of ice. Desalination was based on gravity drainage and assumed to be confined to ice of a porosity above a pre-defined value of critical porosity, φ_C. Desalination rates were calibrated against results of a computational fluid dynamics model.

In the following study, the relationships presented by Toyota et al. (2013) and Petrich et al. (2011) were applied using measurements of ice bulk salinity and $\delta^{18}O$, river $\delta^{18}O$, and seawater $\delta^{18}O$ and salinity to determine the properties of water at the interface and the growth rate at six fjords located in northern Norway (Fig. 1). Findings are compared to a thermodynamic model of ice growth based on daily average air temperature to assess its accuracy. The connection to weather and oceanographic patterns in each fjord, the causes of inconsistencies with modelled growth rate and that calculated, and how this may be tied to ice properties within the ice are also discussed.

2 Methods

2.1 Derivation of growth rate and fraction of seawater from ice properties

In this study, the fraction of seawater in comparison to freshwater, $F_{sw,}$ and ice growth rate, v, were determined from measurements of ice bulk salinity (S_{ice}) and $\delta^{18}O$ (δ_{ice}) and seawater and freshwater properties. Water at the ice-ocean interface is assumed to be a mixture of seawater and freshwater with values for salinity and $\delta^{18}O$ (S_o, δ_o) determined from:

$$S_0 = F_{sw}S_{sw} + (1 - F_{sw})S_w \,, \quad (3)$$

$$\delta_o = F_{sw}\delta_{sw} + (1 - F_{sw})\delta_w \,, \quad (4)$$

Where F_{sw} is the fraction of seawater in comparison to freshwater (F_w= 1 – F_{sw}), S_{sw} and S_w are the salinity of the seawater and freshwater in practical salinity units (psu), respectively, and δ_{sw} and δ_w are $\delta^{18}O$ for seawater and freshwater in parts per thousand (‰). Seawater properties, S_{sw} and δ_{sw}, were measured during each field visit, and δ_w was measured at the main river flowing into each fjord the following season (Table 4). Salinity of freshwater was not measured and is assumed to be S_w =0. Equation 3 therefore simplifies to:

$$S_0 = F_{sw}S_{sw} \,, \quad (5)$$

Seawater properties refer here to values measured >1 m below the ice-ocean interface.

Toyota et al. (2013) linked the fractionation coefficient of sea ice ($\varepsilon_{eff,si}$) to ice growth rate, v, using:

$$\varepsilon_{eff,si} = a_1 + b_1 \exp\left(-\frac{v}{c_1}\right) + d_1 \exp\left(-\frac{v}{e_1}\right), \quad (6)$$

Where a_1= 1.2280 ‰, b_1= 0.7311 ‰, c_1= 8.0100 • 10^{-8} m s, d_1= 0.8441 ‰, e_1= 0.7800 • 10^{-6} m s being valid for 0.8 • 10^{-7} m $s^{-1} < v < 9.3 \cdot 10^{-7}$ m s^{-1}.

A definition for δ_{ice} can therefore be formulated combining Eq. (2), Eq. (4), and Eq. (6) that is dependent on two unknowns, F_{sw} and v:

$$\delta_{ice} = F_{sw}\delta_{sw} + (1 - F_{sw})\delta_w + a_1 + b_1 \exp\left(-\frac{v}{c_1}\right) + d_1 \exp\left(-\frac{v}{e_1}\right), \quad (7)$$

Petrich et al. (2011) linked the bulk salinity of sea ice, S_{ice}, to the interface salinity, S_0, and ice growth rate, v. S_0 depends on F_{sw} according to Eq. (5), and can be related to S_{ice} through the expression presented by Petrich et al. (2011):

$$\frac{S_{ice}}{S_0} \approx \frac{\rho_o}{\rho_{ice}} \frac{C\varphi}{C_0}, \quad (8)$$

Where S_{ice}, ρ_{ice}, and C are the salinity, density, and brine concentration in the ice, respectively, S_0, ρ_0, and C_0 are salinity, density, and solute concentration of seawater at the ice-ocean interface, respectively, and ϕ is porosity. At a critical porosity (ϕ_c), the following is defined as a function of growth velocity, v, incorporated:

$$\frac{(C\varphi)_c}{C_0} = \varphi_C \left(1 + \left(\frac{\varphi_c}{2}\frac{v}{\gamma_s w_0}\left[-1 + \sqrt{1 + \frac{4(1-\varphi_c)}{\varphi_c^2}\frac{\gamma_s w_0}{v}}\right]\right)\right), \quad (9)$$

Where:

$$\gamma_s w_0 = \frac{4.5\ x\ 10^{-8}\frac{m}{s}}{34\frac{kg}{m^3}} C_0, \quad (10)$$

$$C_0 = \frac{\rho_o\left(\frac{S_0}{1000}\right)}{\left(1 - \frac{S_0}{1000}\beta\right)}, \quad (11)$$

With $\gamma_s\omega_0$ being the vertical flux within the permeable zone, ϕ_c=0.05, β=0.8, ρ_0= 1026 kg m^{-3}, ρ_{ice} = 917 kg m^{-3}. Through substitution of Eq. (5) and Eq. (9) into Eq. (8), a definition for S_{ice} dependent on the same two unknowns as Eq. (7), v and F_{sw}, is provided:

$$S_{ice} = F_{sw}S_{sw}\left(\frac{\rho_o}{\rho_{ice}}\right)\varphi_C\left(1 + \left(\frac{\varphi_c}{2}\frac{v}{\gamma_s w_0}\left[-1 + \sqrt{1 + \frac{4(1-\varphi_c)}{\varphi_c^2}\frac{\gamma_s w_0}{v}}\right]\right)\right), \quad (12)$$

To determine v and F_{sw} for each section of core having a measurement of δ_{ice} and S_{ice}, Eq. (7) and Eq. (12) are solved simultaneously through residual minimization.

2.2 Field measurement of ice bulk properties and water endmembers

Six fjords located in northern Norway, shown in Fig.1, were chosen for collection of ice samples in March 2018. While sampling occurred during the two years following, this season of data was chosen due to the minimal snowfall and a sustained period of air temperature below 0 °C (Fig.3-8 (c)). For a complete description of the fjords including bathymetry and geometry see O'Sadnick et al. (2022). In each fjord, at least one ice core was collected near to the center of the ice cover and between 0.5 to 1.5 km from the outlet of the main river. After measuring the depth of any snow cover, snow was removed and an ice core drilled. Upon removal, cores were quickly laid horizontal before being sliced into 0.05 m sections with each placed into a plastic bag. The ice samples were stored at room temperature to melt before measuring bulk salinity (S_{ice}) using a YSI Pro30 temperature/conductivity probe with an accuracy of 0.1 psu and resolution of ±0.1 (psu) or ±1 % of

the reading. After measurement, the melted ice sample was poured into glass bottles, closed with cone-lined caps and stored at +4 °C until transport to the Stable Isotope Laboratory at the Centre for Arctic Gas Hydrate, Environment and Climate (CAGE) located at UiT The Arctic University of Norway, Tromsø, Norway where $\delta^{18}O$ analysis was performed. Details of the analysis were given by O'Sadnick et al. (2022). Additionally, one ice core was also gathered at each fjord for thick sectioning and analysis of ice stratigraphy. It was placed in a cooler immediately after sampling and stored in a -18 °C freezer until it could be processed.

Also collected at each sampling site were measurements of seawater salinity, temperature, and $\delta^{18}O$ under the ice. For the first two, a CTD (CastAway-CTD, Sontek) having a resolution and accuracy of 0.01°C and 0.05 °C respectively for temperature, 0.01 (psu) and ±0.1 (psu) for salinity, and 0.01 m and ±0.25% of the measured value for depth was lowered manually. The measurement provides an endmember of seawater salinity (S_{sw}). To gather a measurement of $\delta^{18}O$ of seawater (δ_{sw}), a manual water pump was lowered to between 1.5 - 2 m below the ice-ocean interface. The sample was stored in the same type of glass bottle as above for eventual measurement with the melted ice samples. Fresh water measurements of $\delta^{18}O$ (δ_w) were gathered in the rivers leading into the fjords at varying distances from the fjords. The glass bottle was similarly filled and delivered with the other samples for stable isotope analysis.

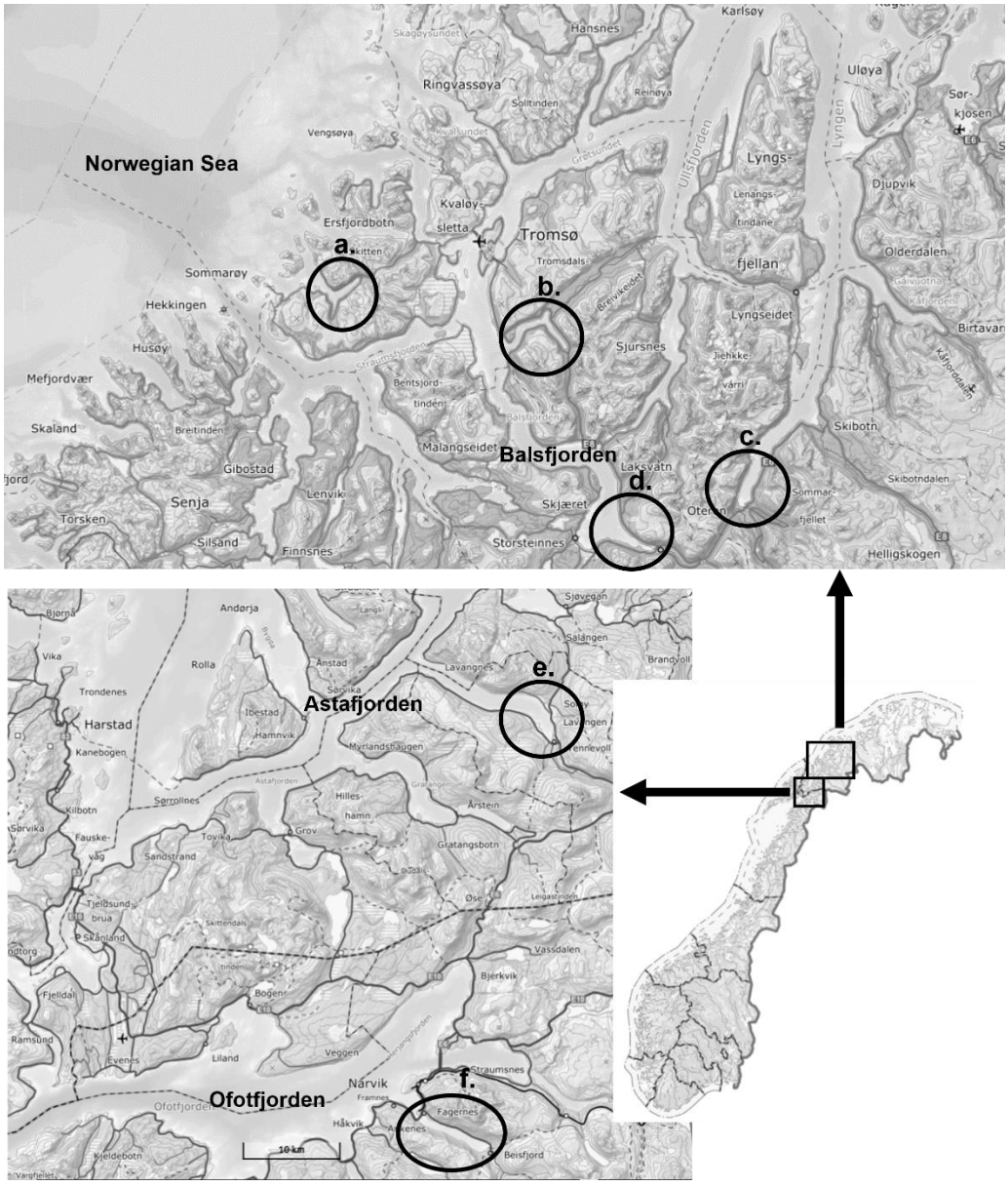

Figure 1: Location of six fjords in northern Norway where ice core samples were gathered. a) Kattfjord; b) Ramfjord; c) Storfjord; d) Nordkjosbotn; e) Lavangen; and f) Beisfjord. ©Kartverket

2.3 Calculation of growth rate from freezing degree days

To assess the accuracy of the above method, growth rate was also calculated independently using daily average air temperature at each fjord combined with the freezing degree model of Anderson (1961), from the date of ice freeze-up to measurement.

While ice formation and breakup can occur several times during a winter season, here freeze-up is defined as the first day of consistent ice coverage with no further breakups occurring until the day of measurement. To determine the date of freeze-up, SENTINEL-1 C-band Synthetic aperture radar (SAR) imagery from the vertical transmit/vertical received were used (Copernicus, 2019) in combination with the Terra satellite MODIS MOD09A1.006 Terra Surface Reflectance 8-Day Global 500m product. The latter does not gather imagery during the period of no sunlight in the upper latitudes (2 November – 2 February) however with correct processing steps (see O'Sadnick et al. (2020)), ice is relatively straight forward to identify. SAR imagery is available year-round but can be more difficult to interpret. While imagery is not gathered every day, a relatively narrow range for the freeze-up date can be determined. Dates of ice formation and measurement were also presented by O'Sadnick et al. (2022) and are shown in Table 1.

Table 1- Summary of ice formation and measurement dates

Fjord	Date of ice formation, 2018	Date of measurement, 2018
Beisfjord	1-5 Feb	13 Mar
Lavangen	27-28 Feb	23 Mar
Nordkjosbotn	29-30 Dec 2017	20 Mar
Storfjord	15-20 Feb	20 Mar
Ramfjord	28-29 Jan	20 Mar
Kattfjord	5-10 Jan	21 Mar

Values for average daily temperature, spatially interpolated onto a 1 km grid, were provided by the Norwegian Meteorological Institute and accessed using seNorge.no (Lussana et al., 2018). At each fjord, one pixel was selected at the head of each fjord located at sea level to provide local temperature. Freezing degree days (θ) were calculated by summing temperatures over the days where daily average air temperature (T_a) was below the freezing point (T_f) from ice freeze-up (i=1) to the date of measurement (i=N):

$$\theta = \sum_{i=1}^{N} \Delta t \begin{cases} T_f - T_{a,i}, & T_{a,i} < T_f \\ 0, & T_{a,i} \geq T_f \end{cases}, \quad (13)$$

Here Δt= 1 day and T_f= 0 °C given the known influence of fresh water on the surface layer. Using the result from each individual fjord, a total ice thickness in cm (H) can be derived (Anderson, 1961):

$$H^2 + aH = b\theta\,, \quad (14)$$

where θ is the number of freezing degree days in °C days (Table 2), a is a constant equal to 5.1 as provided by Anderson (1961), and b has a unique value for each fjord shown (Table 3). For the latter, Anderson (1961) used b=6.7, but here b was fitted to match the measured ice thickness in each fjord.

Table 2- Summary of air temperatures obtained through SeNorge and calculated freezing degree days (FDD)

Fjord	T_{avg} [°C]	T_{min} [°C]	T_{max} [°C]	Days above freezing	θ [° days]
Beisfjord	-8.3	-16.0	-0.8	0	334
Lavangen	-7.6	-13.9	0.5	1	182
Nordkjosbotn	-9.3	-17.3	1.2	4	750
Storfjord	-10.3	-16.8	0.9	2	340
Ramfjord	-7.2	-12.8	3.0	2	367
Kattfjord	-5.3	-10.5	4.0	7	394

205

Table 3- Value for *b* for use in Eq. (14), specific to the fjord

Fjord	*b*
Beisfjord	7.8
Lavangen	9.0
Nordkjosbotn	8.3
Storfjord	4.4
Ramfjord	7.3
Kattfjord	9.7

Ice growth rate was calculated from the difference in daily ice thickness (ΔH) using:

210 $$v = \frac{\Delta H}{\Delta t}, \quad (15)$$

Results were compared to the inversion described in Section 2.1.

3 Results

3.1 Initial Conditions

Thin layers of ice are commonly observed in fjords throughout winter but often break up and disperse quickly. Care was 215 therefore taken to determine the freeze-up date of specifically the ice measured here. Nordkjosbotn had the earliest date of continuous ice cover with freeze up occurring on 29 December 2017 followed by Kattfjord on 5 January 2018. In the other four fjords, formation occurred over a span of several weeks starting with Ramfjord on 28 January, Beisfjord on 2 February, Storfjord on 15 February, and lastly Lavangen on 27 February (Table 4).

220 Seawater salinities (S_{sw}), measured on the same day as ice cores were collected (Table 4), do not show large variation between fjords ranging from 32.4 psu in both Beisfjord and Nordkjosbotn to 33.4 psu in Lavangen. Similarly, $\delta^{18}O$ of

seawater (δ_{sw}) only varies slightly from -0.81 ‰ at Ramfjord to -0.12 ‰ at both Lavangen and Kattfjord. Salinity is assumed to be 0 psu in all rivers (S_w). Measurements of δ_w were only gathered in Beisfjord in March 2018 with all other measurements coming the following ice season in March 2019. These values range from -12.57 ‰ to -10.24 ‰.

Table 4- Summary of measured endmember values for seawater (S_{sw} and δ_{sw}) and freshwater (δ_w), date of measurement for seawater and freshwater samples, and depth of measurement of the seawater sample. S_w= 0 psu for all cases.

Fjord	Date of Measurement	Depth from ice/ocean interface [m]	S_{sw} [psu]	δ_{sw} [‰]	Date of Measurement	δ_w[‰]
Beisfjord	19 Apr 2018	0.4	32.4	-0.34	19 Apr 2018	-12.57
Lavangen	23 Mar 2018	1.0	33.4	-0.12	14 Mar 2019	-11.34
Nordkjosbotn	13 Mar 2019	1.5	32.4	-0.17	13 Mar 2019	-12.15
Storfjord	20 Mar 2018	1.5	32.9	-0.22	12 Mar 2019	-11.55
Ramfjord	20 Mar 2018	1.5	32.5	-0.81	12 Mar 2019	-11.5
Kattfjord	21 Mar 2018	1.5	32.8	-0.12	14 Mar 2019	-10.24

3.2 Bulk Ice Property Measurements

The cores gathered displayed a broad range of both ice bulk salinity and $\delta^{18}O$ values (Table 5, Figs. 3- 8(a))(O'Sadnick, 2022). Thickness ranged from 36 cm in Storfjord to 76 cm in Nordkjosbotn. Between fjords, the lowest average ice bulk salinity (S_{ice}) was found in Kattfjord with a value of only 0.3 psu ranging up to 3.9 psu in Storfjord. The lowest average ice bulk $\delta^{18}O$ (δ_{ice}) was found in Beisfjord, -8.27 ‰, while Storfjord had the highest average value, -1.42 ‰.

Table 5- Summary of bulk ice salinities, S, and $\delta^{18}O$ values

Fjord	Thickness [cm]	S_{min} [psu]	S_{max} [psu]	S_{avg} [psu]	δ_{min} [‰]	δ_{max} [‰]	δ_{avg} [‰]
Beisfjord	48	0.2	1.7	1.1	-8.64	-7.06	-8.27
Lavangen	37	0.9	2.0	1.6	-8.16	-5.95	-7.34
Nordkjosbotn	76	0.9	2.5	1.8	-9.33	-5.55	-7.25
Storfjord	36	2.8	4.9	3.9	-4.46	0.22	-1.42
Ramfjord	49	0.5	2.9	1.6	-9.01	-6.47	-7.68
Kattfjord	59	0.1	1.1	0.3	-9.62	-6.9	-7.78

The cores were primarily composed of congelation ice with granular ice only appearing in the upper 10 cm of the ice core in Kattfjord, 5 cm of the ice core in Beisfjord, and 1 cm in Storfjord and Ramfjord cores (Fig. 2). Pictures of the actual thick sections with and without polarized filters are provided in O'Sadnick et al. (2022). In Beisfjord, this granular ice, presumably snow ice, does not show a clear $\delta^{18}O$ signature differentiating it from the congelation ice below (Fig. 4a). In Kattfjord, the upper 10 cm of the core do show minimum values of $\delta^{18}O$, presumably due to the influence of snow (Fig. 8a).

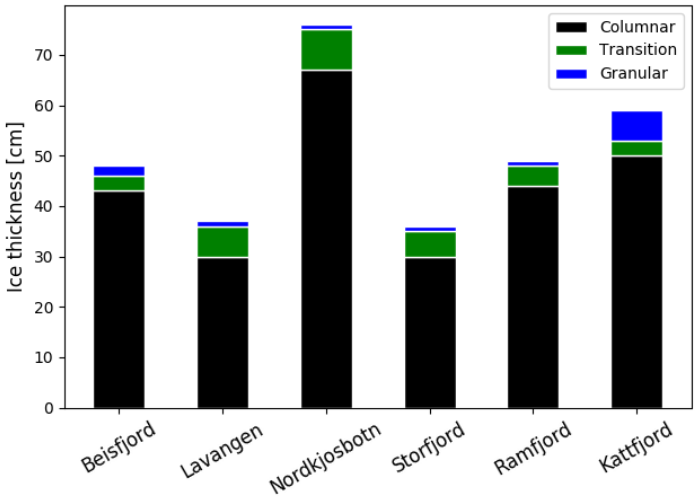

Figure 2 – Schematic of distribution of columnar (black), transition (green), and granular (blue) ice in the six ice cores gathered.

Within one core, measurements of S_{ice} were at times relatively consistent, varying only approximately 1 psu throughout the core as was the case at Lavangen (Fig. 4a) and Kattfjord (Fig. 8a). Other fjords, for example Storfjord (Fig.6a) and Ramfjord (Fig.7a), showed greater variation, with a difference of up to 2 psu between minimum and maximum bulk salinities of core sections. δ_{ice} measurements often showed variability between core sections where little change was recorded in salinity. For example, in ice gathered in Kattfjord (Fig. 8a), salinity hardly increased 0.2 psu in the top 25 cm, δ_{ice} seemingly shows finer detail with a range of 2.0‰ over the same depth.

While bulk ice salinity and $\delta^{18}O$ are often positively correlated, for all but one core, Beisfjord (Fig. 3a), sections of the core also show a negative correlation between these two properties. In Lavangen, this trend is perhaps the most evident with a gradual decrease in S_{ice} while δ_{ice} values increase.

3.3 Growth rate and boundary conditions at the interface

The results of the inversion, the growth rate of the ice (v) and the fraction of seawater at the interface (F_{sw}), a proxy for the mixing occurring at the interface, are presented in Figs.3-8 (b). Findings are examined in line with corresponding ice bulk property measurements, air temperature, and snowfall (Figs. 3-8 (a & c)). For all but one fjord, Storfjord, the fraction of seawater at the interface remains below 0.4 throughout the entirety of the core. This equates to ocean water at the interface not being higher than 13 psu while ice was forming. For Storfjord, the amount of seawater fluctuation from approximately 0.5 to 0.9, equivalent to between 15 – 30 psu water at the ice-ocean interface (Fig. 6b).

While the relationship to bulk properties is not consistent, some trends do appear. For example, Lavangen (Fig. 4a and 4b), where bulk ice salinity and $\delta^{18}O$ are negatively correlated, bulk ice salinity positively correlates to v and $\delta^{18}O$ positively

correlates to F_{sw}. A similar trend is apparent for all other fjords except Kattfjord. In Kattfjord, the uppermost 20 cm of ice having consistently low salinity positively correlates to low values for F_{sw}, while $\delta^{18}O$ positively correlates to v (Fig. 8a and 8b). Additionally, Kattfjord stands out in comparison to other fjords as it has the lowest consistent values for both salinity and $\delta^{18}O$.

3.4 Comparison to growth rate from FDD

While fjords generally maintained air temperatures below 0 °C during ice formation, all but one experienced 1-7 days where temperatures climbed slightly above 0 °C with the highest daily average temperature of 4 °C during this period recorded at Kattfjord (Table 2, Figs.3-8(c)). Kattfjord also had the highest average temperature of -5 °C. The lowest average and individual daily air temperature occurred at Storfjord, with -10 °C and -17 °C, respectively. Snowfall, estimated as snow water equivalent (SWE) is also presented. All fjords experienced relatively little snowfall, only experiencing a few days with 1 – 5 mm SWE accumulation between mid-January and mid-March. This provided ice with a period of both low air temperature and little insulation on the top surface thus allowing for continuous growth except for the few days when temperatures increased above 0 °C.

Estimates of ice growth rate (v) derived from Eqs. 13 – 15 from the day of ice formation to measurement (v_{FDD}), are shown alongside modelled results (v_{inv}) in Figs. 3-8 (b). Both v_{FDD} and v_{inv} generally decrease as ice thickens. This is apparent particularly in Lavangen, Nordkjosbotn, and Kattfjord.

Values for growth rate calculated using both methods fall predominantly within the bounds given by Toyota et al. (2013) although more ice sections do exceed these limits when applying the inversion. Four cores have a calculated ice age within a week of the actual ice age, Beisfjord, Nordkjosbotn, Storfjord, and Ramfjord. The remaining two cores, Lavangen and Kattfjord, overestimate ice age substantially (Table 6).

Table 6: Comparison of actual ice age on day of measurement derived using satellite imagery and the estimated ice age calculated using inversion results.

	Age of Ice (days)	
Fjord	**Actual**	**Calculated from inversion**
Beisfjord	40	39
Lavangen	24	58
Nordkjosbotn	81	86
Storfjord	34	39
Ramfjord	51	44
Kattfjord	75	374

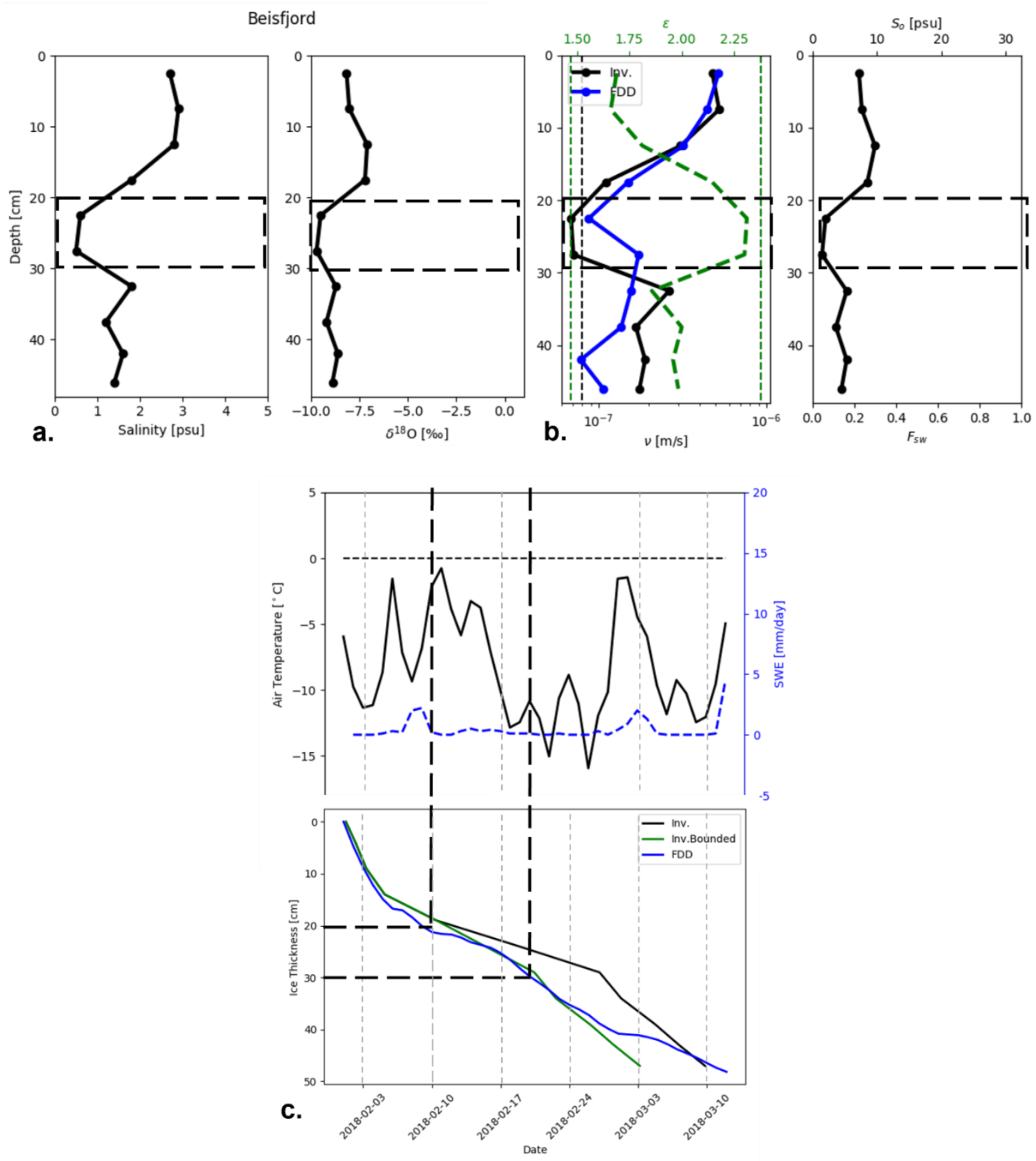

Figure 3: Beisfjord- a) Measured ice salinity S_{ice} (left) and ice bulk salinity δ_{ice} with stratigraphy core superimposed (right). b) Results from the inversion- growth rate in comparison to growth rate derived using freezing degree days (FDD) with calculations of ε also presented in green (left), fraction of seawater (F_{sw}) which is directly in line with equivalent interface salinity also shown (right). c) Top- weather conditions including average daily air temperature and snow water equivalent (SWE) from the time of ice formation to measurement, bottom- evolution of ice growth calculated from growth rates. Black, dashed outlines highlight areas where growth rate extends below bounds (suspected sea ice melt influence), transposed to other data shown.

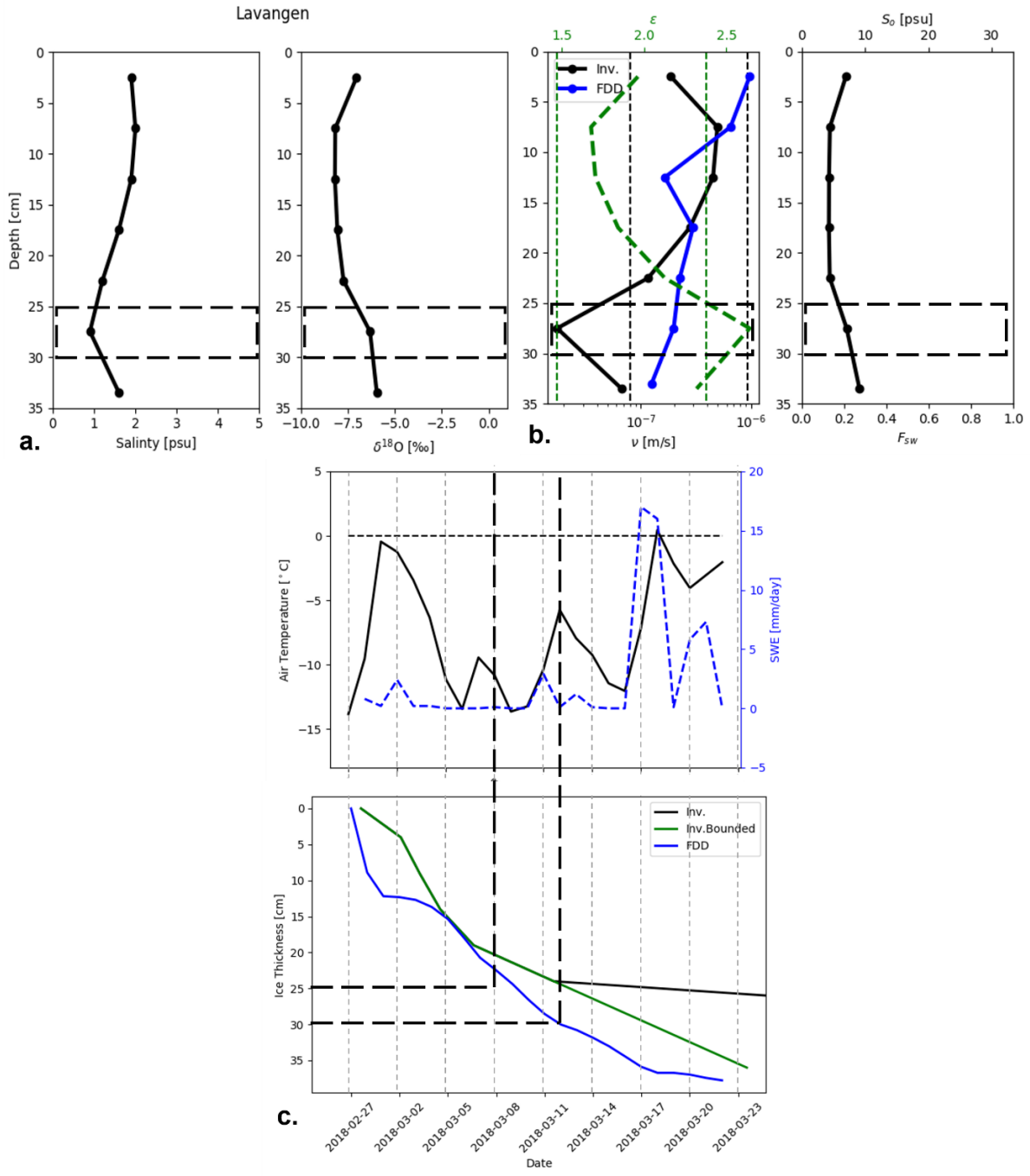

Figure 4: Lavangen- a) Measurements of S_{ice} (left) and measurements of δ_{ice} with stratigraphy core superimposed (right). b) Results from the inversion- growth rate in comparison to growth rate derived using FDD with calculations of ε also presented in green (left), fraction of seawater, the fraction of seawater (F_{sw}) also shown (right). c) Top- weather conditions including average air temperature and SWE from the time of ice formation to measurement, bottom- evolution of ice growth calculated from growth rates. Black, dashed outlines highlight areas where growth rate extends outside of bounds (suspected sea ice melt influence), transposed to other data shown.

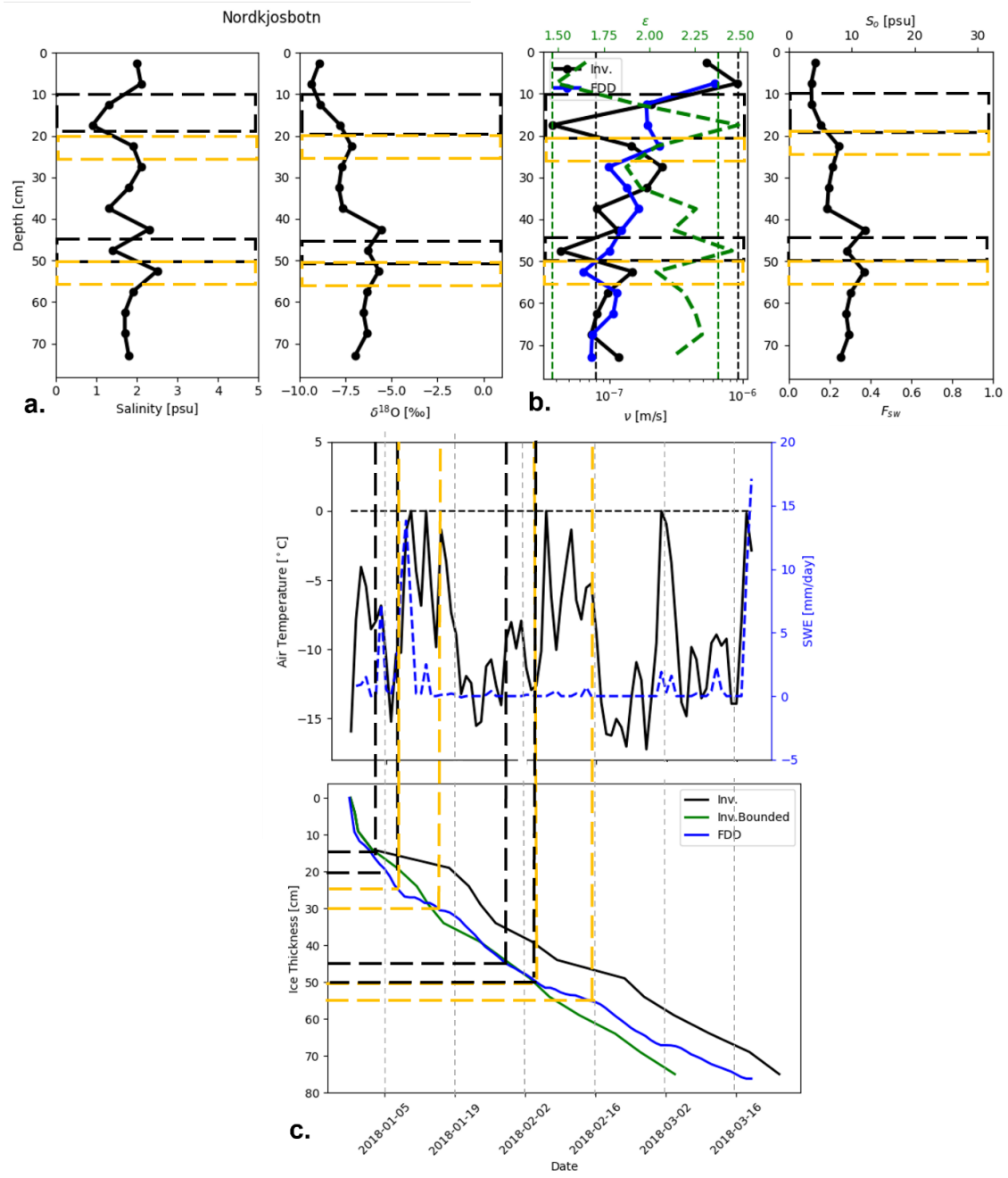

Figure 5: Nordkjosbotn- a) Measurements of S_{ice} (left) and measurements of δ_{ice} with stratigraphy core superimposed (right). b) Results from the inversion- ν in comparison to growth rate derived using FDD with calculations of ε also presented in green (left), fraction of seawater (F_{sw}) which is directly in line with equivalent interface salinity also shown (right). c) Top- weather conditions including average air temperature and SWE from the time of ice formation to measurement, bottom- evolution of ice growth calculated from ν. Black, dashed outlines highlight areas where ν extends outside of bounds (suspected sea ice melt influence), transposed to other data shown. Orange, dashed outlines highlight areas where ν from inversion decreases while ν from FDD increases (suspected snow melt influence).

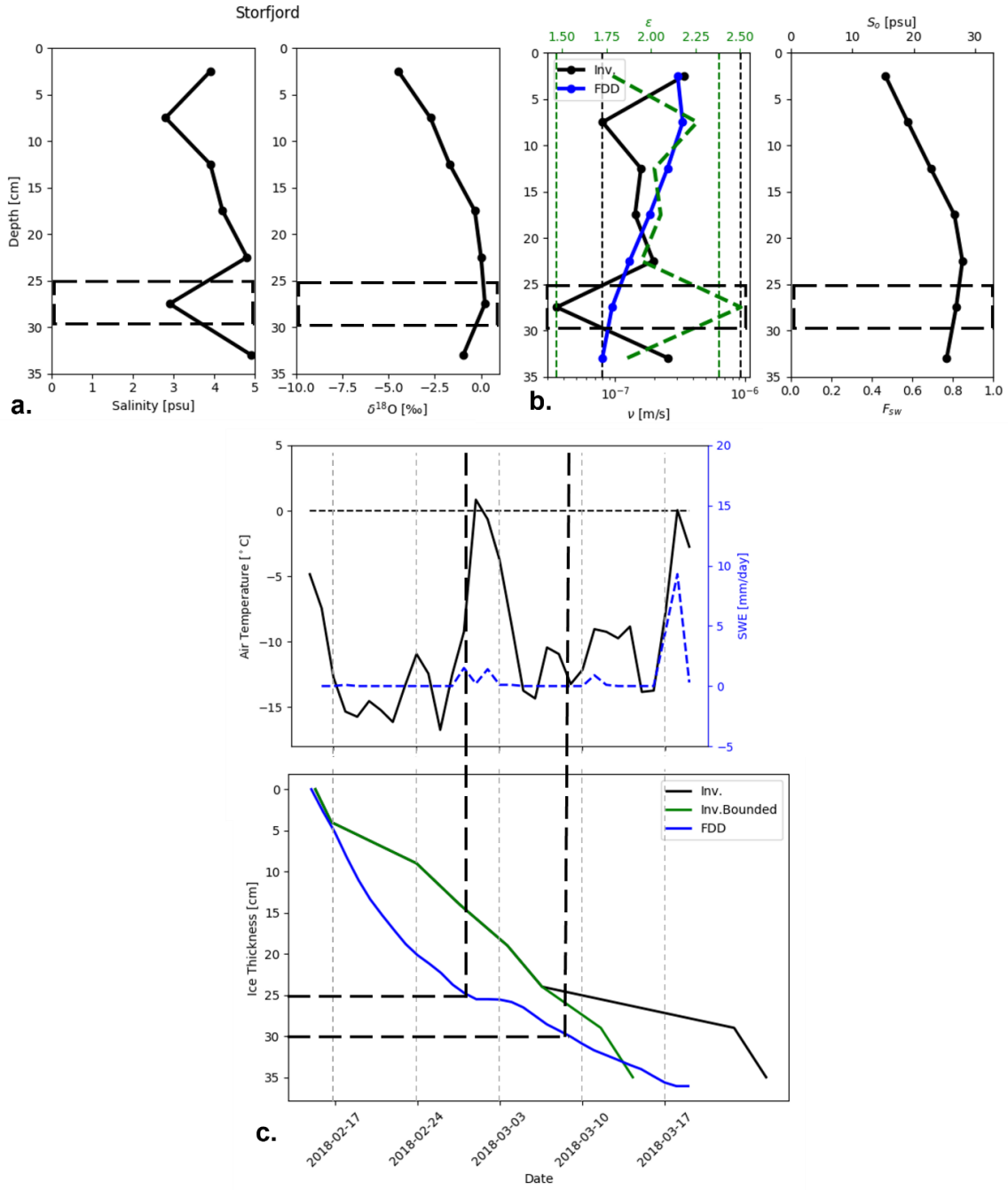

315 **Figure 6: Storfjord- a) Measurements of S_{ice} (left) and measurements of δ_{ice} with stratigraphy core superimposed (right). b) Results from the inversion- ν in comparison to growth rate derived using FDD with calculations of ε also presented in green (left), fraction of seawater (F_{sw}) which is directly in line with equivalent interface salinity also shown (right). c) Top- weather conditions including average air temperature and SWE from the time of ice formation to measurement, bottom- evolution of ice growth calculated from ν. Black, dashed outlines highlight areas where ν extends outside of bounds (suspected sea ice melt influence),**
320 **transposed to other data shown.**

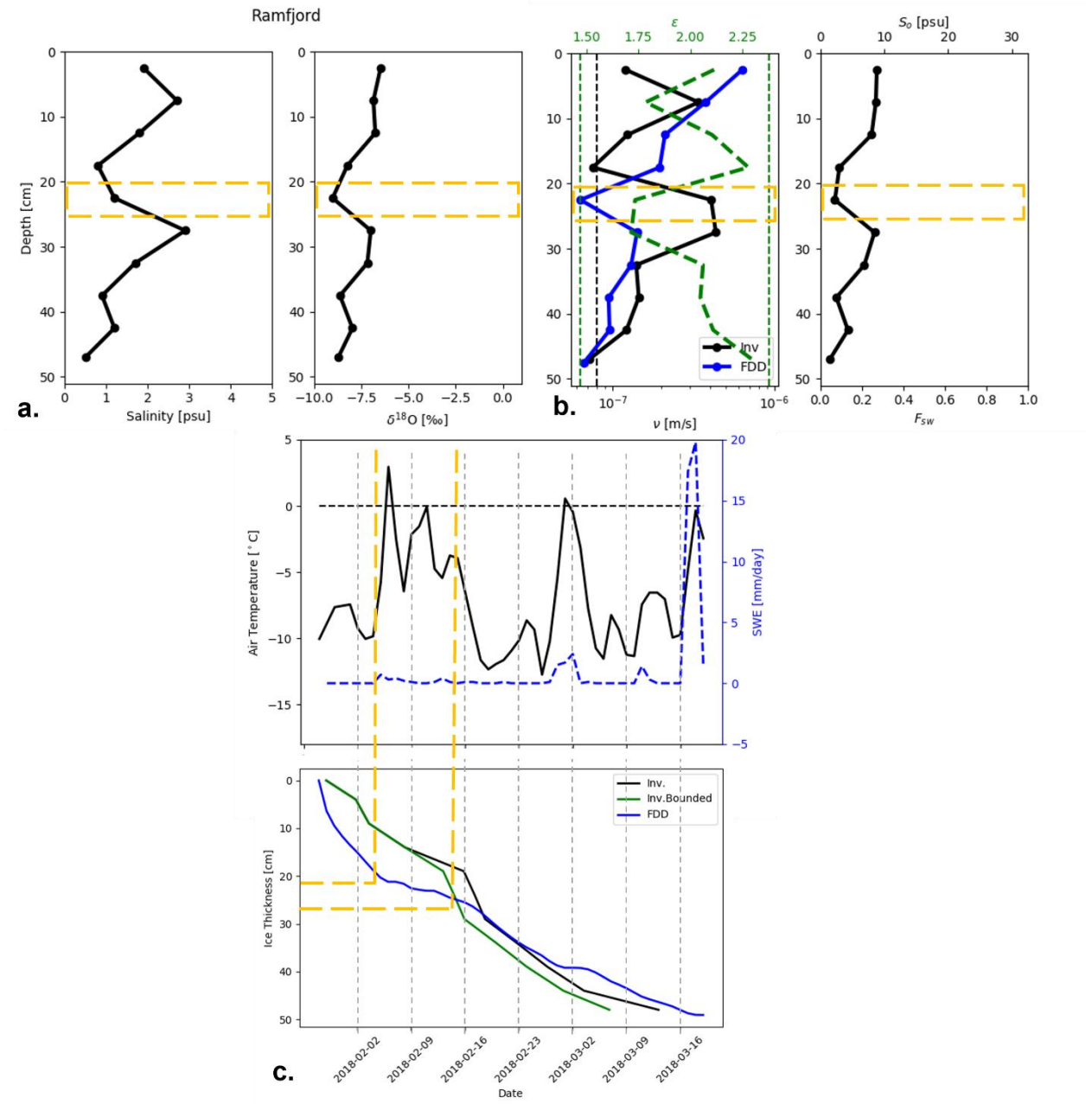

Figure 7: Ramfjord- a) Measurements of S_{ice} (left) and measurements of δ_{ice} with stratigraphy core superimposed (right). b) Results from the inversion- ν in comparison to growth rate derived using FDD with calculations of ε also presented in green (left), fraction of seawater (F_{sw}) which is directly in line with equivalent interface salinity also shown (right). c) Top- weather conditions including average air temperature and SWE from the time of ice formation to measurement, bottom- evolution of ice growth calculated from ν. Black, dashed outlines highlight areas where ν extends outside of bounds (suspected sea ice melt influence), transposed to other data shown. Orange, dashed outlines highlight areas where ν from inversion decreases while ν from FDD increases (suspected snow melt influence).

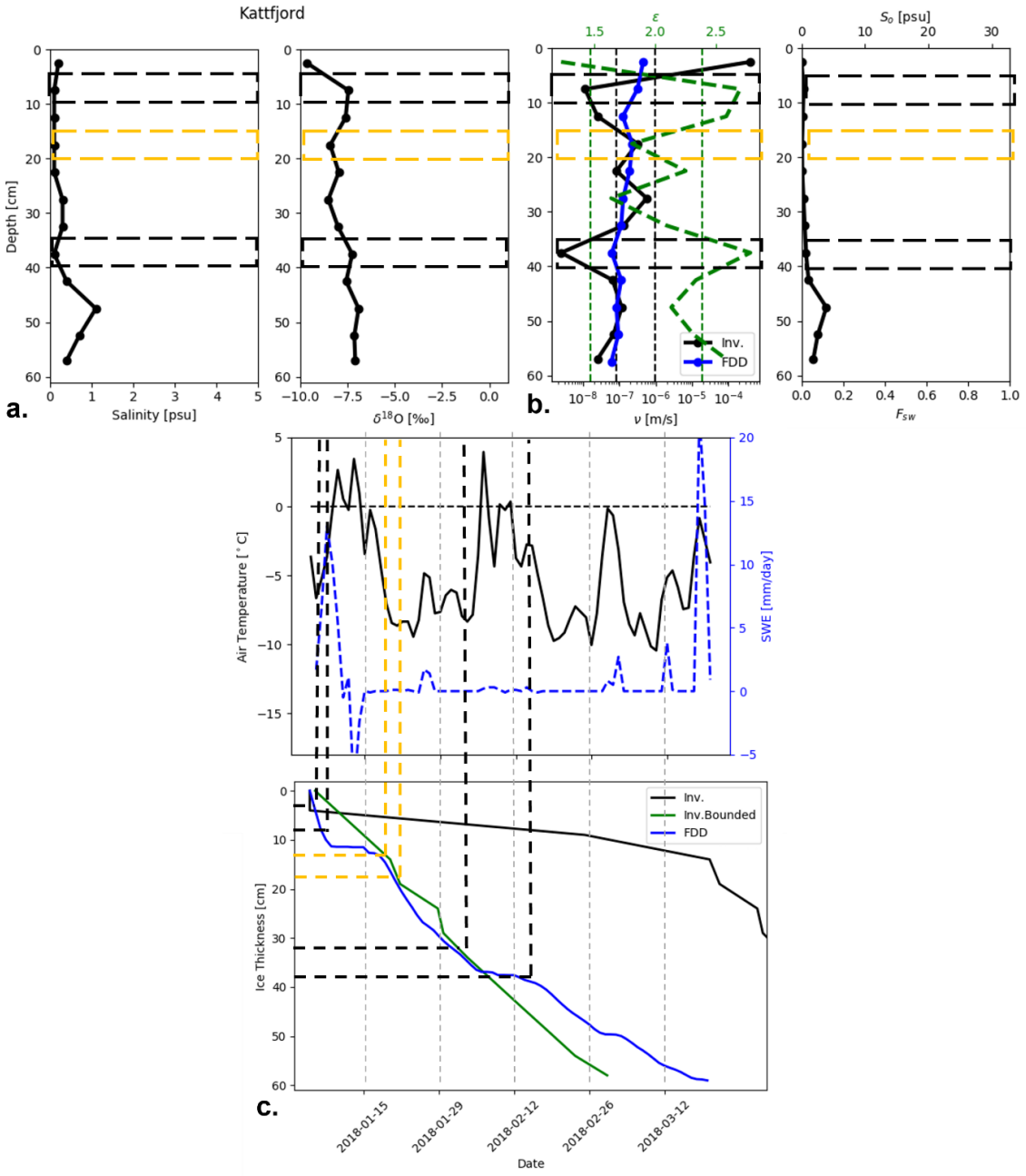

330

Figure 8: Kattfjord- a) Measurements of S_{ice} (left) and measurements of δ_{ice} with stratigraphy core superimposed (right). b) Results from the inversion- ν in comparison to growth rate derived using FDD with calculations of ε also presented in green (left), fraction of seawater (F_{sw}) which is directly in line with equivalent interface salinity also shown (right). c) Top- weather conditions including average air temperature and SWE from the time of ice formation to measurement, bottom- evolution of ice growth
335 **calculated from ν. Black, dashed outlines highlight areas where ν extends outside of bounds (suspected sea ice melt influence), transposed to other data shown. Orange, dashed outlines highlight areas where ν from inversion decreases while ν from FDD increases (suspected snow melt influence).**

4 Discussion

4.1 Endmember sensitivity

A shift in endmember values can lead to different results for growth rate and fraction of seawater at the ice-ocean interface. This may be caused, for example, by exchange between fjords and coastal currents impacting δ_{sw}, or snow and ice melt altering δ_{sw} or δ_w. Here, we examine the impact of each endmember on the final calculations by repeating the inversion defined in Section II.a while using the following values for endmembers:

δ_w : [-13, -12.5, -12, -11.5, -11, -10.5, -10] [‰]

δ_{sw} : [-1, -0.75, -0.5, -0.25, 0] [‰]

S_{sw}: [32, 32.5, 33, 33.5, 34] [psu]

S_w is assumed to be 0 and the inversion is performed for each of the 175 combinations of endmember values (Figs. 9 and 10).

Measurements from Kattfjord offer a good example of the impact of endmembers on results. Values for S_{ice} were substantially lower than all other fjords with $S_{ice,avg}$ = 0.3 psu while δ_{ice} values were the second lowest of the fjords studied, having $\delta_{ice,avg}$= -7.78‰. Values for δ_{sw} were fairly consistent between all fjords with Kattfjord and Lavangen being equal and having the highest value measured δ_{sw} = -0.12‰. The measurement gathered from river water leading into Kattfjord was noticeably higher than all others, however, δ_w= -10.24 ‰ (Tables 3 and 4). In Fig.8b, a small fraction of seawater is shown indicating a high amount of fresh water combined with little mixing at the ice-ocean interface. Through completing the inversion, the degree of influence of freshwater is better defined allowing for deeper analysis of the causes behind changes in the composition of water at the interface. If an inaccurate value for δ_w were assumed, the magnitude of the freshwater influence would not be as well represented with results showing variability upwards of ±0.2 in the fraction of seawater (Fig. 10f). Given the high proportion of freshwater at the interface for the samples presented here, it is the measurement of δ_w that becomes the most important when performing the inversion with the variation shown in Fig. 10a-f primarily coming from a change in this endmember. Accurate measurement of δ_w is therefore imperative to obtain accurate growth rate and fraction of seawater estimates.

Also evident in Fig. 9 is the sensitivity of growth rate to certain combinations of endmembers, skewing results far outside bounds. This is well represented in the Beisfjord core at 27.5 and 37.5 cm depth, Ramfjord at 22.5 and 37.5 cm, and multiple locations in the Kattfjord core. These sudden jumps in estimates can be useful, indicating a sudden shift in conditions at the interface not accounted for in endmember values. In the following, the causes for these deviations are further explored, specifically the impact of snow and ice melt on values of δ_w and the resultant estimates of growth rate and the fraction of seawater derived using the inversion.

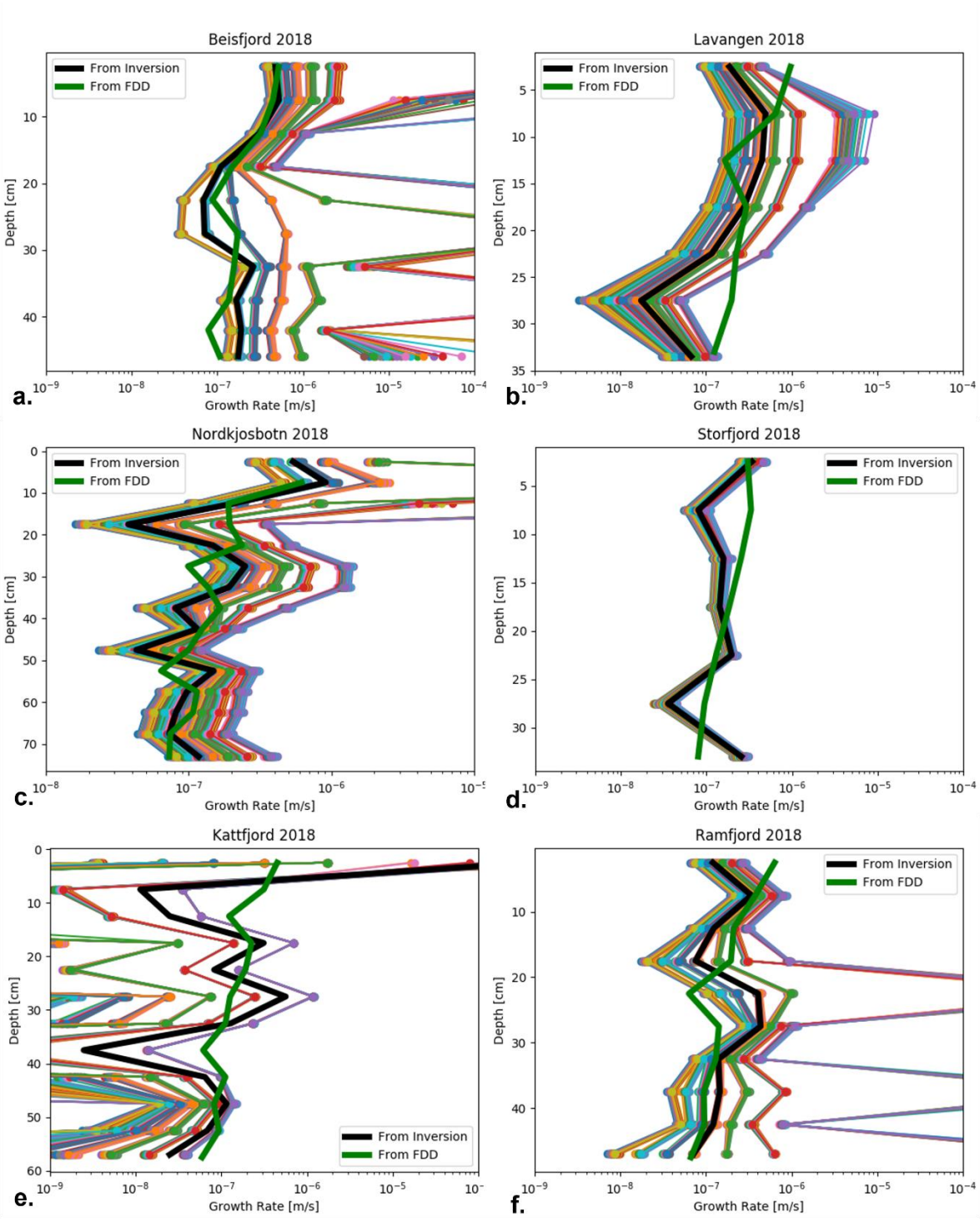

370 **Figure 9: Results of sensitivity study for growth rate. a) Beisfjord, b) Lavangen, c) Nordkjosbotn, d) Storfjord, e) Ramfjord, f) Kattfjord**

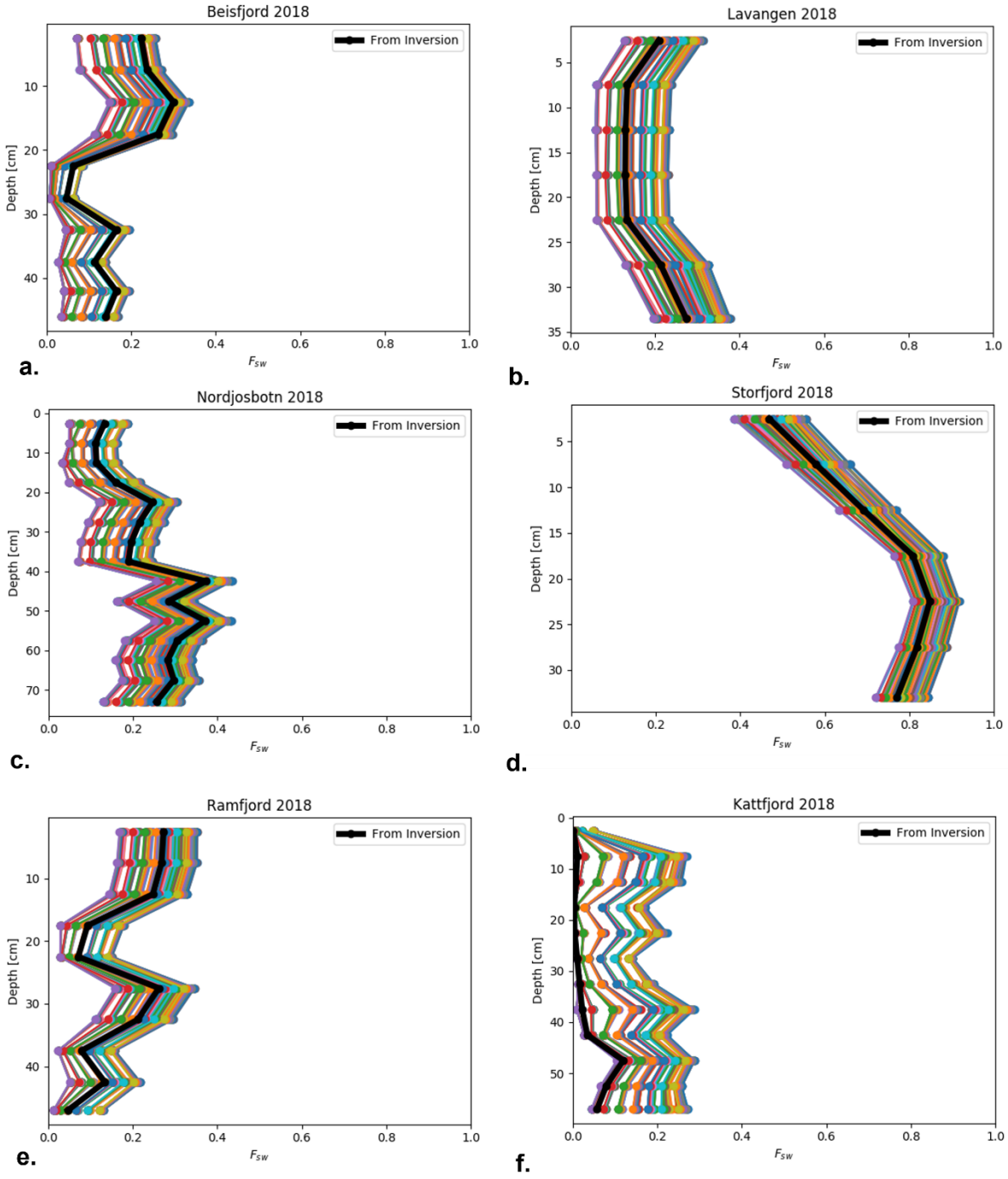

Figure 10: Results of sensitivity study for the fraction of seawater (F_{sw}) . a) Beisfjord, b) Lavangen, c) Nordkjosbotn, d) Storfjord, e) Ramfjord, f) Kattfjord

375

4.2 The impact of temperature on ice bulk properties, and estimates of growth rate and the fraction of seawater

Based on growth rate through each 5 cm thick layer, the evolution of ice thickness through time using the FDD model versus the inversion are presented in Figs.3-8 (c). In O'Sadnick et al. (2022), ice thickness of Norwegian fjord ice calculated from Eqs. 13 and 14 is compared to measured ice thickness highlighting how the two can differ substantially depending on the fjord and year. Here, Eq. (14) was adapted so calculated thickness matches measured thickness. Variations in the constant b are due to primarily surface melt, the insulating effects of snow on the ice surface, and/or heat flux at the ice-ocean interface. Matching calculated and measured thickness provides a method to compare ice properties at specific depths to the weather (including air temperature, snowfall, and melt) at the time of formation. In addition, it provides a second approximation of growth rate to compare inversion results against. The FDD-derived growth rate profiles are estimates, however, with misalignment between weather and ice depth possible.

When comparing the two approximations of growth rate, examples of substantial over-estimation or under-estimation of growth rate by the inversion do stand out. Here, demonstrations of the influence of two specific factors, sea ice melt and snow melt, are provided. When this influence is unaccounted for it leads to inaccurate inversion results. In reality, the mixture of water at the interface may be composed of several sources (e.g. ocean water, river water, snow melt, ice melt), constantly mixing and changing in its composition, being very difficult if not impossible to measure and monitor. A simplified approach is taken here to highlight the influence of separate components which can provide more detailed insight into inversion results and relatedly S_{ice} and δ_{ice} profiles. Findings show the promise of measurement of these two ice bulk properties to gain a better understanding of the conditions through the season- the history of both the ice and fjord during the winter- without in situ or constant observation.

4.2.1 The influence of meltwater beneath sea ice

In Kattfjord, very slow growth rates inferred from the inversion correspond to warm weather (Fig. 8). In two sections of the core (5 – 10 cm depth and 35- 40 cm depth) S_{ice} decreases while δ_{ice} increases. Changes in the composition of seawater at the ice-ocean interface likely contributed to these variations. For example, the refreezing of sea ice melt water that originated during a period of above freezing temperatures would alter seawater endmembers from those assumed, both decreasing S_w while increasing δ_w.

To investigate this possibility, first S_{ice} and δ_{ice} are determined for a section of ice grown at 1.17 x 10^{-7} m s^{-1} (1 cm day^{-1}) from water of a known fraction of fresh and seawater using the using Eqs. 2 – 10 (Fig. 11). Next, a section of this ice is melted resulting in water at the ice-ocean interface being composed of seawater and sea ice melt having the salinity and $\delta^{18}O$ of the ice just formed instead of fresh river water. A new layer of ice is now formed from this mixture at the ice-ocean interface at the same growth rate and S_{ice} and δ_{ice} are again calculated. Lastly, the inversion is run using the resultant values

for bulk ice properties with S_w, S_{sw}, δ_{sw}, and δ_w endmembers being those used for the first layer of ice. This use of inaccurate values for endmembers not reflecting the influence of sea ice melt, results in an underestimation of the ice growth, 4.1×10^{-8} vs. 1.17×10^{-7} m s^{-1}. Sea ice melt is a variable often included when estimating the fraction of different water sources at the ice-ocean interface (Macdonald et al., 1999). In this study, it was not included given the difficulty of measuring both the amount of sea ice melt present under the ice and its composition in terms of salinity and $\delta^{18}O$. Through understanding its influence on inversion results however, an understanding of if, and to what degree, sea ice melt occurred can be gained.

Another fjord that inversion results are hypothesized to be impacted by sea melt is Storfjord despite the estimated ice age being within a week of the actual ice age. Sea ice melt may occur from above (and drain through the ice or through cracks) or below, the latter being tied closely to the amount of oceanic heat flux at the ice-ocean interface. In Fig. 6, growth rate calculated from FDD decreases slowly with depth while inversion results show growth rate to be generally constant outside of two quick decreases hypothesized to be tied to ice melt similar to the example above. The growth rate development from February into March may have resulted from a decrease in oceanic heat flux, allowing ice to hold a constant growth rate despite thickening ice. One indicator of a greater influence from this variable may be the value of *b* (Table 3) being lower than in all other fjords. This constant parameterizes factors such as ice melt, snowfall, ocean-ice heat flux, and/or the difference in air temperature from the effective surface temperature of the ice and can be challenging to determine (Anderson, 1961). This topic, oceanic heat flux and connection to ice formation in fjords, needs further investigation.

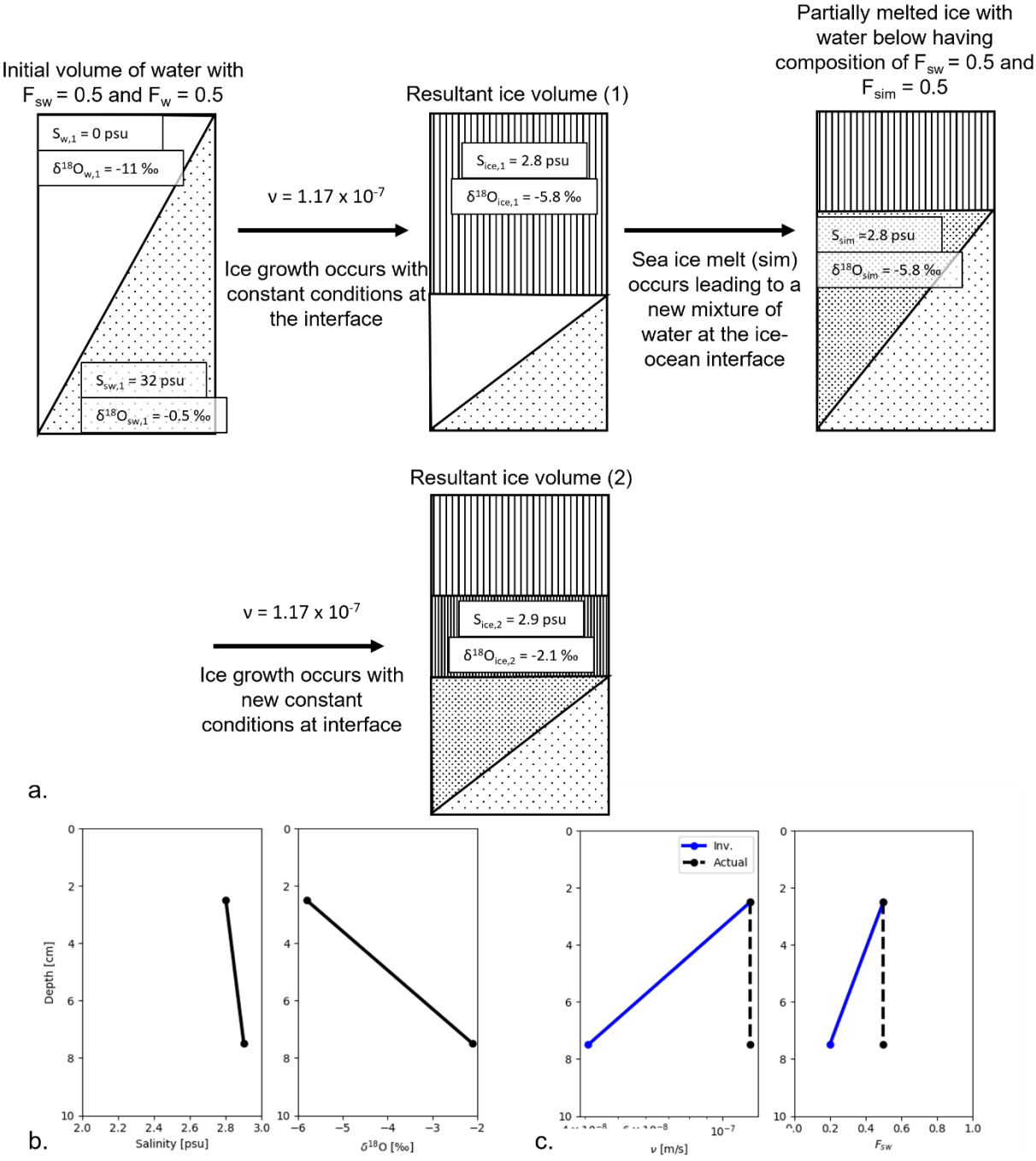

Figure 11: a) Schematic of a sea ice melt and refreeze scenario; b) Bulk ice salinity and $\delta^{18}O$ of the resultant ice; c) Comparison of the actual growth rate and fraction of seawater to those found through the inversion.

4.2.2 The influence of snowmelt

In Ramfjord, while calculated ice age was within one week of the actual ice age, there was an occurrence of a noticeable overestimation of ice growth rate from 20- 30 cm depth (Fig. 7b). During this period of time, temperature is shown to rise to its maximum over the period considered, 2.95 °C, with a small amount of snowfall also apparent. Growth rate calculated from FDD drops significantly, revealing a limitation in the use of Eq. (14) to determine ice thickness as it cannot fully account for the slowing/stopping of growth and potential for melt during these periods of warm weather. In the Ramfjord ice sample, it is hypothesized that this increase in temperature and snowfall led to a mixture of many water sources- seawater, sea ice melt, snow melt, and rainwater - being present at the ice-ocean interface resulting in a decrease in δ_w that are reflected in ice properties

Considered here is the impact of specifically snowmelt and the decrease in δ_w on growth rate estimates. In Fig. 12, a layer of ice is first grown at a rate of 2 x 10^{-7} m s^{-1} assuming only seawater and river water are present at the interface. δ_0 is next changed to be composed of both δ_w = -11 ‰ combined with snowmelt, δ_{sm}= -15 ‰. The value for δ_{sm} originates from a snow sample collected in Ramfjord in March 2019. A layer of ice is grown from this mixture of water at the ice-ocean interface at a rate of 2 x 10^{-7} m s^{-1}, to obtain S_{ice} and δ_{ice}. Last, the inversion is performed assuming the endmember values of δ_w used for the first layer. Results show an overestimation of growth rate, 2.2 x 10^{-6} m s^{-1} versus 2.0 x 10^{-7} m s^{-1}. The derived fraction of seawater present at the interface, F_{sw}, is shown to be less than the original layer as well. This finding assists in interpretation of points in the inversion where growth rate abruptly increases despite a decrease in growth rate based on actual temperature data, revealing the impact of overestimating δ_w values on results for water composition and growth rate. Additionally, this approach shows the use of analyzing inversion results with weather data when it is available. While the latter is not necessary to gain a general approximation of changes at the interface, when combined with other data, a more detailed understanding of conditions under the ice can be developed.

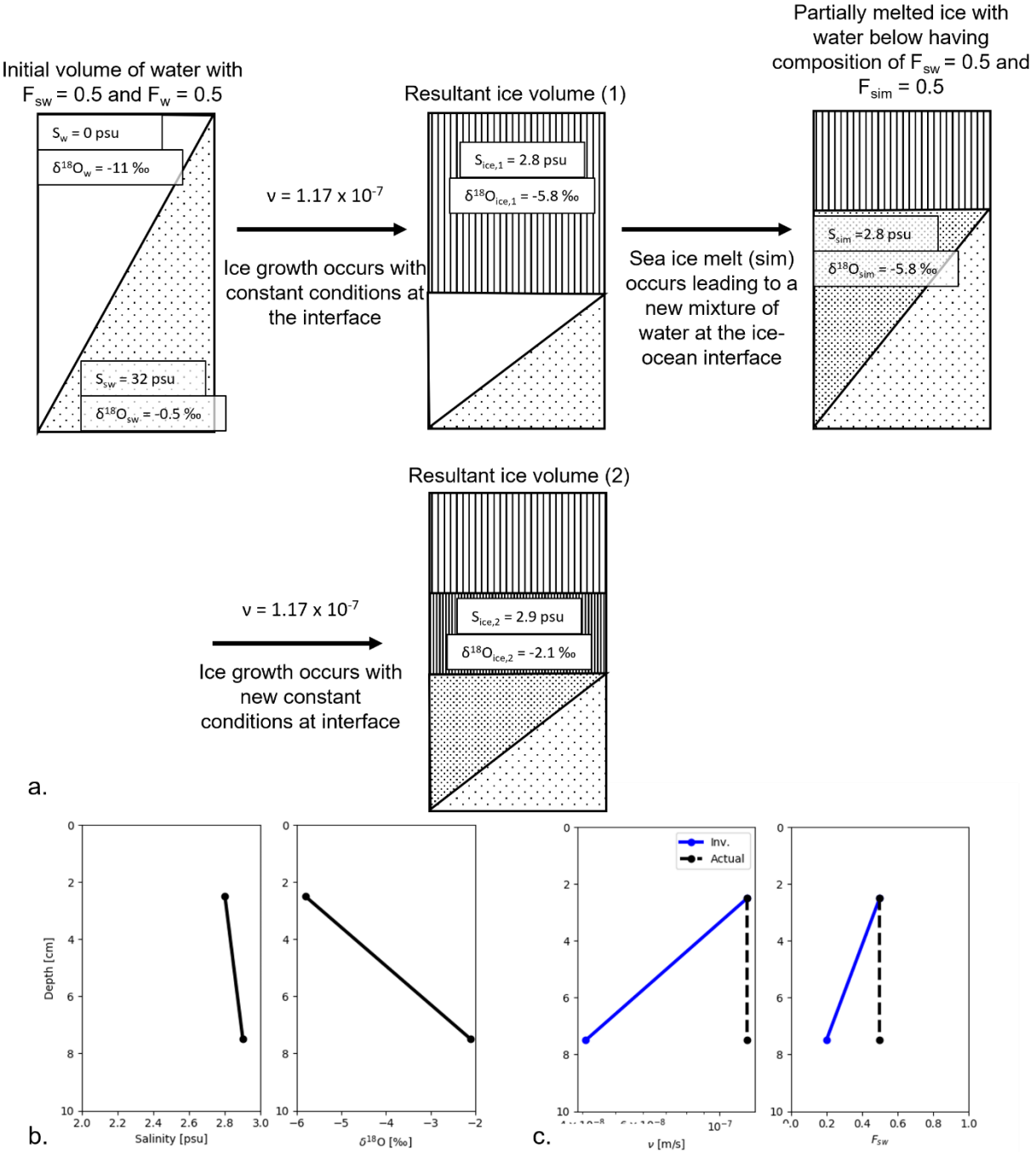

Figure 12: a) Schematic of a snow melt and refreeze scenario; b) Bulk ice salinity and $\delta^{18}O$ of the resultant ice; c) Comparison of the actual growth rate and fraction of seawater to those found through the inversion.

4.3 Scenario Study

Occurrences in the surrounding environment may lead to differences in shape of salinity versus $\delta^{18}O$ profiles that are difficult to interpret. In addition to air temperature and changes to the source of freshwater at the ice-ocean interface, other factors may influence ice growth and overall conditions including currents within the fjord and oceanic heat flux. These factors are difficult to account for without in-situ measurements and when combined with finer scale changes in weather, likely contribute to cores showing variation throughout their depth that are inconsistent between fjords. To simplify, three scenarios are presented in Fig.13 where growth rate and fraction of seawater are known to derive ice bulk salinity and $\delta^{18}O$:

4.3.1 Constant growth rate while the fraction of seawater increases

In a scenario with constant growth rate of 5 x 10^{-7} m s^{-1} we assume the fraction of seawater, F_{sw}, increases from 0.1 to 0.9. In this scenario, F_{sw} and δ_{ice} increase with depth (Fig 12a) and appear to be linearly related with each other. S_{ice} also is shown to increase but begins to curve, increasing at a slower rate, nearer to the bottom of the volume. Similar patterns are apparent in the ice core from Beisfjord, the middle section of the core from Storfjord, and bottom of the core from Ramfjord. In these areas, F_{sw}, S_{ice}, and δ_{ice} are positively correlated while growth rate, v, remains comparatively constant.

4.3.2 Constant fraction of seawater while growth rate decreases

In this scenario, v decreases from 9e-7 m s^{-1} to 1e-7 m s^{-1} while F_{sw} is held constant at 0.5, representing slowing ice growth with increasing thickness. In this scenario, S_{ice} decreases with depth while δ_{ice} increases slightly. This trend was observed in Lavangen through nearly the entirety of the core, and the middle of the Kattfjord core. From these findings it can be hypothesized that in fjords where this trend is present, the amount and mixing of seawater and freshwater were relatively constant during certain parts of the season. As a result, v is reflected well in ice properties.

4.3.3 Decreasing growth rate combined with an increasing fraction of seawater

Here ν decreases from 9e-7 to 1e-7 m s^{-1} while F_{sw} increases from 0.1 to 0.9. The resulting ice properties S_{ice} and δ_{ice} are positively correlated in the upper 10 – 15 cm before S_{ice} nears an inflection point, beginning to decrease around 25 cm while δ_{ice} continues to increase and appears to be linearly related to F_{sw}. The early increase of S_{ice} is dominated by the increase of interface salinity which changes at a very high relative rate (it starts from very low values), while the latter decrease is dominated by a reduced growth rate. These results illustrate that changes in the composition of water at the ice-ocean can affect the ice bulk salinity at high growth rates but have less of an impact as growth rate slows. Meanwhile δ_{ice} will remain primarily related to F_{sw} more so than growth rate when changes to both variables occur simultaneously.

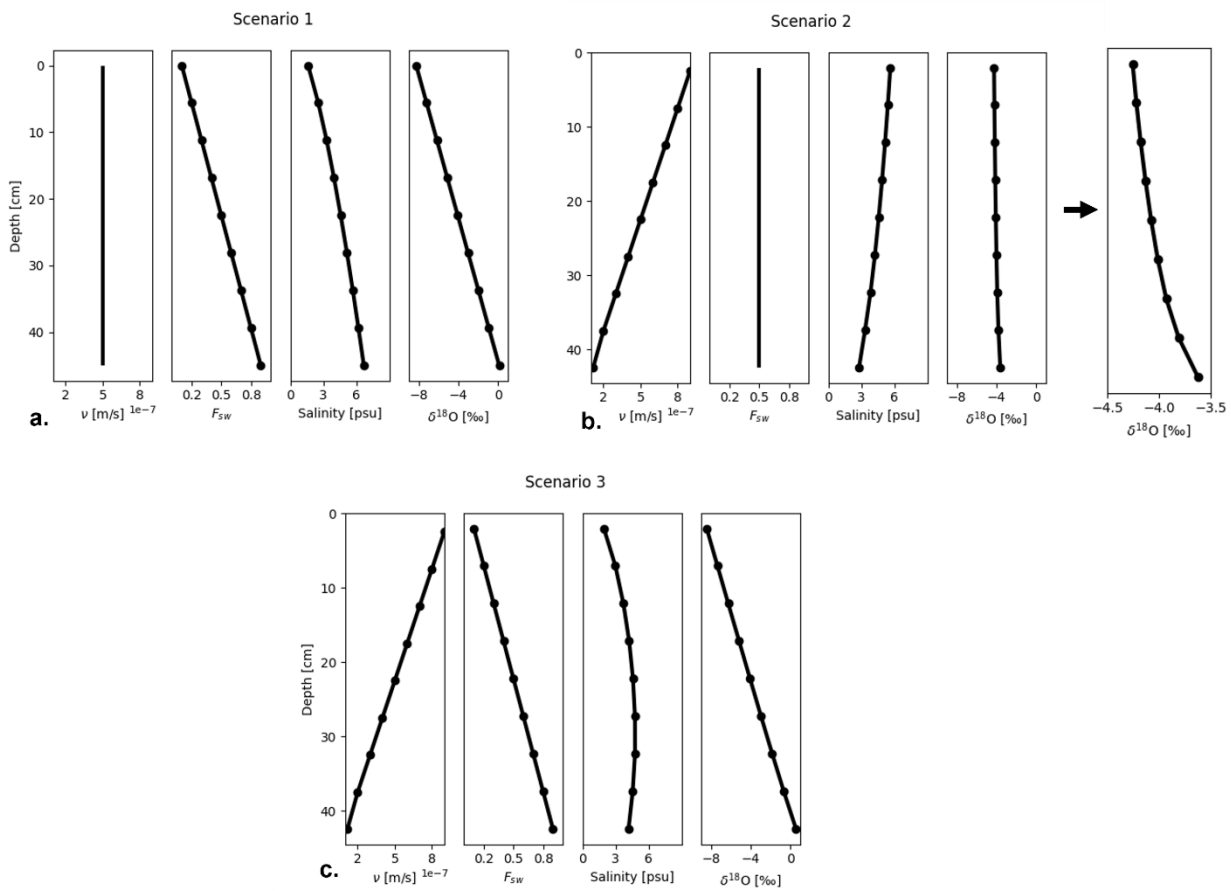

Figure 13 - Results from a scenario study examining the impact of changing growth rate and fraction of seawater on final values of bulk ice salinity and δ^{18}O.

4 Summary and Conclusions

During March 2018, ice cores were collected at six fjords located in northern Norway to obtain measurements of bulk ice salinity and δ^{18}O. Salinity and the isotopic signature of ice depend on growth rate and conditions at the ice-ocean interface making interpretation of profiles non-trivial. This is particularly true in northern Norway, where temperatures may rise above 0 °C throughout winter and the flux of freshwater present at the ice-ocean interface from rain, snowmelt, and ice melt can vary. Using relationships from the literature, a method was developed to invert bulk ice salinity and δ^{18}O simultaneously to determine the history of growth rate and interface composition. Quantitative results depend on knowledge of salinity and δ^{18}O of both freshwater leading into the fjord and seawater and can reveal notable periods of change in the growth history including freshwater incursions events beneath the sea ice.

It was found that five of the six investigated sites had ice grown from a brackish layer with between 0 and 40% seawater content, while one site had ice grown from water with between 50 and 90% seawater content. Evidence of bias was found in the growth rate determination during periods of near to or above freezing temperatures, suggesting that the inversion should not be used as a primary tool for ice age determination when temperatures are not consistently below freezing. When the limitations of the inversion are understood, however, it can provide a valuable approximation of growth rate and interface conditions of fjord ice in regions where in situ measurements and monitoring are uncommon.

In addition, this study supports the following findings:

- Based on the data available for Norwegian mainland fjords, it was found that the shape of the $\delta^{18}O$ profile is indicative of the history of the composition of the water mass at the ice–ocean interface and the shape of the salinity profile is indicative of the growth rate history. This finding does not transfer to regions where either growth rate or interface water composition are primarily constant.
- Substantial periods of air temperatures approaching the melting point of ice will bias the inversion toward either slow or fast growth rates. Such periods of warm weather may modify ice properties due to brine drainage, interface water due to snow or ice melt, and isotopic composition of the freshwater source. Meltwater at the ice–ocean interface can reduce the influence of fresh water from surrounding rivers, leading to ice higher primarily in $\delta^{18}O$, thereby appearing to have grown slower. Snow melting on land may reduce the isotopic ratio of the freshwater source and ice can thus appear to have grown faster.
- The inversion of ice properties resulted in an ice age estimate to within one week for four fjords. The bulk of the error in the remaining fjords can be attributed to individual samples that were expected to have grown under unrealistically low growth rates. However, periods where temperature was near to 0 °C occurred at almost all sites, indicating that errors in the aggregate ice age are to be expected.
- The quality of the inversion depends on the accuracy to which the endmembers are known. Sensitivity is highest to uncertainties in the properties of the dominating water mass, i.e. inversion of ice with predominantly seawater origin will be most sensitive to knowledge of seawater properties. In the current study sensitivity, was highest to uncertainties in the isotopic composition of the river water, δ_w. In Norwegian fjords, the dominating water mass of ice of a fjord may differ between seasons (O'Sadnick et al., 2022).

5 Data Availability

Measurements of ice bulk salinity and $\delta^{18}O$, seawater salinity and $\delta^{18}O$, and freshwater $\delta^{18}O$ can be accessed at https://doi.org/10.5281/zenodo.6607169. All other raw data can be provided by the corresponding author upon request.

6 Author contributions

MO and CP planned the fieldwork campaign, performed the measurements, and designed the method summarized here. MO performed the analysis and wrote the manuscript draft. CP and JS reviewed and edited the manuscript.

7 Competing Interests

The authors declare they have no competing interests.

8 Acknowledgements

This work was funded by the Centre for Integrated Remote Sensing and Forecasting for Arctic Operations (CIRFA), a Centre for Research- based Innovation (Research Council of Norway project number 237906), and partners.

9 References

Alkire, M. B., Nilsen, F., Falck, E., Søreide, J., and Gabrielsen, T. M.: Tracing sources of freshwater contributions to first-year sea ice in Svalbard fjordss, Cont. Shelf Res., 101, 85–97, https://doi.org/10.1016/j.csr.2015.04.003, 2015.

Anderson, D. L.: Growth rate of sea ice, J. Glaciol., 3, 1170–1172, 1961.

Burton, J. A., Prim, R. C., and Slichter, W. P.: The distribution of solute in crystals grown from the melt. Part I. Theoretical, J. Chem. Phys., 21, 1987–1991, https://doi.org/10.1063/1.1698728, 1953.

Cottier, F. R., Nilsen, F., Skogseth, R., Tverberg, V., Skarðhamar, J., and Svendsen, H.: Arctic fjords: a review of the oceanographic environment and dominant physical processes, Geol. Soc. London, Spec. Publ., 344, 35–50, https://doi.org/10.1144/SP344.4, 2010.

Cox, G. F. N. and Weeks, W. F.: Brine Drainage and Initial Salt Entrapment in Sodium Chloride Ice., US Army Corps Eng Cold Reg Res Eng Lab Res Rep, 1975.

Craig, H. and Hom, B.: Relationships of deuterium, oxygen 18, and chlorinity in the formation of sea ice, Trans. AGU, 49, 216–217, 1968.

Eicken, H.: Deriving Modes and Rates of Ice Growth in the Weddell Sea from Microstructural, Salinity and Stable-Isotope Data, Antarct. Sea Ice Phys. Process. Interact. Var. Antarct. Res. Ser, 74, 89–122, https://doi.org/10.1029/ar074p0089, 1998.

Green, J. A. M., Molvaer, J., and Stigebrandt, A.: Hydrographic response of Holandsfjord to changed freshwater runoff, J. Geophys. Res. C Ocean., 109, 1–10, https://doi.org/10.1029/2004JC002295, 2004.

Hunke, E. C., Notz, D., Turner, A. K., and Vancoppenolle, M.: The multiphase physics of sea ice: A review for model developers, 5, 989–1009, https://doi.org/10.5194/tc-5-989-2011, 2011.

Inall, M. E. and Gillibrand, P. A.: The physics of mid-latitude fjords: A review, Geol. Soc. Spec. Publ., 344, 17–33,

https://doi.org/10.1144/SP344.3, 2010.

Kujawa, A., Łącka, M., Szymańska, N., Pawłowska, J., Telesiński, M. M., and Zajączkowski, M.: Could Norwegian fjords serve as an analogue for the future of the Svalbard fjords? State and fate of high latitude fjords in the face of progressive "atlantification," Polar Biol., 44, 2217–2233, https://doi.org/10.1007/s00300-021-02951-z, 2021.

Lehmann, M. and Siegenthaler, U.: Equilibrium oxygen- and hydrogen-isotope fractionation between ice and water, J. Glaciol., 37, 23–26, https://doi.org/10.1017/s0022143000042751, 1991.

Lussana, C., Saloranta, T., Skaugen, T., Magnusson, J., Einar Tveito, O., and Andersen, J.: SeNorge2 daily precipitation, an observational gridded dataset over Norway from 1957 to the present day, Earth Syst. Sci. Data, 10, 235–249, https://doi.org/10.5194/essd-10-235-2018, 2018.

Macdonald, R. W., Paton, D. W., and Carmack, E. C.: The freshwater budget and under-ice spreading of Mackenzie River water in the Canadian Beaufort Sea based on salinity and 18O/16O measurements in water and ice, J. Geophys. Res., 100, 895–919, 1995.

Macdonald, R. W., Carmack, E. C., and Paton, D. W.: Using the d 18 O composition in landfast ice as a record of arctic estuarine processes, Mar. Chem., 65, 3–24, 1999.

Melling, H. and Moore, R. .: Modification of halocline source waters during freezing on the Beaufort Sea shelf: evidence from oxygen isotopes and dissolved nutrients, Cont. Shelf Res., 15, 89–113, 1995.

Nakawo, M. and Sinha, N. K.: Growth rate and salinity profile of first-year sea ice in the High Arctic., J. Glaciol., 27, 313–328, https://doi.org/10.1017/s0022143000015409, 1981.

Notz, D. and Worster, M. G.: Desalination processes of sea ice revisited, J. Geophys. Res. Ocean., 114, 1–10, https://doi.org/10.1029/2008JC004885, 2009.

O'Sadnick, M.: Ice Core Measurements - Northern Norwegian Fjord Ice - Winter 2018/2019 (1.0.0) [Data set], https://doi.org/10.5281/zenodo.6607169, 2022.

O'Sadnick, M., Petrich, C., Brekke, C., and Skarðhamar, J.: Ice extent in sub-arctic fjords and coastal areas from 2001 to 2019 analyzed from MODIS imagery, Ann. Glaciol., https://doi.org/10.1017/aog.2020.34, 2020.

O'Sadnick, M., Petrich, C., Skarðhamar, J., Brekke, C., and Kleven, Ø.: Ice conditions in northern Norwegian fjords: Observations and measurements from three winter seasons, 2017-2020, Cold Reg. Sci. Technol., In Review, 2022.

Olsen, J., Carter, N. A., and Dawson, J.: Community perspectives on the environmental impacts of Arctic shipping: case studies from Russia, Norway and Canada, Cogent Soc. Sci., 5, https://doi.org/10.1080/23311886.2019.1609189, 2019.

Petrich, C., Langhorne, P., and Eicken, H.: Modelled Bulk Salinity of Growing First-Year, Proc. 21st Int. Conf. Port Ocean Eng. under Arct. Cond., 2011.

Skreslet, S. and Loeng, H.: Deep water renewal and associated processes in Skjomen, a fjord in North Norway, Estuar. Coast. Mar. Sci., 5, 383–398, https://doi.org/10.1016/0302-3524(77)90063-9, 1977.

Smith, I. J., Langhorne, P. J., Frew, R. D., Vennell, R., and Haskell, T. G.: Sea ice growth rates near ice shelves, Cold Reg. Sci. Technol., 83–84, 57–70, https://doi.org/10.1016/j.coldregions.2012.06.005, 2012.

Stigebrandt, A.: Hydrodynamics and Circulation of Fjords, in: Encyclopedia of Lakes and Reservoirs. Encyclopedia of Earth Sciences Series., edited by: Bengtsson, L., Herschy, R. W., and Fairbridge, R. W., Springer, Dordrecht, https://doi.org/10.5860/choice.50-3613, 2012.

Svavarsson, J., Guls, H. D., Sham, R. C., Leung, K. M. Y., and Halldórsson, H. P.: Pollutants from shipping - new environmental challenges in the subarctic and the Arctic Ocean, Mar. Pollut. Bull., 164, https://doi.org/10.1016/j.marpolbul.2021.112004, 2021.

Toyota, T., Smith, I. J., Gough, A. J., Langhorne, P. J., Leonard, G. H., Van Hale, R. J., Mahoney, A. R., and Haskell, T. G.: Oxygen isotope fractionation during the freezing of sea water, J. Glaciol., 59, 697–710, https://doi.org/10.3189/2013JoG12J163, 2013.

Vonnahme, T. R.: Microbial diversity and ecology in the coastal Arctic seasonal ice zone, UiT The Arctic University of Norway, 1–238 pp., 2020.

Wassmann, P., Svendsen, H., Keck, a., and Reigstad, M.: Selected aspects of the physical oceanography and particle fluxes in fjords of northern Norway, J. Mar. Syst., 8, 53–71, https://doi.org/10.1016/0924-7963(95)00037-2, 1996.

Weeks, W. F. and Lofgren, G.: Instructions for use The Effective Solute Distribution Coefficient During the Freezing of NaCl Solutions, Phys. Snow Ice, 1967.

Worster, M. G.: Convection in Mushy Layers, Annu. Rev. Fluid Mech., 29, 91–122, https://doi.org/10.1146/annurev.fluid.29.1.91, 1997.

9 Conclusions

The Winter of 2022 provided a clear example of the impact of fjord ice on local communities. An avalanche closed the only road into the town of Beisfjord (located at the head of Beisfjord studied here, 68°22'N, 17°35' E), for several days. While a small dock stands near to town, it was unreachable due to the ice present in the fjord. It is not uncommon for ice to fill the entirety of the fjord; however, ice did not extend past the avalanche path at this time which allowed for a military boat to reach a rocky shoreline at low tide to deliver basic necessities. Approximately a week later, after the avalanche debris had been cleared, ice extended further into the fjord, increasing concern from community members. The ice is often safe to transit near to town, but locals rarely go out nearer to the ice edge given an appropriate fear of soft and inconsistent ice coverage. If the road was again closed, they may need to depend on helicopters or wait for a ship with the proper ice breaking capabilities to arrive. Conversations are ongoing on how to ensure continuous access to Beisfjord through the winter, yet one thing is for certain, the presence of fjord ice greatly complicates any options that depend on access by sea. As a result, the town will likely resort to more costly measures like the building of a tunnel.

Figure 9.1: After a significant avalanche on 21 Feb 2022 closed the road to Beisfjord, Nordland, the military attempted to access the community by boat but was unable because of ice surrounding the dock. This forced the military to land further away from the town on a rocky coastline not always accessible due to tide to provide supplies to residents. Left- picture of fjord two days after the avalanche with the location of avalanche and the dock noted. Photo: SINTEF Narvik. Right- a military boat delivers supplies. Photo: Vidar Løkeng, Fremover.

9.1 Research Conclusions

The results in Paper I revealed that through examination of 386 fjords and coastal areas using MODIS imagery, 47 held > 5 km^2 of ice between 2001 and 2019 with many others having a measurable amount of ice during that time. It is therefore reasonable to surmise that the town of Beisfjord is not entirely unique in how it is impacted by the occasional presence of ice. Sandnessjøen (66°1' N, 12°36' E), provides another example, with fjord ice being noted to halt winter-time shipments of building materials for a factory as early as the 1940s (Dahl, 2013). In current day, fjord ice is still defined as a transportation challenge as it blocks the only alternative route if the single road into town is closed during winter. The simple, yet key, is that a significant amount of ice does form along the coast of Norway during the winter months. Given close proximity to land and year-round freshwater sources,

the properties of fjord and coastal ice found in Norway cannot be assumed constant due to high variability between fjords and over time. Thus, Norwegian fjord and coastal ice should not go overlooked, and perhaps given more focus, because of its potential influence on local communities, industry, and the fjord environment.

In Paper I, ten regions were created to begin investigating trends in ice coverage. For the regions extending from Oslo along the coast to Bergen (60°23' N, 5°19' E), there were several years where ice extent was < 20% of the maximum extent observed if present at all. From Bergen up to Vik (64° 55' N, 10° 57' E), ice extent similarly fluctuated from near to zero to a significant, measurable amount of ice depending on the year. The length of time with ice was shown to be slighter greater, however. In the regions stretching from Vik upwards to Kirkenes (69° 43' N, 30° 2' E), ice coverage was more consistent, having periods of at least 40 % of the maximum ice extent nearly every year over the timespan studied. An analysis of the possible factors driving these differences between regions was undertaken through comparison of ice coverage to the number of freezing degree days, the sum of daily rainfall plus snowmelt, and the sum of snowfall to maximum ice extent. Six out of the ten regions were found to be significantly correlated to freezing degree days, with two being found correlated to snowfall, and one being correlated to rainfall plus snowmelt. The variation found in ice coverage between seasons and regions combined with the differing influence of weather suggest differences in mechanisms for ice formation and resulting ice properties.

Recognizing a need to gather in situ measurements of ice in Norwegian fjords to improve understanding of findings presented in Paper I, a field campaign was run from 2017 to 2020 to collect ice, seawater, and river water data. Seven fjords were chosen, each having a history of ice coverage. In Paper II, the findings are presented revealing clear variations in ice thickness and properties, not only across the seven fjords but at single fjords over the three years of measurements. While the 2017 – 2018 season brought ice primarily columnar in texture, in 2018 – 2019 granular ice composed a much larger portion of the cores. In 2019 – 2020, the other extreme was observed, cores entirely of granular texture if ice was present at all. To help understand these findings, freezing degree days was again used as an initial predictor of ice thickness. A clear difference existed between calculated thickness and measured thickness, however, indicating the strong influence of snow and potentially oceanic heat flux. The former, snow, has an important influence on the ice either acting as an insulator preventing ice growth or adding to the total ice thickness through formation of ice growth. In explanation of why the three seasons of observations differed in the composition of ice gathered, particularly the amount of snow ice, the timing of sub-freezing temperatures, river runoff and additional weather and oceanic variables clearly contributes. This will complicate approaches to prediction of when, how much, and what type of ice will form in a fjord environment.

The majority of fjord ice samples obtained as part of this study had bulk salinities below 2 psu and $\delta^{18}O$ below -5 ‰ despite seawater salinities consistently measured above 30 psu and $\delta^{18}O$ near to 0 ‰. In Paper II, this finding is largely attributed to a de-coupling between the surface and intermediary layers of the fjord waters with intermittent changes to the composition of the water at the ice-ocean interface. The influence of oceanic heat as both an inhibitor of ice growth and cause of bottom melt was also discussed. Paper III utilized bulk salinity and $\delta^{18}O$ combined with river and seawater measurements of salinity and $\delta^{18}O$ to examine these subjects further. Using relationships from the

literature, a method was developed to invert bulk ice salinity and $\delta^{18}O$ to determine the history of growth rate and interface composition. When results from the inversion were used in combination with weather data, an approximation of the timing of both ice and snow melt events that subsequently refroze could be made. In general, however, the inversion performed best when temperatures were consistently below freezing given the unknowns associated with the salinity and isotopic signature of ice and snow melt. This finding relates to the strong influence of endmember measurements and the importance of seawater and river water sampling. Such measurements are logistically simpler to obtain. In combination with ice core measurements, this data can allow for determination of the seasonal history of a fjord in regions where continuous measurements of ocean, ice, and atmosphere are challenging throughout winter.

9.2 Future Work

Through this work, a gap in scientific knowledge has narrowed through the collection of data and completion of analysis focused specifically on Norwegian fjord and coastal ice. More work remains, however, for this gap to be entirely filled to improve our understanding not only of Norwegian fjord ice but extend to other regions where similar ice exists. Here, several potential pathways for future work are provided, divided into two main categories, and described briefly.

1) **The Physics of Fjord Ice and Interaction with the Surrounding Environment**

- *Influence of Oceanic Heat*: In Papers I, II, and III, the potential influence of oceanic heat was noted but not examined in depth. A preliminary study was done to potentially constrain the input of oceanic heat however given the number of factors that needed to be considered including ocean temperature, current speed dependent on tidal patterns and fjord geometry, and stratification and mixing at the ice-ocean boundary, results were not included in published work. Measurement of ice temperature combined with temperature at the ice/ocean interface and ice/atmosphere interface would allow for the most accurate assessment of heat flux through the ice and estimation of oceanic heat flux. Instrumentation was developed to obtain this measurement but the fjord environment proved challenging, with no iterations remaining frozen-in and collecting data while ice formation occurred. This approach is expected to be pursued more in the near future as well as the use of numerical modelling of fjord dynamics.

- *Formation of Snow ice:* As displayed in Paper II, snow ice can compose a large portion of fjord ice cores. The timing of snowfall on ice, flooding of the ice surface, and heat flux through the snow, slush, and ice must all be considered. As snow ice can differ substantially from congelation ice in its engineering properties including mechanical strength and permeability, an investigation into when and where to expect snow ice in fjord and coastal regions specifically is of potentially great use.

- *Linkages to the Fjord Ecosystem and Exchange Processes:* Ice can influence the ecology of a fjord numerous ways including providing a habitat for microbiota, preventing the propagation of light into the upper water column, altering salinity and temperature gradients due to decrease mixing and differences in river plume spread, and potentially altering the timing of deepwater exchange. These topics have been explored in relationship to ice growing in the

high arctic as well as locations like Hudson Bay and the Baltic Sea yet little work exists focused on subarctic fjords. Research into the is topic may be of interest to those in the fishing industry and communities that are invested in the ecological health of ocean and coastal regions.

- *Further work with $\delta^{18}O$:* The method described in Paper III shows promise as a tool to determine conditions at the ice-ocean interface and ice growth rate for fjord ice without constant observation. Further application is recommended however to determine its reliability across seasons and ice of differing properties, formed through differing mixtures of weather and oceanic conditions.

2) **The Impact of Fjord Ice on Marine and Coastal Operations**

- *Ice Mechanics and Application to Infrastructure:* With further study of the type of ice found in fjords including low porosity ice influenced by freshwater and snow ice, a better understanding of the mechanical properties of the ice will be gained. This can be applied to studies of how fjord ice interacts with structures, for example bridges. Roads in places like Norway often run along the edges of a fjords however bridges are continuously being built to shorten travel times and enhance safety. The variability observed in this study highlighted the shortcomings of using ice samples gathered over singular seasons. To obtain an accurate assessment of how fjord ice may impact a structure, the variability observed over a series of seasons must be incorporated. Further study of particularly ice breakup and the movement of ice out of fjord is also recommended.

- *Interaction with Pollutants and Associated Risk:* In addition to mechanical properties, studies of ice permeability when layers of ice types are present are recommended. This includes combinations of congelation ice frozen from saline, brackish, and fresh water with granular frazil and snow ice on top. The samples of fjord ice gathered revealed that it is complex and variable; the movement of oil through would likely be similarly so. As found at the HSVA experiment and displayed in Fig. 1, having one transition will disrupt oil movement, what is the result with more transitions and through ice of the types listed previously? This is an important topic to take into consideration as marine traffic in the Arctic increases. In addition, in the case of an oil spill, having knowledge of where fjord ice is will assist in planning approaches clean up.

- *Long term trends and impacts of climate change:* In Paper I, no long-term trend in ice coverage was found when considering Norway and the ten different regions of focus from 2001 - 2019. In examining fjords and coastal regions independently, however, locations did appear showing both negative and positive trends. Additionally, few records exist focusing on ice coverage before the age of satellite imagery. The questions that first arise upon completion of this study are: If ice formation in fjords is closely connected to fresh water, will winters with more rain lead to more winters with greater ice coverage? What exactly is the timing between weather and oceanic events that allow significant ice to form when ambient ocean temperature is several degrees above freezing and freezing degree days lower than elsewhere

in the Arctic? Could the variability in ice coverage, thickness, and type observed be foreshadowing for other regions where glacier ice is disappearing and winters now bring more rain and melt? To answer these questions, oceanic, atmospheric, and land-based processes must be considered. Therefore, perhaps subarctic fjords are an ideal location to focus studies of changing climate as it is here so many aspects of the natural world collide.

10 Works cited

Anderson, D. L. (1961). Growth rate of sea ice. *Journal of Glaciology*, *3*(30), 1170–1172.

Aure, J., Molvær, J., & Stigebrandt, A. (1996). Observations of inshore water exchange forced by a fluctuating offshore density field. *Marine Pollution Bulletin*, *33*(1–6), 112–119. https://doi.org/10.1016/S0025-326X(97)00005-2

Bergström, S. (1992). The HBV model - its structure and applications. *Swedish Meteorological and Hydrological Institute, Norrköping*, *4*, 1–33.

Beria, H., Larsen, J. R., Ceperley, N. C., Michelon, A., Vennemann, T., & Schaefli, B. (2018). Understanding snow hydrological processes through the lens of stable water isotopes. *Wiley Interdisciplinary Reviews: Water*, *5*(6), 1–23. https://doi.org/10.1002/wat2.1311

Brandvik, P. J., Resby, J. L. M., Daling, P. S., Leirvik, F., & Fritt-Rasmussen, J. (2010). Meso-Scale Weathering of Oil as a Function of Ice Conditions. Oil Properties, Dispersibility, and In Situ Burnability of Weathered Oil as a Function of Time. JIP Report no. 19 (SINTEF A15563)., 116. Retrieved from www.sintef.no/globalassets/project/jip_oil_in_ice/dokumenter/publications/jip-rep-no-19-common-meso-scale-final.pdf

Breivik, H. M. (2014). Palaeo-oceanographic development and human adaptive strategies in the Pleistocene–Holocene transition: A study from the Norwegian coast. *Holocene*, *24*(11), 1478–1490. https://doi.org/10.1177/0959683614544061

Carnat, G., Papakyriakou, T., Geilfus, N. X., Brabant, F., Delille, B., Vancoppenolle, M., … Tison, J. L. (2013). Investigations on physical and textural properties of arctic first-year sea ice in the Amundsen gulf, Canada, November 2007-june 2008 (IPY-CFL system study). *Journal of Glaciology*, *59*(217), 819–837. https://doi.org/10.3189/2013JoG12J148

Cottier, F. R., Nilsen, F., Skogseth, R., Tverberg, V., Skarðhamar, J., & Svendsen, H. (2010). Arctic fjords: A review of the oceanographic environment and dominant physical processes. *Geological Society Special Publication*, *344*, 35–50. https://doi.org/10.1144/SP344.4

Cottier, F. R., Nilsen, F., Skogseth, R., Tverberg, V., Skarðhamar, J., & Svendsen, H. (2010). Arctic fjords: a review of the oceanographic environment and dominant physical processes. *Geological Society, London, Special Publications*, *344*(1), 35–50. https://doi.org/10.1144/SP344.4

Cox, G. F. ., & Weeks, W. F. (1983). Equations for determining the gas and brine volumes in sea - ice samples. *Journal of Glaciology*, *29*(102), 306–316.

Craig, H., & Hom, B. (1968). Relationships of deuterium, oxygen 18, and chlorinity in the formation of sea ice. *Trans. AGU*, *49*, 216–217.

Cronin, M. F., & Sprintall, J. (2001). Wind And Buoyancy-forced Upper Ocean. *Encyclopedia of Ocean Sciences*, 3219–3226. https://doi.org/10.1006/rwos.2001.0157

Cushman-Roisin, B., Asplin, L., & Svendsen, H. (1994). Upwelling in Broad Fjords. *Continental Shelf Research*, *14*(15), 1701–1721.

Dahl, T. D. (2013). *Sauda i den tyske rustnings-økonomien* (Masters Thesis). NTNU.

Darelius, E. (2020). On the effect of climate trends in coastal density on deep water renewal frequency in sill fjords—A statistical approach. *Estuarine, Coastal and Shelf Science*, *243*(January), 106904. https://doi.org/10.1016/j.ecss.2020.106904

Dickens, D. (2011). Behavior of oil spills in ice and implications for Arctic spill response. In *OTC Arctic Technology Conference*. Offshore Technology Conference.

Eicken, H., Fischer, H., & Lemke, P. (1995). Effects of the snow cover on Antarctic sea ice and potential modulation of its response to climate change. *Annals of Glaciology*, *21*, 369–376. https://doi.org/10.1017/s0260305500016086

Eicken, H., Grenfell, T. C., Perovich, D. K., Richter-Menge, J. A., & Frey, K. (2004). Hydraulic controls of summer Arctic pack ice albedo. *Journal of Geophysical Research: Oceans*, *109*(C8), 1–13. https://doi.org/10.1029/2003JC001989

Eicken, H., Dmitrenko, I., Tyshko, K., & Darovskikh, A. (2005). Zonation of the Laptev Sea landfast ice cover and its importance in a frozen estuary. *Global and Planetary Change*, *48*, 55–83. https://doi.org/10.1016/j.gloplacha.2004.12.005

Eicken, H.. (1998). Deriving Modes and Rates of Ice Growth in the Weddell Sea from Microstructural, Salinity and Stable-Isotope Data. *Antarctic Sea Ice: Physical Processes, Interactions and Variability*, *Antarct. Res. Ser*, *74*, 89–122. https://doi.org/10.1029/ar074p0089

Eilertsen, H. C., & Skarðhamar, J. (2006). Temperatures of north Norwegian fjords and coastal waters: Variability, significance of local processes and air-sea heat exchange. *Estuarine, Coastal and Shelf Science*, *67*(3), 530–538. https://doi.org/10.1016/j.ecss.2005.12.006

Farmer, D. M., & Freeland, H. J. (1983). The physical oceanography of Fjords. *Progress in Oceanography*, *12*(2), 147–220. https://doi.org/10.1016/0079-6611(83)90004-6

Fofonoff, N., & Millard, R. (1983). Algorithms for computation of fundamental properties of seawater. *Unesco Technical Papers in Marine Science*, *44*, 54.

Freitag, J., & Eicken, H. (2003). Meltwater circulation and permeability of Arctic summer sea ice derived from hydrological field experiments. *Journal of Glaciology*, *49*(166), 349–358. https://doi.org/10.3189/172756503781830601

Golden, K. M., Eicken, H., Heaton, A. L., Miner, J., Pringle, D. J., & Zhu, J. (2007). Thermal evolution of permeability and microstructure in sea ice. *Geophysical Research Letters*, *34*(16), 2–7. https://doi.org/10.1029/2007GL030447

Gorelick, N., Hancher, M., Dixon, M., Ilyushchenko, S., Thau, D., & Moore, R. (2017). Google Earth Engine: Planetary-scale geospatial analysis for everyone. *Remote Sensing of Environment*. https://doi.org/10.1016/j.rse.2017.06.031

Gow, A., Weeks, W., Kosloff, P., & Carsey, S. (1992). Petrographic and Salinity Characteristics of Brackish Water Ice in the Bay of Bothnia. In *CRREL Report 92-13*. US Army Corps of Engineers.

Granskog, M. A., Ehn, J., & Niemelä, M. (2005). Characteristics and potential impacts of under-ice river plumes in the seasonally ice-covered Bothnian Bay (Baltic Sea). *Journal of Marine Systems*, *53*(1–4), 187–196. https://doi.org/10.1016/j.jmarsys.2004.06.005

Granskog, M., Rosel, A., Dodd, P., Divine, D., Gerland, S., Martma, T., & Leng, M. (2017). Snow contribution to first-year and second-year Arctic sea ice mass balance north of Svalbard. *Journal of Geophysical Research: Oceans*, *122*, 2539–2549. https://doi.org/10.1002/2016JC012398.Received

Granskog, M.A., Martma, T. A., & Vaikmäe, R. A. (2003). Development, structure and composition of land-fast sea ice in the northern Baltic Sea. *Journal of Glaciology*, *49*(164), 139–148. https://doi.org/10.3189/172756503781830872

Granskog, M. A, Kaartokallio, H., Thomas, D. N., & Kuosa, H. (2005). Influence of freshwater inflow on the inorganic nutrient and dissolved organic matter within coastal sea ice and underlying waters in the Gulf of Finland (Baltic Sea). *Estuarine, Coastal and Shelf Science*, *65*, 109–122. https://doi.org/10.1016/j.ecss.2005.05.011

Granskog, M.A., Kaartokallio, H., Kuosa, H., Thomas, D. N., & Vainio, J. (2006). Sea ice in the Baltic Sea - A review. *Estuarine, Coastal and Shelf Science*, *70*(1–2), 145–160. https://doi.org/10.1016/j.ecss.2006.06.001

Green, J. A. M., Molvaer, J., & Stigebrandt, A. (2004). Hydrographic response of Holandsfjord to changed freshwater runoff. *Journal of Geophysical Research C: Oceans*, *109*(7), 1–10. https://doi.org/10.1029/2004JC002295

Hallikainen, M., & Winebrenner, D. P. (1992). The physical basis for sea ice remote sensing. In F. D. Carsey (Ed.), *Microwave remote sensing of sea ice* (68th ed., pp. 29–46). Washington: American Geophysical Union.

Hanssen - Bauer, I., Førland, E. J., Haddeland, I., Hisdal, H., Lawrence, D., Mayer, S., … Ådlandsvik, B. (2017). *Climate in Norway 2100 - a knowlege base for climate adaption*. Retrieved from www.miljodirektoratet.no/M741

Hillig, W. (1958). The kinetics of freezing of ice in the direction perpendicular to the basal plane. In R. H. Doremus (Ed.), *Growth and perfection of crystals* (pp. 350–359). New York: Wiley.

Hobbs, P. V. (1974). *Ice Physics*. Oxford: Clarendon Press.

Horner-Devine, A. R., Hetland, R. D., & MacDonald, D. G. (2015). Mixing and transport in coastal river plumes. *Annual Review of Fluid Mechanics*, *47*, 569–594. https://doi.org/10.1146/annurev-fluid-010313-141408

Hughes, N. (2006). *NP57A, NP57B, NP58A, NP58B Norway Pilot. Sea Ice Conditions: West coast of Norway from: Lindesnes to Statlandet, Statllandet to Risværfjorden. Offshore and coastal waters of Norway from: Risværfjorden to the north part of Vesterrålen, Andfjorden to Varang*. Argyll, UK: Scottish Association for Marine Science.

Hunke, E. C., Notz, D., Turner, A. K., & Vancoppenolle, M. (2011). The multiphase physics of sea ice: A review for model developers. *Cryosphere*, *5*(4), 989–1009. https://doi.org/10.5194/tc-5-989-2011

Ikävalko, J. (1998). Further observations on flagellates within sea ice in northern Bothnian Bay, the Baltic Sea. *Polar Biology*, *19*(5), 323–329. https://doi.org/10.1007/s003000050253

Inall, M., Cottier, F., Griffiths, C., & Rippeth, T. (2004). Sill dynamics and energy transformation in a jet fjord. *Ocean Dynamics*, *54*(3–4), 307–314. https://doi.org/10.1007/s10236-003-0059-2

Inall, M. E., & Gillibrand, P. A. (2010). The physics of mid-latitude fjords: a review. *Geological Society, London, Special Publications*, *344*(1), 17–33. https://doi.org/10.1144/SP344.3

Ingram, R. G., & Larouche, P. (1987). Variability of an under-ice river plume in Hudson Bay. *Journal of Geophysical Research: Oceans*, *92*(C9), 9541–9547. https://doi.org/10.1029/JC092iC09p09541

Jeffries, M. O., Morris, K., & Duguay, C. R. (2012). Floating ice: lake ice and river ice. *Satellite Image Atlas of Glaciers of the World – State of the Earth's Cryosphere at the Beginning of the 21st Century: Glaciers, Global Snow Cover, Floating Ice, and Permafrost and Periglacial Environments*, (January 2014), 381–424.

Jones, D. W. R., & Wells, A. J. (2018). Frazil-ice growth rate and dynamics in mixed layers and sub-ice-shelf plumes. *Cryosphere*, *12*(1), 25–38. https://doi.org/10.5194/tc-12-25-2018

Kovalev, D. P., Kovalev, P. D., & Squire, V. A. (2020). Crack formation and breakout of shore fast sea ice in Mordvinova Bay, south-east Sakhalin Island. *Cold Regions Science and Technology*, *175*(December 2019), 103082. https://doi.org/10.1016/j.coldregions.2020.103082

Lange, M. A., & Eicken, H. (1991). Textural characteristics of sea ice and the major mechanisms of ice growth in the Weddell Sea. *Annals of Glaciology*, *15*(1984), 210–215. https://doi.org/10.3189/1991aog15-1-210-215

Langhorne, P. J. (1983). Laboratory experiments on crystal orientation in NaCl ice. *Annals of Glaciology*, *4*, 163–169. https://doi.org/10.3189/s0260305500005413

LeGrande, A. N., & Schmidt, G. A. (2006). Global gridded data set of the oxygen isotopic composition in seawater. *Geophysical Research Letters*, *33*(12), 1–5. https://doi.org/10.1029/2006GL026011

Lehmann, M., & Siegenthaler, U. (1991). Equilibrium oxygen- and hydrogen-isotope fractionation between ice and water. *Journal of Glaciology*, *37*(125), 23–26. https://doi.org/10.1017/s0022143000042751

Leppäranta, M., & Manninen, T. (1988). *The brine and gas content of sea ice with attention to low salinities and high temperatures*. Helsinki.

Li, S. S., & Ingram, R. G. (2007). Isopycnal deepening of an under-ice river plume in coastal waters: Field observations and modeling. *Journal of Geophysical Research: Oceans*, *112*(C7), 1–15. https://doi.org/10.1029/2006JC003883

Lohse, J. (2020). *On Automated Classification of Sea Ice Types in SAR Imagery*. UiT The Arctic University of Norway.

Lussana, C., Saloranta, T., Skaugen, T., Magnusson, J., Einar Tveito, O., & Andersen, J. (2018). SeNorge2 daily precipitation, an observational gridded dataset over Norway from 1957 to the present day. *Earth System Science Data*, *10*(1), 235–249. https://doi.org/10.5194/essd-10-235-2018

Macdonald, R.W., Carmack, E. C., & Paton, D. W. (1999). Using the d 18 O composition in landfast ice as a record of arctic estuarine processes. *Marine Chemistry*, *65*, 3–24.

Macdonald, R.W, Paton, D. W., & Carmack, E. C. (1995). The freshwater budget and under-ice

spreading of Mackenzie River water in the Canadian Beaufort Sea based on salinity and 18O/16O measurements in water and ice. *Journal of Geophysical Research*, *100*(C1), 895–919.

Maksym, T., & Jeffries, M. O. (2000). A one-dimensional percolation model of flooding and snow ice formation on Antarctic sea ice. *Journal of Geophysical Research: Oceans*, *105*(C11), 26313–26331. https://doi.org/10.1029/2000jc900130

Malmgren, F. (1927). On the properties of sea ice. *Norwegian North Pole Expedition "Maud" 1918-1925*, *1*, 1–67.

McPhee, M. G. (1992). Turbulent heat flux in the upper ocean under sea ice. *Journal of Geophysical Research*, *97*(C4), 5365. https://doi.org/10.1029/92jc00239

Melling, H., & Moore, R. . (1995). Modification of halocline source waters during freezing on the Beaufort Sea shelf: evidence from oxygen isotopes and dissolved nutrients. *Continental Shelf Research*, *15*(1), 89–113.

Merkouriadi, I., Cheng, B., Graham, R. M., Rösel, A., & Granskog, M. A. (2017). Critical Role of Snow on Sea Ice Growth in the Atlantic Sector of the Arctic Ocean. *Geophysical Research Letters*, *44*(20), 10,479-10,485. https://doi.org/10.1002/2017GL075494

Müller-Stoffels, M., Langhorne, P. J., Petrich, C., & Kempema, E. W. (2009). Preferred crystal orientation in fresh water ice. *Cold Regions Science and Technology*, *56*(1), 1–9. https://doi.org/10.1016/j.coldregions.2008.11.003

Myksvoll, M. S., Sandvik, A. D., Asplin, L., & Sundby, S. (2014). Effects of river regulations on fjord dynamics and retention of coastal cod eggs. *ICES Journal Of*, *71*(4), 943–956. https://doi.org/10.1093/icesjms/fst113

Nan, Y., Tian, F., Hu, H., Wang, L., & Zhao, S. (2019). Stable isotope composition of river waters across the world. *Water (Switzerland)*, *11*(9), 1–24. https://doi.org/10.3390/w11091760

Nash, J. D., Kilcher, L. F., & Moum, J. N. (2009). Structure and composition of a strongly stratified, tidally pulsed river plume. *Journal of Geophysical Research: Oceans*, *114*(8), 1–16. https://doi.org/10.1029/2008JC005036

Nilsen, F., Cottier, F., Skogseth, R., & Mattsson, S. (2008). Fjord-shelf exchanges controlled by ice and brine production: The interannual variation of Atlantic Water in Isfjorden, Svalbard. *Continental Shelf Research*, *28*(14), 1838–1853. https://doi.org/10.1016/j.csr.2008.04.015

NORCOR. (1975). *The Interaction of Crude Oil With Arctic Sea Ice*. *Beaufort Sea Technical Report*. Victoria, BC, Canada.

Notz, D., & Worster, M. G. (2008). In situ measurements of the evolution of young sea ice. *Journal of Geophysical Research: Oceans*, *113*(3), 1–7. https://doi.org/10.1029/2007JC004333

Notz, D., & Worster, M. G. (2009). Desalination processes of sea ice revisited. *Journal of Geophysical Research: Oceans*, *114*(5), 1–10. https://doi.org/10.1029/2008JC004885

Oggier, M., Eicken, H., Petrich, C., Wilkinson, J., & O'Sadnick, M. (2019). Crude oil migration in sea-ice: Laboratory studies of constraints on oil mobilization and seasonal evolution. *Cold Regions Science and Technology*, 102924.

Omstedt, A. (1998). Freezing estuaries and semi-enclosed basins. In M. Leppäranta (Ed.), *Physics of Ice-Covered Seas* (pp. 483–516). Finland: Helsinki University Printing House.

Ono, N. (1968). Thermal properties of sea ice: IV, thermal constants of sea ice (in Japanese). *Low Temperature Science Series A*, *26*, 329–349.

Parkinson, C. L., & Washington, W. M. (1979). Large-Scale Numerical Model of Sea Ice. *J Geophys Res*, *84*(C1), 311–337. https://doi.org/10.1029/jc084ic01p00311

Perovich, D. (1998). Optical Properties of Sea Ice. In M. Leppäranta (Ed.), *Physics of ice-covered seas* (Volume 1, pp. 195–230). Helsinki: University of Helsinki.

Persson, P. O. G., Fairall, C. W., Andreas, E. L., Guest, P. S., & Perovich, D. K. (2002). Measurements near the Atmospheric Surface Flux Group tower at SHEBA: Near-surface conditions and surface energy budget. *Journal of Geophysical Research: Oceans*, *107*(10), 1–35. https://doi.org/10.1029/2000jc000705

Petrich, C. (2019). The Color of Ice. In *The International Glaciological Society Sea Ice Symposium*.

Petrich, C., & Eicken, H. (2010). Growth, Structure, and Properties of Sea Ice. In D. Thomas & G. Dieckmann (Eds.), *Sea Ice* (2nd ed., pp. 23–78). Oxford: Wiley Blackwell.

Petrich, C., Karlsson, J., & Eicken, H. (n.d.). Porosity of growing sea ice and potential for oil entrainment.

Petrich, C., Langhorne, P., & Eicken, H. (2011). Modelled Bulk Salinity of Growing First-Year. *Proceedings of the 21st International Conference on Port and Ocean Engineering under Arctic Conditions*.

Petrich, C., Langhorne, P. J., & Sun, Z. F. (2006). Modelling the interrelationships between permeability, effective porosity and total porosity in sea ice. *Cold Regions Science and Technology*, *44*(2), 131–144. https://doi.org/10.1016/j.coldregions.2005.10.001

Petrich, C., O'Sadnick, M., Brekke, C., Myrnes, M., Maus, S., Salomon, M. L., … Reimer, N. (2018). An overview of the Mosideo/Cirfa experiments on behavior and detection of oil in ice. *41st AMOP Technical Seminar on Environmental Contamination and Response, AMOP 2018*, (March 2020), 112–122.

Provost, C., Sennechael, N., Miguet, J., Itkin, P., Rosel, A., Koenig, Z., … Granskog, M. (2017). Observations of flooding and snow-ice formation in a thinner Arctic sea-ice regime during the N-ICE2015 campaign: Influence of basal ice melt and storms. *Journal of Geophysical Research: Oceans*, *122*, 7115–7134. https://doi.org/10.1002/2016JC012011.Received

Rutgersson, A., Carlsson, B., & Smedman, A. S. (2007). Modelling sensible and latent heat fluxes over sea during unstable, very close to neutral conditions. *Boundary-Layer Meteorology*, *123*(3), 395–415. https://doi.org/10.1007/s10546-006-9150-9

Schwerdtfeger, P. (1963). The Thermal Properties of Sea Ice. *Journal of Glaciology*, *4*(36), 789–807.

Serrano, L., Voltas, J., Resco, V., Williams, D., & Ferrio, P. (2005). Stable isotopes in arid and semi-arid forest systems. *Investigación Agraria. Sistemas y Recursos Forestales*, *14*(3), 371–382.

Shirasawa, K., & Ingram, R. G. (1991). Characteristics of the turbulent oceanic boundary layer under

sea ice: Part 1. A review of the ice–ocean boundary layer. *Journal of Marine Systems*, *2*, 153–160.

Skardhamar, J., & Svendsen, H. (2010). Short-term hydrographic variability in a stratified Arctic fjord. *Geological Society Special Publication*, *344*, 51–60. https://doi.org/10.1144/SP344.5

Stigebrandt, A. (1976). Vertical Diffusion Driven By Internal Waves in a Sill Fjord. *Journal of Physical Oceanography*, *6*(4), 486–495. https://doi.org/10.1175/1520-0485(1976)006<0486:vddbiw>2.0.co;2

Stigebrandt, A. (1980). Some aspects of tidal interaction with fjord constrictions. *Estuarine and Coastal Marine Science*, *11*(2), 151–166.

Stigebrandt, A. (2012). Hydrodynamics and Circulation of Fjords. In L. Bengtsson, R. W. Herschy, & R. W. Fairbridge (Eds.), *Encyclopedia of Lakes and Reservoirs. Encyclopedia of Earth Sciences Series.* Dordrecht: Springer. https://doi.org/10.5860/choice.50-3613

Sturm, M., Holmgren, J., König, M., & Morris, K. (1997). The thermal conductivity of seasonal snow. *Journal of Glaciology*, *43*(143), 26–41. https://doi.org/10.3189/s0022143000002781

Sturm, M., Perovich, D. K., & Holmgren, J. (2002). Thermal conductivity and heat transfer through the snow on the ice of the Beaufort Sea. *Journal of Geophysical Research: Oceans*, *107*(C10). https://doi.org/10.1029/2000jc000409

Toyota, T., Smith, I. J., Gough, A. J., Langhorne, P. J., Leonard, G. H., Van Hale, R. J., … Haskell, T. G. (2013). Oxygen isotope fractionation during the freezing of sea water. *Journal of Glaciology*, *59*(216), 697–710. https://doi.org/10.3189/2013JoG12J163

Wang, C., Cheng, B., Wang, K., Gerland, S., & Pavlova, O. (2015). Modelling snow ice and superimposed ice on landfast sea ice in Kongsfjorden, Svalbard. *Polar Research*, *34*(1), 20828. https://doi.org/10.3402/polar.v34.20828

Wassmann, P., Svendsen, H., Keck, A., & Reigstad, M. (1996). Selected aspects of the physical oceanography and particle fluxes in fjords of northern Norway. *Journal of Marine Systems*, *8*, 53–71. https://doi.org/10.1016/0924-7963(95)00037-2

Webster, M., Gerland, S., Holland, M., Hunke, E., Kwok, R., Lecomte, O., … Sturm, M. (2018). Snow in the changing sea-ice systems. *Nature Climate Change*, *8*(11), 946–953. https://doi.org/10.1038/s41558-018-0286-7

Weeks, W. F., & Ackley, S. F. (1986). The growth, structure, and properties of sea ice. In N. Untersteiner (Ed.), *The Geophysics of Sea Ice* ((NATO ASI, pp. 9–164). New York: Plenum Press.

Weeks, W. F., & Lofgren, G. (1967). Instructions for use The Effective Solute Distribution Coefficient During the Freezing of NaCl Solutions. *Physics of Snow and Ice*.

Wettlaufer, J. S., Worster, M. G., & Huppert, H. E. (1997). Natural convection during solidification of an alloy from above with application to the evolution of sea ice. *Journal of Fluid Mechanics*, *344*, 291–316. https://doi.org/10.1017/S0022112097006022

Woodhouse, I. H. (2006). *Introduction to Microwave Remote Sensing*. Boca Raton, FL, USA: CRC Press.